Dissertation zur Erlangung des Doktorgrades

der Fakultät für Chemie und Pharmazie

der Ludwig-Maximilians-Universität München

Sequence-defined carriers for drug and nucleic acid delivery

Lun Peng

aus

Xuzhou, Jiangsu, China

2022

Erklärung

Diese Dissertation wurde im Sinne von § 7 der Promotionsordnung vom 28. November 2011 von Herrn Prof. Dr. Ernst Wagner betreut.

Eidesstattliche Versicherung

Diese Dissertation wurde eigenständig und ohne unerlaubte Hilfe erarbeitet.

München, 28.06.2022

.....……

Lun Peng

Dissertation eingereicht am: 29.06.2022

1. Gutachter: Prof. Dr. Ernst Wagner

2. Gutachter: Prof. Dr. Wolfgang Friess

Mündliche Prüfung am: 28.07.2022

To my family

致家人

„The important thing in life is to have a great aim, and the determination to attain it.”

Johann Wolfgang von Goethe

Table of Contents

1 Introduction

This thesis provides a brief introduction to the research field of molecular therapeutics and associated efficient delivery strategies.

1.1 Combination chemotherapy

Cancer is a public health problem and one of the leading causes of worldwide death. It annually claims more than 8 million lives.[1 2] Cancers are treated with various treatments, such as chemotherapy, hormone therapy, surgery, radiation, immune therapy, and targeted delivery.[3] Further interventions are necessary to lower the rate and manage the disease by implementing various strategies, such as the new treatment methods. With the development of therapeutic modalities, it is essential to identify the most effective treatment. Among several new therapeutic approaches, nanotechnology in cancer plays several roles, including the detection and treatment of cancer, identification of biomarkers, understanding of the progress guiding the development of new diagnostics and imaging agents.[4]

The first trial of chemotherapy began in the 1940s by Goodman and Gilman to examine the potential for a lymphoid tumor.[5] Since then, billions of dollars have been spent every year in the pharmaceutical industry to investigate the discovery and development of new drugs and their approval. However, scientists can not address the clinical need for disease treatments and cancer. The new pharmaceutical anticancer agent is still one of the burning issues for scientists due to cancer remains the leading cause of death and increases the economic and financial burden. It is imperative and essential to find efficient, economically feasible approaches. The new approaches must address several limitations, such as non-specific targeting, drug resistance, excessive toxic effects, and undesired treatment side effects.

The isolation and characterization of the natural drug by Zubrod et al. in the lab in 1956.[6] The cancer drug discovery had gained a reputation for having high risk and little chance of efficiency. Fewer than 10 % of new drugs entering clinical trials achieved Food and Drug Administration (FDA) approval for marketing. During the drug discovery and clinical development of anticancer drugs, scientists found that the significant issue was the acute and long-term toxicities of chemotherapies, which affected virtually every healthy organ of the body. Therefore, seeking new generations of cancer treatment methods with high selectivity for tumor cells is essential.

More and more researchers have paid attention to tumor-targeted combination

therapies recently, especially in nanomedicine. The first combination therapy was proposed in 1965 by Holland, Frei and Freireich for acute leukemia. This approach extended to the lymphomas in 1963.[7] Other promising cases were reported to prove the ability of combination chemotherapy to cure different large-cell tumors.[8] Combination therapy with multiple treatments is more effective than single therapy because it produces synergistic anticancer effects, reduces drug-related toxicity, and inhibits multidrug resistance through different mechanisms.[8]

The strategy for chemotherapy of cancer needs to demonstrate to reach the requirement of successful chemotherapy. With the understanding of molecular and genetic approaches, the signaling networks that regulate cellular activities such as proliferation and survival were radically altered in cancer cells. A breakthrough in medical oncology occurred with the development of targeted therapy in 1980, which determined an improvement in the effectiveness of cancer treatments.[9] This new strategy included growth factors, signaling molecules, cell-cycle proteins, modulators of apoptosis, and molecules.

According to the action mechanism of antitumoral drugs, the cancer cells can be targeted at DNA, RNA, or molecular level, at the organelle or nucleus on a cell level, and at the endothelium and extracellular matrix on a tissue level.[10] Traditional small molecule agents are to damage DNA and interfere with cellular mitosis, and they are the mainstream of cytotoxic anticancer in clinical application. Moreover, most classic chemotherapeutic agents interact with the DNA of cancer cells, whereas monoclonal antibodies are directed against proteins or the endothelium and extracellular matrix.[11] They include alkylating agents, anti-microtubule agents, anti-metabolitesm topoisomerase inhibitors, cytotoxic antibiotics, and so forth.

1.1.1 Co-delivery of different small molecule drugs

Anti-microtubule agents include vinca alkaloids and taxanes. They can prevent the formation of the microtubules, whereas the taxanes, including paclitaxel (PTX) and docetaxel, can prohibit the microtubule disassembly. As a result, cancer cells do not complete mitosis. Cytotoxic antibiotics obtained from the bacterium streptomyces peucetius, for example, doxorubicin (DOX) and daunorubicin, were the first-line chemotherapeutic drugs. Their anticancer mechanisms include 1) DNA intercalation (molecules insert between the two strands of DNA), 2) generation of highly reactive free radicals that damage intercellular molecules, and 3) topoisomerase inhibition. PTX and DOX are most used in nano-drug co-delivery system (NDCDS) chemotherapeutic

drugs, which have different pharmacological mechanisms and subcellular targets.[12-15] It is worth mentioning that NDCDS has developed rapidly in the two decades. This delivery system is recognized to have the advantages of breaking through the biological barrier, improving the target property, and enhancing the penetration ability of the tumor tissue. The nano drug co-delivery system, designed for clinical combination chemotherapy, encapsulates at most minuscule two anticancer drugs with different physicochemical and pharmacological properties into a delivery system. The combination of chemotherapeutic agents and other drugs that target different cellular pathways, such as chemosensitizers, can delay cancer adaptation by reducing the possible cancer cell mutation. In recent decades, NDCDS has emerged as a promising strategy of combined anticancer therapy to combat sophisticated cancer pathways for better therapeutic efficacy. In addition, it can get higher targeting selectivity. Chen and co-workers demonstrated that the co-delivery of polyethylene glycol-polylactic-co-glycolic acid (PEG-PLGA) nanoparticles- loaded DOX and PTX could enhance the anti-tumor efficacy of the combination chemotherapy with free DOX and PTX on non-small cell lung cancer.[16] The drugs exhibited excellent synergistic efficacy in the NDCDS. Furthermore, the co-encapsulation of DOX and mitomycin C within polymer-lipid hybrid nanoparticles (DMPLN) to achieve tumor-targeting delivery in a murine breast tumor model, which was reported by Zhang et al.[17] Compared to the free drug, the formulated nanoparticles showed higher levels of cancer cell apoptosis and reduced organ toxicity. They proved that NDCDS could effectively deliver two therapeutic agents with different chemical properties, such as hydrophobicity and hydrophilicity drugs.

However, there is still a big challenge in NDCDS encapsulating different anti-tumor agents to find the ideal carrier. Many biomaterials have been investigated for constructing therapeutic delivery carriers via tailoring their chemical and physical properties to meet specific needs in different situations. Polymers have been extensively studied for their potential to simultaneously deliver different chemotherapeutic agents with low aqueous solubility. Drugs with poor water-solubility are encapsulated with polymers to form micelle structures, where drugs reside within the hydrophobic core, and hydrophilic chains form the micelle shell.

Liposomes usually comprise phosphatidylcholine, or their hydrogenated derivatives, exhibiting a higher phase transition temperature. Hydrophilic drugs can be easily dissolved in the external aqueous core during liposome preparation using the standard thin layer hydration method, while a hydrophobic drug can dissolve between the lipid bilayers oil phase.[18] In 1975, the liposomal cytarabine materials enhanced the survival

of leukemic mice *in vivo* compared to cytarabine alone, as demonstrated by Kobayashi.[19] In 1995, pegylated liposomal doxorubicin was the first nanocarrier approved by the FDA. Many delivery systems on the market or clinical trials are liposomal or lipid-based products.

Lipid nanocarriers tend to passively accumulate in tumor tissue via the enhanced permeability and retention (EPR) effect caused by tumor vessels' unique anatomical and pathophysiological characteristics. Moreover, the circulation time of liposomes in tumor tissue can be increased with the modification of PEGylation. Patel et al. prepared stealth liposomes encapsulated with P-glycoprotein (P-gp) inhibitor tariquidar and drug Paclitaxel (PTX) by thin-film hydration.[20] Also, liposomes can be designed to respond to specific signals, such as hyperthermia, pH decrease, or an alternation of external magnetic field or ultrasound to release their aqueous content. The triggered release was utilized to avoid unfavorable side effects in non-targeted sites and enhance therapeutic efficacy.

Polymeric nanoparticles are often considered alternatives to liposomal vehicles for their improved *in vivo* stability and loading efficiency. Poly (lactic-co-glycolic acid) (PLGA) is one of the most widely used materials for drug delivery due to its outstanding ease of processing, biodegradability, and biocompatibility.[20] The co-delivery formulation exhibits more effective antitumor effects than free drugs or single-drug-loaded nanoparticles by inducing apoptosis and cell cycle retardation.[20]

Coincidentally, in our working group, Truebenbach et al. demonstrated that the combined effect of polyelectrolyte complexes formed by two drugs, methotrexate, and pretubulysin encapsulated in cationizable lipo-oligomer 454, showed a more efficient delay in tumor growth and a significant increase in mice survival (bearing subcutaneous L1210 tumors) compared to the free drug combination methotrexate and pretubulysin (MTX+PT) (**Figure 1.1**). [21]

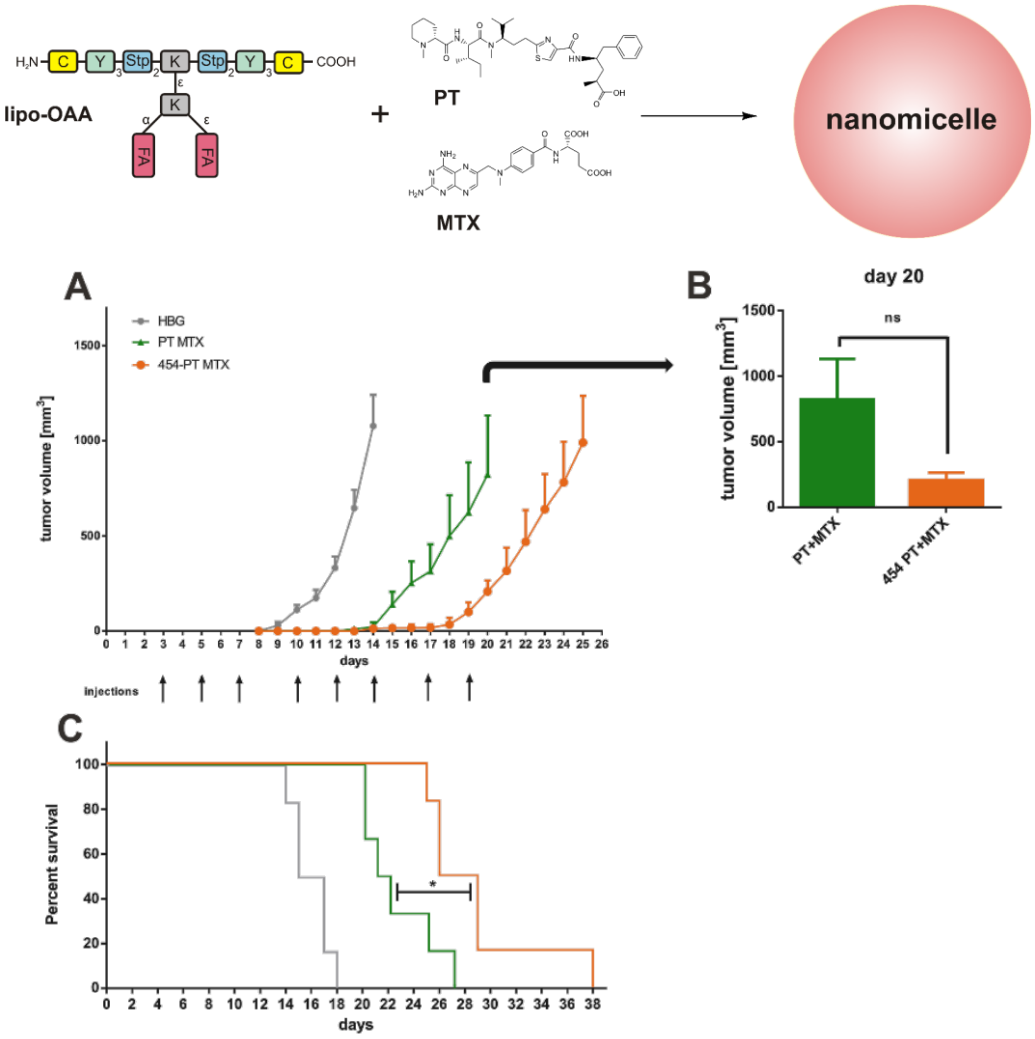

Figure 1.1. Nanomicelle complex formation based on lipooligomer 454, Methotrexate, and Pretubulysin, and the treatment of subcutaneous L1210 tumors.[21]

1.1.2 Co-delivery of Methotrexate and Pretubulysin

Methotrexate (MTX) proved to have antitumor activity in a range of epithelial malignancies when used as a single agent, including breast, ovarian, bladder, head, and neck cancers,[22] see the structure in **Figure 1.2**. In the chemical property of MTX, 10-formyltetrahydrofolate (10-formyl-THF) provides a 1-carbon group for synthesizing purines in the reactions. The reactions are mediated by glycinamide ribonucleotide (GAR) transformylase and amino imidazole carboxamide ribonucleotide (AICAR) transformylase. 5,10-methylenetetrahydrofolate (CH2-THF) donates its 1-carbon group to the reductive methylation reaction converting dUMP to thymidylate dTMP. 5-methyltetrahydrofolate (5-CH3-THF) contributes a methyl group in converting homocysteine to methionine. It can enter the cells through the reduced folate carrier (RFC) by a folate receptor (FR) in an endocytic pathway. In the cell, it competitively inhibits the enzyme dihydrofolate reductase (DHFR) and then blocks the regeneration

of dihydrofolate (FH2) to tetrahydrofolate (FH4).[23] Afterwards, the synthesis of thymidylate is reduced and inhibits the synthesis of DNA and the induction of apoptosis (**Figure 1.3**). Nowadays, MTX is widely used in cancer chemotherapy; even a low concentration of methotrexate inhibits the synthesis of monocytes and the production of superoxide by the cells. The MTX resistance or the loss of drug efficacy could happen in any of those steps, including a decrease in cell uptake, reduction in intracellular retention due to ineffective polyglutamylation, an increase in DHFR activity, reductionrease in binding of MTX to the enzyme. This hurdle can be overcome by combining MTX with a second antitumoral agent.

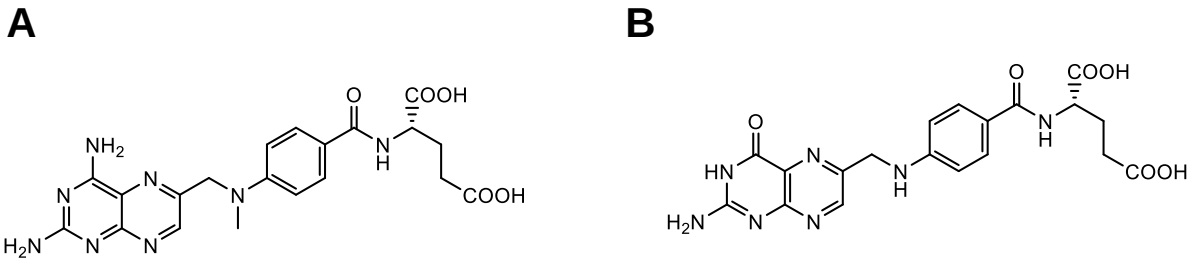

Figure 1.2. Chemical structures of (A) methotrexate and (B) folate.

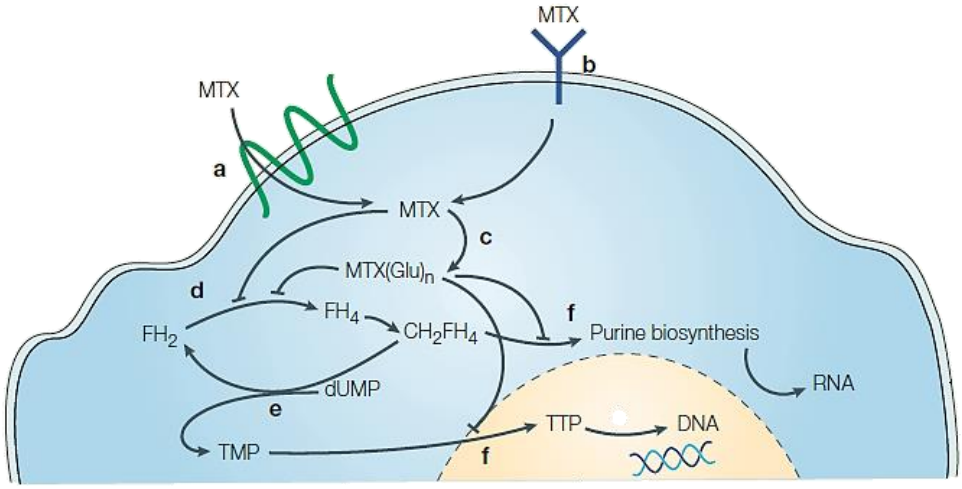

Figure 1.3. Mechanism of the action of methotrexate.

During the development and discovery of drugs, tubulin-binding agents are observed and well-established in the clinical treatment of metastatic cancer. Tubulysins were first discovered by Sasse et al. in 2000, showing potential for experimental anticancer drugs.[24] They consist of N-methyl pipecolic acid (Mep), l-isoleucine (Ile), and two unusual novel amino acids, tubuvaline (Tuv) and unsaturated tubuphenylalanine moiety. They disrupt the microtubule network, prevent tubulin polymerization at low nanomolar concentration, and result in strong G2/M arrest. Tubulysin can also induce

apoptosis in a dose-dependent manner in some cell lines.[25] However, the tubulysins can be obtained from fermentation and isolation procedures, and the synthesis of tubulysin is very challenging.[26] Pretubulysin (PT) is a precursor of tubulysin, containing similar biological properties as tubulysins. It binds to the β-subunit of tubulin, which can lead to microtubule-depolymerize and inhibit tumor cell growth (the structures shown in **Figure 1.4**). PT has been identified as a very potential microtubule-binding agent; it is more easily chemically accessible, which means it can be obtained once in the gram scale. Meanwhile, it possesses simple chemical structures but high efficacy in inducing anoikis and apoptosis in invasive tumor cells.[27] The combined antitumoral effects of pretubulysin and methotrexate have been proved by Kern et al.[28] Consistent with the cell cycle effects, MTX combined at a moderate dose boosts the antitumoral effect of PT in both *in vivo* tumor models. Therefore, the PT+MTX combination may present a promising therapeutic approach for different types of cancer.

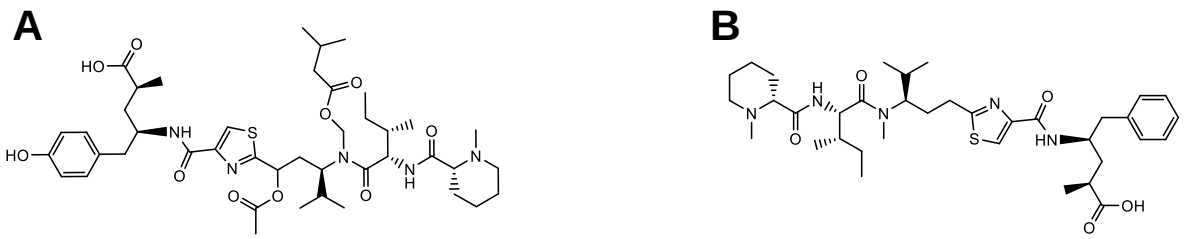

Figure 1.4. Chemical structures of (A) Tubulysin and (B) Pretubulysin.

1.1.3 Targeting ligands for delivery systems

As we know, the targeting drug delivery system (TDDS) is a new means of selectively administering a drug to a target organ, tissue, or cell without affecting healthy normal cells. It showed promising results in the anti-tumor drug delivery[29, 30] The targeting drug delivery system mediated by ligands could improve the specificity of delivery agents to the intended location, increase accumulation in the cellular of disease tissue, and may provide an alternative delivery mechanism. [31]

In combination therapies, especially in synergistic chemotherapy, anticancer drugs lack tumor selectivity, thus increasing potential toxicity in normal tissues. Using a targeted delivery system with nanotechnology to transport chemotherapy drugs can enhance the drug concentration at the target site, significantly reduce the side effects and improve the effectiveness of chemotherapy.[32] The targeted efficacy of drug therapy for cancer was firstly tested after the second world war, and the effects of folic acid on patients with leukemia were investigated at Harvard Medical School.[33] The chemotherapy was a success; the principle was that it blocked the function of folate

requiring enzymes, and the antifolates could suppress the proliferation of malignant cells. In general, the tumor-targeted drug delivery system can eliminate the limit of their cytotoxicity to the normal cells. The ligands help touch the target tumor cells and mediate the cellular uptake. Furthermore, the final combination of chemotherapy with different intracellular targets can target different pathways to create a synergistic effect. The receptor for folate has been identified as a marker for ovarian carcinomas, and it has also been found to be frequently overexpressed in many other types of tumors targeted drug delivery.

Folate receptors (FRs) designated α and β form, frequently found in organs like lung, kidney, and placenta, are overexpressed in human tumors. They bind folic acid (FA) with high affinity[33, 34]. Meanwhile, the receptor generally does not exist in most normal tissues. FA is the synthetic oxidized form of folate. It plays a significant role in DNA synthesis and replication, cell division, growth, and survival. Klein et al. synthesized siRNA polyplexes modified with folate-targeted PEG shielding agent, and they show that the targeted, bivalent DBCO agent with a short PEG24 sequence was superior in terms of particle size, receptor targeting, cellular uptake, and gene silencing *in vitro* (**Scheme 1**).[35] MTX, as a folic acid analog, inhibits the synthesis of FH2 and decreases the availability of FH4. So, FA and MTX can serve as the selective targeting ligand for the targeted combination chemotherapy.

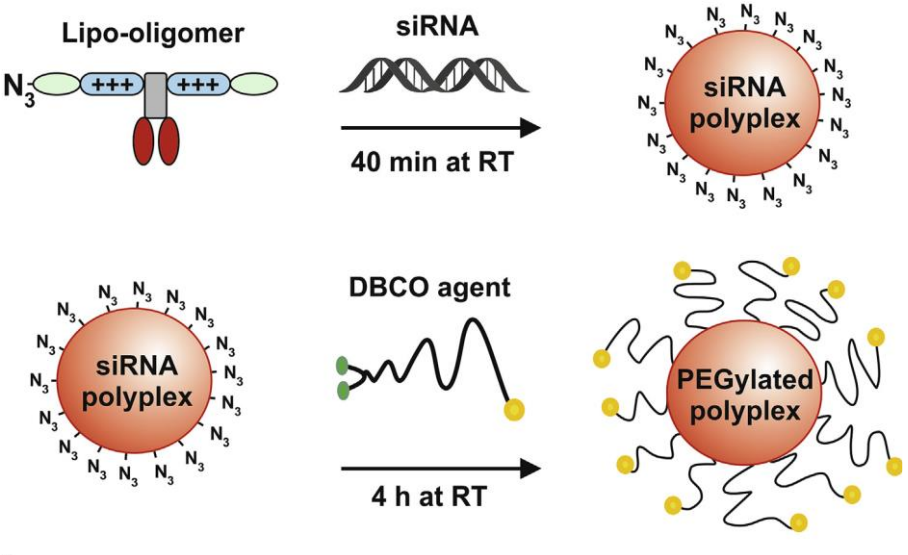

Scheme 1. Formulation of a polyplex with siRNA functionalized with DBCO-Folate.[35]

The epidermal growth factor receptor (EGFR) is another targeting ligand explicitly used for chemotherapy.[36] EGFR was found in 1984 by Drebin[37] as a protein tyrosine kinase that shows overexpression in many cancer cell lines. The signal-transducing tyrosine

kinase activity of the EGFR and related receptors is dormant when the receptors are isolated. When some specific ligands bind to the receptor extracellular portion, dimerization could happen. The dimerized receptor can activate the receptor enzymatic activity through the phosphorylation of tyrosine residues in the receptor C-terminal portion, resulting in intracellular signal transmission activation.[38] GE11(the sequence is YHWYGYTPQNVI, Molecular weight is1540 g/mol) consisting of 12 amino acids, a small peptide, demonstrates excellent EGFR affinity.[39] Several reports have proved that the nanoparticles coupling with GE11 possesses efficient delivery to EGFR overexpressing tumors.[40-42]

1.2 Non-viral gene delivery

With the development of nanotechnologies for solid tumor and cancer treatment, the strategies for natural drugs combination chemotherapy have improved significantly. A series of novel therapeutic nucleic acids entered research and clinical evaluation. Today gene therapy is a promising approach to treating genetic diseases, including mitochondrial-related diseases like blindness, muscular dystrophy, cystic fibrosis, and some cancers.[43-45] Gene delivery is the transport of genes of therapeutic values into the chromosomes of the cells or tissues which can target to replace the faulty genes. Initially, non-viral gene therapy focused on DNA-based gene transfer, immunostimulatory oligonucleotides, and gene inhibition by antisense oligonucleotides or ribozymes. Then include small interfering RNA (siRNA) and micro RNA in various variations and chemical modifications, stabilized message RNA (mRNA), splicing-modifying oligo-nucleotides, or single guide RNA (sgRNA) for genome-modification were found and utilized in evaluation. However, the extracellular and intracellular trafficking barriers represent a significant limitation in delivering fragile therapeutics. Systemically administered macromolecules are rapidly sequestered by the reticuloendothelial system (RES), and internalized molecules are quickly trafficked to lysosomes for acidic and enzymatic degradation. It is vital to address the challenges, including that these macromolecules must be stabilized against degradation in the bloodstream and clearance, taken up by the target cells, and reach the intracellular site of action.

siRNAs can silence the expression of virtually any gene through the activated pathway with high efficiency and specificity. The therapeutic potential of this method is far-reaching, and siRNA-based therapeutics are under development for the treatment of diseases ranging from viral infections[46, 47] to hereditary disorders and cancers[48, 49]. There are around 22 RNAi-based materials under evaluation in clinical trials, including

the naked siRNA, Cyclodextrin NP, and lipid nanoparticles (LNP). Unmodified siRNA is unstable in the bloodstream, can be immunogenic, and does not readily cross membranes to enter cells.[50] For utilizing the siRNA therapeutics, the critical challenge of safety and efficiency inside has to be solved. Chemical modifications and delivery materials are required to bring siRNA to its site of action without adverse effects. Polymers[51], lipids[52, 53], peptides[54], antibodies[55], aptamers[56], and small molecules[57, 58] are under exploration by innovative scientists to address the challenges. It is worth mentioning that successful lipid-siRNA systems have been developed by rational design or discovered by using high-throughput screens.[53]

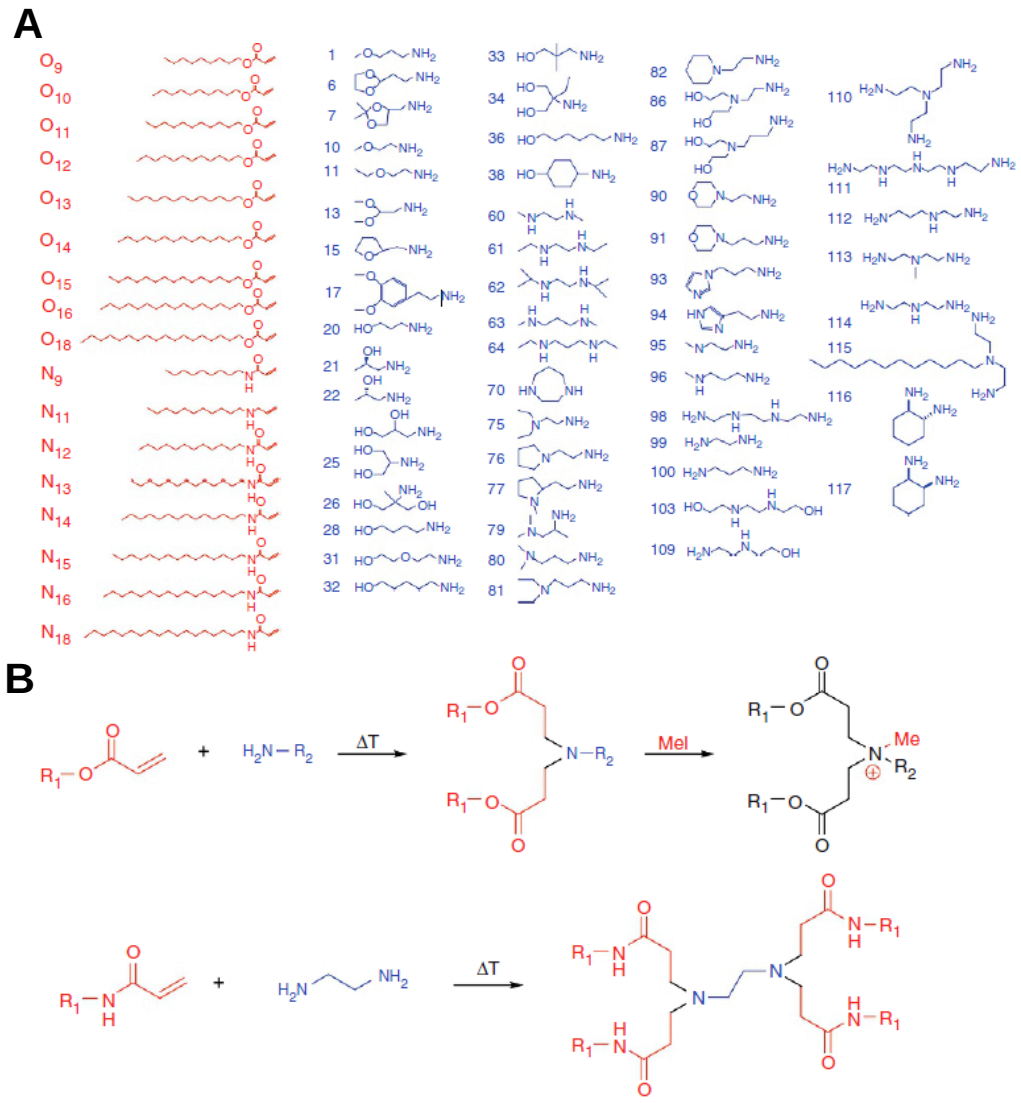

Figure 1.5. Synthesis of lipidoid using high-throughput screens for siRNA delivery.[53]

The non-viral delivery systems of mRNA and plasmid deoxyribonucleic acid (pDNA) have been demonstrated in the vaccines against the novel SARS-CoV-2 (COVID-19). Two formulations of mRNA vaccines from Pfizer–BioNTech and Moderna were approved for emergency use within one year after the pandemic outbreak and have

been administered to billions worldwide.[59] A pDNA vaccine developed also was approved in India by Zydus Cadila, exhibiting high efficiency for preventing infection in a large clinical trial.[60] These successful examples prompt further research and the development of vaccines and therapeutics based on mRNA and pDNA. pDNA is widely used for transient gene delivery applications due to its ability to accommodate large gene payloads, ease of construction, low production cost, and resistance to degradation.[61] Delivering mRNA is another method for achieving transient gene expression in target cells.[62] mRNA as a novel therapeutic payload can be readily translated in the cytoplasm and does not need to translocate through the restrictive nuclear barrier. However, there are still some improvements for the delivery systems, such as preventing extracellular mRNA and pDNA degradation by nucleases, increasing intracellular targeting of mRNA and pDNA to the desired sites, and prolonging the duration of protein expression from mRNA and pDNA.[63] The mRNA stability and immunogenicity improvements have helped increase its popularity as a transgene vector.[64]

Many gene therapies are focused on permanently altering the genome of target cells within a patient in a process known as gene editing. These therapeutic strategies utilize nucleic acid and protein-based machinery. Moreover, gene therapy strategies have embraced technologies that can achieve genomic manipulations, such as gene insertions and knockouts, with greater precision. The most common non-viral gene-editing platforms include zinc finger nucleases, transcription activator-like effector nucleases (TALENs), meganucleases, and the CRISPR/Cas9 system.[65] These nuclease systems induce a double-strand break (DSB) in a precise location of the genome, which stimulates endogenous cellular repair machinery. Repair of the DSB can occur through nonhomologous end-joining (NHEJ) or homology-directed repair (HDR). The NHEJ pathway ligates the broken ends and often introduces insertions and/or deletions that can disrupt genes at the site of the break (knockout). In contrast, the HDR pathway can repair the break by using a DNA template containing a homologous sequence, and by doing so, the repair can lead to the insertion of an exogenous gene of choice (knock-in).[66, 67] The lipid-based systems get a fantastic process in delivering these cargos obtaining impressive therapy.[68, 69]

1.3 Delivery strategies for different therapeutics

Nanomaterials-based cancer therapy is essential in increasing the therapeutic efficiency against cancer by combining nanomaterials and chemo-therapeutic agents. Nanoparticles are promising drug carriers. They could deliver the hydrophobic and/or

hydrophilic drug molecules, peptides, small molecule drugs, antibodies, or nucleic acids to the tumor site with minimum toxicity to surrounding tissues; this safe delivery is based on their penetration capacity. The collective physicochemical properties, such as the size, polydispersity, shape, charge, and surface hydrophobicity/hydrophilicity, can affect the biological identity of the nanoparticles.

The size of nanoparticles plays a crucial role in cellular uptake. It can affect the physical interaction between the nanoparticles and the cell membrane, leading to the segregation and clustering of nanoparticles on the cell surface and a subsequent cell membrane response.[70, 71] For example, de Planque et al. reported that the permeability and integrity of membranes strongly depend on the size and surface chemistry of the interacting nanoparticles.[72] Besides nanoparticle size, the shape is another crucial factor for cellular uptake. Besides nanoparticle size, the shape is another critical factor for cellular uptake. Using a simulation approach showed the role of shape and orientation in the cellular uptake of nanorods and nanocubes of different aspect ratios and edge curvatures, respectively.[73] Herd et al. reported that clathin-mediated endocytosis is the most favorable mechanism for spherical NPs, whereas their helminth-like counterparts undergo micropinocytosis or phagocytosis.[74] Also, electrostatic interactions between charged nanoparticles and the cell membrane are of great biological significance. The charged NPs have been proved that they show a more favorable thermo-dynamical interaction than their uncharged counterparts.[75] Additionally, the adhesion of positively charged NPs to the cell membrane can promote the membrane wrapping phenomenon. Hühn et al. explored how surface charge indirectly affects cell-NP interactions via the alteration of the protein corona around the nanoparticles.[76]

The surface hydrophobicity/ hydrophilicity plays a vital role in the interaction between nanoparticles and cells.[77] The hydrophobic nanoparticles are thermo-dynamically stable around the middle of the hydrophobic core of the cell membrane. Moreover, semi-hydrophilic nanoparticles energetically prefer to adsorb on the bilayer surface rather than into the core, which leads to membrane wrapping (endocytosis).[78] In addition, the functionality of the surface is also one of the significant effects of dominating the ability of nanoparticles. It is essential to understand the role of surface functionalization in the biological effects of nanoparticles is required to facilitate the efficient engineering of nanomedicines. Functionalized nanoparticles can take advantage of overexpressed or unique receptors on the cell surface. In this context, targeting small molecules, aptamers, peptides, proteins, and antibodies that can

interact with these receptors are widely used to functionalize particles.[79-81]

1.3.1 Nanoparticles for drug delivery

The shortcomings of monotherapies are apparent, such as limited stability, nonspecific tumor targeting ability, and severe side effects. It is well-known that the small molecule chemotherapy always needs a high dose but with unfavorable pharmacokinetic properties, such as rapid drug clearance, short circulation half-life, limited tumor accumulation, and significant systemic toxicity. The realization of the goal could be affected by some challenges, for instance, the design and preparation techniques and the physicochemical and pharmaceutical properties (**Figure 1.6**),[15] In addition, the pharmacological and toxicity of NDCDS passive targeting of large nanoparticles by the enhanced permeability and retention (EPR) effect is crucial for solid tumor targeting in cancer nanomedicine. With the rapid development of modern nanotechnology, nanoparticles have been investigated in a wide range of applications. The biodegradable and biocompatible materials mostly form nanoparticles with droplet sizes between 100 and 300 nm as carriers for encapsulating various agents such as proteins, nucleic acids, peptides, and drugs for cancer therapy. Different formulations containing drugs are proven to enhance the drug tumor accumulation, reduce the toxic side effects, increase the antitumor efficiency, and overcome the drug resistance.[82] Liposomes[83, 84], micelles[85], polymers[86], inorganic nanoparticles, and polyplexes have achieved excellent therapeutic effects in tumor treatments.[87, 88] There are several formulations of lipid-based drug delivery systems have been approved by the US Food and Drug Administration (FDA) and European Medicines Agency (EMA) to delivery different drugs.[89, 90]

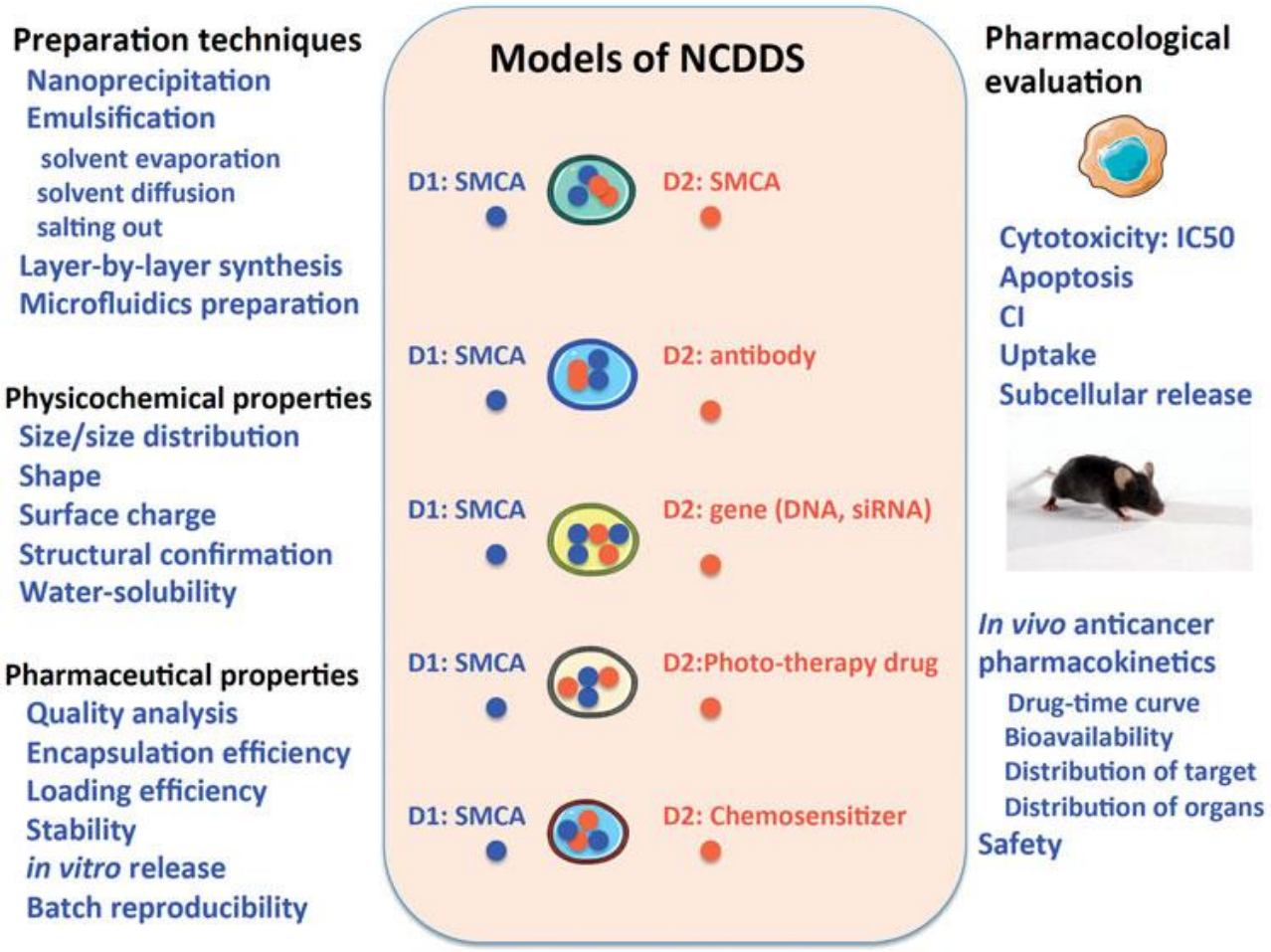

Figure 1.6. Schematic illustration of nano-drug co-delivery system (NDCDS) models: the physicochemical and pharmaceutical properties, pharmacodynamic, and pharmacokinetic profiles.[15]

1.3.2 Strategies for developing drug-loaded nanoparticles

One of the most significant challenges encountered when developing nanoparticle delivery is their poor stability.[91] The formed nanoparticles generally need a stabilizing environment to prevent aggregation and maintain high reactivity. A nanoparticle is not a single component substance but a composite with a solid core surrounded by a suitable surface chemical microenvironment. The stability of nanoparticles can be affected by the size, the polarity of materials, the number of molecules coated on the surfaces, the pH of the environment, and the solvent. When the nanoparticles are not naked but rather coated with some ligands, they can be more stable by saturating the dangling bonds and shielding them from the external environment.

The nanoparticles encapsulating lipophilic anticancer agents can be self-assembled from amphiphilic biodegradable block copolymers through different strategies to encapsulate drugs, such as chemical conjugation of drugs, chemical crosslinking of

nanoparticles, and introduction of physical interactions (for instance, hydrogen bonding, electrostatic interaction, and π-π stacking between the carrier and loaded drug). In these ways, the drug loading efficacy was enhanced, and the stability was systemically increased. [92]

1.3.3 Strategies for nucleic acids delivery platforms

Many delivery systems are being developed to deliver gene products safely and effectively. Non-viral vectors for gene delivery utilize natural or synthetic materials to deliver the gene of interest to target cells. The compounds used to make non-viral vectors do not elicit an immune response and are less toxic. Additional functionality of non-viral vectors increases their specificity for target sites. They are relatively easy to produce and can be used for repeated administration. There are mainly two different strategies for the non-viral gene delivery system: inorganic and organic.

For the inorganic strategy, magnetic nanoparticles, gold nanoparticles, carbon nanotubes, carbon quantum dots (CDs), and silica nanoparticles are mainly used for gene delivery or as an emerging therapeutic tool due to their nanostructures' size, shape, and surface properties.[93-96] For instance, gold nanoparticles exhibit photothermal properties, which are used in biomedical applications in different diseases such as cancer.[96] The surface of gold nanoparticles can be modified to improve their stability and selectivity. The functionalized particles can be used for gene transfection and silencing, targeted drug or gene delivery, intracellular detection, bioimaging, cancer studies, and biosensors.[97-99] Carbon quantum dots, possessing high brightness, resistance to photobleaching, multiplexing capacity, and high surface-to-volume ratio, are excellent candidates for intracellular tracking, diagnostics, *in vivo* imaging, and therapeutic delivery.[100]

Organic materials mainly include cationic lipids and polymers that interact with negatively charged nucleic acids. Lipid-based delivery strategy is one of gene delivery's most attractive for non-viral vectors. These systems take advantage of the self-assembling properties of amphiphilic lipids, such as phospholipids, to generate carriers that protect nucleic acids. Lipoplexes are electrostatic complexes spontaneously formed when liposomes composed of cationic lipids such as DOTAP interact with negatively charged oligonucleotides.[84, 101] However, liposomes are highly dynamic systems that lack stability, which can significantly impact nucleic acid encapsulation, causing the genetic material's release before it arrives at the site of action. Lipid nanoparticles have become widely known vectors for delivering genetic material since

the recent success of COVID-19 vaccines.[102, 103] These spherical vesicles are composed of ionizable lipids, possessing a positive charge at low pH, allowing interaction with nucleic acids through electrostatic forces and the endosomal escape once cells internalize them. In addition, these lipids are neutral at physiological pH, which reduces their toxicity and immunogenicity.[104] Moreover, lipid nanoparticles can deliver CRISPR/Cas9 components to achieve clinically relevant levels of genome editing *in vivo*, which is reported by Kalra et al.[105] Polymer-based systems have also been widely studied for the delivery of gene therapeutics. Positively charged polymers, such as poly-ethylenimine (PEI) or chitosan, can form nanoparticles, called polyplexes, upon interaction with negatively charged nucleic acids.[106] Lipoplexes and polyplexes can achieve high *in vitro* transfection. However, their use *in vivo* is hindered by their toxicity and immunogenicity.[107] The cationic lipid-based delivery systems have a positively charged surface leading to interaction with negatively charged membranes and proteins in the physiological environment. The positively charged surface consequently prompts the recognition and uptake of these systems.

Since the development of lipids, most lipids consist of positively charged headgroups that bind with the anionic phosphate groups of nucleic acids via electrostatic interactions to form lipoplexes. Due to the self-assembling lipid tail structures, lipoplexes are often present as liposomes, solid lipid nanoparticles, or lipid emulsions. Compared with other carrier materials, lipids are biodegradable, less toxic, and can incorporate hydrophilic and hydrophobic substances. For example, lipidoids are lipid-like materials synthesized by conjugating amines with lipophilic acrylates, acrylamides, or epoxide. The simple synthetic process makes it possible to evaluate an extensive library of lipidoids with diverse structures.[53] The screening test demonstrated lipidoids' safety and efficacy in three animal models: mice, rats, and nonhuman primates. The studies reported here suggest that these lipidoid materials may have broad utility for both local and systemic delivery of RNA therapeutics.[53]

Critical issues of nucleic acid delivery via manufactured vehicles are (1) extracellular stability by stable polyplex formation and shielding to avoid rapid decay, clearance, and unspecific interactions, (2) specific target cell binding and uptake through receptor-mediated endocytosis, (3) efficient endosomal escape and (4) release of the cargo in the cytosol (**Figure 1.7**).[108]

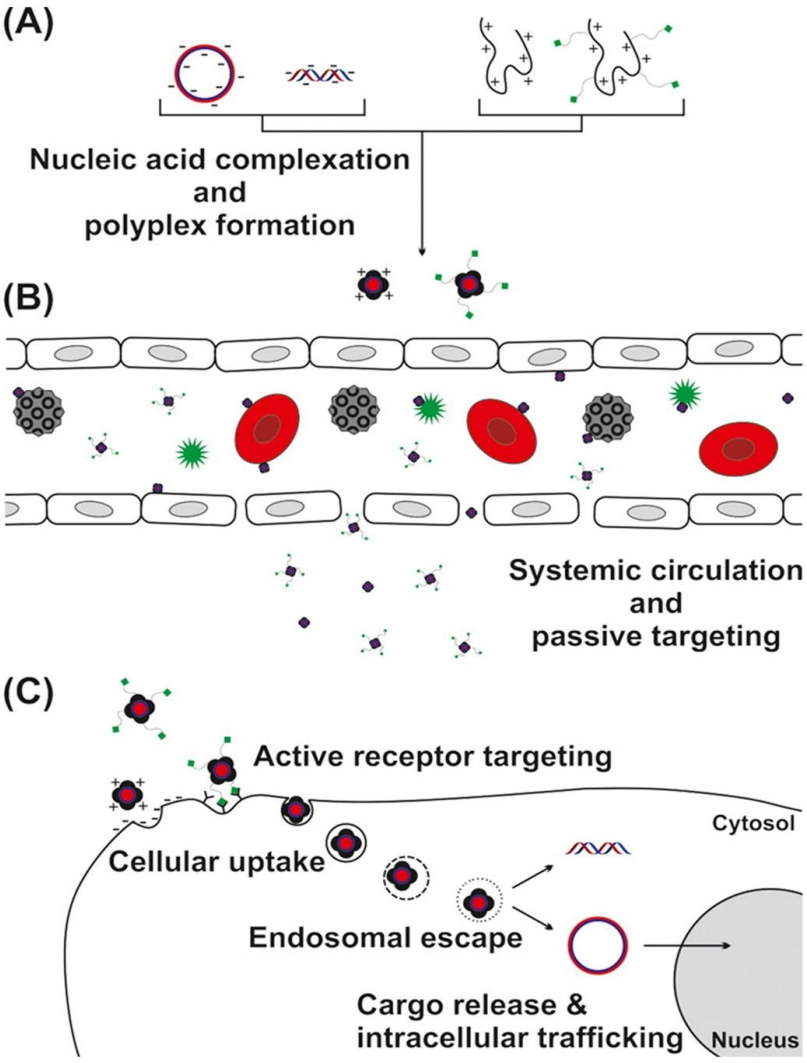

Figure 1.7. The nucleic acid delivery pathway of polyplexes: A) Formation of stable polyplexes, B) avoidance of rapid clearance and unspecific interactions with blood components, and C) receptor targeting, endocytosis, endosomal escape, and cytosolic cargo release.[108]

With continuous developments of the advanced polymer synthetic and analytical methods, the synthetic chemical requirements in the quest for optimized nanocarriers become less challenging compared with the supramolecular nano assembly and, predominantly, the design of the best, most relevant screening systems. In a nutshell, screening in an artificial cell culture system will eventually yield the carrier system which is most effective within these artificial conditions.

pH plays an essential role in many biological processes, including endosome/lysosome maturation, protein and lipid metabolism, and tumor pathophysiology.[109, 110] The advantages of intelligent, pH-responsive delivery systems can carry potent therapeutics. For many biological processes, pH variations are minor from normal physiological pH (7.4).[111, 112] For example, extracellular pH of tumors is reported to be ~6.8, and early endosomal pH is at 6.5. Various pH-sensitive polymers and

nanoparticles have been developed for therapeutic delivery and imaging applications.[113] Small molecular or non-cooperative polymeric pH-sensitive systems are not efficient in responding to these subtle pH differences, which prompted the successful development of various intelligent materials with improved pH sensitivity and response.

Synthetic polymers have been designed to enhance endosomal release through known mechanisms buffering in acidic pH (proton sponge effect) and incorporation of membrane-active peptides and alkylated carboxylic acid.[114, 115] Gao and co-workers developed ultra pH-sensitive (UPS) nanoparticles by introducing a hydrolytically active polycarbonate backbone and the ionizable tertiary amines with different hydrophobic substituents to improve the therapeutic efficiency.[116-118] Coincidentally, VIPER material reported by Pun et al. combines serum stable nucleic acid condensation with a pH-sensitive display of a potent lytic peptide to achieve safe and highly efficient plasmid and siRNA delivery *in vivo*.[119, 120]

1.3.4 Cationic carriers synthesized by solid-phase synthesis

Cationic delivery systems require clear-cut structure-activity relationships to be drawn. Therefore, a technique for obtaining polymers with a precisely defined sequence is needed. A series of researchers have applied the well-established solid-phase-assisted synthesis method to develop linear and branched peptide-based and lipid-based nucleic acid carriers. Our lab developed a diverse platform facilitating the intracellular transport of different cargos, like siRNA, proteins, and drugs.[42, 121-123] These oligoaminoamides (OAAs, also called oligomers or oligoamides) consist of natural α-amino acids, artificial amino acids, and fatty acids. Truebenbach and Steinborn et al. have recently reported on the nanoparticle formation properties of cationic lipo-oligomer 1198 or 454 with the negatively charged drug MTX and various polyglutamylation polyanionic MTX analogs and applied it for siRNA and MTX and siEG5 with PT codelivery, respectively.

In recent years, many reports have demonstrated impressive progress in synthetic and physicochemical aspects of macromolecules and expanded knowledge about the intracellular bottlenecks in delivery. Thus, further refinement of polymeric carriers both in design and accurate synthesis may play a tremendous role in future nucleic acid therapeutics. The current development of stimuli-responsive formulations is directed toward multifunctional nanomachines, which might be supported by physical forces (such as near-infrared light, ultrasound, or magnetic fields) in a remote-controlled

manner. Most importantly, evolutionary algorithms will have to be developed for optimizing polymeric nanosystems for the actual disease targets and target locations in the human patient. Dynamic bioresponsive polymers and sequence-defined multifunctional polymers with different synthetic building blocks have been investigated for the gene therapeutic delivery.[120, 124, 125] Synthetic lipids have been used to deliver genes for a long time. Most lipids contain positively charged head groups that bind with the anionic phosphate groups of nucleic acids via electrostatic interactions. The hydrophobic alkane chain inserts and disrupts the membrane bilayer to form lipopolyplexes. [29] Subsequent designs of ionizable amino lipids focused on improving the potency of the pDNA, siRNA, and mRNA delivery. A structure-activity relationship guided the synthesis and screening of many ionizable lipids with various linkers connecting the amino group and the acyl chains.[52, 126]

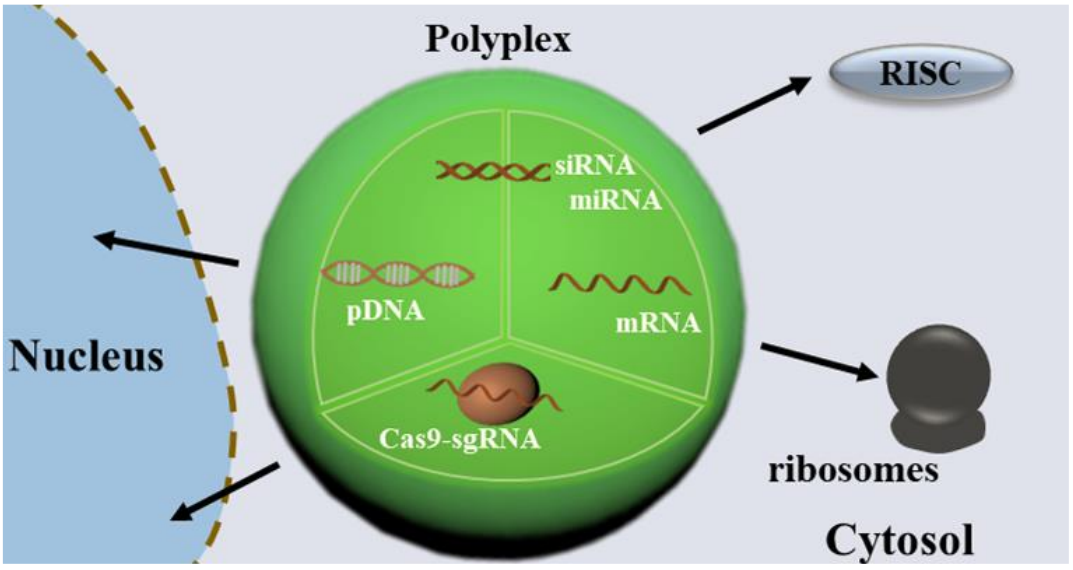

Figure 1.8. Intracellular trafficking of non-viral nucleic acid polyplexes.

Sequence-defined polymers[124, 127, 128] can be prepared with high precision by solid-phase synthesis (SPS) for different non-viral nucleic acid delivery (**Figure 1.8**). For example, Schaffert et al. designed peptide-like polyaminoamides based on artificial oligoamino acids.[129] By generating polymers with a defined structure in various topologies (for example, linear, branched three-arm or four-arms, i-shapes, T-shapes, u-shapes), clear-cut structure-activity relations could be made.[129-131] Kuhn et al. demonstrated the delivery of Cas9/sgRNA ribonucleoprotein complexes via hydroxystearyl oligoamino amides.[132] Upon further optimization, including SPS integration of shielding, targeting, and other functional units, it was realized soon that the different specific cargos required different carrier sequences, for example, for pDNA[133, 134] or siRNA[35] delivery.

2 Aim of the thesis

The recent development of a solid-phase synthesis platform for assembly sequence-defined oligo(ethane amino)amides enables the quick and accessible synthesis of cationic oligomers complexing and delivering nucleic acids.[135] Different shaped oligomers were synthesized by introducing artificial amino acids based on the diaminoethane motif of PEI, which is well known for its nucleic acid binding and endosomal buffering abilities.[136] Additionally, SPS can introduce different functionalities such as shielding, polyplex stabilization, and targeting into these oligomers. The three aims of the thesis addressed in three main chapters were as described in the following.

The first main chapter of this thesis aimed at optimized formulations for co-delivering chemotherapeutic MTX/PT. Combination chemotherapy is still an effective strategy in cancer treatment nowadays. The main problems of this strategy are the limited tumor accumulation, significant toxicity, rapid drug clearance from the bloodstream, and the lack of target effect. By optimizing the nanoparticulate co-delivery of different therapeutic drugs, the drawbacks of the chemotherapy had to be overcome, and therapy efficiency should be increased with the targeted drug delivery system. Derivatives of the antimetabolite MTX and cationic carriers had to be synthesized by SPS. MTX was modified with more glutamic acids to increase the negative charge intensity to strengthen the electrostatic interactions between cationic carriers and MTX and its analogs. Meanwhile, the addition of stabilizing domains in the polyplexes should help to stabilize the particles. The oligomers had to be designed to contain azide groups for subsequent click-modification with FR ligands. This strategy was supposed to make the synthetic polyplexes more effective on FR-overexpressing L1210 leukemia cells.

Aim of the second main chapter was to review novel strategies and technologies for therapeutic nucleic acid delivery. The specific requirements for the various therapeutic cargos were to be discussed. Furthermore, a conclusion on future directions, including dynamic bioresponsive polymers as components of nanomachines, multifunctional sequence-defined carriers for evolution-based selective optimization, and organic−inorganic multicomponent nanoassemblies should be provided.

The third main chapter of this thesis had to synthesize a series of novel dialkylated lipo-amino fatty acids and incorporate them into novel carriers for gene therapy. Recently, the frequently researched non-viral vectors are polymers, lipids, inorganic particles, or combinations of different types. Non-viral vectors are low in their cytotoxicity, immunogenicity, and mutagenesis, attracting more researchers to explore the

promising delivery system and move the gene therapy field forward. Nevertheless, to improve gene transfer efficiency, specificity, gene expression duration, and safety, it is significant to develop novel non-viral vectors. Lipidoids are lipid-like materials synthesized by conjugating amines with lipophilic acrylates, acrylamides, or epoxide. It is possible to do the screening of an extensive library of lipidoids with diverse structures due to their simple synthetic progress. This chapter aimed at the synthesis of ionizable domain tertiary amines with hydrophobic substituents (lipo-amino fatty acid) and hydrophilic cationizable building blocks (such as Stp) into a defined combination sequence by solid-phase synthesis. A new library containing such structures should be developed for evaluation as effective nucleic acid carriers.

3 Combination therapy of antitumoral drugs

This chapter introduces chemically designed artificial carriers for optimizing the efficient co-delivery of two drugs (Pretubulysin and methotrexate).

3.1 Introduction

The previously reported beneficial properties of the drug combination PT+MTX were evaluated in this chapter using novel carriers. PT and MTX (analogs) were co-incorporated into a delivery system using the previously established lipo-oligoaminoamide 1198 and its novel analog 1444 with six more tyrosines. The cationizable oligomers, containing hydrophobic and hydrophilic segments, spontaneously self-assemble into micellar structures in an aqueous solution. Four units of the artificial amino acid succinoyl tetraethylene pentamine (Stp) serve as a hydrophilic protonatable segment in 1198 or 1444. The Stp units, partially protonated at physiological pH, can facilitate the polyelectrolyte complex (PEC) formation with negatively charged cargo molecules, such as MTX, E2MTX, and E5MTX, via electrostatic interaction. And the zwitterionic lipophilic PT interacts with oligomer independently from PEC formation via hydrogen bonding, hydrophobic, or other interactions. Upon cell uptake, additional protonation of the Stp units under acidifying endosomal conditions promotes the escape of complexes out of these intracellular vesicles. In addition to the ionic building blocks, lipo-oligomers contain two oleic acid chains (OleA) and tyrosine tripeptide units which might serve as a further stabilizing domain of the micellar structures by hydrophobic or aromatic π-π stacking interactions. N- and C-terminal cysteines were shown to stabilize complexes due to their disulfide crosslinking potential. As a helper lipid, cholesterol may act as another stabilizing domain in nanoparticle formation. To improve the circulation and equip the delivery system with targeting functionality, copper-free click chemistry was utilized to modify the surface of the nanoparticles. The high ring strain of a cyclooctyne derivate facilitates click reaction with an azide. The structures containing PEG of 24 ethylenoxide monomers, targeting ligand folic acid, and two DBCO units were synthesized by SPS and used to synthesize lipo-oligomers.

3.2 Materials

3.2.1 Materials

The solvents, reagents and buffers used for the experiments are summarized in **Table 3.1**, **Table 3.2**, and **Table 3.3**.

Table 3.1 Solvents used for experimental procedures.

Chemicals and solvents (abbreviations)	CAS-No.	Manufacturer
Dichloromethane (DCM)	75-09-2	Bernd Kraft, Duisburg, Germany
N,N-Dimethylformamide (DMF)	68-12-2	Iris Biotech, Marktredwitz, Germany
Chloroform	67-66-3	VWR Int. (Darmstadt, Germany)
Chloroform-d	865-49-6	Sigma-Aldrich, Munich, Germany
Ethyl acetate	141-78-6	Staub & Co. (Nürnberg, Germany)
Methyl-tert-butyl ether	1634-04-4	Brenntag (Mülheim/Ruhr, Germany)
anhydrous DCM AcroSeal®	75-09-2	Acros Organics, Germany
Methanol	67-56-1	Fisher Scientific (Schwerte, Germany)
Acetonitrile (ACN)	75-05-8	VWR Int. (Darmstadt, Germany)
Methanol-d3	1849-29-2	Sigma-Aldrich, Munich, Germany
Ethanol absolute	64-17-5	VWR Int. (Darmstadt, Germany)
Methanol anhydrous AcroSeal®	67-56-1	Acros Organics, Germany
Deuterium oxide	7789-20-0	Euriso-Top (Saint-Aubin Cedex, France)
Water	7732-18-5	In-house purification
n-Heptane	142-82-5	Grüssing (Filsum, Germany)

Table 3.2 Reagents used for experimental procedures.

Chemicals and solvents (abbreviations)	CAS-No.	Manufacturer
O-Benzotriazole-N,N,N',N'-tetramethyluronium-hexafluoro-	94790-37-1	Multisyntech (Witten, Germany)
4-[[(2,4-diamino-6-pteridinyl) methyl] methylamino] benzoic acid	19741-14-1	Niels Clauson-Kaas A/S (Farum, Denmark)
Methotrexate (MTX)	59-05-2	Sigma-Aldrich (Munich, Germany)
Pretubulysin (PT)		In-house synthesis1
HEPES	7365-45-9	Biomol (Hamburg, Germany)

Phenol	108-95-2	Sigma-Aldrich (Munich, Germany)
Hydrazine monohydrate	7803-57-8	Merck Millipore (Darmstadt, Germany)
Ninhydrin	485-47-2	Sigma-Aldrich (Munich, Germany)
Ammonia solution 25 %	1336-21-6	Carl Roth (Karlsruhe, Germany)
Piperidine	110-89-4	Iris Biotech (Marktredewitz, Germany)
Folic acid	59-30-3	Sigma-Aldrich (Munich, Germany)
Sodium hydroxide (anhydrous)	1310-73-2	Sigma-Aldrich (Munich, Germany)
6- aminocaproic acid	60-32-2	Sigma-Aldrich, Munich, Germany
4-aminobutyric acid	56-12-2	TCI, EUROPE N.V.
Triisopropylsilane (TIS)	6485-79-6	Sigma-Aldrich, Munich, Germany
Oleic acid	112-80-1	Sigma-Aldrich (Munich, Germany)
D-(+)-Glucose monohydrate	28718-90-3	Sigma-Aldrich (Munich, Germany)
Benzotriazol-1-yl-oxy tripyrrolidinophosphonium	128625-52-5	Sigma-Aldrich, Munich, Germany
1-Hydroxybenzotriazole (HOBt)	2592-95-2	Sigma-Aldrich, Munich, Germany
N,N-Diisopropylethylamine (DIPEA)	7087-68-5	Iris Biotech, Marktredwitz, Germany
Di-tert-butyl dicarbonate (Boc2O)	24424-99-5	Sigma-Aldrich, Munich, Germany
Fmoc-Stp(Boc_3)-OH building block		In-house synthesis
Fmoc-L-Lys(Fmoc)-OH	78081-87-5	Iris Biotech, Marktredwitz, Germany
2-chlorotrityl chloride resin	42074-68-0	Iris Biotech, Marktredwitz, Germany
Fmoc-L-Lys(Dde)-OH	204777-78-6	Iris Biotech, Marktredwitz, Germany
Boc-L-Lys(Fmoc)-OH	84624-27-1	Iris Biotech, Marktredwitz, Germany
Fmoc-L-Tyr(tBu)-OH	71989-38-3	Iris Biotech (Marktredewitz, Germany)
Cholesterol	57-88-5	Sigma-Aldrich (Munich, Germany)
Fmoc-OSu	82911-69-1	Iris Biotech (Marktredewitz, Germany)
Fmoc-*N*-amido-$dPEG_{12}$-acid	756526-01-9	Quanta Biodesign (Powell, Ohio, USA)
Fmoc-*N*-amido-$dPEG_{24}$-acid	756526-01-9	Quanta Biodesign (Powell, Ohio, USA)
Sephadex® G-10	9050-68-4	GE Healthcare (Freiburg, Germany)
Hydrochloric acid solution (1 M) (1 M HCl)	7647-01-0	Bernd Kraft, Duisburg, Germany

Linear polyethylenimine (LPEI)	9002-98-6	In-house synthesis
(3-(4,5-dimethylthiazol-2-yl)-2,5 diphenyltetrazolium bromide) (MTT)	298-93-1	Sigma-Aldrich, Munich, Germany
Trifluoro acetic acid (TFA)	76-05-1	Iris Biotech, Marktredwitz, Germany
1,2-Ethanedithiol (EDT)	540-63-6	Sigma-Aldrich, Munich, Germany

Table 3.3 Buffers used for experimental procedures.

Buffer	Composition
10 mM HCl solvent for size exclusion chromatography	693 mL water, 300 mL acetonitrile, 7 mL 1 M HCl solution
Electrophoresis loading buffer	6 mL glycerine, 1.2 mL 0.5 M EDTA solution (pH 8.0), 2.8 mL H_2O, 20 mg bromophenol blue
ACN buffer (0.1 %TFA) for High-performance liquid chromatography (HPLC)	899.1 mL ACN, 0.9 mL TFA
Water (0.1 %TFA)	899.1 mL water, 0.9 mL TFA
HEPES buffered glucose (HBG)	20 mM HEPES, 5 % glucose, pH 7.4
Kaiser test solutions	A: 80 % (w/v) phenol in EtOH; B: 5 % (w/v) ninhydrine in EtOH; C: 20 µM KCN in pyridine (2 mL of 1 mM KCN (aq) in 98 mL of pyridine)

3.2.2 Instrumentation used in solid-phase synthesis (SPS)

Automated parallel synthesis or synthesis supported with microwave irradiation was carried out using a Biotage Syro Wave (Biotage, Uppsala, Sweden) peptide synthesizer. Disposable polypropylene (PP) syringe microreactors with the volume size 2 mL, 5 mL, and 10 mL were purchased from Multisyntech (Witten, Germany). Itwas conducted with polytetrafluoroethylene (PTFE) filters. The recommended size of the reactors was chosen according to the amount of resin. For manual solid-phase synthesis, microreactors with polyethylene filters (Multisyntech, Witten, Germany) were used. Reactions were carried out under steady shaking with an overhead shaker.

3.3 Methods

3.3.1 General Synthesis of oligomers, MTX analogs, PEGylation reagents and via SPS

3.3.1.1 Loading of a 2-chlorotrityl chloride resin with a Fmoc protected amino acid

Typically, 1000 mg of 2-chlorotrityl chloride resin (1.56 mmol chloride) is pre-swollen in anhydrous DCM in the 10 mL of syringe for 20 min, the DCM was then removed by filtration. Dissolved the first Fmoc protected amino acid (e.g. Fmoc-L-Lys(Dde)-OH 0.3 eq, with DIPEA 3 eq) dissolved in anhydrous DCM and added to the resin for reaction for 75 min. The reaction solvent was drained and a capping solution consisting of DCM/MeOH/DIPEA (4 mL DCM, 3 mL MeOH and 500 µL DIPEA per 1000mg of resin) was added to the resin for 60 min to transform residual free chlorides into unreactive methoxy ethers. After removal of the reaction mixture, the resin was washed 3 times with DMF and 3 times with DCM. The resin was dried under the vacuum, and then weighed 5-10 mg of the resin for 3 eppes to determine the loading efficiency of the resin. 1 mL Fmoc deprotection solution (20 % piperidine in DMF, v/v) was added to each sample and incubated for 75 min at 700 rpm, 25 °C. The samples were then vortexed and got the beads to settle down. The 25 µL of reaction solution supernatant was diluted with 975 µL of DMF, and 25 µL of Fmoc deprotection solution diluted in 975 µL of DMF was used as blank control, the absorption of the dilution was measured by a Genesys 10S UV−vis photometer (Fisher Thermo Scientific, U.S.A.) at 301 nm. The loading of each sample in the eppes was then calculated according to the following equation: resin load [mmol g^{-1}] = (A× 1000)× (m [mg] × 7800× df)$^{-1}$ with df as dilution factor. The average of three values gave the respective resin loading efficiency. The remaining resin was treated 3 times with Fmoc deprotection solution to remove the Fmoc protection group. The reaction progress was monitored by Kaiser test. The resin was washed with 3 times of DMF, 3 times of DCM after each coupling step and deprotection step. Afterwards, the resin was dried in vacuo and stored at 4°C.

3.3.1.2 Procedure of manual coupling steps via solid phase synthesis

After pre-loading the resin with the first building block as described in **3.3.1.1** and swelling it in in 10 mL/g resin DCM for 30 minutes, a cycle of iterative coupling and deprotection steps with the respective building blocks was carried out until the final desired structure was obtained which was then cleaved from the resin. If not stated

otherwise, coupling steps were generally performed with 4 eq Fmoc-building block-OH, 8 eq DIPEA, 4 eq PyBOP and 4 eq HOBt. The respective molar amount of free amine present on the resin beads was regarded as 1 eq, whilst an identical excess of HOBt and PyBOP was used for preactivation, DIPEA was added with an eightfold excess (also related to free amines). In case of structures synthesized manually, the activating reagents HOBt and PyBOP were dissolved in 5 mL of DMF/g of resin and the Fmoc protected amino acid/the building block was dissolved in 5 mL of DCM/g of resin with the addition of corresponding amount of DIPEA. It is worth mentioning that for synthetic approaches utilizing the automated synthesizer, DCM was replaced with NMP. Routinely coupling time was chosen as 1 h, using an overhead shaker for steady shaking. After each coupling step (as well as after each step of deprotection), three washes with DMF and with DCM (10 mL/g of resin) were carried out. 20 % (v/v) piperidine/DMF was applied for Fmoc-removal four times per 10 min by default (10 mL/g resin). Coupling and deprotection were verified by testing for free amines qualitatively using Kaiser test. If the result was unsatisfying the previous coupling or deprotection step was repeated. After a completed cycle (coupling and deprotection, with washing steps in between), the procedure was repeated until the desired oligomer is obtained. After the last coupling, the resin was dried, and cleavage conducted. Synthesis conditions for manual synthesis are summarized in Table 4 and synthesis is displayed schematically in Scheme 2.1**.** Moreover, to avoid the stearic hinderance of bulky building blocks, the building block solutions were supplemented with Triton X-100, leading to a final concentration of 1 % (v/v) in DMF and 1 % in DCM. Deprotection was carried out with 20 % piperidine/DMF, supplemented with 1 % Triton X-100, for 3 × 15 min.

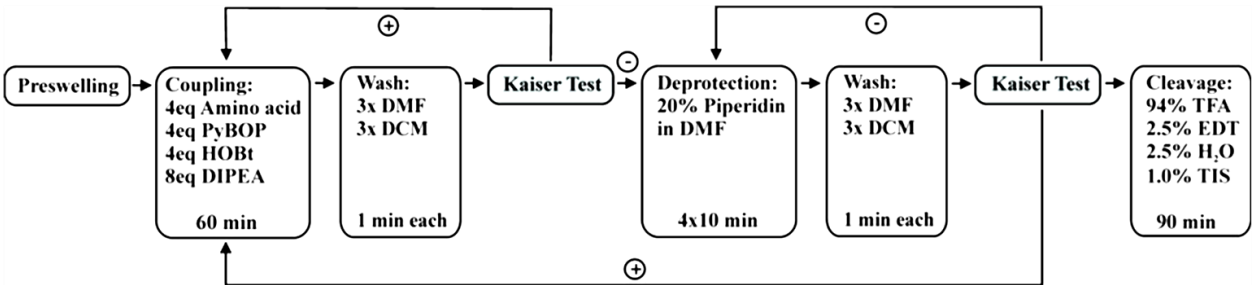

Scheme 2.1. Illustration of a manually conducted solid phase synthesis cycle.

Table 3.4 General steps of a manually conducted synthesis cycle.

Step	Description	Solvent	Volume	Time
1	Coupling	DCM/DMF 50/50	10 mL/g resin	75 min
2	Wash	DMF and DCM	10 mL/g resin	3 times each
3	Kaiser test	Kaiser test solutions	2 drops of each	2 min
4	Fmoc deprotection	20 % piperidine/DMF	10 mL/g resin	3 x 15 min
5	Wash	DMF and DCM	10 mL/g resin	3 times each
6	Kaiser test	Kaiser test solutions	2 drops of each	3 min

3.3.1.3 Kaiser test

Free amines of deprotected amino acids on the resin were determined qualitatively by the Kaiser test.[137] Briefly, a small sample of DCM washed resin was taken into an Eppendorf reaction tube, 2 to 3 drops of each reagent A, B and C solution were added to the test tube. The tube was heated at 99°C for 1-3 min under shaking and compare the color with the following reference: colorless or faint blue colorless (⊖): complete coupling, proceed with synthesis. A deep blue color (⊕) indicated the presence of free amines, proceed with deprotection or coupling incomplete.

3.3.1.4 Procedure of an automated solid phase synthesis

For the long sequence of oligomers or the large number of beads, automated solid phase synthesis was used. After amino acid loading and Fmoc removal, automated synthesis also follows a repetitive cycle of coupling, washing, deprotection, washing after the deprotected resin is preswelled. Nevertheless, compared to manual synthesis, severalsteps required optimization. Firstly, during automated synthesis, all washing steps were conducted with the system liquid DMF (5 × 1 min). Also, within automated synthesis, special reactors had to be used and DCM, as a volatile solvent, was replaced by NMP. During coupling, PyBOP was replaced by HBTU, providing improved stability of the activation reagent in solution within syntheses. Since the automated synthesis does not offer the opportunity to separate resin samples for the Kaiser test, improved coupling conditions and extended deprotection steps were applied. Briefly, during automated synthesis, coupling steps were conducted twice. The calculated 4 eq Fmoc-protected amino acid on the resin was dissolved together with 4 eq. of HOBt in NMP, 4 eq activation reagent HBTU dissolved in DMF, and 8 eq. of DIPEA in NMP were set up

in separate bottles.

3.3.2 General description of cleavage conditions

3.3.2.1 General cleavage of oligomers

After the desired coupling steps, in order to maximize the yields, all resins were dried completely under high vacuum prior to cleavage. This following protocol for cleavage was applied for the T-shaped oligomers containing unsaturated oleic acid (OleA). The structures were cleaved from resins with a mixture of TFA/ EDT/ TIS/ H_2O (94: 2.5: 2.5: 1, v/v), the cleavage solution was dosed according to the amount of resin. To avoid the destroy of unsaturated acid OleA, after 30 minutes of incubation under agitation, the cleavage solution was concentrated by nitrogen flow, and then oligomers were precipitated dropwisely in 40 mL of pre- cooled cocktail MTBE–n-hexane (1: 1, v/v). After precipitation, the tube was shaken vigorously, centrifuged (10 min, 4°C, 4000 rpm, Megafuge 1.0R, Heraeus, Hanau, Germany) and the supernatant removed. The obtained pellets were dried under nitrogen flow. Afterwards, the T-shape oligomers were purified by size exclusion chromatography (SEC) using an Äkta purifier system (GE Healthcare Bio-Sciences AB, Uppsala, Sweden), a Sephadex G-10 column and 10 mM hydrochloric acid (HCl), dissolved in 30 % acetonitrile in water (v/v), frozen in liquid nitrogen and freeze-dried (Christ Alpha 2–4 LD plus, Martin Christ Gefriertrocknungsanlagen GmbH, Osterode, Germany). The relevant fractions were lyophilized, obtaining HCl salts of all oligomers. Purity was evaluated and confirmed by MALDI-TOF-MS and ^{1}H-NMR.

3.3.2.2 Cleavage and purification of DBCO containing reagents

Due to the acid sensitive nature of DBCO, the complete solid-phase synthesis of DBCO-bearing agents is only possible if a certain concentration of TFA in the cleavage cocktail is not exceeded. For this reason, the cleavage is performed at only 5 % of TFA and protecting groups can only be used if they can be deprotected under these mild conditions. The cleavage of the structures off the resin was performed by incubating the dried resin with DCM: TFA: TIS (92.5: 5: 2.5) for 60 min followed by immediate precipitation in 40 mL of pre-cooled MTBE: n-hexane (1: 4). The precipitate was then dissolved in 0.05 M NaOH solution. The pH was adjusted to 7 and the structure was purified by dialysis with a 1000 Da cut-off membrane against deionized water. The obtained DBCO reagents were lyophilized.

3.3.3 Synthesis of oligomers and functional ligands

3.3.3.1 Synthesis of T-shape oligomers 1198 and 1444

1198 and 1444 both were synthesized using a 2- chlorotrityl resin preloaded with the first C-terminal amino acid cysteine (C). The sequence (N→C) of 1198: C(Trt)-[Y(tBu)]$_3$-[Stp (Boc)$_3$]$_2$-K(Dde)-[Stp(Boc)$_3$]$_2$-[Y(tBu)]$_3$-C(Trt) and the sequence (N→C) of 1444: C(Trt)-[Y(tBu)]$_6$-[Stp(Boc)$_3$]$_2$-K(Dde)-[Stp(Boc)$_3$]$_2$-[Y(tBu)]$_6$-C(Trt) were synthesized via SyroWave^{TM} synthesizer (Biotage, Uppsala, Sweden) separately. Coupling steps were carried out as described herein before. All further synthesis steps were performed manually under standard Fmoc solid-phase peptide synthesis conditions using syringe microreactors. Coupling steps were carried out using 4 eq. of Fmoc-protected amino acid and 8 eq. DIPEA in DCM, 4 eq. PyBOP and 4eq. HOBt in DMF (DMF/DCM 1:1, v/v; 10 mL g^{-1} resin) for 75 min. Fmoc deprotection was accomplished by 3 × 15 min incubation with 20 % piperidine in DMF. The resin was washed with DMF 3 times and then DCM 3 times after each coupling and deprotection step, followed by a Kaiser Test. Fmoc-Lys(N_3)-OH was coupled to the backbone and after the removal of the Fmoc protecting group, the N-terminal NH_2-group was protected with 10 eq Di-tert-butyl dicarbonate (Boc anhydride) and 10 eq DIPEA in DCM. Dde-deprotection protocol was accomplished by using Dde-deprotection solution (2 % hydrazine in DMF, v/v, 15 x 2 min). Afterwards, the resin was washed with DMF5 times, with 10 % DIPEA in DMF 5 times and then with DCM 3 times (10 mL g^{-1} resin). A symmetrical branching point was introduced using Fmoc-Lys (Fmoc)- OH. In the final coupling step oleic acid was coupled to produce lipo-oligomer 1198. It is worth mentioning here that for the two of free amines at the branching point, two-fold of normal equivalent of Fmoc-protected amino acid and activating agents. The lipo-oligomer was cleaved off the resin using the optimized cleavage protocol for oleic acid containing structures. TFA cleavage condition (TFA/ EDT/ TIS/ H_2O = 94: 2.5: 2.5: 1, v/v) with pre-cooling to avoid hydroxylation of the oleic acid double bonds. Lipo-OAA 1198 and 1444 was then purified by size exclusion chromatography (SEC) using a Äkta purifier system (GE Healthcare Bio- Sciences AB, Uppsala, Sweden), a Sephadex G-10 column (60 cm) and 10 mM hydrochloric acid solution: acetonitrile (7:3) as solvent. The lipo-oligomer 1198 was lyophilized. The identity of the synthesized structures was confirmed by MALDI mass spectrometry and ^{1}H NMR.

3.3.3.2 Solid phase syntheses of MTX analogs E2-MTX and E5-MTX

After swelling the preloaded resin Fmoc-Glu-OtBu (loading efficiency is 0.25 mmol/mg), the structures were synthesized manually under standard Fmoc solid-phase peptide synthesis conditions using syringe microreactors. Briefly, Fmoc-L-Glu-OtBu was coupled stepwise to the deprotected α‑amine of the loaded resin using 4 eq. Fmoc-L-Glu-OtBu and 8 eq. DIPEA in DCM, 4 eq. PyBop 4 eq and HOBt in DMF and a coupling time of 90 minutes under agitation. After each coupling step, the resin was washed (3 × DMF, 3 × DCM) and the absence of remaining free amines determined by Kaiser test. Upon a negative Kaiser test indicating complete coupling, the resin was Fmoc-deprotected with 3 × 15 min Fmoc deprotection solution, subsequently, washed with 3 × DMF and 3 × DCM. For E2-MTX, a total of two additional Fmoc-L-Glu-OtBu coupling steps was performed, whereas a total of five additional Fmoc-L-Glu-OtBu coupling steps took place for the synthesis of E5-MTX. For both structures, in the last coupling, 4-[[(2,4-diamino-6-pteridinyl) methyl]methylamino] benzoic acid was dissolved in the mixture of 1:1 NMP/ DMSO solution with 8 eq DIPEA reacting for 90 min under agitation. After subsequent washing with 3 × DMF and 3 × DCM, the resin was fully dried under vacuum. The peptide was then cleaved under agitation in the cleavage condition TFA/ TIS/ H_2O 95: 2.5: 2.5. The reactor was washed with 1 mL of TFA, and the combined eluate was collected in a flask and concentrated under nitrogen flow. The obtained flaky yellowish product was dissolved in 10 mL of 25 % (v/v) acetonitrile in water, frozen in liquid nitrogen and freeze‑dried (Martin Christ, Osterode am Harz, Germany) over 2 days. Successful synthesis was confirmed by MALDI-TOF-MS.

3.3.3.3 Synthesis of bisDBCO-PEG-FolA (or E4-FolA) agents for polyplex post-modification

After swelling the preloaded resin Fmoc-L-Lys (Dde)-OH or Fmoc-N-amido-dPEG24-acid, the structures were synthesized manually under standard Fmoc solid-phase peptide synthesis conditions using syringe microreactors. Coupling steps were carried out using 4 eq Fmoc-amino acid, 8 eq. DIPEA in DCM, 4 eq. PyBop 4 eq and HOBt in DMF (DCM/DMF 1: 1) for 90 min. Fmoc deprotection was processed by 3 × 15 min incubation with 20 % piperidine in DMF. A washing procedure comprising 3 × DMF, 3 × DCM incubation and a Kaiser test were performed after each coupling and deprotection step. In case of folate targeted structures, folic acid was first synthesized by coupling of Fmoc-Glu-O-2-PhiPr at a Lys (Dde)-loaded resin followed by N10-(trifluoroacetyl) pteroic acid (dissolved in DMF only), whereas a total of four additional

Fmoc-L-Glu-OtBu coupling steps took place for the synthesis of bisDBCO-PEG-E4-FolA. Dde-deprotection was then performed 15 × 2 min with in a 2 % hydrazine in DMF solution (v/v). The reaction solvent was drained, and fresh solution was added again. Afterwards, the resin was washed with 5 × DMF 5 × 1 min 10 % DIPEA/DMF and 3 × DCM. For the deprotection of the trifluoroacetyl-group of pteroic acid the resin was treated with 25 % aqueous ammonia solution: DMF (1: 1) four times for 30 min. After each deprotection cycle, the resin was washed with DMF. Then, Fmoc-dPEG24-OH was coupled. For the synthesis of bisDBCO-PEG24 structures, the branching points was introduced using Fmoc-Lys (Fmoc)-OH. Finally, 6 eq DBCO acid were coupled using 12 eq DIPEA and 12 eq PyBOP in DCM/DMF. After completion of the reaction, the resin was washed with DMF and DCM and dried in vacuo. The dried resin with DCM: TFA: TIS (92.5: 5: 2.5) for 60 min followed by immediate precipitation in 40 mL of pre-cooled MTBE: n-hexane (1: 4). The precipitate was then dissolved in 0.05 M NaOH solution. The pH was adjusted to 7 and the structure was purified by dialysis with a 1000 Da cut-off membrane against deionized water. The obtained DBCO reagents were lyophilized.

3.3.3.4 Synthesis of bisDBCO-PEG-GE11 agents for polyplex post-modification

For the synthesis of bisDBCO-PEG24-GE11, a 2-chlorotrityl resin was preloaded with Fmoc- Ile-OH, the first C-terminal amino acid of the GE11 sequence. After deprotection, the GE11 sequence was completed via automated SPS. After the final automated deprotection step, Fmoc-dPEG24-OH was coupled manually under the conditions described above, and the branching points was introduced using Fmoc-Lys (Fmoc)-OH. To avoid the stearic hinderance, after the branched Lys coupling, the Fmoc-STODTA-OH was coupled with the general coupling conditions. In the final coupling step, 6 eq DBCO acid were coupled using 12 eq DIPEA and 12 eq PyBOP in DCM/DMF (1: 1). After the completion of the reaction, the resin was washed with DMF and DCM and dried in vacuo. The dried resin with DCM: TFA: TIS (92.5: 5: 2.5) for 60 min followed by immediate precipitation in 40 mL of pre-cooled MTBE: n-hexane (1: 1). The precipitate was then dissolved in 0.05 M NaOH solution. The pH was adjusted to 7 and the structure was purified by dialysis with a 2000 Da cut-off membrane against deionized water. The obtained DBCO reagent was lyophilized, the successful coupling reaction was confirmed via MALDI-MS and analytical HPLC.

3.3.3.5 Synthesis of cy5-labeled oligomer 1198

The azide-containing oligomer 1198 can be labeled using Cy5-NHS ester by the

conjugation of the free amine at the end of N-terminus of 1198 with NHS ester. Oligomer 1198 were dissolved in 0.5 mL of HEPES buffer (pH 7.4), then to avoid the oxidation of Cys-SH group to disulfide, the mixture solution was bubbled for removing air under the argon gas. The pH of solution was then adjusted to 8 using 1 M NaOH with keeping argon bubbles. The label can change the properties of oligomers because the difference of N-terminus; therefore, not every azido oligomer needs to be labeled, 0.5 equivalents of Cy5-NHS ester (the ratio to the free amine) was dissolved in DMSO and added to the lipo-oligomer solution. After 4 h reaction time at room temperature, the 1198-Cy5 conjugate will be purified by dialysis under the argon condition at 4°C. Afterwards, the solution was lyophilized, blue powder was obtained, and the successful labeling reaction was confirmed by MALDI-TOF-MS.

3.3.4 Analytical methods

3.3.4.1 MALDI-TOF mass spectrometry

The MALDI-TOF mass spectrometry matrix solution contains 10 mg/mL Super-DHB (90/10 m/m mixture of 2,5-dihydroxybenzoic acid and 2-hydroxy-5-methoxybenzoic acid) in 69.93/30/0.07 (v/v/v) H_2O/acetonitrile/trifluoroacetic acid. 1 µL of matrix solution was spotted on an MTP AnchorChip (Bruker Daltonics, Germany). After crystallization of 1 µL matrix solution, 1 µL of sample solution (1 mg/mL in water) was added onto the matrix spot. Samples were analyzed using an Autoflex II mass spectrometer (Bruker Daltonics, Germany). All spectra were recorded in positive ion mode.

3.3.4.2 Proton ^{1}H NMR spectroscopy

Proton ^{1}H NMR spectroscopy spectra were recorded using an Advance III HD 400 MHz Bruker BioSpin (400 MHz) with CryoProbe™ Prodigy probe head. All spectra were recorded without TMS and chemical shifts were calibrated to the residual proton signal of the solvent and are reported in ppm. The spectra were analyzed using MestreNova (MestReLab Research). Integration was performed manually.

3.3.4.3 Analytical reversed-phase high performance liquid chromatography (RP-HPLC)

Reversed-phase HPLC (RP-HPLC) was carried out with a VWR-Hitachi Chromaster 5160 Pump System (VWR, Darmstadt, Germany), VWR-Hitachi Chromaster 5260 Autosampler (VWR, Darmstadt, Germany) and a Diode Array Detector (VWR-Hitachi Chromaster 5430; VWR, Darmstadt, Germany) at 214 nm detection wavelength. As a

column either a YMC Hydrosphere 302 C18 (YMC Europe, Dinslaken, Germany) or a Waters Sunfire C18 (Waters, Saint-Quentin en Yvelines Cedex, France) was used. A gradient starting at 95: 5 (water / acetonitrile) to 0: 100 within 20 min was applied. All solvents were supplemented with 0.1 % trifluoroacetic acid.

3.3.4.4 UV-Vis Spectroscopy

UV-vis absorbance spectra were recorded using a V-630 spectrophotometer (Jasco) with water being the solvent.

3.3.4.5 ESI mass spectrometry

The testing samples were dissolved in $CHCl_3$ to a concentration of 1 mg/mL. Electrospray ionization (ESI) mass spectrometry was carried out using a Thermo scientific LTQ FT Ultra Fourier transform ion cyclotron and an IonMax source. Data is shown after positive ionization as (M+X). Samples were kindly processed by Dr. Werner Spahl from the analytical core facility at the Department of Chemistry, LMU Munich.

3.3.5 Preparation of 1198 MTX and PT nanomicelles

The T-shape lipo-oligomer 1198 was dissolved in HEPES-buffered glucose (HBG, 20 mM HEPES, 5 % glucose [w/w], pH 7.4) at a concentration of 3 mM. PT and MTX were dissolved in 10 % DMSO separately, and the solutions were diluted with 90 % HBG at a stock concentration of 10 mM. The drug solution was further diluted with HBG to final concentrations of 1 mM for MTX and 0.5 mM PT. The nanomicelle was formed by adding an equal volume of drug solution PT+MTX (0.5 mM, 1 mM) to the oligomer solution (3 mM), and the solution was mixed by vigorous pipetting. This resulted in final concentrations of 250 µM PT, 500 µM MTX and 1.5 mM lipo-oligomer 1198 in the nanoparticle. Nanomicelles started to form immediately. The ratios of oligomer to drug concentrations were optimized and their effects on particle formation are investigated as described below.

3.3.6 Formation of d E2-MTX or E5-MTX and 1198 nanoparticles

For these nanoparticles consisting of MTX analogs E2-MTX and E5-MTX formulation, E2-MTX and E5-MTX were separately dissolved in 10 % DMSO and diluted with HBG solutions containing 20 mM HEPES to a final concentration of 1 mM. Pretubulysin (PT) was dissolved in 10 % DMSO and diluted with 90 % HBG and further diluted to a final concentration of 0.5 mM. The drug solution was prepared by adding equal volume of

E2-MTX or E5-MTX and PT, then the mixture drug solution was added to equal volume of the prepared 3 mM of 1198 solution to result in a final concentration of 250µM PT, 500 µM E2 or E5-MTX and 1.5 mM 1198. The solutions containing 1198 with drugs were mixed by pipetting up and down (approximately 10 times), the nanoparticles formed, and then further incubated for 45 min at room temperature.

3.3.7 Formation of MTX or E2-MTX or E5-MTX and 1198 or 1444 nanoparticles with the addition of cholesterol

For this, the MTX and MTX analogs solutions were prepared as described herein before. The powder cholesterol was dissolved in ethanol to a stock solution concentration of 15 mM. Lipo-oligomer 1198 was dissolved in ethanol at a concentration of 3 mM. The oligomer 1198 solution was mixed with cholesterol at the volume ratio of 1198/ Cholesterol 5/1 to result in an equal molar concentration of solution. For instance, the 100 µL mixture solution was the concentrated by a rotary concentrator to remove some ethanol and resulted in a 10 µL solution. The solution was diluted to a concentration of 3 mM of 1198 and further mixed with the MTX/PT drug solution, the final concentrations of 250 µM PT, 500 µM MTX and 1.5 mM lipo-oligomer 1198 with 50 % molar ratio of Cholesterol in the nanoparticle were produced. The nanoparticles were formed and then further incubated for 45 min at room temperature.

3.3.8 Post-modification with PEGylation reagents

For post-modifying 1198 or 1444 drug nanoparticles with click agents bisDBCO-PEG24, bisDBCO-PEG24-FolA and bisDBCO-PEG24-E4-FolA, drug solutions and oligomers with/without cholesterol solutions were mixed and incubated for 20 min to form the core polyplex. Then PEGylation reagents were added in ¼ of the volume of the polyplex solution, the concentration of the solution was calculated according to the respective equivalents (eq). Equivalents represent the molar ratio of shielding agents to oligomers in the polyplex solution. All polyplexes were modified with 0.5 eq. of click agent. The polyplex solution was gently mixed and further incubated 4 h.

3.3.9 Measurements of particle size and zeta potential

To confirm the formation of antitumoral drugs nanoparticles and to determine particle size and zeta potential, the freshly prepared polyplexes according to the formation protocol of nanoparticles were measured by dynamic laser-light scattering (DLS) using a Zetasizer Nano ZS (Malvern Instruments, Worcestershire, UK). Nanoparticle solution (65 µL) contained 250 µM PT, 500 µM MTX and 1.5 mM lipo-oligomer 1198 with 50

% molar ratio of cholesterol was transferred to a capillary cell (DTS1070) and measured. For size measurements, the equilibration time was 0 min, the temperature was 25°C and an automatic attenuator was used. The refractive index of the solvent was 1.337 and the viscosity was 1.0336 mPa x s. Each sample was measured three times runs with 13 subruns. For Zeta potential (ZP) measurements, 65 µL of each sample was diluted to 800 µL with 20 mM HEPES pH 7.4 buffer. The zeta potential is displayed as average (mV) of three runs with up to 15 sub-runs each.

3.3.10 Transmission electron microscopy (TEM) of polyplexes

Samples were prepared in HBG as described in paragraph 2.2.7 and 2.2.8, polyplexes contained 250 µM PT, 500 µM MTX and 1.5 mM lipo-oligomer 1198 with 50 % molar ratio of cholesterol. Transmission electron microscopy (TEM) images were taken by Özgür Öztürk (Pharmaceutical Biotechnology, LMU München). The formvar/carbon-coated 300 mesh copper grids(Ted Pella Inc., Redding, CA, USA) were activated by plasma cleaning (420 V, 1 min, argon atmosphere). Afterwards, 5 µL of nanomicelle solution were incubated on the grids for 3 min before it was removed and stained by a 1.0 % uranyl formate solution according to the following procedure: First, 5 µL uranyl formate solution was placed on the grid and removed immediately, second, 5 µL of the same solution were left on the grid for five seconds before removal. Afterwards, the grids were dried for 30 min at room temperature. The stained nanomicelles were visualized by a JEM/1011 transmission electron microscope with 80 kV acceleration voltage.

3.3.11 Drug incorporation efficiency

The drug Incorporation efficiency was determined by ultrafiltration of nanoparticles and subsequent HPLC analysis of the filtrate. Nanoparticles were formed in HBG solution (1198 PT+MTX: 250 µM PT, 500 µM MTX and 1.5 mM 1198 with cholesterol). Amicon Ultra- 0.5 mL (Ultracel 3 K) centrifugal filters were used according to the manufacturer's protocol. The filters were pre-rinsed and washed with 200 µL of Millipore water 3 times. The 140 µL of prepared nanoparticle solution in HBG was added to the ultrafilter, the filled device was inserted into a microcentrifuge tube and centrifuged at 18 000 g for 30 min. The 90 µL of each filtrate was injected and analyzed by HPLC (C- column, YMC column, HS-302, HS12S05-1546WT, 150 x 4.6 mm I.D., S-5 µm, 12 nm, YMC Europe GmbH, Dinslaken, Germany) with a gradient of 5 % to 100 % acetonitrile with 0.1 % TFA in 20 min. Unincorporated drugs PT and MTX were filtrated from the filter and can be detected at 214 nm. Incorporation efficiency was calculated by comparing the peak areas of ultrafiltered, incorporated drug to the peak areas of ultrafiltered free drug. All

experiments were performed in triplicates.

3.3.12 Polyplex stability in the presence of in HBG, 154 mM NaCl and FBS

The stability of drug incorporation in 1198 PT+MTX with cholesterol nanomicelles incubated in HBG, 154 millimolar sodium chloride (154 mM NaCl, same as physiological saline) and 10 % - 50 % FBS in HBG was determined at different temperatures and incubation time points. Drug polyplexes were prepared in HBG as previously described (1198 PT+MTX: 250 µM PT, 500 µM MTX and 1.5 mM 1198 with 50 % molar ratio of cholesterol). Particle solution (70 µL) was added to the equal volume of respective incubation medium (HBG, 308 mM NaCl and 20- 100 % FBS in HBG). After incubation at room temperature or 37°C in a shaker for 1 h or 12 h, nanomicelles were ultrafiltered at 18 000 g for 30 min. Depending on the incubation medium, filtration devices with different cut-offs were used. Amicon Ultra 0.5 mL (Ultracel 3 K) were used to measure drug release upon incubation in serum- free HBG or NaCl solution. Due to interactions of PT and FBS components, 100 K cut off filtration devices (Amicon Ultra-0.5 mL, Ultracel 100 K) were used in case of FBS containing solutions. Control experiments demonstrated that MTX or PT, only if released from nanomicelles, would be detectable in the filtrates in both settings. T The 90 µL of each filtrate was injected and analyzed by HPLC (C- column, YMC column, HS-302, HS12S05-1546WT, 150 x 4.6 mm I.D., S-5 µm, 12 nm, YMC Europe GmbH, Dinslaken, Germany) with a gradient of 5 % to 100 % acetonitrile with 0.1 % TFA in 20 min. Unincorporated drugs PT and MTX were filtrated from the filter and can be detected at 214 nm. The amount of released drug upon incubation was determined for MTX and PT and calculated in relation to free PT+MTX which was incubated under the same conditions. All experiments were performed in triplicates.

3.3.13 Cell culture

Cell culture work was carried out by Mina Yazdi (Pharmaceutical Biotechnology, LMU München). Cell culture media, antibiotics, and fetal bovine serum (FBS) were purchased from Invitrogen (Karlsruhe, Germany), Sigma Aldrich (Munich, Germany) or Life Technologies (Carlsbad, USA). L1210 (Mouse lymphocytic leukemia cells) cells were cultured with RPMI-1640 (+/- folate) were supplemented with 10 % FBS, 4 mM stable glutamine, 100 U/mL penicillin and 100 µg/mL streptomycin. Cell lines were cultured at 37°C and 5 % CO_2 in an incubator with a relative humidity of 95 %.

Exponentially growing cells were detached from the culture flasks using Millipore water, supplemented with 0.05 % trypsin-EDTA (Invitrogen, Karlsruhe, Germany), and

followed by resuspension in the required culture media. Cell suspensions were seeded at the desired density for each experiment. Luciferase cell culture lysis buffer and D-luciferin sodium salt was purchased from Promega (Mannheim, Germany).

Table 3.5. Overview of the used cell lines and corresponding culture media.

Cell line	Description	Medium
L1210	Mouse lymphocytic leukemia cells	RPMI-1640, +/- folate

3.3.14 Cell viability assay (MTT)

L1210 cells were seeded at density of 5000 cells/well 4 h before treatment. After the desired incubation times with polyplexes, 3-(4,5-dimethylthiazol-2-yl)-2,5-diphenyltetrazolium bromide (MTT, 10 µL, 5 mg/mL in PBS) was added to each well and cells were incubated for 2 h. For cell lysis of L1210 cells, a solution of 10 % sodium dodecyl sulfate (SDS) in 0.01 M hydrochloric acid (HCl) was added to each well and incubated overnight. The absorption was measured at a wavelength of 590 nm against a reference wavelength of 630 nm using a SpectraFluor™ Plus microplate reader (Tecan, Groedig, Austria). Cell viability was calculated as percentage of absorption compared to wells treated with HBG only. All experiments were performed in triplicate.

3.4 Results and discussion

3.4.1 Design and evaluation of sequence-defined oligoaminoamide copolymer for targeted combination chemotherapy

It is well recognized today that chemotherapy is a crucial modality in today's clinical oncology practice, and anticancer drugs are often most effective when used in combination. There are still some problems, such as limited efficacies and poor safety and resistance profiles,[138] despite major spending on research and development and technological advances.[139] Synergistic and potentiation drug combinations have been explored to achieve several favorable outcomes: enhanced efficacy, reduced or delayed drug resistance, and decreased dosage at equal or increased efficacy.

The previous study in our working group has reported that the combination of two low-dose drugs, Pretubulysin and Methotrexate, has effective tumor treatment *in vivo*.[28] Pretubulysin (PT), a natural product-derived compound, has been a potent tubulin-binding drug. PT disrupts the microtubule network at nanomolar concentrations. It abrogates proliferation and long-term survival and induces apoptosis in invasive tumor cells equally potent to tubulysin. Due to these potencies, PT is a possible candidate for cancer therapy.[21, 27, 42] Methotrexate (MTX), a chemotherapy agent and immune system suppressant binds to the folic acid's target enzyme dihydrofolate reductase (DHFR). It is well established in cancer therapy.[140] Compared to some small molecules, the formulated polyplexes exhibit improved structural stability and facile functionalization, whereas the delivery system remains challenging to fabricate codelivery polymeric vesicles possessing encapsulation stability and structural stability in blood circulation and synchronized corelease features triggered by specific pathological milieu.[141]

This chapter investigates cationic sequence-defined oligoaminoamides as vectors for the combination chemotherapy. The negatively-charged drug binding element, a stabilizing unit, a shielding block, and a tumor-specific targeting domain are required in the delivery system. Solid-phase synthesis (SPS) derived T-shape oligomers, MTX analogs, and Folate acid ligands were applied as nanoparticles for receptor-targeted drug delivery *in vitro*.

Several structural motifs were crucial in designing the drug delivery vehicles. A bioreducible dynamic covalent bond, cysteine–cysteine disulfide bond, is introduced in the oligomers to form stable dimers within other cysteine-any-cysteine peptides.[142] In

this strategy, C- and N- terminal cysteines can stabilize the drug nanoparticles due to their cross-linking ability. The artificial amino acid succinoyl tetraethylene pentamine (Stp) acts as hydrophilic protonatable segment which can facilitate the incorporation of negatively charged cargo molecules via electrostatic interaction due to being partly protonated at physiological pH.[143] The oleic acid (OleA) and tyrosine enhance the stabilization of nanomicelle by hydrophobic or aromatic π-π stacking interactions.[92, 144, 145] Zhong et al. found that polytyrosine blocks significantly enhance the drug loading efficiency and stability of the particles.[92]

It is also interesting to note that the increased negative charge intensity would enhance water solubility by modifying the hydrophobic drug. The increased electrostatic interaction could bind to the positively charged region of the oligomer more firmly. So, amino glutamic acid, used widely in peptide synthesis, is a promising unit to enhance the negative charge. Besides, impaired intracellular polyglutamylation resulting in insufficient cytosolic MTX accumulation has also been described as contributing to MTX resistance. To address this drug resistance, two pre-polyglutamylated MTX structures, E2- MTX and E5- MTX, and PEGylated E4-FolA ligand were introduced in the nanoparticulate for the codelivery of drugs.

Cholesterol is the principal sterol component in most mammalian membranes and is non-homogeneously distributed among different organelles. One of the specific physical features of the cholesterol molecule is the steroid tetracycle, a relatively conformationally rigid structure. It governs much of the interactions of cholesterol in a lipid bilayer and increases its mechanical stiffness while keeping the membrane fluid.[146, 147] Cholesterol can serve as a stabilizing domain in the complex micelles for *in vivo* delivery due to the increased stability in the proteinous medium and the bloodstream.[148-150]

3.4.2 Oligomers and PEGylated ligands synthesis

The T-shape oligomers 1198 and 1444 containing previously mentioned crucial domains were synthesized by SPS. The sequence-defined T-shape oligomers with their internal polymer numbers, the synthetic glutamylated versions E2-MTX, E5-MTX, helper lipid cholesterol, bisDBCO-PEG ligands are included in **Figure 3.1**. Both sequence-defined cationic lipo-oligomers contain hydrophobic and hydrophilic domains. They can complex negatively charged MTX and its gamma-glutamylated derivatives (E2-MTX and E5-MTX) and neutral antitumoral drug PT by electrostatic and hydrophobic interactions in an aqueous solution. The prepared nanoparticles can

further be modified with PEGylated folate ligands to obtain the targeted function, see **Scheme 3.1**.

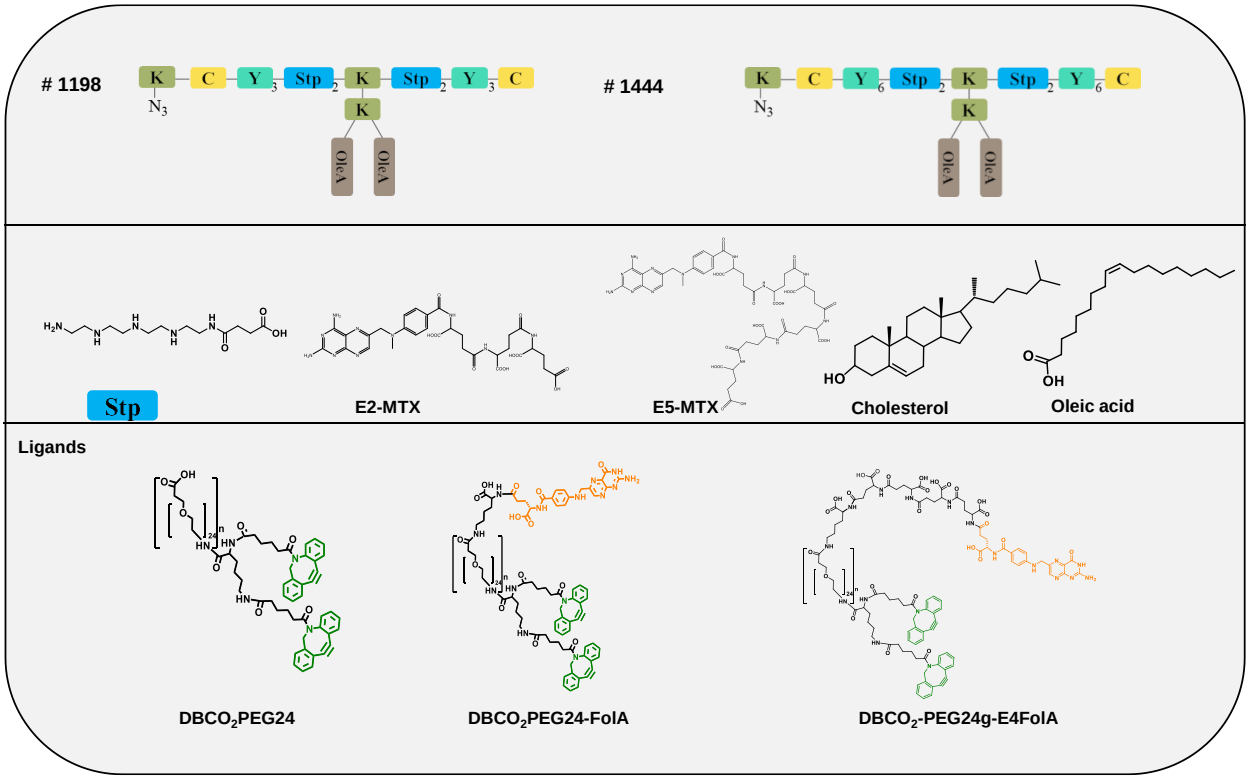

Figure 3.1. Sequences, topologies, and abbreviations of oligomers and MTX derivatives. The different structural segments of the lipo-oligomer are represented in different colors: hydrophilic regions: blue (Stp), hydrophobic: grey (oleic acid) and aromatic: green (tyrosine). Additional nanoparticle stabilization is facilitated by disulfide crosslinkages (yellow: cysteine). Chemical structure of oleic acid, cholesterol, succinyl- tetraethylene pentamine (Stp), and $DBCO_2$-PEG_{24} ligands.

3.4.3 Formation and characterization of nanomicelle complexes

MTX and its analogs acting as the negatively charged cargo molecules were bound to the positively charged lipo-oligomers to form polyelectrolyte complexes. The zwitterionic lipophilic tubulin-binding drug PT interacts with 1198 or 1444 via the interactions of hydrogen bonding, hydrophobic, or other interactions.[21] To enable the successful formation of polyelectrolyte complexes, the ratio of oligomer (1198) to MTX were firstly investigated. Steinborn et al. have examined the particles of MTX and 454 or polyglutamylated analogs of MTX,[82] and Truebenbach et al. have previously found a promising ratio for the nanoparticle formation. This study examined several different ratios of 1198 to MTX based on their work.

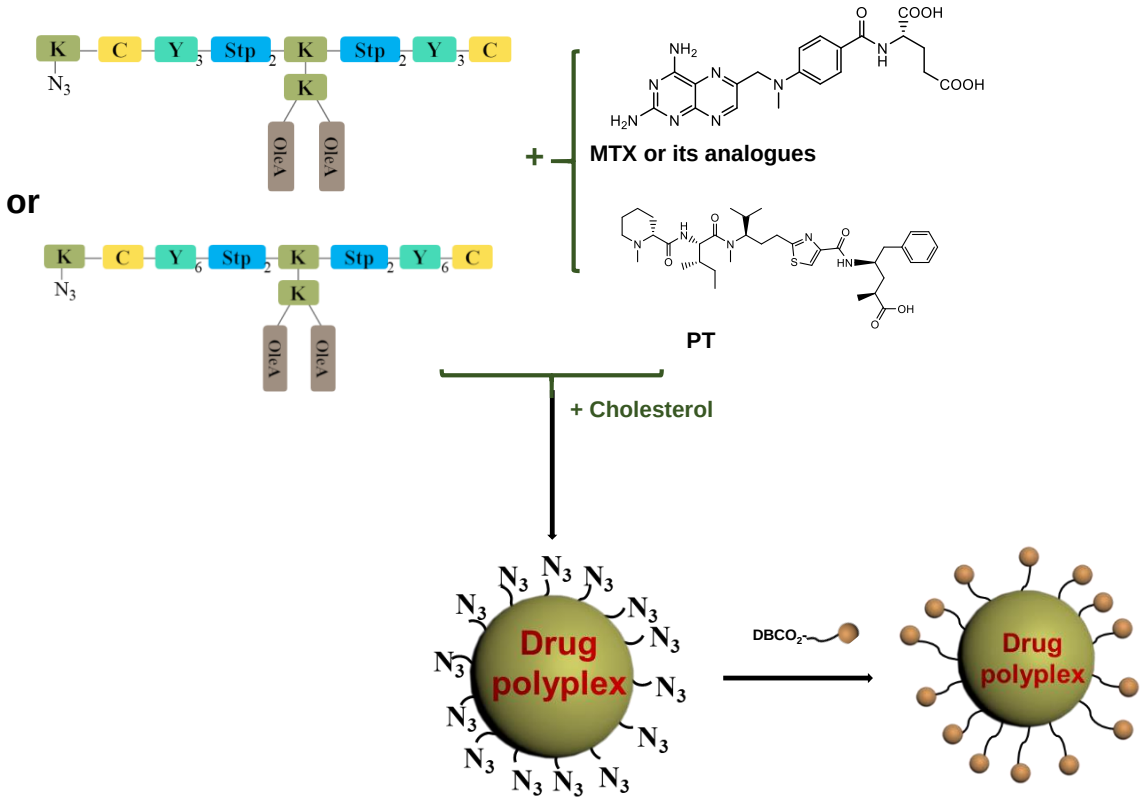

Scheme 3.1. Schematic illustration of polyplex formation. lipo-oligomer 1198 (Y_3) or 1444 (Y_6), MTX or its analogs and PT form a polyplex including addition of cholesterol. In the second step, the polyplex was modified with bisDBCO ligands via “click-chemistry”.

Dynamic light scattering (DLS) measurements demonstrated that once the ratio of the oligomer to MTX is too high, the solution mixture forms an inhomogeneous nanoparticle, one is 20 nm, and the other peak appears at more than 300nm. Truebenbach et al. also proved that in their work.[21] It is recognized that particles that are smaller than 5-10 nm are reported to be rapidly cleared by the kidneys. In contrast, particles with sizes above 200 nm are recognized by the reticuloendothelial system (RES) and degraded by macrophages. By decreasing the ratio of 1198 to MTX, the optimized particle could be obtained at physiological pH. It shows that in **Figure 3.2 A,** at a 3-fold surplus of the oligomer, 1198/MTX nanoparticles (3: 1) possessing 100 nm in size with a polydispersity index (PDI) of 0.25 were formed. By further lowing oligomer amounts to a molar ratio of 3 to 2 or 3 to 4, excellent particles 100 nm – 180 nm in size were obtained as well with lower than 0.3 of PDI. However, when the ratio of the oligomer to the drug was inversed using these ratios, particle aggregation and precipitation would appear in the drug solution. In further evaluating these particles, 1198 MTX at 3 to 1 ratio polyplex properties did not change when the particles were incubated for 12 hours at 25°C or even body temperature (37°C). Therefore, a 3:1 molar ratio was used for subsequent 1198 MTX and analogs of MTX formation studies (**Figure 3.2B**).

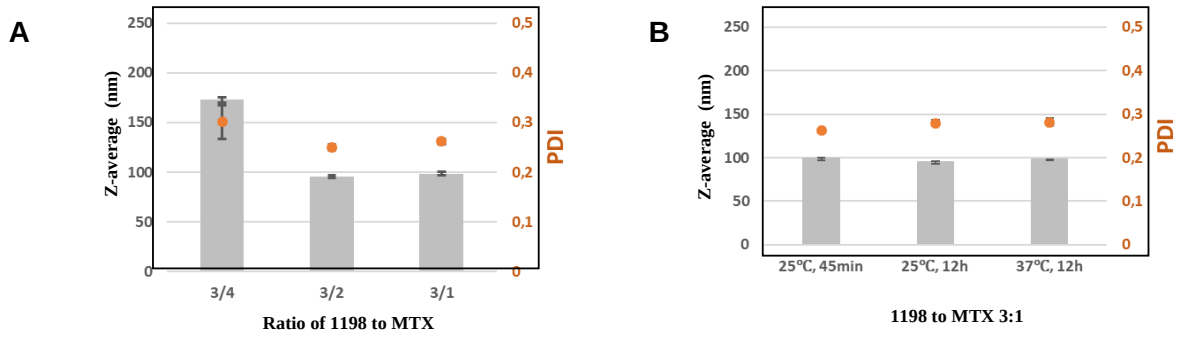

Figure 3.2. Size and polydispersity index of (A) 1198 MTX formed upon different molar ratios of 1198: MTX and (B) polyplexes (3: 1 ratio) incubated at indicated temperature condition for different time point in HBG solution.

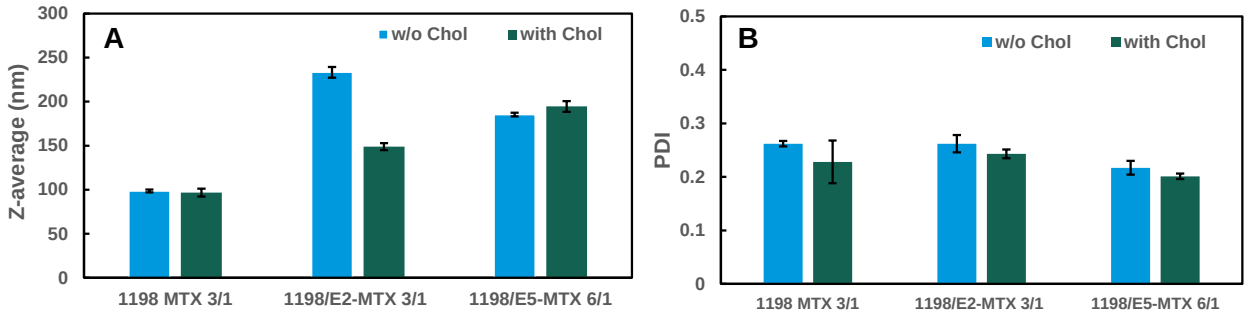

Figure 3.3. Size (A) and polydispersity index (B) of 1198 with MTX analogs, E2-MTX, E5-MTX with or without the addition of cholesterol.

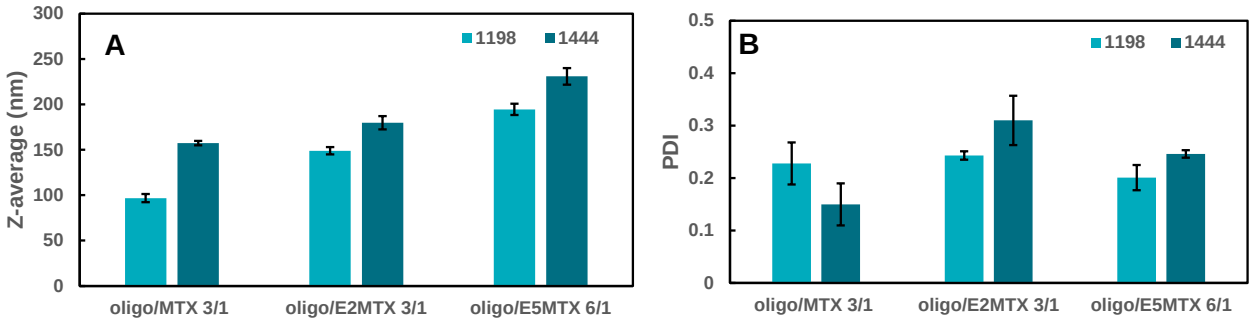

Figure 3.4. Size (A) and polydispersity index (B) of 1198 or 1444 with MTX analogs, E2-MTX, E5-MTX with the addition of cholesterol.

The other strategies were also investigated and optimized in the formation of polyplexes. From the evaluation of nanoparticle properties, we can see that in **Figure 3.3,** with the increase of amounts of glutamic acids in the conjugation of the MTX analogs, the size of the polyplex (1198 E0 or 2 or 5- MTX) increased. They are still below 200 nm with 0,3 below PDI. The particles did not change after adding 50 % of cholesterol into the polyplexes. Cholesterol was applied to stabilize lipid bilayers and

enhance the stability of the lipidic protein nanoparticles. Coincidentally, adding cholesterol was also proved to be a crucial factor in the prepared particle properties in the following drug incorporation efficiency experiment. 1444 (1198 analog with six more tyrosines) was also used for encapsulating MTX and analogs. The 1444 polyplexes are slightly larger than the 1198 polyplexes with cholesterol; the particle size is around 250 nm, and the PDI is below 0.35.

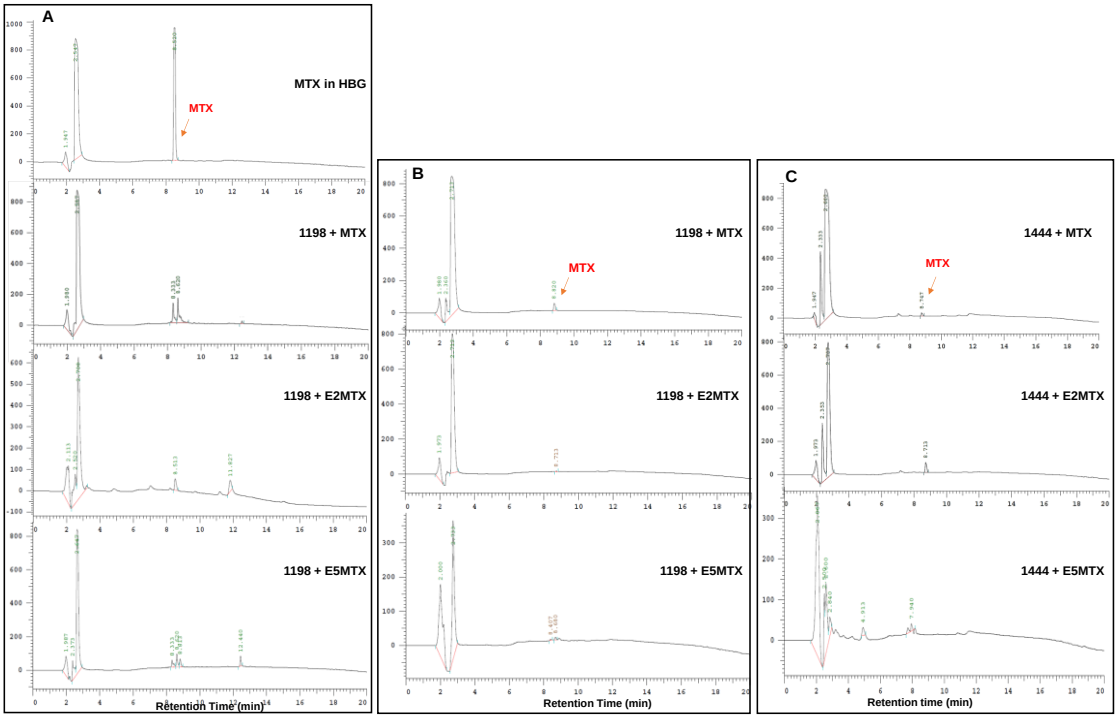

Figure 3.5. Free MTX, MTX, E2-MTX and E5-MTX drug incorporation into 1198 nanomicelles upon exposure to HBG (A) without cholesterol and (B) with cholesterol addition, and (C) MTX, E2-MTX and E5-MTX drug incorporation into 1444 nanomicelles with cholesterol at room temperature. HPLC chromatograms (C18 column, 5 % to 100 % acetonitrile gradient in 0.1 % aqueous TFA in 20 min, detection wavelength 214 nm) oligomer and MTX particles after ultrafiltration. Nanoparticle solution (500 µM MTX, 1.5 mM 1198 or 1444; 100 µL) was diluted with 100 µL of HBG. The respective filtrates were evaluated by HPLC for released drug. The upper chromatogram in **Figure 3.5A** serves as a concentration standard to calculate free, unincorporated drug.

3.4.4 Drug incorporation efficiency of oligomers

A nanoparticle system with maximal drug loading and a high incorporation efficiency will reduce the number of carriers required to administer a sufficient amount of active compound and is crucial for the therapeutic effect. The incorporation efficiency of E0 or 2 or 5- MTX into 1198 and 1444 nanomicelles was determined by ultrafiltration. Nanoparticles were formed in HBG and then ultrafiltered using centrifugal filters with a cut-off of 3 kDa. HPLC analyzed the filtrate containing a non-incorporated drug for drug

content. In **Figure 3.5A**, the intensity of the peaks represents the amounts of unincorporated drug MTX. The area of separated peaks was calculated compared to the standard concentration. The polyplexes1198 combined with single drug MTX show nearly 90 % drug incorporation efficiency at the optimized molar ratio oligomer/ MTX of 3:1. The negatively charged drug was encapsulated into cationic oligomers by the electrostatic interactions. With two or five more negative charged glutamate residues attached, the incorporation efficiency of the PECs stays unchanged. We could see very tiny peaks in E2- and E5-MTX particles. Upon increasing the amount of stabilizing domain tyrosines and cholesterol in the nanomicelles, little more drugs were incorporated into the polyplexes, with the drug incorporation of 91.5 % (**Figure 3.5 B** and **C**).

3.4.5 Stability of the drug nanomicelles

It is essential to ensure the stability of a micelle under physiological conditions. Different parameters, like salt changes and contact with numerous proteins, endanger its structural integrity. For the optimized screening experiments, single drug MTX and its analogs were examined to confirm the strategy. The availability and shortage of pretubulysin (PT) was also one of the reasons for single drug encapsulating condition screening. The stability of the nanomicelles was determined by HPLC chromatograms (C18 column, 5 % to 100 % acetonitrile gradient in 0.1 % aqueous TFA in 20 min, detection wavelength 214 nm) particles after ultrafiltration. Nanoparticle solution (500 µM MTX, 1.5 mM 1198; 100 µL) was diluted with 100 µL of incubation medium (HBG, 308 mM NaCl, 20 % or 40 % or 90 % of FBS containing HBG). PECs were incubated at final concentrations of 154 mM NaCl in HBG, 10 % or 20 % or 45 % FBS in HBG for 1 h at room temperature and ultrafiltered. For nanoparticles incubated in physiological NaCl solution (154 mM NaCl), filters with a 3 K cut-off (Amicon Ultracel 3 K) were used to separate the nanoparticle from free, unincorporated drugs. For nanoparticles incubated in an FBS-containing medium, filters with a 100 K cut-off (Amicon Ultracel 100 K) served to separate the free drug. The respective filtrates for the released drug. While MTX incorporation efficiency of the polyplexes is as high as 95 %, **Figure 3.6** shows us that 36 % to 40 % of MTX is not entrapped from the MTX encapsulated particles incubated in the FBS medium. Moreover, around 42 % MTX is released in physiological NaCl solution (**Figure 3.7**).

We can see from **Table 3.6** that the stability of the E2- and E5- MTX polyplexes increased, especially the polyplexes with cholesterol incubated in a different medium

but did not vary significantly, and the 1444 polyplexes with cholesterol showed minor drug release compared to the 1198 polyplexes. 1444 +MTX polyplexes with 96 % drug incorporation efficiency are stable in HBG and 20 % FBS medium, and the drug release ratios are below 10 %. However, 43 % of the drug was released incubated in 45 % FBS medium from 1444+E5-MTX.

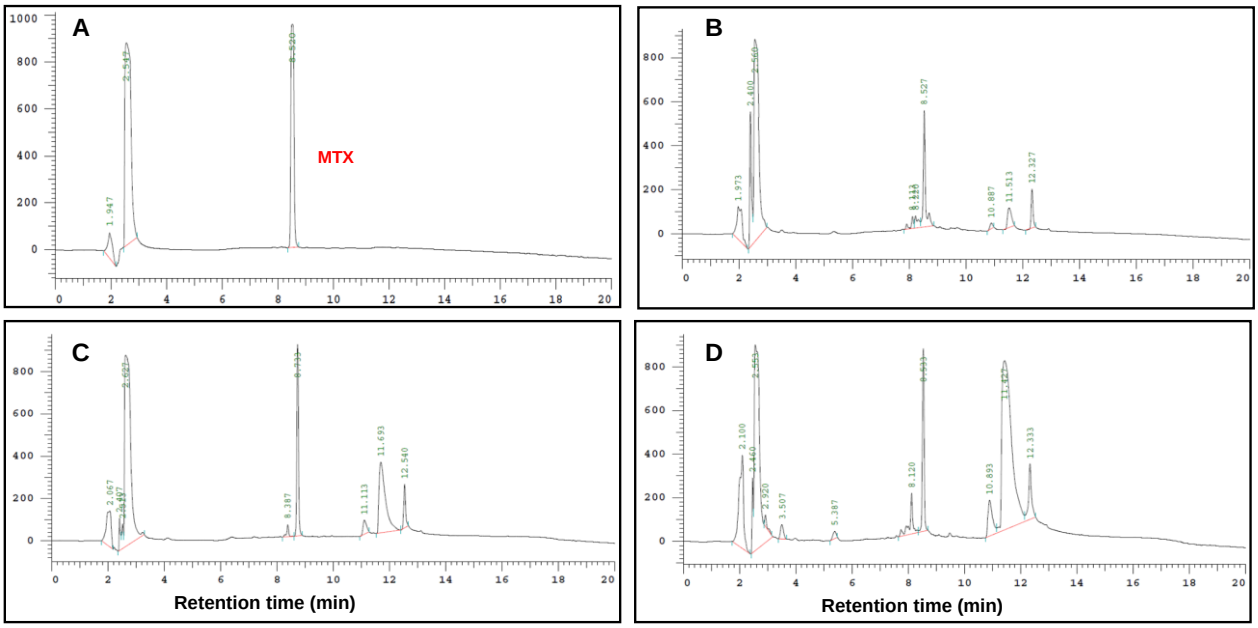

Figure 3.6. Stability of MTX drug incorporation into 1198 nanomicelles upon exposure to (A) free MTX in HBG, (B) 10 % serum containing HBG, (C) 20 % serum containing HBG (D) 45 % serum containing HBG at room temperature. HPLC chromatograms (C18 column, 5 % to 100 % acetonitrile gradient in 0.1 % aqueous TFA in 20 min, detection wavelength 214 nm) particles after ultrafiltration. Nanoparticle solution (500 µM MTX, 1.5 mM 1198; 100 µL) was diluted with 100 µL of incubation medium (20 % or 40 % or 90 % of FBS containing HBG). PECs were incubated at final concentrations 10 % or 20 % or 45 % FBS and for 1 h at room temperature and ultrafiltered. For nanoparticles incubated in FBS containing medium (B, C and D), filters with a 100 K cut off (Amicon Ultracel 100 K) served to separate the free drug. The respective filtrates were evaluated by HPLC for released drug.

Based on these finds and knowledge, when more glutamate units were introduced in the drug analogs, nanomicelle polyelectrolyte complexes (PECs) could entrap more drugs due to the stronger electrostatic interactions, whereas the stability was not increased in the FBS medium. Tyrosine and cholesterol help provide hydrophobic interactions beyond fundamental electrostatic interactions, thereby enhancing polyplex stability. Meanwhile, the nanoparticle properties changed slightly in size and PDI. 1444 nanomicelle PECs were stable over time. In the subsequent evaluation of combination codelivery of drugs, 1198 used as mainly cationic carrier encapsulated MTX and PT to form a nanoparticle.

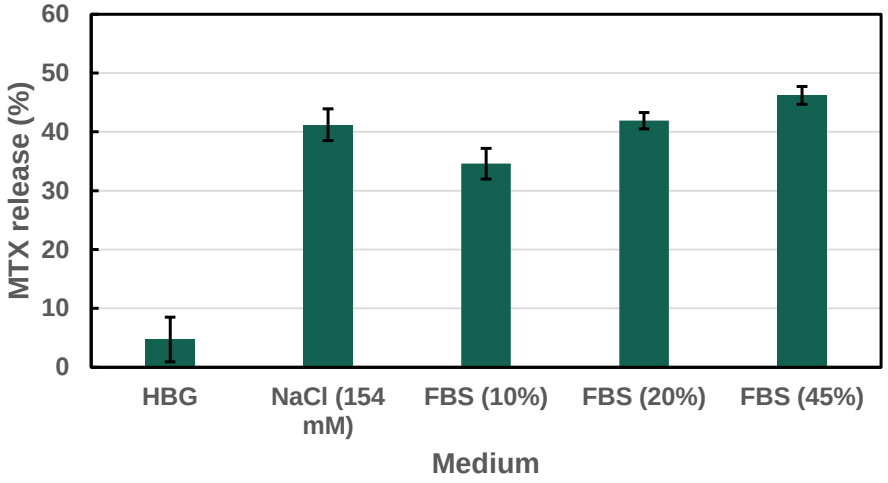

Figure 3.7. Stability of MTX drug incorporation into 1198 nanomicelles upon exposure to HBG, 154 mM sodium chloride solution, 10 %, 20 % and 45 % FBS serum containing HBG at room temperature. HPLC chromatograms (C18 column, 5 % to 100% acetonitrile gradient in 0.1 % aqueous TFA in 20 min, detection wavelength 214 nm) particles after ultrafiltration. Nanoparticle solution (500 µM MTX, 1.5 mM 1198; 100 µL) was diluted with 100 µL of incubation medium (308 mM NaCl, 20 % or 40 % or 90 % of FBS containing HBG). PECs were incubated at final concentrations 154 mM NaCl in HBG, 10 % or 20 % or 45 % FBS in HBG for 1 h at room temperature and ultrafiltered. For nanoparticles incubated in physiological NaCl solution (154 mM NaCl), filters with a 3 K cut off (Amicon Ultracel 3 K) were used to separate the nanoparticle from free, unincorporated drug. For nanoparticles incubated in FBS containing medium, filters with a 100 K cut off (Amicon Ultracel 100 K) served to separate the free drug. The respective filtrates were evaluated by HPLC for released drug.

Table 3.6. The ratio of MTX released from different nanomicelle PECs from different incubation medium.

Nanomicelle PECs	Cholesterol Addition	HBG	20 % FBS	45 % FBS
1198 + MTX	Without	4.4	41.9	46.2
1198 + MTX	With	9.6	33.8	30
1198 + E2MTX		2.2	14.8	23.8
1198 + E5MTX		4.6	26.4	33.5
1444 + MTX		3.4	33.5	62.6
1444 + E2MTX		9.4	7.5	24.3
1444 + E5MTX		7.5	4.7	43.2

The ability of lipo-OAA 1198 incorporating MTX (1198 MTX) and PT (1198 MTX+PT)

with or without the addition of cholesterol is shown in **Figure 3.8**. Pretublysin, a zwitterionic lipophilic drug, did not form a good particle when it interacted with 1198 (the size 20 nm). MTX particles revealed sizes around 100 nm with 0.2 of PDI. 1198 (MTX+ PT) particles were considerably bigger, around 120 nm. TEM images show 1198 (MTX+ PT) PECs to be uniform and spherical in shape. Data correspond well with DLS measurements in terms of particle size. The size of 1198 (MTX+ PT) particles with cholesterol was not changed, and the zeta potential was the same as that of 1198 MTX nanomicelles. Particle sizes between 10 and 200 nm have previously been shown to passively target tumors by the EPR effect.[151]

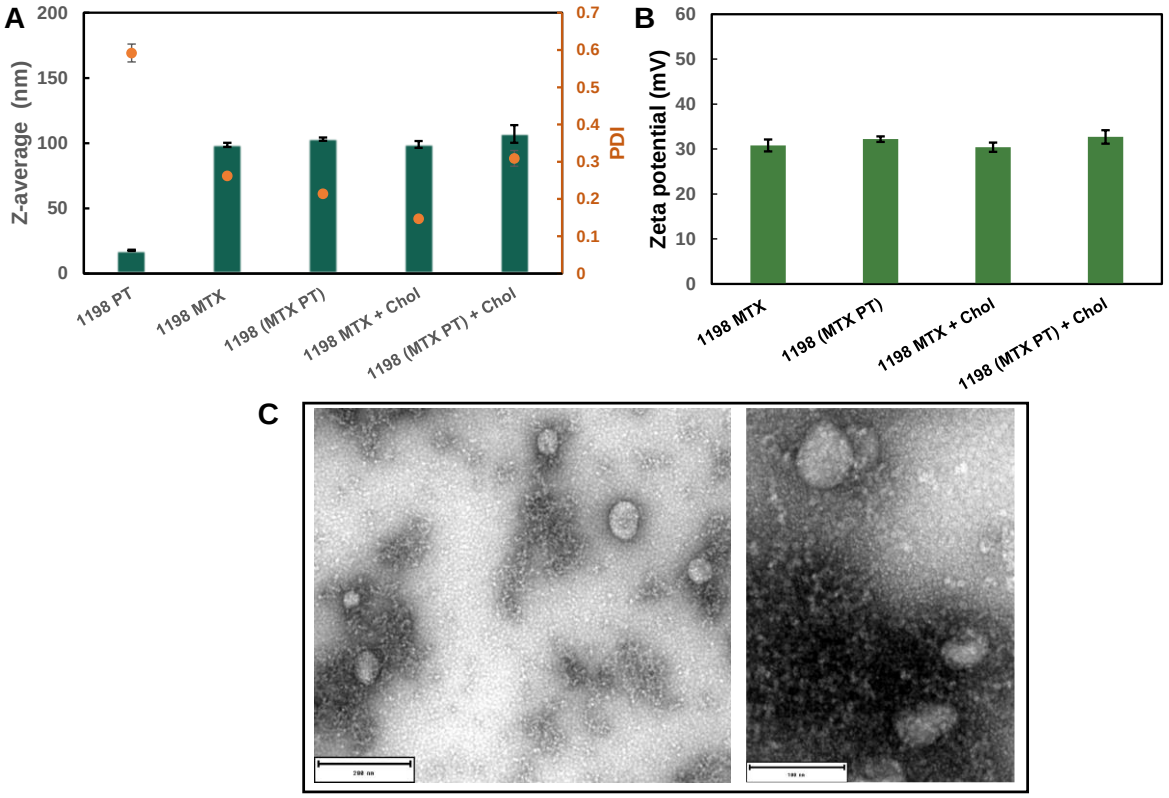

Figure 3.8. (A) Size and polydispersity index and (B) Zeta potential of the polyplexes. DLS measurements of 1198 PT and 1198 MTX PT with/without cholesterol, the polyplexes were formed at ratio of 1198: MTX: PT = 6: 2: 1 with 45 % molar ratio of cholesterol addition. (C) Morphology of 1198 (MTX PT) + Cholesterol nanoparticles in HBG. The scale bar is 200 nm in the left picture, 100 nm in the right picture.

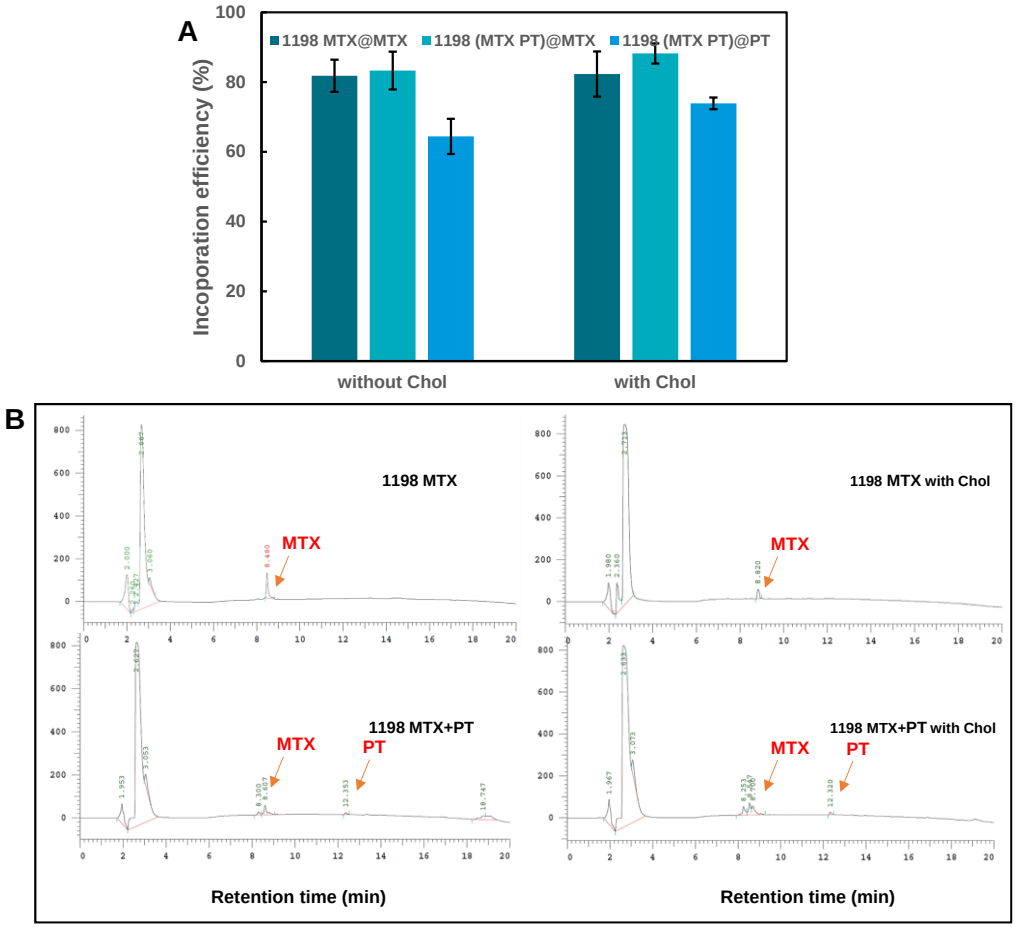

Figure 3.9. Drug incorporation efficiency (A) 1198 MTX and 1198 MTX+PT with/without the addition of cholesterol, the polyplexes were formed at ratio of 1198: MTX: PT = 6:2:1 (250 µM PT, 500 µM MTX, 1.5 mM 1198; 100 µL) with 45 % molar ratio of cholesterol addition. The calculated efficiency was determined by ultrafiltration of polyplexes and (B) high-performance liquid chromatography (HPLC, C18 column of 5 % to 100 % gradient of acetonitrile in 0.1 % aqueous TFA, detection wavelength 214 nm).

Drug incorporation efficiency (**Figure 3.9**) and stability (**Figure 3.10**) of 1198 MTX and 1198 (MTX+ PT) with or without cholesterol were further investigated by HPLC after ultrafiltration. At the optimized molar ratio 1198: MTX: PT = 6: 2: 1 (250 µM PT, 500 µM MTX, 1.5 mM 1198; 100 µL), lipo-OAA 1198 (MTX+ PT) incorporates 80 % of MTX and 62 % of PT. After adding 45 % cholesterol, the incorporation efficiency of the PECs increased to 86 % and 74 %, respectively (**Figure 3.9**). The stability of a micelle under physiological conditions is crucial. 1198 MTX and 1198 (MTX+ PT) nanomicelles were incubated in HBG, 154 mM sodium chloride, and FBS in HBG for one h, the particles were ultrafiltered. In **Figure 3.10**, we can see that all the nanomicelles incubated in HBG, whether with or without the addition of cholesterol, stayed stable, and less than 7 % drug was released from PECs. However, 40 % of MTX or PT was released when nanomicelles were incorporated and exposed to the physiological solution and FBS-

containing solution, the salt changes and contact with proteins can affect the system. Cholesterol helps to stabilize lipid bilayers and enhance the stability of the nanoparticles. It also seems like a potential domain for increasing the stability of 1198 MTX and 1198 (MTX+ PT), as less than 20 % of drugs are released from both nanomicelles.

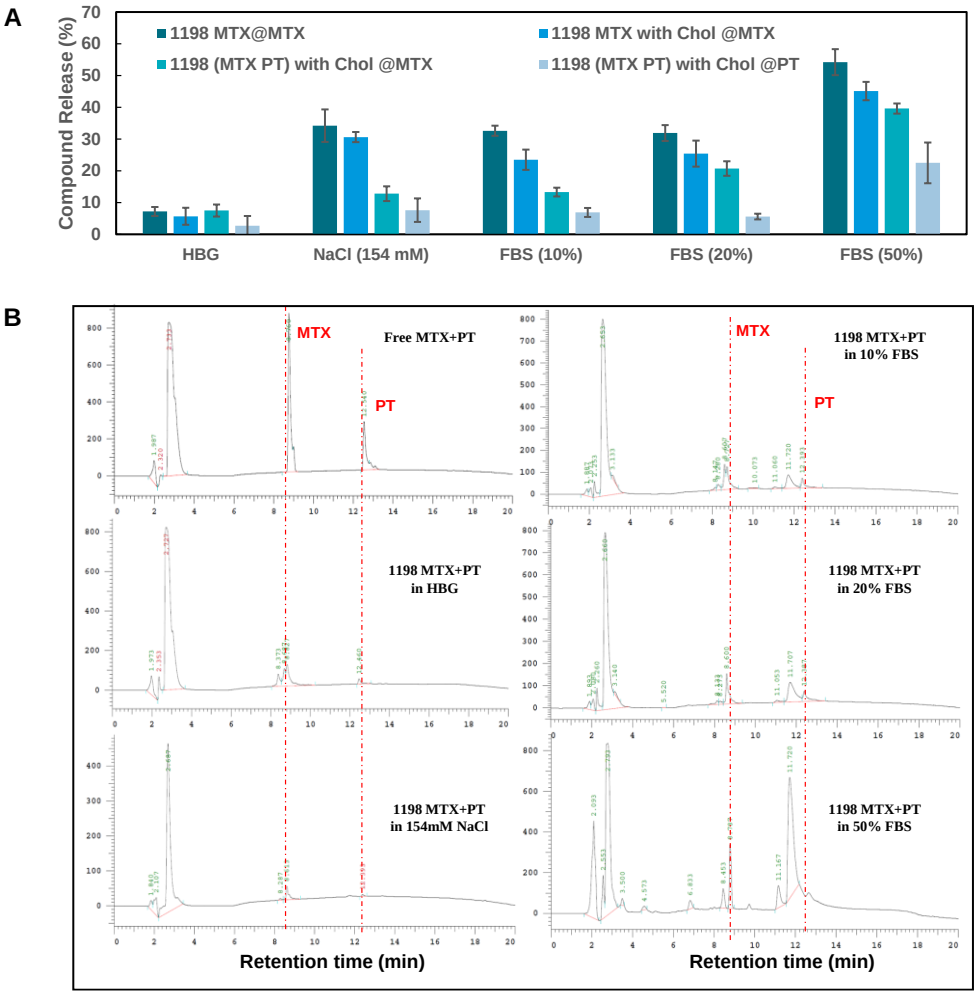

Figure 3.10. Stability of MTX or MTX+PT drug incorporation into 1198 polyplexes upon exposure to different medium solution, including HBG, 154 mM NaCl solution and 10 %, 20 % and 50 % FBS containing serum containing HBG at 37 h. (A) MTX or PT release of 1198 polyplexes in different medium. (B) HPLC chromatograms of polyplexes incubated in different mediums.

3.4.6 Therapeutic activity of free or formulated MTX or MTX+ PT

PT shows a strongly antiproliferative effect on L1210 leukemia cells *in vitro*. L1210 cells are susceptible to MTX treatment, and Truebenbach and Kern have already reported the combination effect of (MTX+ PT).[21] This new strategy for co-delivering negatively charged MTX (and its analogs) has been developed using sequence-defined cationic lipooligomers. All cell culture experiments were performed by Mina Yazdi, PhD student

at LMU Pharmaceutical Biotechnology. In **Figure 3.11**, we can see that stable polyplexes 1198 encapsulating MTX, E2-, or E5-MTX with cholesterol show the similar trend in tumor therapeutic efficiency at different concentration of drug, and it demonstrates that 1198+MTX formulation possessed higher cancer cells killing ability even though 1198+E2 or E5-MTX have less MTX release.

The cell viability results in **Figure 3.12A** also demonstrated that the cell viability upon the combination of drugs (MTX+PT) after 48 h can be decreased compared to free MTX (**Figure 3.11**) from 40 % of cells to 20 %. 1198 (MTX+ PT) incorporation also increased the antitumoral effects on L1210 cells, significantly at lower concentrations compared to 1198 MTX nanomicelles and combined drugs without carrier. The increased tumor cell killing effects of the 1198 formulations over the free drugs could not be attributed to lipo-OAA toxicity, which was negligible. However, the therapeutic efficiency of 1444 polyplexes is not better than 1198 with the addition of cholesterol. Considering more tyrosine in 1444 than 1198, more tyrosines could affect the stability of polyplexes and the encapsulation efficiency of drugs, whereas the antitumoral effect keeps a similar level as the original one 1198 (**Figure 3.12B**).

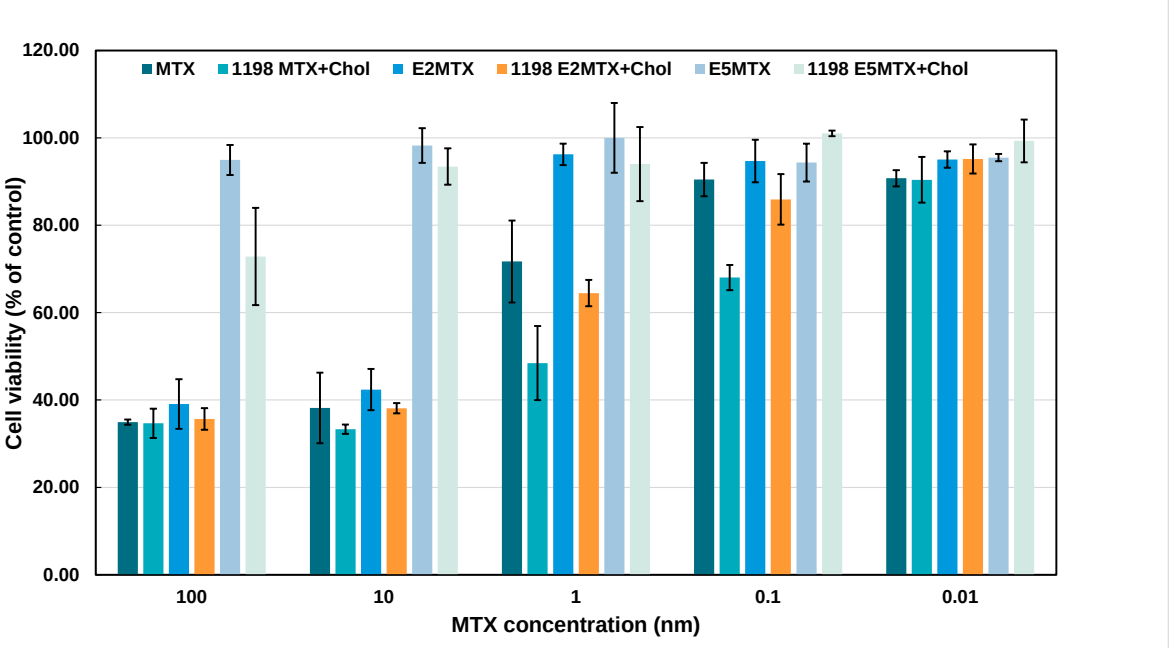

Figure 3.11. L1210 cell viability upon treatment with free MTX and their analogs compared to their formulation with 1198 + Chol. Experiment performed by Mina Yazdi (PhD student at LMU Pharmaceutical Biotechnology).

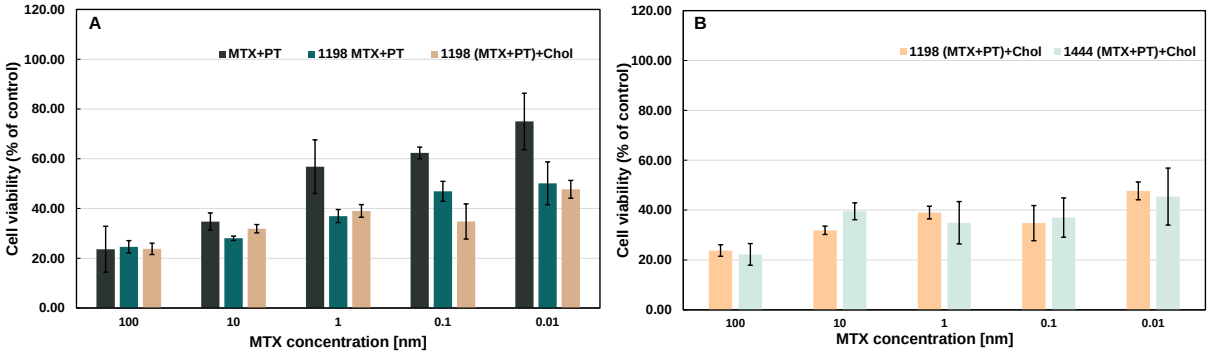

Figure 3.12. L1210 cell viability upon treatment with (A) MTX+PT, 1198 (MTX+PT) and 1198 (MTX+PT) + Chol for 48h; (B) L1210 cell viability upon treatment with 1198 (MTX+PT) and 1444 (MTX+PT) with the addition of Chol for 48h. Experiment performed by Mina Yazdi (PhD student at LMU Pharmaceutical Biotechnology).

Shielding and directing polyplexes specifically towards the tumor by introducing a specific targeting molecule or peptide are essential for targeted chemotherapy. The cationic oligomers can be post-modified with PEG reagents comprising a targeting domain. For this study, the 1198 MTX nanomicelles were modified with bisDBCO-PEG24, bisDBCO- PEG24- FolA, and bisDBCO- PEG24- E4FolA reagents, and the particle properties were determined by DLS and zeta potential measurements. The ratio of PEG reagents to the azido group at the N-terminus of each oligomer was screened, and the 0.25 eq was considered for post-modification of polyplexes with shielding and targeting agents. At this ratio, good particles formed without much agglomeration and precipitation (**Figure 3.13**). Compared to the nonmodified polyplexes, the modified polyplexes get larger than 150 nm in size, and the zeta potential was decreased from 30 mV to 20mV by the shielding effect of PEGylation. The addition of cholesterol in the 1198 polyplexes modified ligands does not significantly change the particle size or zeta potential. The efficiency of the 1198 (MTX+PT) nanomicelle complexes including optionally cholesterol and ligand modifications were determined by MTT assay.

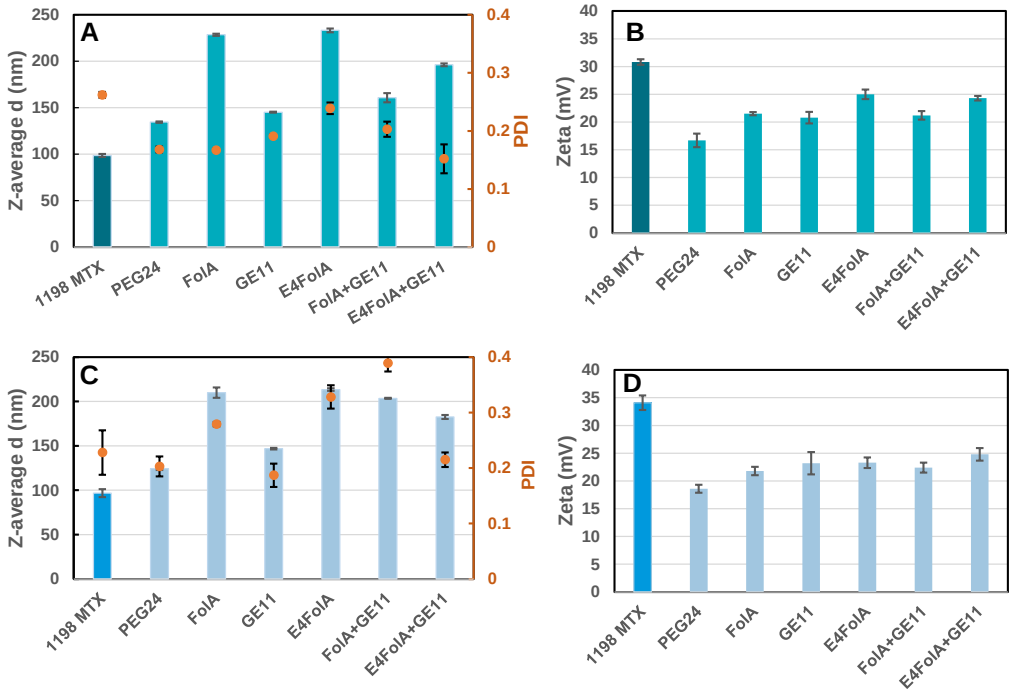

Figure 3.13. Particle size of 1198 MTX nanomicelles (A) without cholesterol and (C) with cholesterol and zeta potential (B) without cholesterol and (D) with cholesterol modified with different PEG reagents. The 0.25 equivalent of PEG reagents to 1198 was used for the post-modification.

L1210 cells were treated with modified and unmodified 1198 (MTX+PT) for 48 h. We can see that modified 1198 (MTX+PT) particles show therapeutic efficiency compared to unmodified polyplexes. Although, there is not much different targeting efficiency between FolA and glutamate FolA (E4FolA) *in vitro*, the tumor selective effect of targeting polyplexes might be promising (**Figure 3.14**).

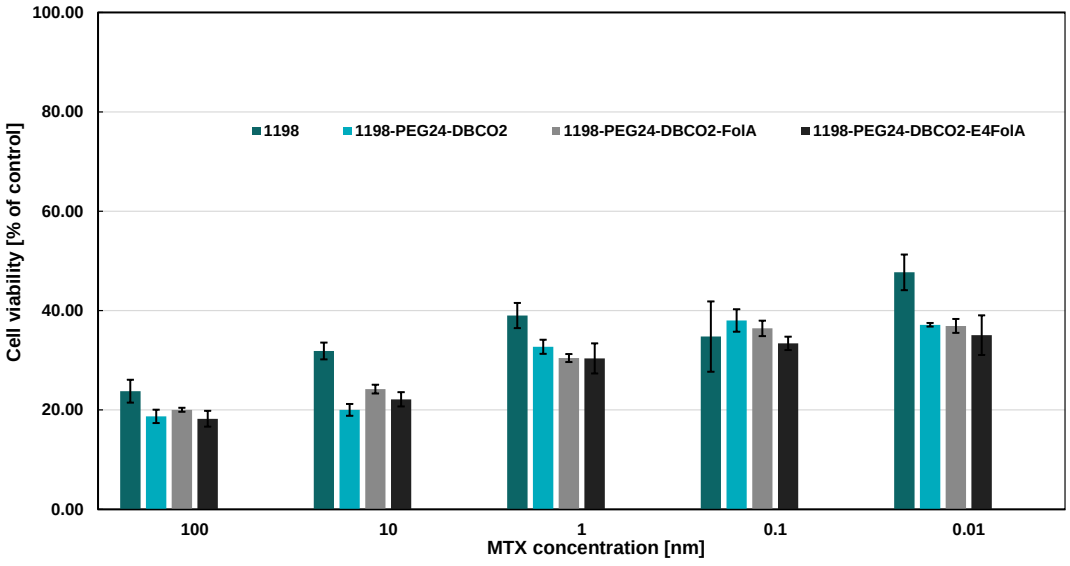

Figure 3.14. L1210 cell viability upon treatment with targeting polyplexes (1198 encapsulating MTX and PT) compared to unmodified polyplexes (non) with cholesterol for 48 h. Experiment performed by Mina Yazdi (PhD student at LMU Pharmaceutical Biotechnology).

3.5 Conclusions

For a successful combination drug delivery by artificial vectors, these carriers must display several functionalities to increase their efficiency and reduce the risk for chemoresistance. In the current chapter, the novel tubulin-binding drug Pretubulysin and polyglutamylated methotrexate were encapsulated with a cationic carrier with several significant domains. To reach the target site, the folate receptor targeting ligand FolA were modified onto the nanomicelles. For the carriers and PEGylated ligands, solid-phase synthesis (SPS) was utilized.

The ratio of 1198 to MTX was optimized. The polyplexes at a 3:1 ratio is 100 nm in size and stable after a long time of incubation at different temperatures. The E2 and E5MTX can also be encapsulated in 1198 or 1444 to form a good particle with 100-150 nm in size. The MTX incorporation efficiency of the polyplexes is 80 % to 90 %. We could see that the stability of the E2- and E5- MTX polyplexes increased, especially the polyplexes with cholesterol incubated in a different medium. Also, the 1444 polyplexes with cholesterol show less drug release than the 1198 polyplexes. 1198 MTX polyplexes with or without cholesterol show more efficiency in cell killing than the free drug. 1444 MTX polyplexes showed similar efficiency as 1198.

The increased tumor cell killing effects of 1198 MTX+PT polyplexes were higher than the free drug solution and slightly higher than the polyplexes without cholesterol. The effect could be seen in L1210 cells. The drug incorporation efficiency of the 1198 polyplexes is high, around 80 % of MTX and 65 % of PT, the polyplexes with the cholesterol show more drug encapsulation.

The cell-killing effects of the polyplexes can be increased with the ligand modification E4FolA and FolA compared to the non-modified ones. Especially the efficiency can be seen after higher incubation time such as 72h.

4 Polymeric carriers for nucleic acid delivery: current designs and future directions

This chapter was adapted from: Lun Peng and Ernst Wagner. Polymeric Carriers for Nucleic Acid Delivery: Current Designs and Future Directions. Biomacromolecules 2019, 20, 10, 3613–3626.

Abstract:

Within the last two decades, a series of novel therapeutic nucleic acids entered research and clinical valuation. Their differences both in biophysical properties as well as in mode and site of biological action provide polymer-based carriers with new delivery challenges. Recent tailor-made designs of polymeric carriers are reviewed that were optimized for nucleic acid cargos such as plasmid DNA, siRNA, and micro RNA, mRNA, or genome-modifying nucleic acids. The specific requirements for the various therapeutic cargos are discussed. Future directions include dynamic bioresponsive polymers as components of nanomachines, multifunctional sequence-defined carriers for evolution-based selective optimization, and organic−inorganic multicomponent nanoassemblies.

4.1 Introduction

Polymeric carriers have been explored for nucleic acid delivery for over five decades,[108, 152-155] with initial application in transfections for molecular virology and genetic engineering, followed by the development of therapeutic nucleic acid formulations. Initially, nonviral gene therapy focused on DNA-based gene transfer, immunostimulatory oligonucleotides, and gene inhibition by antisense oligonucleotides or ribozymes. Since the new millennium, the field has been enriched by a series of novel therapeutic nucleic acid entities entering research and clinical evaluation. These include small interfering RNA (siRNA) and micro-RNA in various variations and chemical modifications, stabilized mRNA, splicing-modifying oligonucleotides, or single guide RNA (sgRNA) for genome-modification. Here we illustrate current efforts to meet the delivery requirements with recent examples of polymer design. We highlight the challenges and bottlenecks, which can be different for the different therapeutic nucleic acid cargos,[156-160] based on their different biophysical characteristics as well as their cellular site and mode of action.

4.2 Recent designs

4.2.1 Different nucleic acid cargos demand different delivery solutions

Plasmid DNA (pDNA) and CRISPR Cas9/sgRNA need to act in the cellular nucleus, whereas siRNA, micro-RNA, or mRNA act in the cytosol. siRNA and microRNA are rather small (~21−25 bp) nucleic acid molecules which may limit stability of purely electrostatic polyelectrolyte complexes. pDNA and mRNA are larger nucleic acid materials, where compaction into smaller nano-sized structures is important in the initial delivery process, whereas in the later phase the release in the proper compartments as intact materials accessible for functional conversion by transcription or translation, respectively, is critical. For medium-sized single guide RNA, proper biochemical interaction with the Cas9 protein is essential for the genome editing function. Polymer libraries such as generated from poly(amine-co-esters) (PACE;[161] **Scheme 4.1 A**) or poly(2-ethyl-2-oxazoline)/poly (ethylene imine) copolymers (PEtOx-PEI)[162] (**Scheme 4.1 B**) have been screened for different nucleic acid cargos; it was found that different members of each library were most effective for the different cargos. For example, Blakney et al. synthesized and screened a library of poly(2-ethyl-2-oxazoline)/poly (ethylene imine) copolymers with varying molar mass and charge densities for polyplex transfection efficiency by different nucleic acids. The optimal copolymer molar mass and charge density (%) was found as 83 kDa/ 100 %, 72 kDa/ 100 %, and 45 kDa/ 80 % for pDNA, RepRNA, and mRNA, respectively.[162]

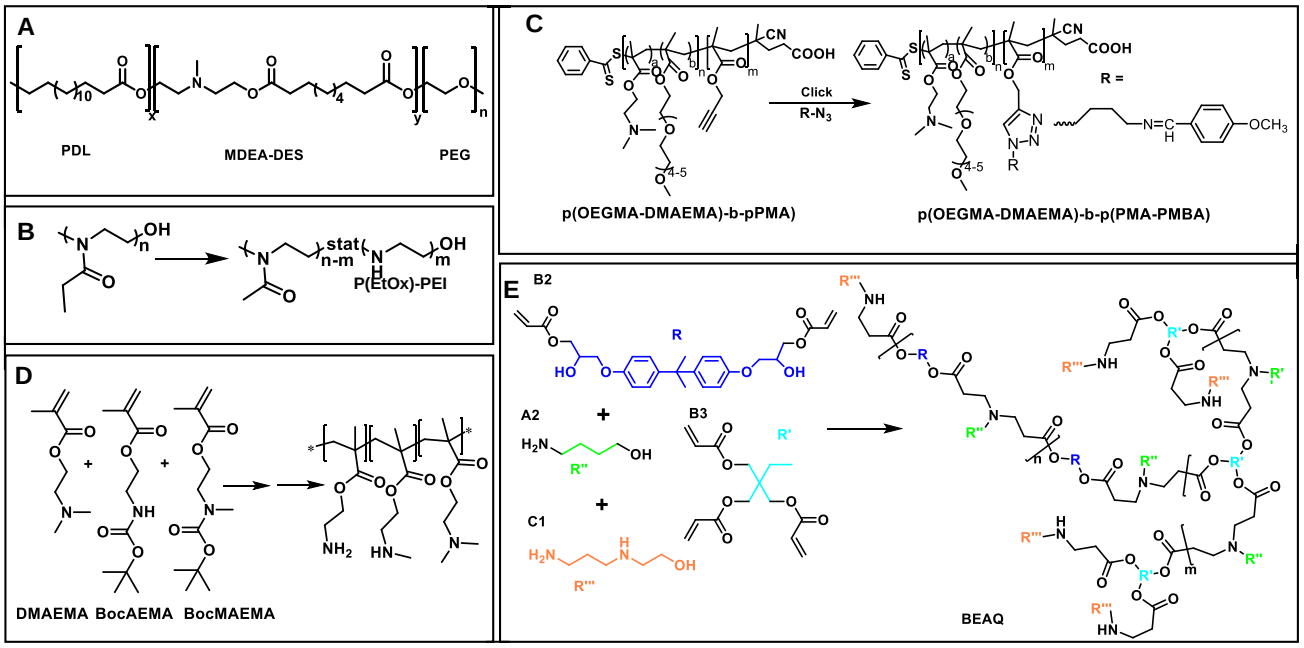

Scheme 4.1. Schematic Illustration of Different Polymers for Nucleic Acid Delivery. (A)

Representative PACE chemical structure.[161] (B) Synthesis of PEtOx-PEI statistical copolymer.[162] (C) p(PMA−PMBA)-b-(p(OEGMADMAEMA).[174] (D) Polymethacrylate bearing primary, secondary, and tertiary amino groups.36 (E) BEAQ quadpolymer (A2 + B2/B3 + C1).[183]

4.2.2 DNA based gene transfer

DNA requires compaction into suitable size for systemic circulation with proper surface shielding, intracellular uptake by endocytosis, crossing of endosomal vesicle barrier, and intranuclear delivery. Only sub-50 nm DNA/PEI polyplexes were observed in a *Xenopus* oocyte system to enter across the nuclear pore complex without compromising the integrity of the nuclear envelope.[163] Delivery of minicircle DNA, which formed small sub-50 nm polyplexes, resulted in higher and cell-cycle independent gene transfer than analogs plasmid DNA (pDNA) polyplexes.[164] On the one hand, instability of PEI polyplexes *in vivo* after systemic administration had been identified as a critical concern.[165, 166] On the other hand, stable nanoparticle characteristics can be disadvantageous inside the cell, because they may prevent nuclear entry (if nanoparticles are too large) and also accessibility for transcription.[167] For example, 22 kDa linear PEI forming less stable DNA polyplexes than 25 kDa branched PEI mediates the higher gene expression and less cell-cycle dependence.[168-170] Histidinylation of linear PEI further improved endosomal escape and cytosolic unpackaging of delivered DNA, which would improve its transport toward and into the nucleus.[159] Nuclear uptake is still a not well-understood barrier, also depending on aspects of cell type and cell division.[158] In a quantitative study by flow cytometry, only 0.1 % of added poly(β-amino ester)/DNA polyplexes was taken up by human brain cancer cells, but 12 % of internalized DNA successfully entered the nucleus.[171] A recent screen of inhibitors of histone-modifying enzymes identified compounds which enhance polyplex-mediated gene expression.[172]

Several recent polymeric strategies shed light on the “polyplex dilemma” in delivery and provide directions for overcoming the bottleneck. For example, incorporated PEG blocks in polylysine block polymers were found to significantly affect DNA condensation, including effects on nanoparticle shape and transcriptional availability.[173] More extended rod-shaped nanoparticles mediated higher gene expression efficiency in a cell-free system than globular shaped nanoparticles. Related work, based on ligand-targeted and PEG shielded pDNA polyplexes, showed potent c-Met receptor-targeted hepatoma or prostate cancer transfection *in vitro* despite limited DNA compaction; however, *in vivo* tumor-targeted delivery of a luciferase marker gene only was

successful with slightly modified, better compacted bioreversibly cross-linked polyplexes.[133] These finding were confirmed using a theragnostic antitumoral gene (sodium iodide symporter, NIS) in the same subcutaneous hepatoma model[174] or using IL6-receptor-targeted antitumoral ING4 pidan polyplexes targeting orthotopic glioma in mice (**Figure 4.1**).[134]

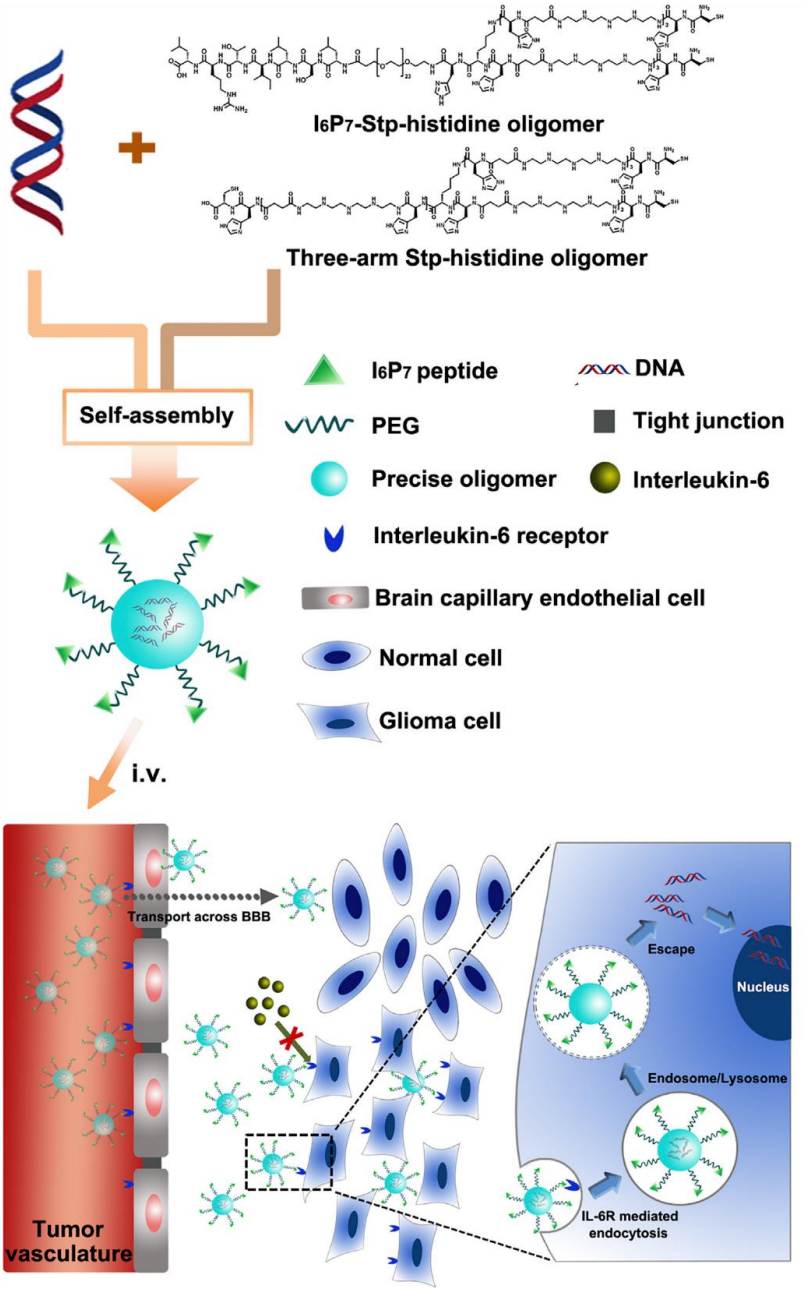

Figure 4.1. Formation of I6P7 peptide-Stp-His/DNA nanoparticles and delivery process *in vivo*. Reprinted with permissions from Wang et al.[134] Copyright 2017 American Society of Gene and Cell Therapy.

To address the polyplex dilemma of suboptimum stability in the extracellular environment and insufficient intracellular DNA release of polycationic carriers, Pun and co-workers reported the design of a pH-sensitive polymer, poly(oligo-(ethylene glycol)

monomethyl ether methacrylate)-co-poly(2- (dimethylamino) ethyl methacrylate)-block-poly(propargyl methacrylate-graft-propyl- (4-methoxy-benzylidene) -amine) (p(PMA−PMBA) -b-(p(OEGMA- DMAEMA), see **Scheme 4.1 C**, for successful *in vitro* and *in vivo* gene transfer.[175] The hydrophobic p(PMA−PMBA) domain significantly enhanced the polyplex stability under physiological extracellular condition, but undergoes an acid-triggered hydrophilic transition within endosomes through the cleavage of benzoic imines, thus, allowing the release of nucleic acid cargo due to the loss of hydrophobic functionalization.

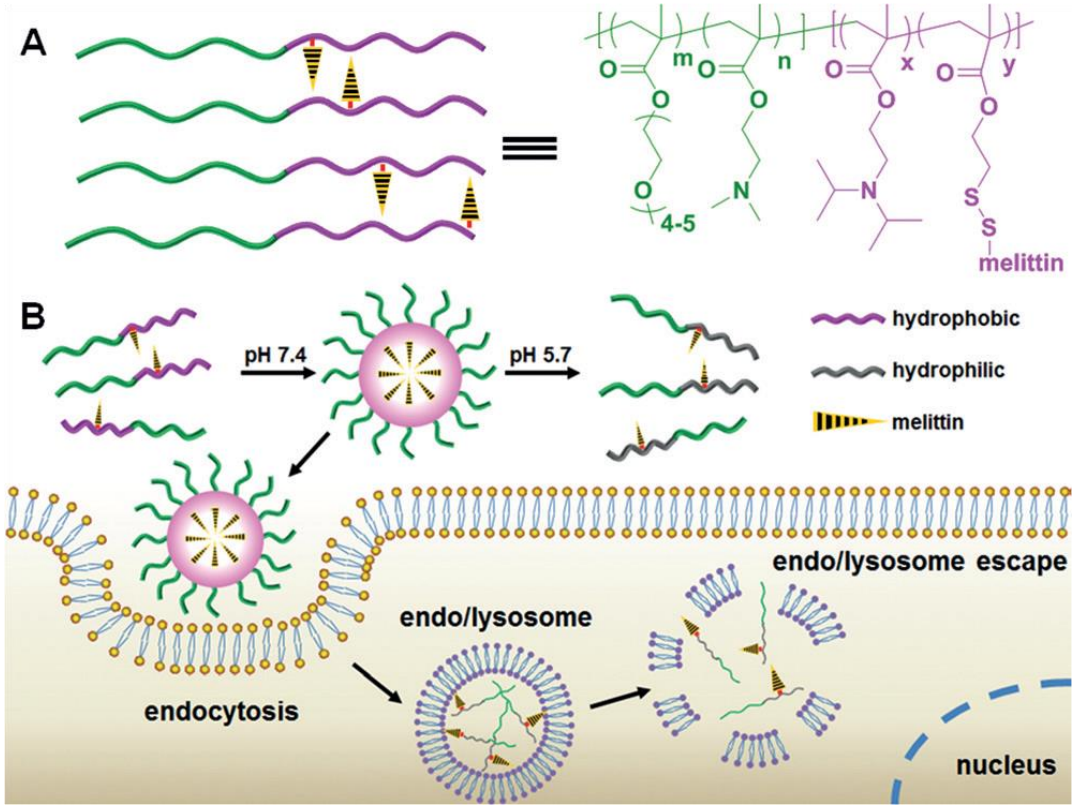

Figure 4.2. (A) Structure of VIPER. (B) Melittin coupled in VIPER next to the hydrophobic DIPA domain is exposed upon endosomal acidification and solubilization of the DIPA domain, which promotes endosome escape into the cytosol. Reproduced from Cheng et al.[124] with permissions of John Wiley and Sons. Copyright 2016 Wiley-VCH Verlag GmbH & Co. KGaA, Weinheim.

Escape of internalized polyplexes out of the endosome is a known critical bottleneck within the delivery process. Incorporation of endosomolytic agents such as whole virus particles[176] or lytic peptides[177-179] into nanoagents had been pursued to overcome this limitation. Cheng et al. optimized methacrylate copolymers as transfection carriers by designing a virus-inspired polymer for endosomal release (VIPER, **Figure 4.2**).[125] VIPER is a block copolymer based on four different monomers. The first block is a hydrophilic copolymer of OEGMA for nanoparticle surface shielding and cationic DMAEMA block for binding and compaction of DNA. The second block is reversibly

hydrophobic, containing a pH-sensitive 2-diisopropylaminoethyl methacrylate (DIPAMA) and the pyridyl disulfide ethyl methacrylate (PDSEMA). DIPAMA provides a sharp endosomal pH phase transition from hydrophobic to hydrophilic state, thus exposing PDSEMA. The activated disulfide function of the latter unit was utilized for coupling the lytic peptide melittin which thus could be displayed in an acid-triggered fashion, promoting endosomal escape into the cell cytosol. This VIPER carrier facilitated effective gene transfer upon intratumoral administration to KB tumor-bearing mice. In subsequent work, the same research group replaced melittin with a series of other lytic peptides.[120] Peptide conjugates with highly lytic but not pH-selective peptides achieved safe and effective transfection both *in vitro* and *in vivo*. Apparently, the sharp pH-transition of VIPER compensated for potential advantages from pH-sensitive but less lytic peptides.

Another strategy of improving endosomal escape agents was reported by Duat, Kichler, and Guichard.[180, 181] Starting from the amphipathic histidine-rich peptide LAH4,[178] analogs urea-based foldamers were generated. A pH-responsive, bioreducible cell-penetrating foldamer was developed through covalent dimerization of a short (8-mer) amphipathic oligourea sequence bearing histidine-type units which mediates efficient gene transfer. Most recently, the cell-penetrating foldamer strategy was extended by conjugation to a ligand that binds cell surface expressed nucleolin, to facilitate both assemblies with DNA and mediating receptor-targeted cell entry.[181]

The group of Schubert evaluated the influence of the amino substitution pattern of linear cationic methacrylate-based transfection carriers.[182] For this purpose, they prepared a library of defined linear polymers based on (2-aminoethyl)- methacrylate (AEMA), N-methyl-(2-aminoethyl)-methacrylate (MAEMA), and N,N-dimethyl-(2-aminoethyl)-methacrylate (DMAEMA) monomers, bearing pendant primary, secondary, and tertiary amino groups (**Scheme 4.1**). In contrast to previous experiences with PEI based polyplexes, successful transfection was not affected by the buffer capacity. Polyplexes containing a high content of primary amino groups (AEMA) offered the highest transfection efficiency, whereas polyplexes bearing tertiary amino groups (DMAEMA) exhibited the lowest transfection efficiency. Further insights into the cellular uptake and release mechanisms by fluorescence and transmission electron microscopy support the theory of lipid-membrane pore formation as an effective process in endosomal release of methacrylate-based polyplexes.

Other strategies to solve the “polyplex dilemma” involve the integration of

biodegradable ester functions or disulfide bonds. To provide polyplex stability during blood circulation and high transfection ability, Barz and colleagues designed reactive triblock copolypept(o)ides.[183] These triblocks include a stealth-like polysarcosine block for efficient shielding, a hydrophobic block based on reactive disulfides for multiple cross-linking, and a cationic polylysine block for complexation of pDNA. Bifunctional aminoethylene cross-linkers were employed for simultaneous introduction of bioreversible stabilization by disulfide bond formation and endosomolytic properties of polyplexes. Upon screening cross-linkers, pDNA polyplexes were developed which transfect dendritic cells and resulted in successful immunological presentation of a model antigen.

Green and co-workers synthesized multifunctional poly(ester amine) quadpolymers (BEAQs) with well-defined branching structure via A2 + B2/B3 + C1 Michael addition reactions from small molecule acrylate and amine monomers and then end-capped with amine-containing small molecules (**Scheme 4.1**).[184] BEAQs with moderate degrees of branching were found highly effective for pDNA transfer to retinal pigment epithelial cells, exceeding potency of previously reported leading linear poly(β-amino esters). Defined structural properties including tertiary amine content correlated with transfection efficacy.

Polyplex stabilization by surface shielding is an important aspect for *in vivo* application. Ishihara and colleagues coated the surfaces of pDNA/chitosan complexes with hyaluronic acid (HA) of varying molecular masses. pDNA complexes were lyophilized and subsequently stored under defined conditions.[185] Transfection efficiencies of pDNA/chitosan/HA ternary complexes were dependent on the average size of HA; the coating with high-molecular-weight HA augmented the stability and transfection ability of polyplexes after lyophilization-rehydration. Intratumoral injection of lyophilized, rehydrated polyplexes encoding the thymidine kinase suicide gene showed a suppression of tumor growth in Huh7 tumor-bearing mice.

A frequent observation is lack of correlation between *in vitro* and *in vivo* gene transfer. The tetrafunctional block copolymer 704, consisting of four PEG/PPO blocks centered on an ethylene diamine moiety, can complex DNA but was found ineffective *in vitro*. In mice, the block copolymer was found as more effective in lung gene transfer than the well-established cationic liposomal carrier GL67A. In the newborn piglet as a larger-animal model, the 704 pDNA formulation was more than 10-fold more effective than a corresponding cationic liposomal formulation, without inducing IL-6 as inflammation

marker.[186]

4.2.3 Stabilized Messenger RNA

Delivery of mRNA, on the one hand replacing DNA-based gene expression constructs, on the other hand replacing recombinant proteins, presents a new therapeutic focus for protein replacement therapies, treatment of genetic diseases, or vaccination.[187-189] Chemical modifications of the quite labile mRNA have resulted in stabilized and less immunogenic mRNAs.[190] The novel therapeutic modality also provides novel challenges and opportunities for polymeric delivery. Dohmen and colleagues evaluated PEI-like cationic carriers. They noted that a small difference within the PEI repeat unit, introducing a methylene group into every second aminoethylene unit, resulting in aminoethylene-aminopropylene-aminoethylene sequence (**Scheme 4.2A**), strongly enhanced mRNA delivery *in vitro* and *in vivo*, in the murine liver or the porcine lungs after systemic or aerosol administration, respectively.[191] Nuhn, Zentel, and co-workers designed reductive decationizable block copolymers with disulfide-linked primary amines (**Scheme 4.2B**).[192]The cationized amines allow effective polyplex formation with mRNA and subsequent release under the reductive conditions of the cytosol.

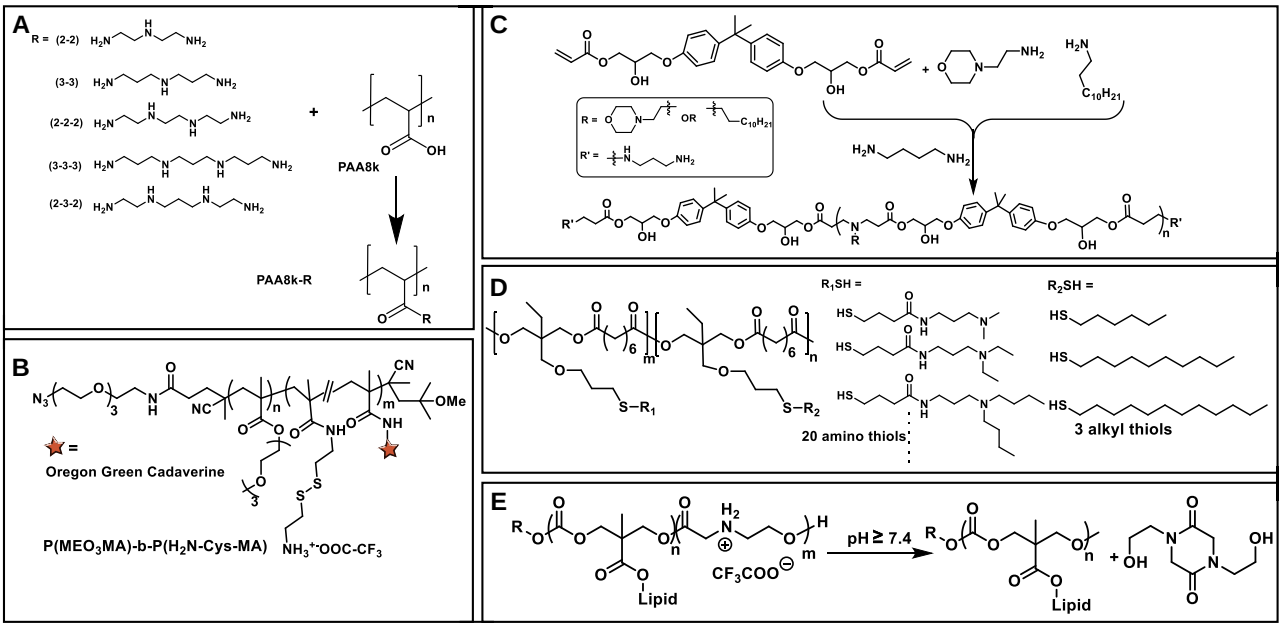

Scheme 4.2. Synthetic routes and chemical structures as carriers for stabilization and delivery of mRNA. b(A) Carriers bearing aminoethylene-aminopropylene-aminoethylene sequence.[191] (B) Reductive block polymer.[192] (C) Poly amino esters formRNA formulation.[193] (D) Modified polyester series.[194] (E) CART copolymer and its physiological degradation.[197-200]

Formulations for systemic delivery of mRNA to the lung were developed by several researchers.[193-195] Kaczmarek et al. coformulated mRNA with poly(β-amino esters) (PBAEs, **Scheme 4.2C**) and lipid-PEG for functional delivery to the lungs after

intravenous administration in mice.[193] Optimization in terms of polymer synthesis and nanoparticle formulation strongly increased potency; using genetically engineered Cre reporter mice, they demonstrate functional mRNA delivery to both the lung endothelium and pulmonary immune cells.[194] Siegwart and collaborators generated a combinatorial 480-member polyester library based on poly(trimethylolpropane allyl ether-co-suberoyl chloride (**Scheme 4.2D**). The mRNA polyplex nanoparticles (NPs) stabilized with 5 % pluronic F127 enabled upon intravenous application luciferase marker expression predominantly in the lungs of mice.[195] A new ionizable amino-polyester library was synthesized by Kowalski et al.[196] via ring-opening polymerization of lactones with tertiary amino-alcohols and used for formulating mRNA into lipid nanoparticles (LNPs). Aiming at tissue and cell type selective delivery, mRNA LNPs were identified that can preferentially home to and express in lung endothelium, liver hepatocytes, and splenic antigen presenting cells.

For systemic delivery of mRNA to tumors, Dong and colleagues formed polyplexes with poly (N-isopropylacryla- mide) (PNIPAM)-polylysine (PLys)-thiol and cRGD-PEG-PLys-thiol.[197] Incorporation of the thermoresponsive PNIPAM and the redox-responsive disulfide linkages were supposed to stabilize and protect mRNA during systemic circulation. cRGD ligand was attached for receptor-targeted mRNA transfer. Intravenous administration of the formulation demonstrated improved accumulation in subcutaneous U87 tumors and expression of luciferase or eGFP marker mRNAs.

Waymouth and colleagues developed a novel tunable class of synthetic biodegradable nucleic acid delivery materials: amphiphilic charge-altering releasable transporters (CARTs).[198-201] CART co-oligomers (**Scheme 4.2E**) were synthesized in two steps via sequential organocatalytic ring-opening polymerization of lipid-containing cyclic carbonate monomers and morpholinone monomers. Efficient carriers for mRNA were identified from combinatorial libraries of such transporters with varied lipid domains. The transporters are highly degradable; initially the oligo (α-amino ester) cationic block mediates electrostatic stabilization of mRNA nano-complexes, but subsequently degrades by charge-neutralizing intramolecular rearrangement, leading to intracellular release of mRNA. This release appears as essential requirement for transcriptional accessibility and functionality of mRNA. The lead lipid CART combination showed enhanced lymphocyte transfection in primary T cells and *in vivo* in mice.[199] For example, systemic antitumor immune responses were generated upon intratumoral injection of the CART/Ox40L-, CD80-, and CD86-encoding mRNA complexes, curing tumors.[200] Lipid variations of the CARTs substantially impacted the delivery efficiency of pDNA,

with oleyl- and linoleyl-based CARTs showing enhanced performance.[201]

4.2.4 siRNA and MicroRNA for RNA Interference

Patisiran (Onpattro) is the first siRNA drug formulation which was approved by FDA and EMA and reached the medical market. It contains siRNA directed against TTR mRNA in a PEGylated lipid nanoparticle (PEG-LNP) formulation.[202] Gene silencing is targeted to liver hepatocytes via apolipoprotein which incorporates into the LNP during circulation in blood. Gene silencing to other organs is far less effective. First tumor-targeted siRNA polyplexes evaluated in cancer patients were based on transferrin-coated nanoparticles.[49]

siRNA is much smaller than pDNA or mRNA, providing far fewer negative charges for electrostatic polyplex stabilization. One alternative to overcome this problem is covalent conjugation with polymers.[203, 204] A single chemical entity (SCE) siRNA, GalNac-PEG siRNA for hepatocyte targeting, is currently being tested in human clinical trials.[205, 206] Application of this strategy, which targets the highly abundant asialoglycoprotein receptor, to receptor targeting beyond the liver using an alternative ligand has not been successful thus far.

Improved polyplex stability requires significant changes in polymer structure and hydrophobic modifications. For example, Ling Peng and co-workers optimized dendrimers for siRNA delivery via self-organizing the hydrophilic and hydrophobic components.[207] Merkel and Pun applied the VIPER polymer system bearing polycation and pH sensitive segments previously established for pDNA delivery for *in vivo* delivery of siRNA to the lung.[208] The excellent DNA transfection agent PEI is rather inefficient in siRNA delivery and substantially cytotoxic; chemical modifications can enhance the ability of self-assembly and stabilization of siRNA nanoparticles. For instance, grafting aromatic domains such as tyrosine onto PEI does not trigger difference in endosomal buffering capability, but higher bioresponsiveness and stability in delivery. Zuber and collaborators demonstrated that PEI modified with tyrosine or pyridylthiourea (πPEI) enhances the efficiency of siRNA mediated gene silencing.[209-211] Ewe and Aigner extended the strategy to design tyrosine-modified nontoxic, low molecular weight polyethylenimine (P10Y) for efficient siRNA delivery *in vitro* and *in vivo*.[212] Tumor-inhibitory effects were observed in a melanoma xenograft mouse model upon systemic application of survivin siRNA polyplexes, indicating therapeutic efficacy in the absence of adverse effects such as hepatotoxicity, immunostimulation, or weight loss. Tyrosine trimers (Y3) were also utilized as stabilizing components via hydrophobic or aromatic

π–π stacking interactions in siRNA polyplexes based on sequence-defined lipo-oligomers.[213] For that purpose, artificial amino acids had been designed that contain the repeated aminoethylene motif of PEI. Different fatty acids were incorporated for nanomicelle stabilization.[130] Combined with integrated tyrosine trimers, these aminoethylene-based artificial lipopeptides displayed good biocompatibility and mediated gene anti-EG5 antitumoral gene silencing *in vitro* and *in vivo* in mouse tumor models.[35, 214] It is worth to be mentioned that tyrosine oligomers were also applied in form of PEG-pTyr (DP~ 30) for receptor-targeted polymerosomes for antitumoral drug delivery.[144]

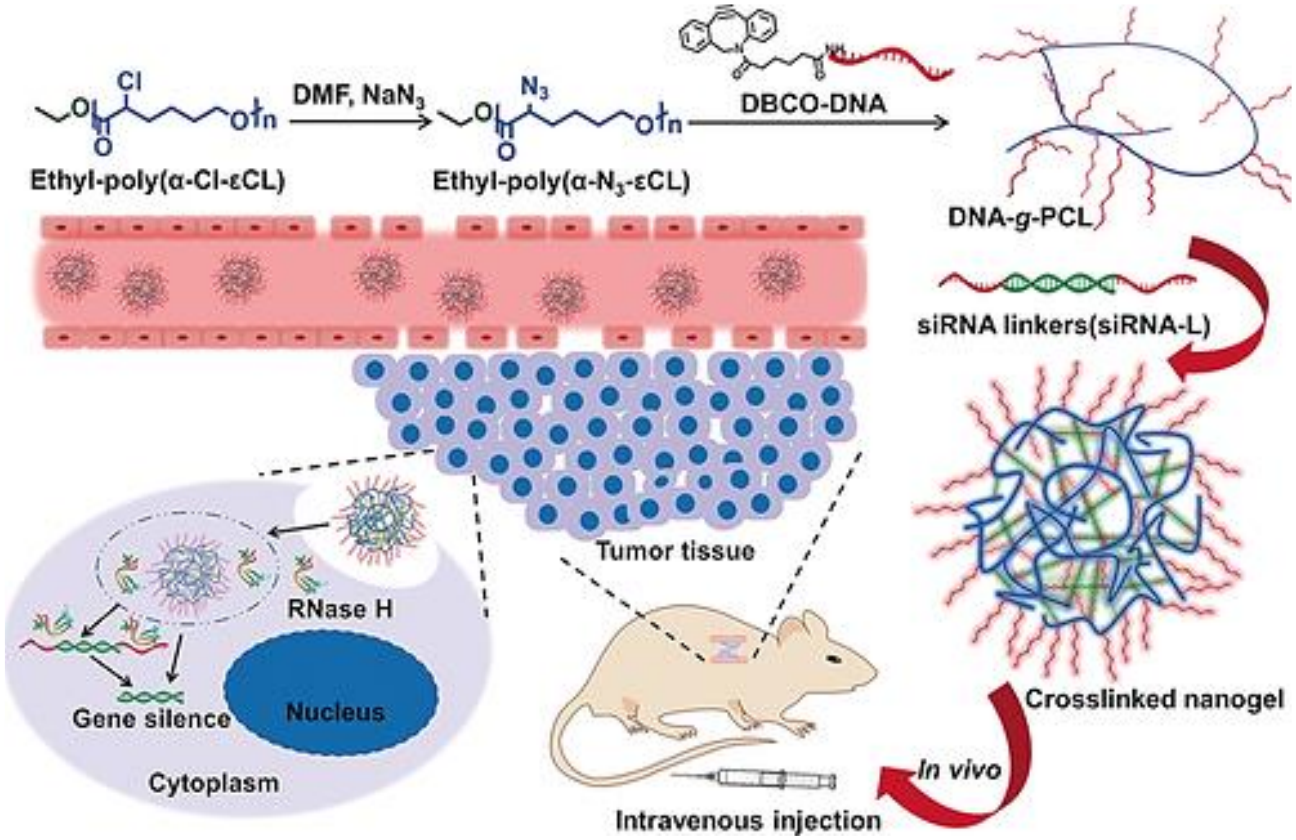

Figure 4.3. Schematic representation of DNA-grafted-PCL brushes forming with siRNA-L (containing RNA linkers for DNA hybridization) crosslinked nanogels for siRNA delivery *in vivo*. Reproduced with permissions of John Wiley and Sons from Ding et al.[215] Copyright 2018 Wiley-VCH Verlag GmbH & Co. KGaA, Weinheim.

As alternative strategy to overcome the limited stability of electrostatically formed siRNA polyplexes, Hammond and colleagues applied a polymeric form of siRNA, termed periodic short hairpin RNA (p-shRNA). p-shRNA is synthesized by rolling circle transcription (RCT) of DNA and, due to its higher charge valency, can form more stable complexes than monomeric siRNA. Biodegradable PBAE polymers were optimized containing hydrophobic domains and stabilizing PEG domains.[215] Silencing STAT3 in the B16F10 mouse melanoma model significantly prolonged survival, demonstrating

therapeutic applicability. Ding et al. applied conjugated siRNA both as antitumoral therapeutic agent and as stabilizing cross-linker.[216] For this purpose, DNA-grafted-polycaprolactone (PCL) brushes were specifically hybridized with complementary single-stranded overhangs at both ends of the siRNA, resulting in self-assembly into cross-linked nanogels of sizes tunable between 80 nm up to micrometer range (**Figure 4.3**). Intravenous administration of anti-PLK1 siRNA nanogels resulted in growth reduction of MDA-MB231 breast carcinoma in the mouse xenograft.

The peptide angiopep 2 (ANG) has high affinity to low-density lipoprotein-receptor-related protein (LRP), which is overexpressed both on surface of the brain capillary endothelial cells (BCECs) and glioma cells. Consistently, ANG should be able to pass the blood−brain barrier (BBB) and deliver into brain tumor cells. ANG−PEG-containing peptide-like lipopolymers were applied to siRNA lipopolyplex formation;[217] intravenous administration resulted in delivery into orthotopic glioblastomas in mice and tumoral BAG3 gene silencing. Zhong and co-workers designed ANG-decorated chimaeric polymersomes (ANG-CPs) to package siRNA in their interior (**Figure 4.4A**). These ANG-CPs were found to effectively permeate a BCEC monolayer as *in vitro* BBB model, transport siRNA into the cytosol of glioblastoma cells via the LRP-1- mediated pathway, releasing the siRNA payload within the reductive environment in the cytosol, and silencing PLK1 mRNA. The ANG-PEG-CP-siRNA polymersomes showed a prolonged circulation time and accumulated in glioblastoma. siPLK1 induced a strong antiglioblastoma effect and significantly improved the survival time of glioblastoma carrying mice.[218]

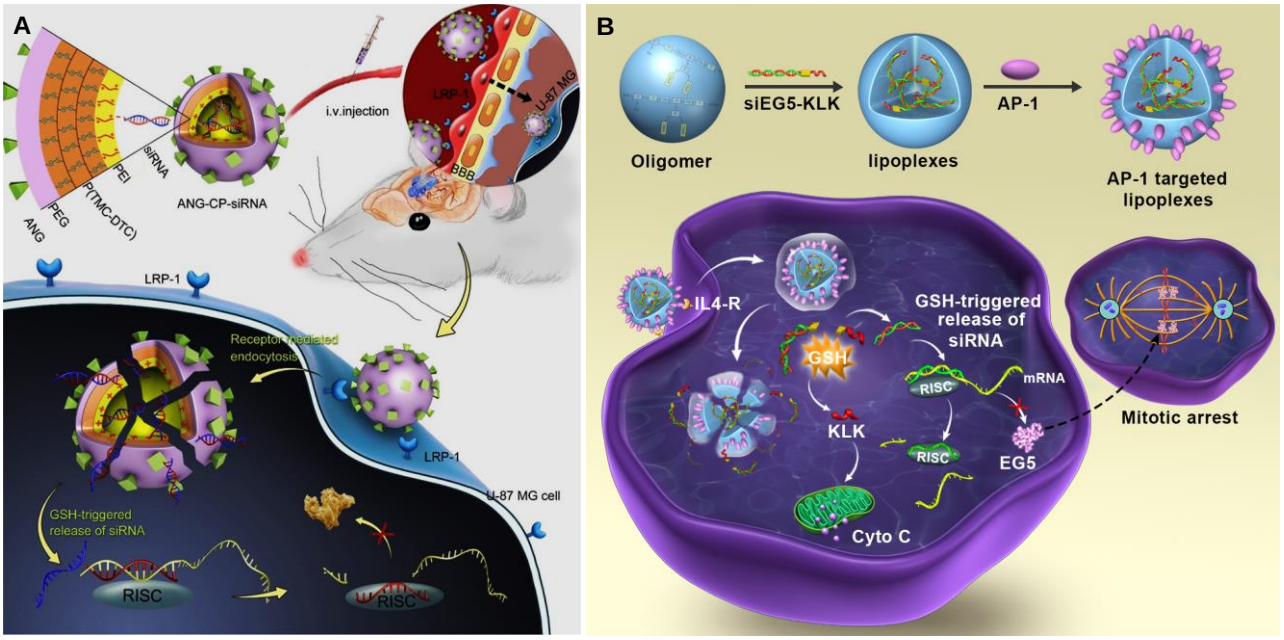

Figure 4.4. (A) Illustration of improved RNAi therapy for human glioblastoma *in vivo* using

siRNA-loaded nontoxic brain-targeting chimaeric polymersomes (ANG-CP-siRNA). Reprinted with permission from Shi et al.,[218] Copyright 2018 Elsevier. (B) siEG5-KLK peptide conjugates into IL4-receptor-targeted lipopolyplexes resulted in enhanced apoptotic tumor cell killing. Reprinted with permission from John Wiley and Sons from Luo et al.[219] Copyright 2019 Wiley-VCH Verlag GmbH & Co. KGaA, Weinheim.

Antitumoral siRNA has been combined with other antitumoral active components; for example, Luo et al.[219] synthesized bioreducible covalent conjugates of EG5 siRNA with mitochondria-interacting peptide KLK (**Figure 4.4B**). Formulating siEG5-KLK peptide conjugates into IL4-receptor-targeted lipopolyplexes resulted in enhanced apoptotic tumor cell killing due to the combined effect of mitotic arrest by EG5 gene silencing and mitochondrial membrane disruption by KLK.

Almost 2000 micro RNAs (miRs) are naturally expressed in our body and regulate the expression of our genome at the post-transcriptional level. They participate in the physiological cellular processes, but also have a decisive impact under pathophysiological conditions. For example, loss of tumor suppressor miRs and activation of onco-miRs are key events in tumor progression. Therefore, therapeutic treatments by delivery of suppressor miRs or delivery of antionco-miRs (antagomirs) have been considered.[220, 221] In early days, Aigner and colleagues applied PEI polyplexes for miR-145 and miR-33 delivery which exhibited antitumor effects in colon carcinoma.[222] Müller et al. designed miR-200c lipopolyplexes based on cationizable T-shaped lipo-oligoaminoamines.[41] The core nanoparticles were surface-modified with a PEG shield exposing peptide GE11 as artificial EGF receptor targeting ligand; miR-200c delivery to EGFR-positive breast cancer cells resulted in reduced tumor cell proliferation, reduced cell migration, and enhanced chemosensitivity. Green and co-workers optimized bioreducible PBAE polyplexes for delivery of cancer stem cell (CSC)-inhibiting miRNAs into gliomas. Polyplexes containing multiplexed CSC-inhibiting miRNAs inhibited glioblastoma growth; intratumoral infusion of miR-148a and miR-296-5p polyplexes into orthotopic xenografts prolonged survival of mice.[223]

In summary, for polymer-mediated siRNA and miRNA delivery a stabilized extracellular delivery, efficient cellular uptake, and endosomal release into the cytosol appear as key measures. However, research can be full of surprises; recently hyaluronic acid was found to stabilize siRNA via hydrogen bondings and hydrophobic interactions, and the negatively charged HA mediated siRNA delivery into CD44-positive human osteosarcoma cells and in mesenchymal stromal cells (hMSCs), resulting in

approximately 60 % gene knockdown in both cell types without any toxicity.[224] The *in vivo* translation of these encouraging results remains to be demonstrated.

4.2.5 Single guide RNA for CRISPR Cas9-mediated genome Modification

A series of highly precise genome-modifying nucleases, such as zinc finger nucleases, TALENs, or CRISPR Cas9 present new powerful tools for genome repair or genetic modification of cells. Intracellular delivery has been achieved in form of DNA[225] or mRNA[226] based expression constructs, as proteins or (in case of CRISPR Cas9) as protein/sgRNA ribonucleoprotein formulations.[227, 228] For example, Huang and colleagues used PEI β-cyclodextrin for efficient delivery of plasmid DNA encoding Cas9 and sgRNA and demonstrated efficient genome editing at two targeted genome loci, namely, hemoglobin subunit beta and rhomboid 5 homologue 1.[225] Green and co-workers optimized a series of reducible branched ester-amine quadpolymers (rBEAQs, **Figure 4.5**) for their ability to coencapsulate and deliver Cas9 DNA plasmids and sgRNA.[229] Variation of rBEAQs polymer branching, reducibility, and hydrophobicity resulted in efficient Cas9 DNA and sgRNA codelivery as well as CRISPR-mediated gene editing utilizing. The group of Siegwart designed zwitterionic amino lipids nanoparticles (ZNLs) for combined delivery of Cas9 mRNA and sgRNAs.[230] Intravenous codelivery of optimized Cas9 mRNA/sgLoxP ZNLs induced expression of floxed tdTomato protein in the liver, kidneys, and lungs of transgenic mice. Polymers have also been applied for direct delivery of the Cas9/sgRNA ribonucleoprotein complex. For example, Sun et al. formulated Cas9/sgRNA into DNA nanoclews (synthesized by rolling circle amplification) which were coated with PEI.[227]Kang et al. generated cationic polymer- conjugated Cas9 for subsequent complexation with sgRNA targeting antibiotic resistance. The formed sgRNA polyplexes were efficiently delivered into methicillin-resistant Staphylococcus aureus (MRSA), resulting in bacterial genome editing.[228] Recently, Liu et al. modified cationic PAMAM G5 dendrimers with phenylboronic acid (PBA) residues; this modification enables binding with both negatively or positively charged proteins and mediated potent cytosolic delivery of proteins. Among several examples, successful Cas9 protein/ sgRNA delivery and genome editing was demonstrated.[231]

4.3 Conclusions and future perspectives

Up to the mid of 2019, approximately 2930 gene therapy trials have been performed, with nine gene therapy products, eight oligonucleotide products, and one siRNA drug

approved by the major medical agencies. About 15 gene therapy clinical trials have reached phase 3, and numerous oligonucleotide and siRNA clinical trials the phases 2 and 3. More information on gene therapy clinical trials worldwide[232] can be obtained from the web http://www.abedia.com/wiley. Currently, the marketed oligonucleotides and siRNA are all synthetic products, often presenting chemically modified nucleic acids in many different variations. Vectors applied in gene therapy products, however, are all based on viral vectors such as retroviral or adeno-associated viral (AAV) vectors, reflecting their superior efficacy. Within cationic carriers, lipofection and LNPs have been most frequently used in clinical translation, as they benefit from a strong experience of the liposome technology field and straightforward syntheses of rather small cationic lipids. Their still lower efficacy in comparison to viruses is illustrated, for example, by the fact that even optimized LNPs deliver less than 1 % of the nucleic acid cargo into the cytosol.[233] The endosomal barrier presents a large delivery hurdle. Macromolecular carriers may combine several delivery functions in one chemical entity. In the past, polymer-based carrier development, however, faced more challenges than the far more established liposome technology; especially precise synthesis of monodisperse macromolecules, site-specific introduction of functionalities, and high-resolution macromolecule analytics were critical factors hindering clinical translation of polymeric carriers. The recent years demonstrate impressive progress in synthetic and physicochemical aspects of macromolecules and an expanded knowledge about the intracellular bottlenecks in delivery. Thus, with further refinement of polymeric carriers both in design and accurate synthesis, these may play a tremendous role in future nucleic acid therapeutics. Current development of stimuli-responsive formulations is directed toward multifunctional nanomachines, which might be supported by physical forces (such as near-infrared light, ultrasound or magnetic fields) in a remote-controlled manner. Most importantly, evolutionary algorithms will have to be developed for optimizing polymeric nanosystems for the real disease targets and target locations in the human patient.

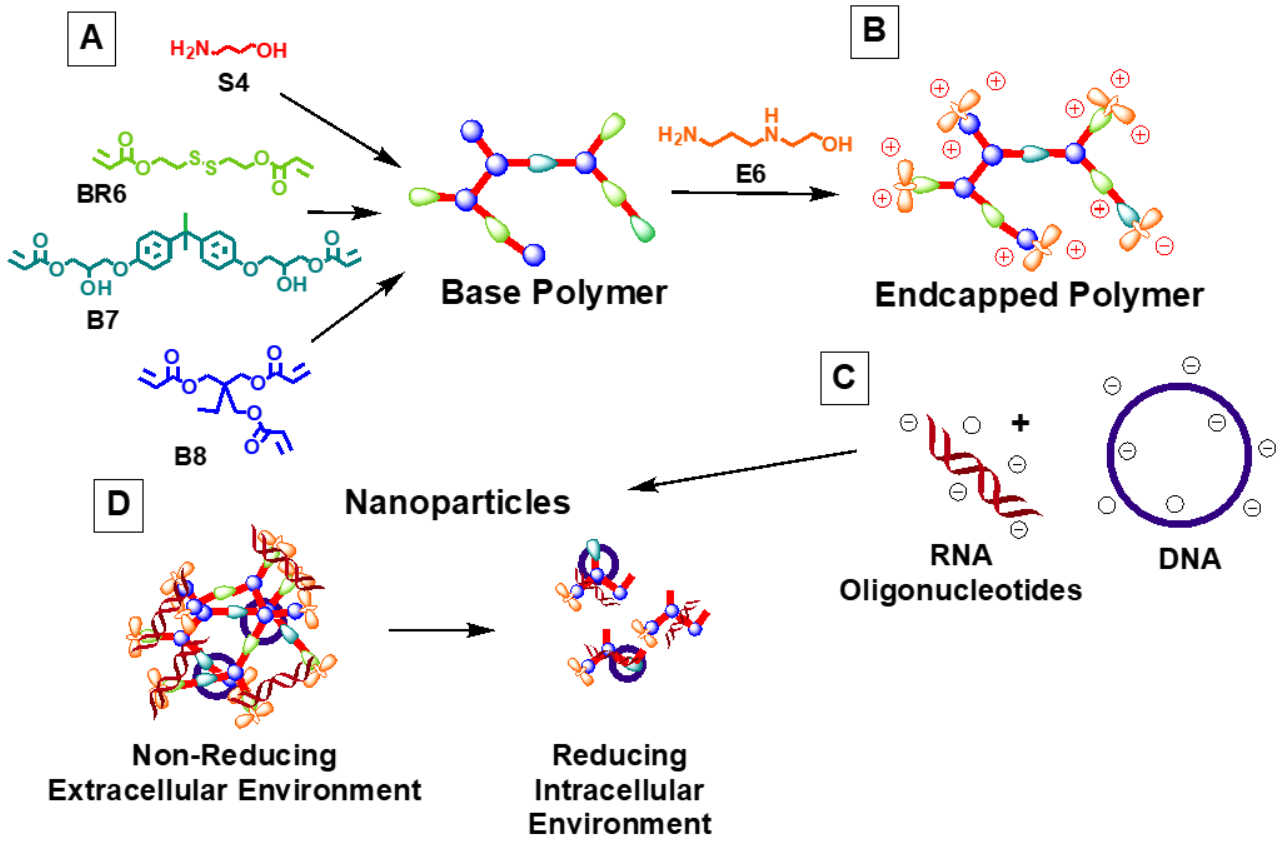

Figure 4.5. Synthetic route of rBEAQs and formation of nucleic acid nanoparticles. Reproduced with permission from Rui et al.[229] Copyright 2019 American Chemical Society.

4.3.1 Dynamic bioresponsive polymers: toward active nanomachines

As noted in the previous sections, we often face a “delivery dilemma” due to the very different biophysical requirements during the different steps of delivery. For example, nanoformulations need to be dynamic in properties, stably transporting their therapeutic cargo within the bloodstream to the target site, but effectively releasing it at the intracellular target location. As a solution for this dilemma, stimuli-response carriers have been proposed,[234-236] which can sense the subsequent different biological microenvironments and respond with changes favorable for the upcoming delivery step. Alterations in the microenvironment include concentration of protons (such as acidification in endosomal vesicles or tumor environment) or other ions and low-molecular weight substrates, differences in specific enzyme concentrations or microRNAs, or differential oxygenation and redox conditions. Scientists have programmed their nucleic acid delivery systems by incorporating appropriate sensor molecules.[119, 237] For example, endogenous miR-122 expression levels were utilized as condition for controlled release of an antagomiR and chemical inhibitor from mesoporous silica nanoparticles into the diseased cells.[238] Within polymeric delivery systems, precise bioreducible disulfide or cathepsin B cleavage sites have been

integrated into lipo-oligoaminoamides to strongly reduce residual carrier cytotoxicity after the delivery process.[239, 240] The sharp endosomal pH phase transition of pDIPAMA has been capitalized in block copolymers to trigger a timely and potentiated activity of lytic peptides for effective endosomal release (VIPER).[120, 125] This completely synthetic design actually resembles the natural endosomal lipid membrane interaction mechanism of influenza virus, where in a “spring-loaded” process a conformational change of the hemagglutinin HA2 unit relocates the amphipathic terminal fusion peptide by 10 nm from the HA interior toward the endosomal target membrane.[241, 242] It is not surprising that the impressive performance of natural viruses has inspired many scientists to generate dynamic nanoagents mimicking viruses in delivery functions but being based on completely different synthetic building blocks.[243, 244]

Neither natural nor current synthetic viruses present autonomous, smart, and active nanoagents. Smart scientists need to design the nanoagent components to undergo preprogrammed dynamic changes as part of the delivery process. Current agents are passive and reactive. Nevertheless, remote control is possible by external physical triggers such as light, ultrasound, electric or magnetic fields.[235, 245-248] This, on the one hand, may trigger location-selective chemical and structural changes, on the other hand, this may provide nanoagents with energy and convert them into nanomachines.[249-251] As a recent example, refined plasmonic Janus nanopens were made consisting of a gold nanoparticle attached to a dielectric alumina shaft.[248] Balancing optical and thermophoretic forces allowed Janus nanopens to be positioned on the surface of cells. The subsequent optical injection into cells involves strong heating of the plasmonic gold side, but not the alumina shaft, which allowed the functionalization with sensitive payloads like DNA and, hence, the spatially controlled injection of genetic material.

In summary, there is still a lot of space for refined stimuli-responsive sensors and effective spacio-temporal integration into dynamic carrier systems. Future development from purely passive nanoagents toward remote-controlled and active nanomachines can be expected.

4.3.2 Sequence defined multifunctional polymers: optimizing by artificial evolution

As outlined above, viruses present perfect models of bioresponsive dynamic nanoagents. One basis of their success is the definition of all of their multifunctional nucleic acid and protein components as sequences; these sequences were optimized by natural evolution. Conceptually, designing polymers as a precise sequence of

artificial subunits would enable (i) the design of multifunctional polymers with high precision and (ii) their optimization as delivery carrier by artificial evolution processes. Such strategies may yield highly functional carriers, devoid of the immunogenicity problem that natural viruses and viral proteins face upon their host interaction. Sequence-defined polymers[124, 127, 128] can be prepared with high precision by solid-phase synthesis (SPS). For example, Schaffert et al. designed peptide-like polyaminoamides based on artificial oligoamino acids.[129] By generating polymers with a defined structure in various topologies (for example, linear, branched three-arm or four-arms, i-shapes, T-shapes, u-shapes) clear-cut structure− activity relations could be made.[129-131, 252] Upon further optimization, including SPS integration of shielding, targeting, and other functional units, it was realized soon that the different specific cargos required different carrier sequences, for example for pDNA[133, 134] or siRNA[35, 130, 213, 214, 219] delivery.

With continuously refined polymer synthetic and analytical methods, the chemical synthetic requirements in the quest for optimized nanocarriers become less challenging compared with the supramolecular nanoassembly and, predominantly, the design of the best, most relevant screening systems. In a nutshell, screening in an artificial cell culture system will eventually yield the carrier system which is most effective within these artificial conditions. But it becomes evident that the far more relevant *in vivo* conditions pose drastically different request toward the carrier.[253] Dahlman and co-workers developed a novel strategy for evolutionary *in vivo* selection, named “Fast identification of nanoparticle delivery (FIND)”. This is a DNA barcode-based system designed to measure functional delivery of hundreds differently barcoded nanoparticles into the cytoplasm of target cells in a single mouse. By these means, *in vivo* delivery of mRNA was optimized.[254]

Summarizing from the current perspective, multifunctional polymeric carriers can be synthesized with high precision and need to be optimized and selected for the intended therapeutic purpose by innovative evolution-based screening technologies.

4.3.3 Multicomponent nanoassemblies: integrating inorganic with organic materials

The combination of polymeric carriers with inorganic nanoparticles presents a novel encouraging direction; advantages of hard nanomaterials, such as precise nanoparticle sizes and shapes, may synergize with the soft dynamic properties of more flexible organic polymers. For example, Möller and colleagues optimized mesoporous silica

nanoparticles (MSN) in inner surface and pore size for interior loading of siRNA. Very high siRNA loading of up to 380 µg/mg MSN was obtained with charge-matched amino-functionalized mesoporous cores, with up to 80 % siRNA release at 24 h. These nanoparticles were coated with a lipo-oligoaminoamide polymer, serving as pore capping and endosomal release agent.[255] In an opposite approach, hybrid nanoparticles for nucleic acid delivery were generated starting with a polymeric core, which was surface-coated with an inorganic silica shell. Sukhorukov and colleagues[256] generated layer-by-layer assembled nanocapsules by alternative deposition of polyarginine and dextran sulfate onto calcium carbonate particles, followed by removal of the carbonate core. EGFP marker gene mRNA or pDNA, or CRISPR Cas9 sgRNA expressing pDNA LeGO-Cas-gTom were deposited as shell layers. Tetraethyl orthosilicate (TEOS) was used as precursor to form a biocompatible surface silica shell. These carriers mediate more efficient transfection than a commercially available liposomal reagent for mRNA and pDNA). Delivery of pDNA expressing CRISPR-Cas9 components in a dTomato- expressing HEK293T cell model translated in high-level knockout in 70 % of cells.

Generation of a poly (DAMA-HEMA) multishelled cationic corona onto AuNP cores by surface-initiated atom transfer radical polymerization (ATRP) was reported as effective systemic siRNA delivery strategy.[257] The amount of siRNA electrostatically incorporated into the nanoparticle was tuned by the number of polymeric shells, which influenced the cellular uptake and gene silencing. Interlayer disulfide bonds release the siRNA from the polymeric shells under bioreductive cellular environment. Intravenously injected c-Myc siRNA nanoparticles accumulated in the tumor site and suppressed tumor growth in a murine lung carcinoma model. Gold nanoparticle cores were also the basis for polymer- based siRNA delivery in a recent publication by Kataoka and colleagues.[258] A glucose-PEG-block-p(L-lysine) polymer modified with lipoic acid (LA) at the ω-end formed unimer nanoplexes with siRNA. About 65 of these small polyplexes were loaded onto a 20 nm gold through Au−S bonding. The resulting <50 nm glucose-containing targeted nanoparticles (Glu-NPs) exhibited higher cellular uptake into MBA-MB-231 breast cancer spheroid compared with glucose-free control nanoparticles. Probably due to the higher glucose transporter 1 (GLUT1) expression level on the cancer stem-like cells (CSCs), the Glu-NPs became more efficiently internalized and also resulted in enhanced gene silencing in CSC-rich orthotopic MDA-MB-231 tumors following systemic administration to mice. Repeated administrations of polo-like kinase 1 (PLK1) siRNA nanoparticles significantly suppressed the tumor growth.

5 Sequence-defined lipo amino cationic carriers for nucleic acid delivery

5.1 Introduction

The delivery of nucleic acids with transient activity for genetic engineering is a promising methodology with potential applications in treating diseases ranging from cancer and infectious diseases to heritable disorders. Within the last two decades, a series of novel therapeutic nucleic acids (such as plasmid DNA, antisense oligonucleotides, siRNA, and miRNA) entered a research and clinical evaluation.[232] Nucleic acids are negatively charged and are occasionally unstable molecules, and thus their intracellular delivery, in the appropriate place at the appropriate time. In addition, naked DNA or RNA is prone to degradation. The protective shield must be efficient in attaching to the cell membrane and enable cell entry, which remains challenging for the chemistry, materials, and biotechnology fields. Regarding nucleic acids, DNA- and mRNA-based technologies have been established as extremely promising approaches to therapy and prevention of numerous diseases. Although plasmid DNA was the first nucleic acid to be pursued as a therapeutic[259], *in vitro*-transcribed (IVT) mRNA offers several advantages: it does not integrate into the genome, which is associated with a risk of carcinogenesis[260], and a natural degradation pathway is in place to ensure that its activity is temporary. From a delivery perspective, mRNA, which lives in the cytoplasm, does not require transport across the formidable nuclear membrane[261]. mRNA-based drug technologies have attracted serious attention over the past years.[187, 262] mRNA has shown therapeutic potential in a range of applications, including viral vaccines, protein replacement therapies, cancer immunotherapies, cellular reprogramming, and genome editing. [188, 230, 263-268]

We may notice that scientists have frequently researched non-viral vectors for gene therapy to solve the problems associated with protecting the mRNA molecules and ensuring efficient and safe delivery across cell membranes. They include lipids, lipid-like materials, polymers, and protein derivatives.[262, 269-271]. Particularly, lipid nanoparticles (LNP) have been thoroughly investigated and successfully entered the clinic for mRNA delivery, for example, the approved in emergency mRNA-1273[272] and BNT162b[273] for the COVID-19. Polyethylenimine (PEI), one of the most intensively investigated polycations, was utilized for high transfection efficiency.[274-276] Polyplexes also present excellent therapies due to their inherent electrostatic abilities to condense

nucleic acid and promote cellular uptake.[196, 277, 278] pH also plays a vital role in many biological processes. The synthetic polymer VIPER contains several blocks, including the hydrophilic unit OEGMA, cationic domain DMAEMA, and the hydrophobic and pH-sensitive block DIPAMA. The pH-responsive structures self-assemble into particles at physiological pH, triggers sharp endosomal pH phase transition, and create effective endosomal release.[208, 279, 280]

Compared with other carrier materials, lipid materials are biodegradable, less toxic, and can incorporate hydrophilic and hydrophobic substances. Solid-phase synthesis (SPS) derived oligomers have been successfully applied as carriers for pDNA, siRNA, and mRNA as a well-established method for synthesizing cationic polymers.[35, 143, 214, 277, 281, 282] However, the intravenous administration of cationic lipoplexes or polyplexes often results in particle instability and nonspecific interactions with blood components that induce opsonization, aggregation of red blood cells, platelet activation, excessive biodistribution to the lungs, and, in extreme cases, rapid mortality. [283, 284] Thus, we focus on designing peptide-like sequence-defined polymers that combine multifunctionality with pharmaceutical precision via solid-phase synthesis. The cationic domain and the hydrophobic units are introduced into one structure to obtain the functionalities of the components of the structures. In which, the cationic domain is for condensing nucleic acids. Hydrophobic units are for serum stabilizing, and membrane binding, which improve the dissociation in the cytoplasm, and decrease cytotoxicity.[285-287] A new series of structures containing hydrophilic cationizable building blocks (such Stp) and lipophilic building blocks (lipo amino fatty acid, LAF) were synthesized in a library approach with sequence variations, in order to identify suitable carriers for packaging of various nucleic acids into polyplexes or lipopolyplexes. In a 'chemical evolution' strategy, physical-chemistry properties and transfection efficiencies as determined by team colleagues (as will be described in detail in the LMU PhD theses of Paul Folda for pDNA, Mina Yazdi for siRNA, and Sophie Schlögl for mRNA) provides feedback for further sequence-optimization of the carriers.

5.2 Materials and methods

5.2.1 Materials

The solvents, reagents and buffers used for the experiments are summarized in **Table 5.1**, **Table 5.2**, and **Table 5.3**.

Table 5.1 Solvents used for experimental procedures.

Chemicals and solvents (abbreviations)	CAS-No.	Manufacturer
Dichloromethane (DCM)	75-09-2	Bernd Kraft, Duisburg, Germany
N,N-Dimethylformamide (DMF)	68-12-2	Iris Biotech, Marktredwitz, Germany
Chloroform	67-66-3	VWR Int. (Darmstadt, Germany)
Chloroform-d	865-49-6	Sigma-Aldrich, Munich, Germany
Ethyl acetate	141-78-6	Staub & Co. (Nürnberg, Germany)
Methyl-tert-butyl ether	1634-04-4	Brenntag (Mülheim/Ruhr, Germany)
anhydrous DCM AcroSeal®	75-09-2	Acros Organics, Germany
Methanol	67-56-1	Fisher Scientific (Schwerte, Germany)
Acetonitrile (ACN)	75-05-8	VWR Int. (Darmstadt, Germany)
Methanol-d3	1849-29-2	Sigma-Aldrich, Munich, Germany
Ethanol absolute	64-17-5	VWR Int. (Darmstadt, Germany)
Methanol anhydrous AcroSeal®	67-56-1	Acros Organics, Germany
Water	7732-18-5	In-house purification
HEPES	7365-45-9	Biomol (Hamburg, Germany)

Table 5.2. Reagents used for experimental procedures.

Chemicals and solvents (abbreviations)	CAS-No.	Manufacturer
Oleic acid	112-80-1	Sigma-Aldrich (Munich, Germany)
Phenol	108-95-2	Sigma-Aldrich (Munich, Germany)
Hydrazine monohydrate	7803-57-8	Merck Millipore (Darmstadt, Germany)
Sodium hydroxide (anhydrous)	1310-73-2	Sigma-Aldrich (Munich, Germany)
6- Aminocaproic acid	60-32-2	Sigma-Aldrich, Munich, Germany
4-Aminobutyric acid	56-12-2	TCI, EUROPE N.V.
Triisopropylsilane (TIS)	6485-79-6	Sigma-Aldrich, Munich, Germany

Ammonia solution 25 %	1336-21-6	Carl Roth (Karlsruhe, Germany)
Piperidine	110-89-4	Iris Biotech (Marktredewitz, Germany)
Potassium permanganate (KMnO4)	7722-64-7	Sigma-Aldrich (Munich, Germany)
D-(+)-Glucose monohydrate	28718-90-3	Sigma-Aldrich (Munich, Germany)
Triton® X 100	9036-19-5	Sigma-Aldrich, Munich, Germany
Benzotriazol-1-yl-oxy tripyrrolidinophosphonium	128625-52-5	Sigma-Aldrich, Munich, Germany
Octanal	124-13-0	Sigma-Aldrich, Munich, Germany
Decanal	112-31-2	Sigma-Aldrich, Munich, Germany
Dodecyl aldehyde	112-54-9	Sigma-Aldrich, Munich, Germany
Sodium cyanoborohydride ($NaBH_3CN$)	25895-60-7	Sigma-Aldrich, Munich, Germany
1-Hydroxybenzotriazole (HOBt)	2592-95-2	Sigma-Aldrich, Munich, Germany
N,N-Diisopropylethylamine (DIPEA)	7087-68-5	Iris Biotech, Marktredwitz, Germany
Di-tert-butyl dicarbonate (Boc_2O)	24424-99-5	Sigma-Aldrich, Munich, Germany
Fmoc-Stp(Boc_3)-OH building block		In-house synthesis
Fmoc-L-Lys(Fmoc)-OH	78081-87-5	Iris Biotech, Marktredwitz, Germany
2-Chlorotrityl chloride resin	42074-68-0	Iris Biotech, Marktredwitz, Germany
Fmoc-L-Lys(Dde)-OH	204777-78-6	Iris Biotech, Marktredwitz, Germany
Boc-L-Lys(Fmoc)-OH	84624-27-1	Iris Biotech, Marktredwitz, Germany
Fmoc-STODTA-OH	172089-14-4	Sigma-Aldrich (Munich, Germany)
Fmoc-*N*-amido-$dPEG_{12}$-acid	756526-01-9	Quanta Biodesign (Powell, Ohio, USA)
Fmoc-*N*-amido-$dPEG_{24}$-acid	756526-01-9	Quanta Biodesign (Powell, Ohio, USA)
Acetic acid	64-19-7	Bernd Kraft, Duisburg, Germany
Hydrochloric acid solution (1 M) (1 M HCl)	7647-01-0	Bernd Kraft, Duisburg, Germany
Linear polyethylenimine (LPEI)	9002-98-6	In-house synthesis
(3-(4,5-dimethylthiazol-2-yl)-2,5 diphenyltetrazolium bromide) (MTT)	298-93-1	Sigma-Aldrich, Munich, Germany
Trifluoro acetic acid (TFA)	76-05-1	Iris Biotech, Marktredwitz, Germany
1,2-Ethanedithiol (EDT)	540-63-6	Sigma-Aldrich, Munich, Germany
Plasmid DNA pDNA		Plasmid pCMVLuc Plasmid Factory GmbH, Bielefeld, Germany

siRNA	Axolabs, Kulmbach, Germany
CleanCap FLuc mRNA (5moU)	Trilink Biotechnologies, San Diego
CleanCap Fluc mRNA	Trilink Biotechnologies, San Diego

Table 5.3. Buffers used for experimental procedures

Buffer	Composition
10 mM HCl solvent for size exclusion chromatography	693 mL water, 300 mL acetonitrile, 7 mL 1 M HCl solution
Electrophoresis loading buffer	6 mL glycerine, 1.2 mL 0.5 M EDTA solution (pH 8.0), 2.8 mL H_2O, 20 mg bromophenol blue
ACN buffer (0.1 %TFA) for High-performance liquid chromatography (HPLC)	899.1 mL ACN , 0.9 mL TFA
Water (0.1 %TFA)	899.1 mL water, 0.9 mL TFA
HEPES buffered glucose (HBG)	20 mM HEPES, 5 % glucose, pH 7.4
Kaiser test solutions	A: 80 % (w/v) phenol in EtOH; B: 5 % (w/v) ninhydrine in EtOH; C: 20 µM KCN in pyridine (2 mL of 1 mM KCN (aq) in 98 mL of pyridine)
$KMnO_4$ staining solution for thin layer chromatography (TLC) plate	1.5 g $KMnO_4$ + 10 g K_2CO_3 + 1.25 mL 10 % NaOH (w/v) + 200 mL H_2O.

5.2.2 Cell culture

Cell culture work was carried out by Sophie Schlögl, Paul Folda and Mina Yazdi (Pharmaceutical Biotechnology, LMU München) using the murine Neuro 2A neuroblastoma cell line (N2a wt) or its eGFP-luciferase gene modified version N2a eGFPLuc.

Table 5.4. Overview of the used cell lines and corresponding culture media.

Cell line	Description	Medium
Neuro-2a (N2a cell)	Mouse neuroblastoma cells	DMEM

5.2.3 Methods

5.2.3.1 Synthesis of lipo amino fatty acid (LAF) 8Oc

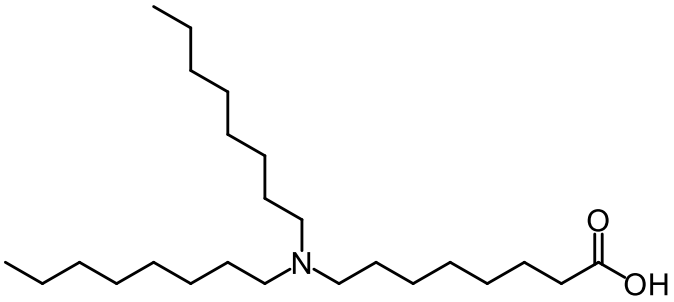

The lipo amino fatty acids (LAFs) 8Oc (C8 dialkylated 8-aminooctanoic acid) was synthesized by the reductive amination via reactions of octanal with 8-aminooctanoic acid. The synthesis of 8Oc is briefly described as below: the 8-aminooctanoic acid (200 mg, 1.26 mmol, 1 eq) and octanal (644.2 mg, 5.02 mmol, 4 eq) in a 20 mL of anhydrous methanol solution were added in the 100 mL of round bottom flask followed by the addition of the sodium cyanoborohydride ($NaBH_3CN$, 315.6 mg, 5.02 mmol, 4 eq). The reaction mixture stirred for 20 min. Afterwards, 1.5 eq of acetic acid (108 µL, 1.88 mmol) was added to the solution, the reductive amination reaction was performed for 48 hours at room temperature. The mixture was monitored by thin layer chromatography (TLC) using the optimized ratio of solvent DCM/MeOH, basic potassium permanganate $KMnO_4$ stain to check the aldehyde complete consumption. The mixture solvent was removed under reduced pressure evaporator. To remove the excess of reducing agents, the dry mixture was redissolved in pure DCM, the insoluble sodium solid was filtered, and the filtrate was further concentrated to 5 mL. The crude product was purified by silica gel column chromatography (gradient: CH_2Cl_2/MeOH from 100:0 to 15:1). The products were confirmed by ESI-MS and ^{1}H-NMR.

$C_{24}H_{49}NO_2$, the yield was 72 %, colorless oil.

5.2.3.2 Synthesis of LAF 10Oc

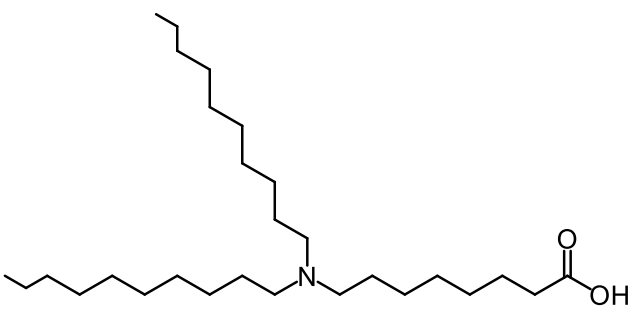

The dialkylated lipo amino fatty acid 10Oc (C10 dialkylated 8-aminooctanoic acid) was synthesized by the reductive amination reactions of decanal with 8-aminooctanoic acid.

8-Aminooctanoic acid (200 mg, 1.26 mmol, 1 eq) and decanal (784.9 mg, 5.02 mmol, 4 eq) in a 20 mL of anhydrous methanol solution were added in the 100 mL of round bottom flask, then the sodium cyanoborohydride ($NaBH_3CN$, 315 mg, 5.02 mmol, 4 eq) was added, and the mixture stirred for 20 min. Afterwards, 1.5 eq of acetic acid (107.83 µL, 1.88 mmol) was added to the solution, the reductive amination reaction proceeded for 48 hours at room temperature. The mixture was monitored by thin layer chromatography (TLC) using the optimized ratio of solvent DCM/MeOH, basic potassium permanganate $KMnO_4$ stain to check the aldehyde complete consumption. The mixture solvent was removed under reduced pressure evaporator. To remove the excess of reducing agents, the dry mixture was redissolved in pure DCM, the insoluble sodium solid was filtered, and the filtrate was further concentrated to 5 mL. The The crude product was purified by silica gel column chromatography (gradient: CH_2Cl_2/MeOH from 100:0 to 20:1). The products were confirmed by ESI-MS and ^{1}H-NMR.

$C_{28}H_{57}NO_2$, colorless oil.

5.2.3.3 Synthesis of LAF 12Oc

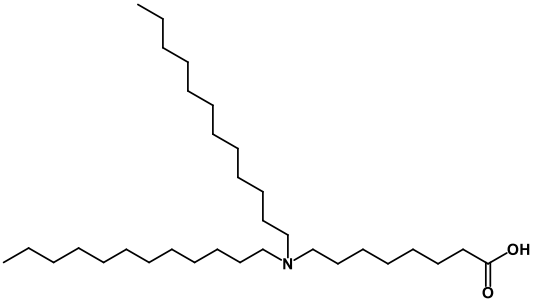

The dialkylated lipo-amino fatty acid 12Oc (C12 dialkylated 8-aminooctanoic acid) was synthesized by the reductive amination reactions of dodecanal with 8-aminooctanoic acid. Because the different solubility of 8-aminoocanoic acid and dodecanal, the protocol for the synthesis was changed compared to the previous one. Briefly, the synthesis of 12Oc is according to this protocol: the 8-aminooctanoic acid (200 mg, 1.26 mmol, 1 eq) was added to a 100 mL round bottom flask, and the mixture solution of Dodecanal (925.8 mg, 5.02 mmol, 4 eq) in 10 mL of THF was added into the flask followed by the addition of a 15 mL of anhydrous methanol solution. The corresponding amount of sodium cyanoborohydride ($NaBH_3CN$, 315.6 mg, 5.02 mmol, 4 eq) was added, and the mixture stirred for 20 min. Afterwards, 1.5 eq of acetic acid (107.8µL, 1.88 mmol) was added into the solution, the reductive amination reaction was kept for 48 hours at room temperature. The mixture was monitored by thin layer chromatography (TLC) using the optimized ratio of solvent DCM/MeOH, basic

potassium permanganate $KMnO_4$ stain to check complete consumption of the aldehyde. The mixture solution was diluted with 5 mL of water and extracted with ethyl acetate (20 ml) three times. The organic phase was dried with anhydrous sodium sulfate, and the solvent was removed and concentrated to a volume of 5 mL under reduced pressure evaporator. The crude product was purified by silica gel column chromatography (gradient: CH_2Cl_2/MeOH from 100:0 to 25:1). The products were confirmed by ESI-MS and ^{1}H-NMR.

$C_{32}H_{65}NO_2$, colorless oil.

5.2.3.4 Loading of a 2-chlorotrityl chloride resin with an Fmoc protected amino acid

Typically, 1000 mg of 2-chlorotrityl chloride resin (1.56 mmol chloride) is pre-swollen in anhydrous DCM in the 10 mL of syringe for 20 min, the DCM was then removed by filtration. Dissolved the first Fmoc protected amino acid (e.g. Stp loading for comb, bundle and T-shape structures; Fmoc-L-Lys (Dde)-OH for U-shape structures; 0.3 eq, with DIPEA 3 eq) in anhydrous DCM and added to the resin for reaction for 75 min. The reaction solvent was drained and a capping solution consisting of DCM/MeOH/DIPEA (4 mL DCM, 3 mL MeOH and 500 µL DIPEA per 1000 mg of resin) was added to the resin for 60 min to transform residual free chlorides into unreactive methoxy ethers. After removal of the reaction mixture, the resin was washed 3 times with DMF and 3 times with DCM. The resin was dried under the vacuum, and then weighed 5-10 mg of the resin for 3 eppes to determine the loading efficiency of the resin. 1 mL Fmoc deprotection solution (20 % piperidine in DMF, v/v) was added to each sample and incubated for 75 min at 700 rpm, 25°C. The samples were then vortexed and got the beads to settle down. The 25 µL of reaction solution supernatant was diluted with 975 µL of DMF, and 25 µL of Fmoc deprotection solution diluted in 975 µL of DMF was used as blank control, the absorption of the dilution was measured by a Genesys 10S UV−vis photometer at 301 nm. The loading of each sample in the eppes was then calculated according to the following equation: resin load [mmol g^{-1}] = (A×1000) × (m [mg] × 7800×df)$^{-1}$ with df as a dilution factor. The average of three values gave the respective resin loading efficiency. The remaining resin was treated 3 times with Fmoc deprotection solution to remove the Fmoc protection group. The reaction progress was monitored by Kaiser test. The resin was washed with 3 times of DMF, 3 times of DCM after each coupling step and deprotection step. Afterward, the resin was dried in vacuo and stored at 4°C.

5.2.3.5 Synthesis of comb structures containing LAFs

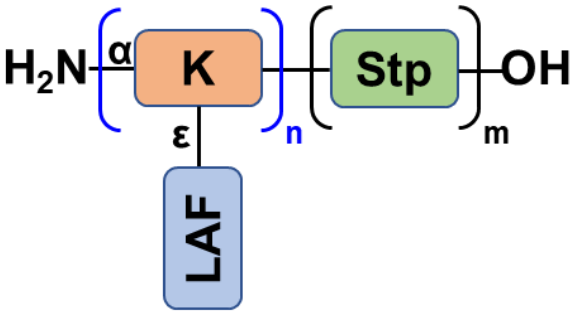

The Fmoc-protected Stp-loading resin was pre-swollen for 20 min in DCM or overnight in DMF (peptide grade) before the first deprotection step. Fmoc was cleaved by the 20 % piperidine in DMF treatments, followed by extensive washing with DCM and DMF three times. The next couplings of polyamine building block Fmoc-protected Stp or amino acid Fmoc-Lys (Dde)-OH were done by dissolving of Fmoc-building block/amino acid (4 eq), PyBOP (4 eq), HOBt (4 eq), DIPEA (8 eq) in the minimal amount of DMF/DCM and transferred to the reactor. After 75 min the completeness of the coupling reaction was checked by Kaiser test. The last Fmoc-Lys (Dde)-OH was coupled to the backbone and after the removal of the Fmoc protecting group, the N-terminal NH_2-group was protected with 10 eq Di-tert-butyl dicarbonate (Boc anhydride) and 10 eq DIPEA in DCM. Dde-deprotection protocol was accomplished by using Dde-deprotection solution (2 % hydrazine in DMF, v/v, 15 x 2 min). Afterwards, the resin was washed with 5 times DMF, 5 times 10 % DIPEA in DMF and then 3 times DCM (10 mL g^{-1} resin). The LAFs coupling was done by dissolving the LAFs/DIPEA and Pybop/HOBt in DCM and DMF with 1 % of Triton, respectively, reacting for 2- 4 hours, the equivalences were changed referring to the number of free amines after the Dde deprotection. After the final reaction step the resin was washed with DMF, DCM and checked by Kaiser test, and dried in vacuo. For cleavage, the pre-cooled resin was suspended in a pre-cooled solution of TFA/TIS/H_2O (95/2.5/2.5, v/v/v) and agitated for 1 hour. The cleavage solution was drained and collected. The resin was washed once with TFA. The collected solutions were concentrated with nitrogen flow to approximately 1 mL, and further mixed with 2 mL ethanol. The clear solutions were dialyzed against pure ethanol using a Spectra/Por® Dialysis Membrane, MWCO 2K Da for 4 hours and further dialyzed against water with 10 mM HCl for another 24 h. The samples were lyophilized to obtain the products, characterization was performed by MALDI-TOF-MS and ^{1}H-NMR.

5.2.3.6 *Synthesis of bundle structures containing LAFs*

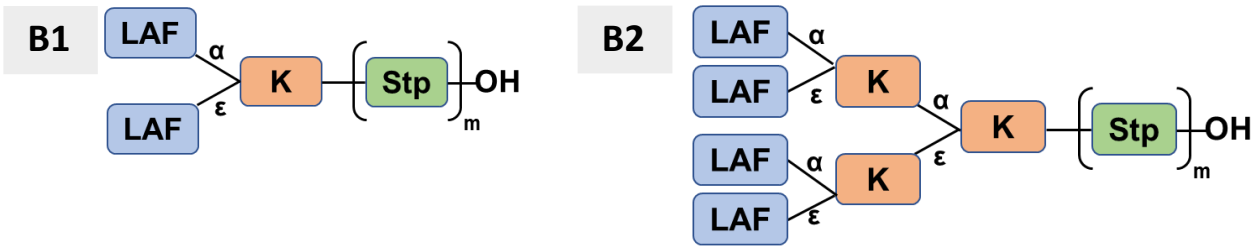

The Fmoc-protected Stp-loading resin was pre-swollen for 20 min in DCM or overnight in DMF (peptide grade) before the first deprotection step. Fmoc was cleaved by the 20 % piperidine in DMF treatments, followed by extensive washing with DCM and DMF three times. The next couplings of polyamine building block Fmoc-protected Stp or amino acid Fmoc-Lys (Fmoc)-OH were done by dissolving of 4 eq Fmoc-building block/amino acid, 4 eq PyBOP,4 eq HOBt, 8 eq DIPEA (two-fold equivalence for the second Fmoc-Lys (Fmoc)-OH coupling of **B2** structures) in the minimal amount of DMF/DCM and transferred to the reactor. After 75 min the completeness of the coupling reaction was checked by Kaiser test. After the Fmoc deprotection, the LAFs coupling was done by dissolving the LAFs/DIPEA and Pybop/HOBt in DCM and DMF with 1 % of Triton, respectively, reacting for 2- 4 hours, the equivalences were changed referring to the number of free amines. After the final reaction step the resin was washed with DMF, DCM and checked by Kaiser test, and dried in vacuo. For cleavage, the r pre-cooled resin was suspended in a pre-cooled solution of TFA/TIS/H_2O (95/2.5/2.5, v/v/v) and agitated for 1 hour. The cleavage solution was drained and collected. The resin was washed once with TFA. The collected solutions were concentrated with nitrogen flow to approximately 1 mL, and further mixed with 2 mL ethanol. The clear solutions were dialyzed against pure ethanol using a Spectra/Por® Dialysis Membrane, MWCO 1000 Da for 4 hours and further dialyzed against water with 10 mM HCl for another 24 h. The samples were lyophilized to obtain the products, characterization was performed by MALDI-TOF-MS and ^{1}H-NMR.

5.2.3.7 *Synthesis of T-shape structures containing LAFs*

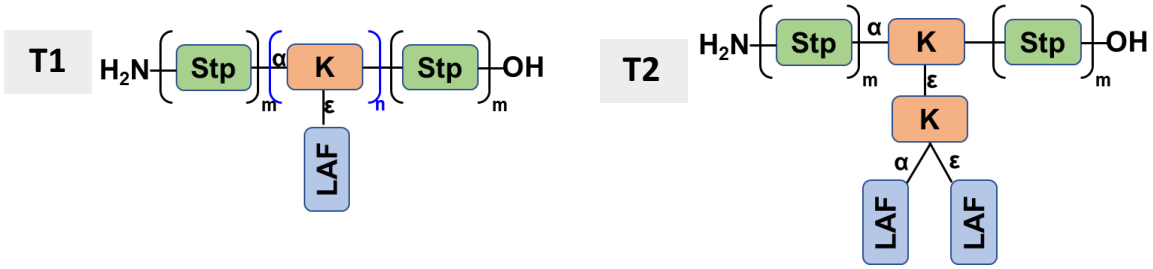

The Fmoc-protected Stp-loading resin was pre-swollen for 20 min in DCM or overnight

in DMF (peptide grade) before the first deprotection step. Fmoc was cleaved by the 20 % piperidine in DMF treatments, followed by extensive washing with DCM and DMF three times. The next couplings to the backbones of polyamine building block Fmoc-protected Stp or amino acid Fmoc-Lys (Dde)-OH were done by dissolving of 4 eq Fmoc-building block/amino acid, 4 eq PyBOP,4 eq HOBt, 8 eq DIPEA in the minimal amount of DMF/DCM and transferred to the reactor. After 75 min the completeness of the coupling reaction was checked by Kaiser test. The last Fmoc-protected Stp was coupled to the backbone and after the removal of the Fmoc protecting group, the N-terminal NH_2-group was protected with 10 eq Di-tert-butyl dicarbonate (Boc anhydride) and 10 eq DIPEA in DCM. Dde-deprotection protocol was accomplished by using Dde-deprotection solution (2 % hydrazine in DMF, v/v, 15 x 2 min). Afterwards, the resin was washed with 5 times DMF, 5 times 10 % DIPEA in DMF and then 3 times DCM (10 mL g^{-1} resin). For **T2** structures, before the LAFs coupling step, another Fmoc-Lys (Fmoc)-OH was coupled using the same coupling conditions. The LAFs coupling was done by dissolving the LAFs/DIPEA and Pybop/HOBt in DCM and DMF with 1 % of Triton, respectively, reacting for 2- 4 hours, the equivalences were changed referring to the number of free amines after the Dde/Fmoc deprotection. After the final reaction step the resin was washed with DMF, DCM and checked by Kaiser test, and dried in vacuo. For cleavage, the pre-colded resin was suspended in a pre-colded cleavage solution of TFA/TIS/H_2O (95/2.5/2.5, v/v/v) and agitated for 1 hour. The cleavage solution was drained and collected. The resin was washed once with TFA. The collected solutions were concentrated with nitrogen flow to approximately 1 mL, and further mixed with 2 mL ethanol. The solutions were dialyzed against pure ethanol using a Spectra/Por® dialysis membrane, MWCO 1000 Da for 4 hours and further dialyzed against water with 10 mM HCl for another 24 h. The samples were lyophilized to obtain the products, characterization was performed by MALDI-TOF-MS.

5.2.3.8 Synthesis of U-shape (U1 and U2) structures containing LAFs

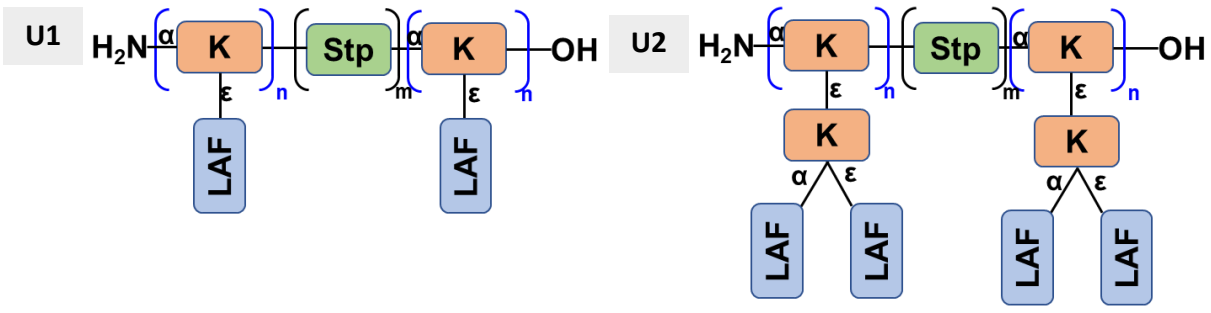

The Fmoc- Lys (Dde) OH -loading resin was pre-swollen for 20 min in DCM or overnight in DMF (peptide grade) before the first deprotection step. Fmoc was cleaved by the 20 %

piperidine in DMF treatments, followed by extensive washing with DCM and DMF three times. The next couplings to the backbones of polyamine building block Fmoc-protected Stp or amino acid Fmoc-Lys (Dde)-OH were done by dissolving of 4 eq Fmoc-building block/amino acid, 4 eq PyBOP,4 eq HOBt, 8 eq DIPEA in the minimal amount of DMF/DCM and transferred to the reactor. After 75 min the completeness of the coupling reaction was checked by Kaiser test. After the completeness of Fmoc-Lys (Dde)-OH, the N-terminal NH_2-group was protected after the Fmoc deprotection with 10 eq Di-tert-butyl dicarbonate (Boc anhydride) and 10 eq DIPEA in DCM. Dde-deprotection protocol was accomplished by using Dde-deprotection solution (2 % hydrazine in DMF, v/v, 15 x 2 min). Afterwards, the resin was washed with 5 times DMF, 5 times 10 % DIPEA in DMF and then 3 times DCM (10 mL g^{-1} resin). For **U2** structures, before the LAFs coupling step, Fmoc-Lys (Fmoc)-OH was coupled using the same coupling conditions. The LAFs coupling was done by dissolving the LAFs/DIPEA and Pybop/HOBt in DCM and DMF with 1 % of Triton, respectively, reacting for 2- 4 hours, the equivalences were changed referring to the number of free amines after the Dde/Fmoc deprotection. After the final reaction step the resin was washed with DMF, DCM and checked by Kaiser test, and dried in vacuo. For cleavage, the pre-colded resin was suspended in a pre-colded cleavage solution of TFA/TIS/H_2O (95/2.5/2.5, v/v/v) and agitated for 1 hour. The cleavage solution was drained and collected. The resin was washed once with TFA. The collected solutions were concentrated with nitrogen flow to approximately 1 mL, and further mixed with 2 mL ethanol. The solutions were dialyzed against pure ethanol using a dialysis membrane, MWCO 1000 Da for 4 hours and further dialyzed against water with 10 mM HCl for another 24 h. The samples were lyophilized to obtain the products, characterization was performed by MALDI-TOF-MS and ^{1}H-NMR.

5.2.3.9 Synthesis of U-shape (U3 and U4) structures containing LAFs

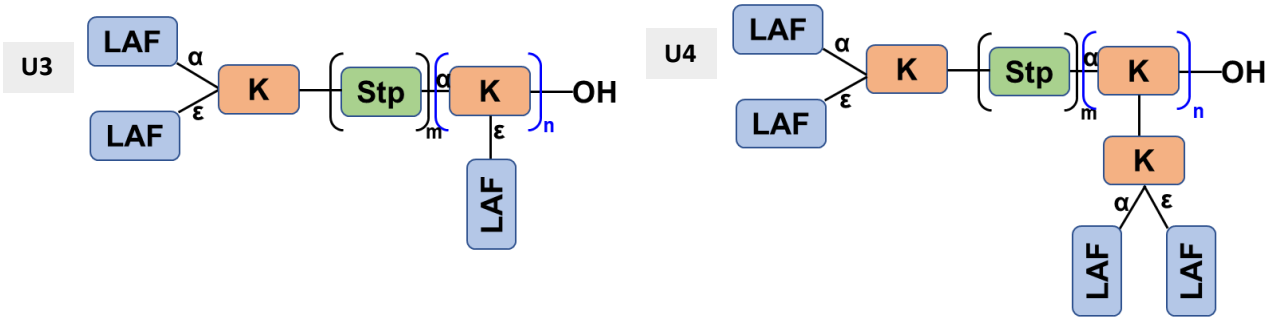

The Fmoc- Lys (Dde) OH -loading resin was pre-swollen for 20 min in DCM or overnight in DMF (peptide grade) before the first deprotection step. Fmoc was cleaved by the 20 %

piperidine in DMF treatments, followed by extensive washing with DCM and DMF three times. The next couplings to the backbones of polyamine building block Fmoc-protected Stp or amino acid Fmoc-Lys (Dde)-OH were done by dissolving of 4 eq Fmoc-building block/amino acid, 4 eq PyBOP,4 eq HOBt, 8 eq DIPEA in the minimal amount of DMF/DCM and transferred to the reactor. After 75 min the completeness of the coupling reaction was checked by Kaiser test. For **U3** structures, after the completeness of Fmoc-protected Stp, one more Fmoc-Lys (Fmoc)-OH was coupled to the backbone, followed by the Fmoc deprotection using the 20 % piperidine in DMF solution and Dde deprotection using the Dde deprotection cocktail (2 % hydrazine in DMF, v/v, 15 x 2 min; afterwards, the resin was washed with 5 times DMF, 5 times 10 % DIPEA in DMF and then 3 times DCM). For **U4** structures, after the last Stp coupling step, the Fmoc protecting group and the Dde protecting group were cleaved by using the Fmoc deprotection cocktail and Dde deprotection protocol, respectively. The resin was further washed with 5 times 10 % DIPEA in DMF and then 3 times DCM. Then, Fmoc-Lys (Fmoc)-OH was coupled using the common coupling conditions. The LAFs coupling of **U3** and **U4** structures was done by dissolving the 12 eq LAFs and 24 eq DIPEA, 12 eq Pybop/ 12 eq HOBt in DCM and DMF with 1 % of Triton, respectively, reacting for 2- 4 hours. After the final reaction step the resin was washed with DMF, DCM and checked by Kaiser test, and dried in vacuo. For cleavage, the pre-colded resin was suspended in a pre-colded cleavage solution of TFA/TIS/H_2O (95/2.5/2.5, v/v/v) and agitated for 1 hour. The cleavage solution was drained and collected. The resin was washed once with TFA. The collected solutions were concentrated with nitrogen flow to approximately 1 mL, and further mixed with 2 mL ethanol. The solutions were dialyzed against pure ethanol using a Spectra/Por® Dialysis Membrane, MWCO 1000 Da for 4 hours and further dialyzed against water with 10 mM HCl for another 24 h. The samples were lyophilized to obtain the products, characterization was performed by MALDI-TOF-MS and ^{1}H-NMR.

5.2.3.10 Kaiser test

Free amines of deprotected amino acids on the resin were determined qualitatively by the Kaiser test.[137] A small sample of DCM washed resin was transferred into an Eppendorf reaction tube. One drop of each 80 % phenol in EtOH (w/v), 5 % ninhydrin in EtOH (w/v) and 20 µM potassium cyanide (KCN) in pyridine (mixture of 1 mL aqueous 0.001 M KCN solution and 49 mL pyridine) were added. The tube was incubated at 99 °C for 4 min under shaking. The presence of free amines was indicated by blue color.

5.2.4 Analytical methods

5.2.4.1 ESI mass spectrometry

The testing samples were dissolved in $CHCl_3$ to a concentration of 1 mg/mL. Electrospray ionization (ESI) mass spectrometry was carried out using a Thermo scientific LTQ FT Ultra Fourier transform ion cyclotron and an IonMax source. Data is shown after positive ionization as (M+X). Samples were kindly processed by Dr. Werner Spahl from the analytical core facility at the Department of Chemistry, LMU Munich.

5.2.4.2 MALDI-MS Analysis

The MALDI-TOF mass spectrometry matrix solution contains 10 mg/mL Super-DHB (90/10 m/m mixture of 2,5-dihydroxybenzoic acid and 2-hydroxy-5-methoxybenzoic acid) in 69.93/30/0.07 (v/v/v) H_2O/acetonitrile/trifluoroacetic acid. 1 µL of matrix solution was spotted on an MTP AnchorChip (Bruker Daltonics, Germany). After crystallization of 1 µL matrix solution, 1 µL of sample solution (1 mg/mL in water) was added onto the matrix spot. Samples were analyzed using an Autoflex II mass spectrometer (Bruker Daltonics, Germany). All spectra were recorded in positive ion mode.

5.2.4.3 Proton ^{1}H NMR spectroscopy

^{1}H NMR spectra were recorded using an AVANCE III HD 400 (400 MHz) by Bruker with a 5 mm CPPBBO probe. All spectra were recorded without TMS as internal standard and therefore all signals were calibrated to the residual proton signal of the Chloroform-d ($CDCl_3$) or Methanol-d4 (CD_3OD) solvent. Chemical shifts are reported in ppm and refer to the solvent as internal standard. Integration was performed manually. The spectra were analyzed using MestreNova (Ver. 9.0 by MestReLab Research).

5.2.4.4 Analytical RP-HPLC

Reversed-phase HPLC (RP-HPLC) was carried out with a VWR-Hitachi Chromaster 5160 Pump System (VWR, Darmstadt, Germany), VWR-Hitachi Chromaster 5260 Autosampler (VWR, Darmstadt, Germany) and a Diode Array Detector (VWR-Hitachi Chromaster 5430; VWR, Darmstadt, Germany) at 214 nm detection wavelength. As a column either a YMC Hydrosphere 302 C18 (YMC Europe, Dinslaken, Germany) or a Waters Sunfire C18 (Waters, Saint-Quentin en Yvelines Cedex, France) was used. A gradient starting at 95: 5 (water / acetonitrile) to 0: 100 within 20 min was applied. All solvents were supplemented with 0.1 % trifluoroacetic acid.

5.2.5 Polyplex formation

Nucleic acid and calculated amounts of aminolipid at indicated N/P (nitrogen/phosphate) ratios were diluted in separate tubes of HBG (20 mM of HEPES, 5 % glucose (w/v), pH 7,4). All protonable nitrogens of the Stp (succinoyl-tetraethylene pentamine) units and tertiary amines of the LAFs were considered in the N/P ratio calculations. Equal volumes of nucleic acid solution and aminolipid solution were mixed by rapid pipetting and incubated 40 minutes at room temperature in a closed Eppendorf reaction tube. The final concentration of nucleic acid in the polyplex solution was 12,5 ng/µL for mRNA (CleanCap FLuc mRNA (5moU) (Trilink Biotechnologies, San Diego) or CleanCap Fluc mRNA (Trilink Biotechnologies, San Diego)), 10 ng/µL for pDNA (Plasmid pCMVLuc Plasmid Factory GmbH, Bielefeld, Germany) and 25 ng/µL for siRNA (Axolabs, Kulmbach, Germany) siRNA silencing eGFPLuc (siGFP) (sense: 5′-AuAucAuGGccGAcAAGcAdTsdT-3′; antisense: 5′-UGCUUGUCGGCcAUGAuAUdTsdT-3′); control siRNA (siCtrl) (sense: 5′-AuGuAuuGGccuGuAuuAGdTsdT-3′; antisense: 5′-CuAAuAcAGGCcAAuAcAUdTsdT-3′); small letters indicate 2′methoxy modifications; “s” indicates phosphorthioate linkages).

5.2.6 Transfection efficiency of polyplexes in neuroblastoma cells

Transfection efficiency of polyplexes was evaluated in N2a neuroblastoma cells as will be described in detail in the LMU PhD theses of Paul Folda (for pDNA), Mina Yazdi (for siRNA) and Sophie Schlögl (for mRNA). For luciferase pDNA and luciferase mRNA ;10 000 N2a wt cells/well were seeded in 96-well plates. For siRNA, 5 000 N2a eGFPLuc cells/well were seeded in 96-well plates. Luciferase activity of cell lysate was measured and transfection efficiency (for pDNA and mRNA) was presented as relative light units (RLU) per well. For siRNA polyplex transfection, gene silencing activity was presented as percentage of the luciferase gene expression (100 %) obtained with HBG buffer-treated cells, comparing siGFP transfected cells with siCtrl transfected N2a eGFPLuc cells.

5.3 Results and discussion

5.3.1 Design of novel lipids

Nucleic acid therapy is highly dependent on safe and effective delivery systems to protect cargo from degradation and deliver it to target cells for efficient uptake. Non-viral vectors, compared to the viral vectors, for nucleic acid delivery have many advantages, such as more safety, less toxicity, and immunogenicity.[288, 289] A number of cationic lipid-based carriers have also been shown to be very efficient in cell transfection *in vitro* and *in vivo* in nucleic acid delivery.[290, 291] The cationic lipid molecules mainly contain three functional domains: a positively charged polar head group, a hydrophobic region, and a linker that tethers the cationic group and hydrophobic groups. The previous work proved that the single-tailed lipids are less effective and more toxic than their double-tailed counterparts.[292] The ionizable cationic lipids, especially for both COVID-19 vaccines as mRNA-LNP formulation, consist of tertiary amine with branched long alkyl chains and a polar head. The lipids are required to form complexation with mRNA and then delivered into cytosol. In our lab's previous work with cationic polyplexes, the results have shown that the lipopolyplexes, composed of synthetic positively charged oligomers and negatively charged nucleic acid, possess effective results in siRNA, pDNA and mRNA via chemical evolution through libraries with sequence variations of the carrier.[277, 282, 293]

Based on these findings, firstly we designed a set of lipo-amino-fatty acids (LAFs) with tertiary amines and long alkyl chains. The LAFs, lipophilic cationizable building blocks, can be synthesized via reductive amination from small molecule aldehyde and fatty acid carrying an amino group. The carboxylic acid group in the LAFs can be applied for the next coupling in SPS. Stp, a short linear oligoethylenimines instead of propylenimine used as amine building blocks, were previously found to possess superior gene transfer properties. Then next, we explored the novel combination of lipophilic cationizable building blocks (LAFs) and cationizable hydrophilic building block (Stp) necessary for an astonishingly high effect. The method to achieve the combination is solid-phase synthesis (SPS), as it is an ideal tool for the synthesis of precise, sequence defined polymers and can with the right set of protocols. Branching points were introduced by lysines, which provide two amines after deprotection during synthesis. So, these synthetic structures via SPS allow the study of structure-activity relationships (SAR) in more detail and offer increased control over the polymer and thereby the possibility of fine-tuning their properties. By screening them for *in vitro*

transfection capabilities and correlating these to their biophysical parameters, useful SARs and promising lead candidates should be identified.

5.3.2 Synthesis of LAFs via reductive amination

The lipo-amino-fatty acids (LAFs) were synthesized via reductive amination reaction. The reductive amination of aldehydes and ketones is an important and efficient method for synthesizing primary, secondary, and tertiary amines. It involves a one- or two-step procedure in which an amine and a carbonyl compound condense to afford an imine or iminium ion that is reduced in situ or subsequently to form an amine product. This reaction procedure's common mild reducing agents are $Na(OAc)_3BH$ and $NaBH_3CN$. Acetic acid (AcOH) is frequently employed as a proton donor, in reductive amination, it also acts as catalyst, as the reactions are generally conducted at pH ~ 5. Sodium borohydride ($NaBH_3$) is a reducing agent frequently used in this imine reducing reaction process. However, carbonyl compounds or the carboxylic group are reduced to alcohols under acidic conditions after a long incubation, presumably via a protonated carbonyl cation, which is not as our desired structures. The carboxylic group is also necessary for our next coupling and compatibility with solid phase synthesis.

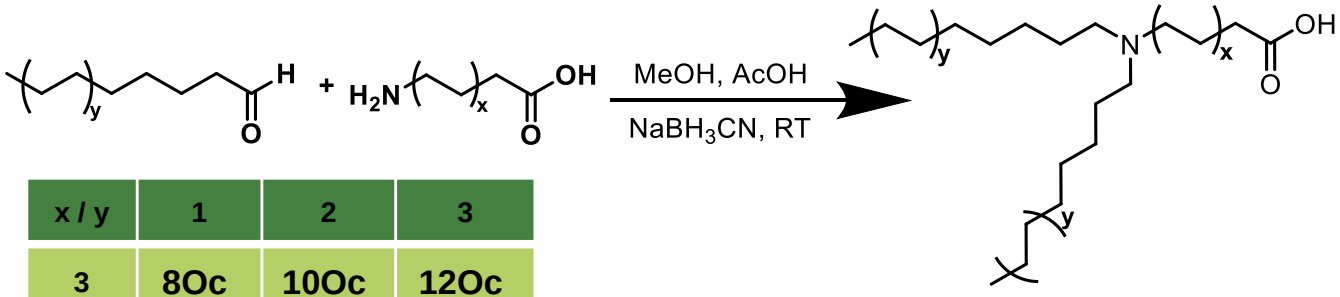

x / y	1	2	3
3	8Oc	10Oc	12Oc

Scheme 5.1. Schematic of the LAFs synthesis via reductive amination. x or y is the number of ethylene units in the aldehyde, amino fatty acid, or the products (x = 3, y = 1, y = 2, y = 3 is 8Oc, 10Oc and 12Oc, respectively). The reaction condition: MeOH as solvent, AcOH as catalyst, $NaBH_3CN$ as reducing agent, at room temperature.

The synthetic strategy to convert aldehyde and amino fatty acid reactants into the lipo-amino-fatty acid building block required the specific condition via reductive amination in one step (shown in **Scheme 5.1**). The carbonyl group is reacted with an amine to form an imine (Schiff base), which is then reduced to an amine with reducing agents. The reaction should be carried out under weak acid conditions, because on the one hand, weak acid conditions make carbonyl protonation to enhance the electrophilicity and promote the reaction. On the other hand, it also avoids the occurrence of nucleophilic decline caused by excessive protonation of amines. To avoid the side

products (reduced to alcohol), the mild reducing agent $NaBH_3CN$ was utilized for reducing the imine, because the electricity-absorbing induction effect of the cyano group of $NaBH_3CN$ weakens the activity of boron-hydrogen bonds so that sodium cyanoborohydride can only selectively reduce Schiff bases without reducing the carbonyl group of aldehydes and ketones, thus avoiding the occurrence of side reactions. The common solvent used here is methanol, the mixture THF/MeOH is more suitable for dissolving the longer chain of aldehyde such dodecanal reactants. Excess of aldehyde was added in the reaction for avoiding the mono-alkylated reaction. Thin layer chromatography (TLC) is important for monitoring the reaction process. Staining the TLC plate with basic potassium permanganate ($KMnO_4$) stain, alcohols, amines, and aldehyde will appear readily on a TLC plate following immersion into the stain solution as yellow spots, the product was further treated and purified.

The excess of reducing agents were filtered after mixing the dry mixture in DCM, the crude product was purified by column chromatography with the gradient DCM/MeOH. The purification of the LAFs was examined by some characteristic methods, as ESI-MS and ^{1}HNMR identified the products, 12Oc as example, see **Figure 5.1**. Other characterizations of structures are shown in the **Appendix**.

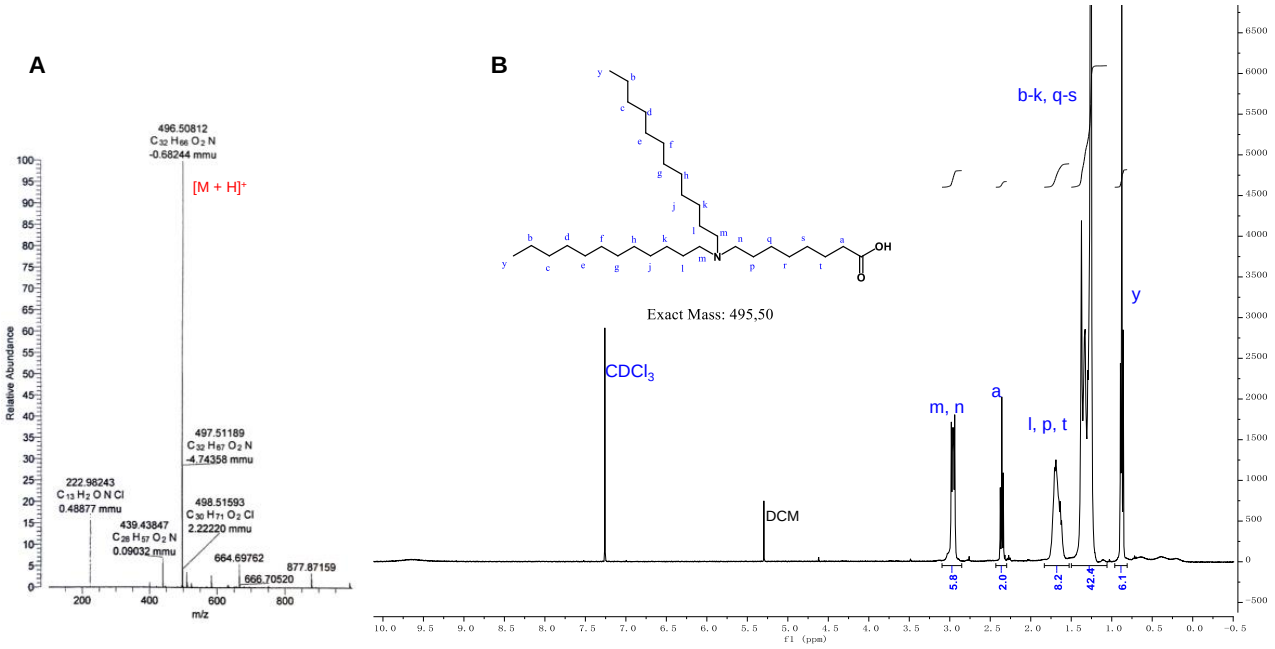

Figure 5.1. (A). Exemplary ESI-MS spectrum of 12Oc in positive mode. (B). The ^{1}HNMR spectrum of 12Oc in solvent Chloroform-d ($CDCl_3$). The integration of every specific peak that refers to the hydrogens of the structure was performed manually.

5.3.3 Synthesis of different topologies of carriers

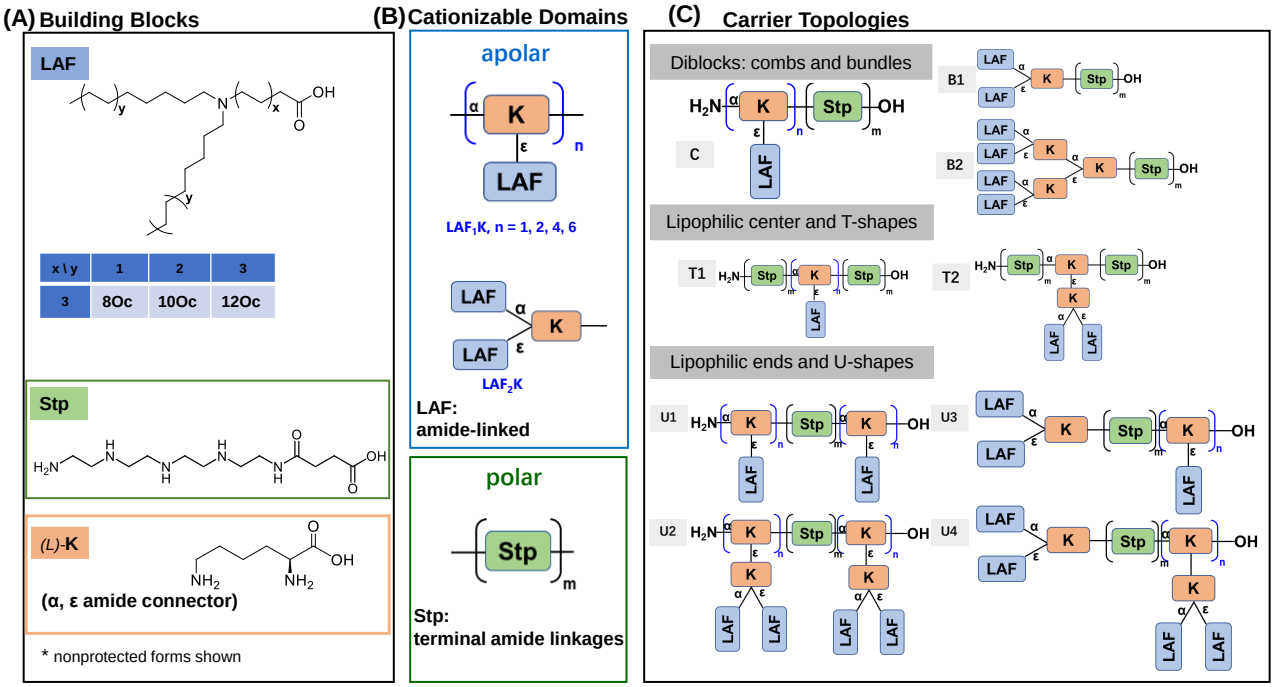

Figure 5.2. Overview over (A) the used building blocks, (B) the cationizable domains and (C) different carrier topologies in the novel lipid design.

Polyethylenimines (PEI) show the high transfection activity, due to the protonatable diaminoethane motif possessing unique properties as a “proton sponge” for the endosome buffering and destabilization.[294, 295] The inspired artificial amino acid succinoyl tetraethylene pentamine (Stp), as a polar domain, was applied together with lysine (K, as branching connectors) and LAFs (apolar cationizable domain) to generate a library of defined structures. Different topologies of carriers were designed and synthesized via SPS approach. **Figure 5.2** and **Table 5.1** give an overview over the set of compounds. The first variant class, the first topologies (diblocks: combs and bundles) consist of a continuous Stp sequence with the branched LAF1K or LAF2K domains. The Stp was placed at the head or central position of the branched lysine for complexing and condensing to form particles with the hydrophobic LAFs. The next topologies are chains with lipophilic domain at the center (T-shape), and chains with two diacylation sites at the ends (U-shape). In the second carrier class, each domain's influence in the structures was investigated, such as applying replacements for the Stp and LAF, respectively.

For the synthesis of these carriers, the standard Fmoc SPS conditions were used. The addition of Triton-X increased the efficiency of coupling reactions to eliminate the steric hindrance. All compounds were identified by MALDI-TOF-MS. Some of ^{1}H-NMR and

RP-HPLC data can be found in the **Appendix.**

Table 5.1. ID numbers, topologies, sequences, and the amount of polar domain (**m**) and apolar domain (**n**) of the synthesized Stp/12Oc-contained structures.

ID	Topology	m	n	Sequence (N→C)
Blocks (comb)				
1700	C	10	-	Stp_{10}
1701	C	10	2	$[K]_2$-Stp_{10}
1615	C	1	2	$[K(12Oc)]_2$-Stp
1616	C	1	4	$[K(12Oc)]_4$-Stp
1617	C	1	6	$[K(12Oc)]_6$-Stp
1704	C	10	2	$[K(12Oc)]_2$-Stp_{10}
1705	C	10	4	$[K(12Oc)]_4$-Stp_{10}
1706	C	10	6	$[K(12Oc)]_6$-Stp_{10}
1707	C	2	4	$[K(12Oc)]_4$-Stp_2
1708	C	2	2	$[K(12Oc)]_2$-Stp_2
1709	C	4	4	$[K(12Oc)]_4$-Stp_4
Lipidic Center / T-Shapes				
1563	T1	2	1	Stp_2-K(12Oc)-Stp_2
1714	T1	1	2	Stp-$[K(12Oc)]_2$-Stp
1715	T2	1		Stp-K[$K(12Oc)_2$]-Stp
Bundles				
1614	B1	1		$K(12Oc)_2$-Stp
1710	B1	2		$K(12Oc)_2$-Stp_2
1613	B2	1		K[$K[12Oc)_2]_2$-Stp
1713	B2	2		K[$K[12Oc)_2]_2$-Stp_2
Lipidic Ends / U-Shapes				
1611	U1	1	1	K(12Oc)-Stp-K(12Oc)
1718	U1	1	2	$[K(12Oc)]_2$-Stp-$[K(12Oc)]_2$
1612	U3	1	2	$K(12Oc)_2$-Stp-K(12Oc)-K(12Oc)
1681	U1	2	1	K(12Oc)-Stp_2-K(12Oc)
1719	U1	2	2	$[K(12Oc)]_2$-Stp_2-$[K(12Oc)]_2$
1720	U2	1	1	K[$K(12Oc)_2$]-Stp-K[$K(12Oc)_2$]
1721	U2	2	1	K[$K(12Oc)_2$]-Stp_2-K[$K(12Oc)_2$]
1722	U3	2	2	$K(12Oc)_2$-Stp_2-K(12Oc)-K(12Oc)
1716	U4	1	1	$K(12Oc)_2$-Stp-K[$K(12Oc)_2$]
1717	U4	2	1	$K(12Oc)_2$-Stp_2-K[$K(12Oc)_2$]

* The structures were synthesized via SPS, and identified by MALDI-TOF-MS.

5.3.4 Evaluation of precise, sequence-defined carriers for nucleic acids delivery

To identify promising structures for subsequent structure activity model's library members were screened to evaluate their nucleic acid delivery potential in a luciferase reporter gene assay pDNA and mRNA delivery, and a Neuro2A/eGFPLuc gene silencing model siRNA delivery.

5.3.4.1 Evaluation of LAFs Oligomers for in vitro pDNA Delivery

Figure 5.3 shows an exemplary comparison of topology constructed structures under the experimental conditions in the pDNA delivery. It presents the luciferase gene

transfer activity of selected structures complexed with pDNA at indicated protonatable nitrogen/phosphate (N/P, 6, 12, 18) molar ratios. Oligomers like the comb structures (C) with 10 Stp units but without LAFs (**1700**, **1701**) or with fewer than 6 LAF units (**1704**, **1705**, **1706**) show gene- transfer activity about 10- to 100-fold lower the gold standard, linear PEI (LPEI). Some other comb structures with single Stp unit like **1615**, **1616** and **1617** do not transfect, while two and four Stp units -bearing structures (**1707** and **1709**) shows slightly higher transfection efficiency about 100-fold above the background of untransfected cells (ctrl, HBG), surprisingly **1708** shows the same efficiency as LPEI at N/P ratio 18.

T-shape oligomers were generated to obtain the lipophilic center structures with different amount of the cationizable domain Stp. Compared to the comb structures, the T-shape structures **1563**, **1714** and **1715** show similar effects. The transfection results also demonstrated that the **1715** shows 2 to 10-fold above the positive control LPEI in pDNA polyplexes, which contains the LAF2K domain, is better than **1714** that containing LAF1K apolar domain.

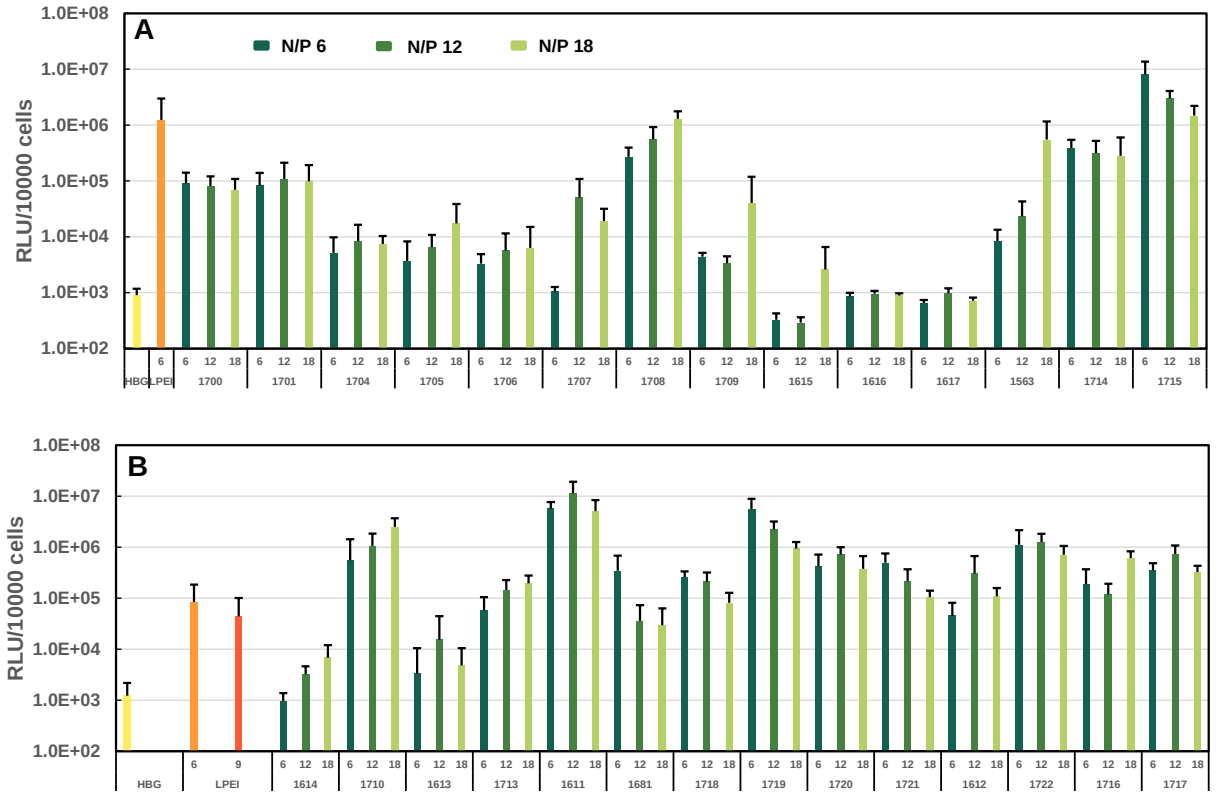

Figure. 5.3. Gene transfer with pDNA lipopolyplexes into Neuro2A neuroblastoma cells. (A) comb and T-shape structures, (B) bundle and U-shape structures. 200 ng pCMVL pDNA/well were prepared in HBG at a concentration 10 µg/mL and indicated N/P ratio (6, 12, or 18) for transfection of 10,000 Neuro2A cells /well. Luciferase protein expression was determined at 24 hours after transfection. Positive control = LPEI, linear polyethylenimine; negative control =

HBG, HEPES buffered saline. The experiment was performed by Paul Folda, PhD student at LMU Pharmaceutical Biotechnology.

The structures with one or two polar cationic Stp units and moderate amounts of hydrophobic domain LAFs perform better, and the topologies play additional important roles for the biological activity. Based on the good performance, the bundles and U-shape structures were produced, and were evaluated in pDNA delivery (see **Figure 5.3**). The transfection efficiency of the bundles with two Stp units (**1710** and **1713**) is much higher than **1614** and **1613** with one Stp. It is worth mentioning that **1710** is better than LPEI, and some U-shape structures, such as **1611**, **1719**, **1720**, **1722**, and **1717** also outperform the excellent standard in transfection efficiency. In addition, **1611, 1719** and **1722** show highest potent of gene-transfer activity in pDNA, the results were shown in **Figure 5.3**. The structures consisting of Stp as lipophilic center and cationizable apolar domains (LAF1K, LAF2K or combination of LAF1K/LAF2K) show encouraging performance in pDNA delivery.

These structures can form 100-200 nm polyplexes by assembly of the complex the pDNA. Some of structures (**1710**, **1715**, **1611**, **1719** and **1722**) performed extremely well, however, considering the toxic effect of lipids, dose-response efficacy was determined for selected polyplexes. The results were displayed in **Figure 5.4**. With the decrease of the dose in pDNA polyplexes of **1611** and **1719** maintain very high efficacy at N/P 12 and 18.

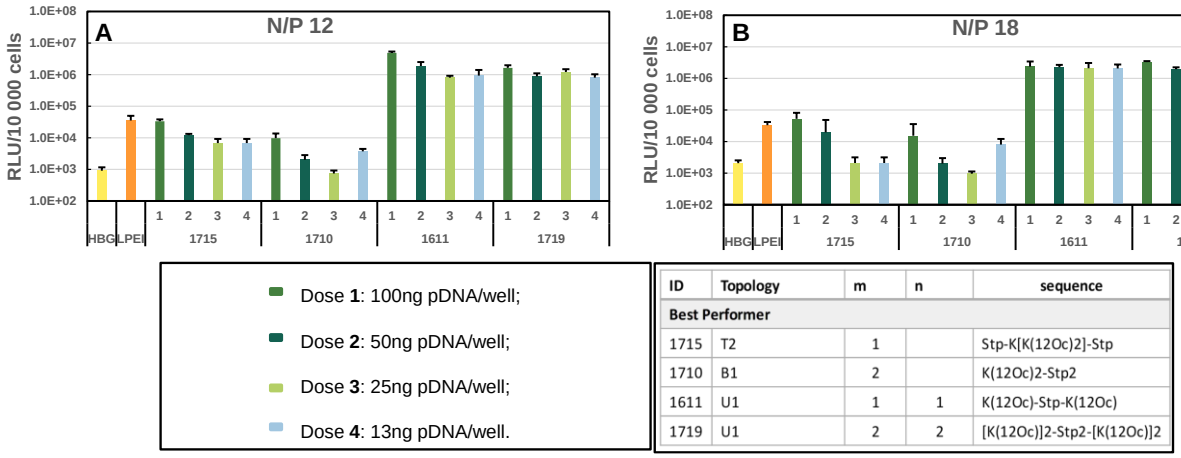

ID	Topology	m	n	sequence
Best Performer				
1715	T2	1		Stp-K[K(12Oc)2]-Stp
1710	B1	2		K(12Oc)2-Stp2
1611	U1	1	1	K(12Oc)-Stp-K(12Oc)
1719	U1	2	2	[K(12Oc)]2-Stp2-[K(12Oc)]2

Figure 5.4. Gene transfer with pDNA lipopolyplexes into Neuro2A neuroblastoma cells. pCMVL polyplexes were prepared at indicated N/P ratio ((A)12 or (B) 18) in HBG and applied in indicated doses (13 ng to 100 ng /well) for transfection of 10,000 Neuro2A cells /well. Luciferase protein expression was determined at 24 hours after transfection. The experiment was performed by Paul Folda, PhD student at LMU Pharmaceutical Biotechnology.

Cationizable hydrophobic domains (LAFs) contain protonatable (tertiary) amines, which is an essential factor in the pDNA gene transfer into N2A cells. We also explored one of the best performers U-shape with the replacement of DodOc. The DodOc domain consists of 8-aminooctanoic acid coupled with dodecanoic acid (C12 acid), resulting in an amide, possessing the same length of chain as 12Oc but without the branched point or tertiary amine. The DodOc containing structure **1725** does not transfect, compared to the high efficiency of **1722** polyplexes, **1725** shows same activity as control group of HBG treated cells.

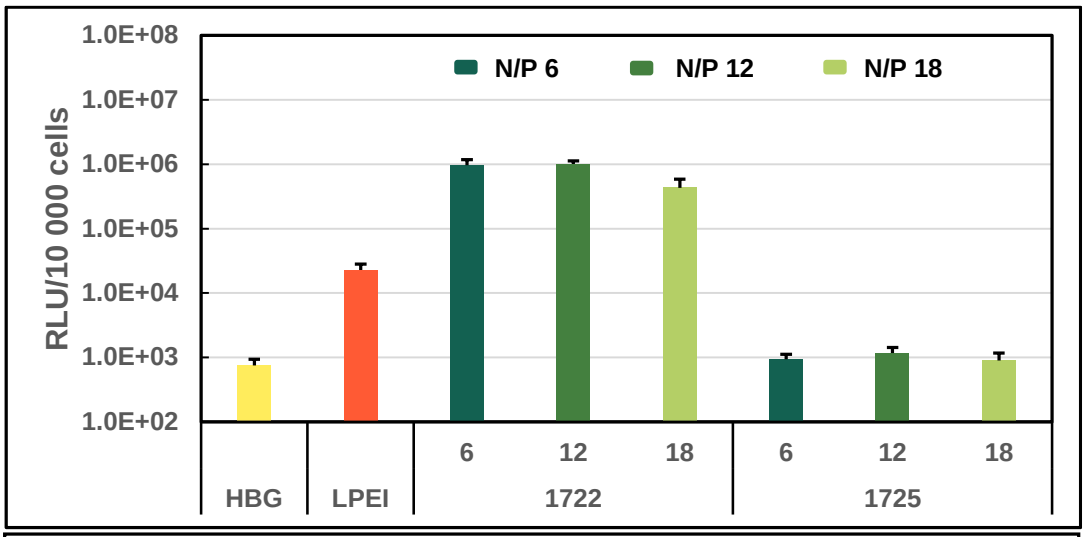

ID	Topology	m	n	sequence
1722	U3	2	2	K(12Oc)2-Stp2-K(12Oc)-K(12Oc)
1725	U3	2	2	K(DodOc)2-Stp2-K(DodOc)-K(DodOc)

Structure of DodOc:

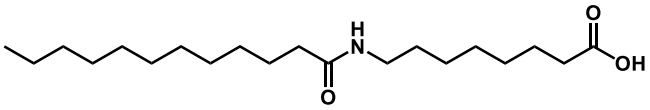

Figure 5.5. Gene transfer with pDNA lipopolyplexes into Neuro2A neuroblastoma cells using oligomer **1722** or negative control oligomer **1725**. 200 ng pCMVL polyplexes were prepared at indicated N/P ratio (6, 12 or 18) in HBG and applied for transfection of 10,000 Neuro2A cells /well. Luciferase protein expression was determined at 24 hours after transfection. The experiment was performed by Paul Folda, PhD student at LMU Pharmaceutical Biotechnology.

5.3.4.2 Evaluation of LAFs Oligomers for in vitro mRNA Delivery

We also applied the structure library with new topologies to mRNA carriers. The first carriers such as 1218 for mRNA formulations have already been developed with this technology in our lab reported by Krhac Levacic/Berger et al.,[277] 1218 has no lipophilic

cationizable building blocks but only permanently lipophilic fatty acid residues and are significantly less active. During the optimization of 1218, it was noticed that the labilization of the lipophilic fatty acid region through reductive cleavage from the oligomer had an advantageous. For comparison, SuccPEI and 1218 as control in the evaluation of mRNA delivery. Some of the structures that were already described for pDNA delivery such as **1611**, **1719** and **1722** also show good transfection efficiency in mRNA delivery at lower dose, as it shown in **Figure 5.6.** In detail, the effect of positive control SuccPEI was decreased more than 15 times with the dose decreasing from 125 to 31.25 ng/well. In contrast, U-shape structures **1611**, **1719** and **1722** keep their high effective effect in mRNA even the doses were decreased. We can not only see the high efficiency in the delivery of 5moU modified mRNA (**Figure 5.6 A**) but also the mRNA without base modification (**Figure 5.6 B**). Compared to the 1218 polyplexes, perturbation of lipophilicity introduced via a different route through protonatability of the lipophilic building block shows a much more dramatic improvement (~20- to 100-fold efficiency).

Table 5.2. The structures for comparison of lipo-oligomers for mRNA delivery.

ID	Topology	m	n	sequence
1722	U3	2	2	K(12Oc)2-Stp2-K(12Oc)-K(12Oc)
1732	U4	2	1	K(8Oc)2-Stp2-K[K(8Oc)2]
1725	U3	2	2	K(DodOc)2-Stp2-K(DodOc)-K(DodOc)
1614	B1	1		K(12Oc)2-Stp
1621	B2	1		K[K[8Oc)2]2-Stp

We can also conclude that the U-shape structures **1611**, **1719** and **1722** show effective effect in mRNA even for the decreased doses of mRNA from 125 ng/well to 31.25 ng/well from **Figure 5.6**, Whereas the efficiency decreased 100 times from the highest dose to the lowest one for the bundle **1614**. In addition, structures with a different kind of LAF were evaluated for mRNA delivery. The U4 backbone with another LAF 8Oc **1732** and B2 with 8Oc **1621** still maintain high transfection efficiency when the dose of each well was decreased. The structures are shown in **Table 5.2**. Overall, the structures containing LAFs not only 12Oc but also 8Oc in some topologies are very effective carriers for mRNA delivery. Furthermore, we also explored the impact of DodOc replacement for the LAF in mRNA polyplexes, see **Figure 5.7**. The DodOc containing structure **1725** does not transfect at all, compared to the high efficiency of

1722 polyplexes. This demonstrates that the LAF plays a significant role in the polyplexes formation and nucleic acid delivery.

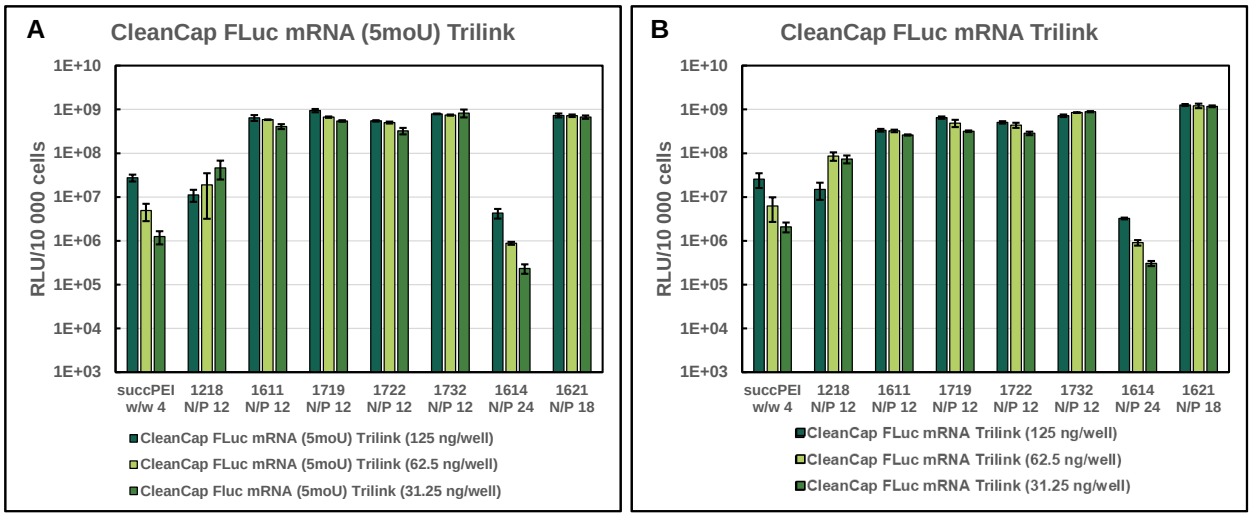

Figure 5.6. Transfer of luciferase mRNA lipopolyplexes into Neuro2A neuroblastoma cells. Polyplexes were prepared at indicated N/P ratios in HBG and applied in indicated mRNA doses (31.25 ng to 125 ng /well) for transfection of 10,000 Neuro2A cells /well. Luciferase protein expression was determined at 24 hours after transfection. CleanCap FLuc mRNA with or without 5moU modification was tested. SuccPEI at w/w 4 was used as positive control. The experiment was performed by Sophie Schlögl, PhD student at LMU Pharmaceutical Biotechnology.

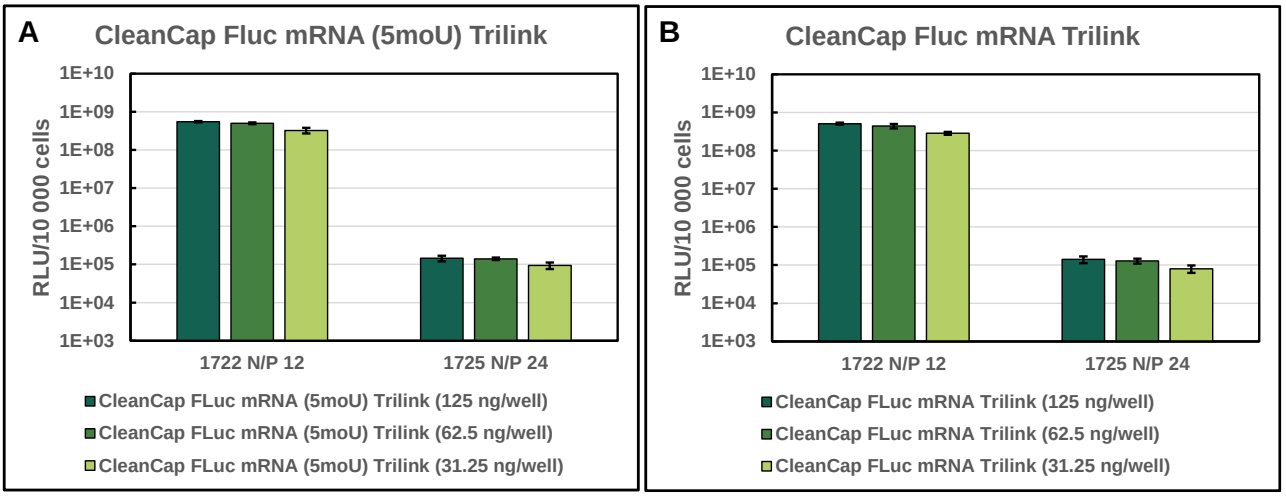

Figure 5.7. Transfer of luciferase mRNA lipopolyplexes into Neuro2A neuroblastoma cells using oligomer 1722 or negative control oligomer 1725. Polyplexes were prepared at indicated N/P ratios in HBG and applied in indicated doses (31,25 ng to 125 ng /well) for transfection of 10,000 Neuro2A cells /well. Luciferase protein expression was determined at 24 hours after transfection. CleanCap FLuc mRNA with or without 5moU modification was tested. SuccPEI at w/w 4 was used as positive control. The experiment was performed by Sophie Schlögl, PhD student at LMU Pharmaceutical Biotechnology.

5.3.4.3 Evaluation of LAFs Oligomers for in vitro siRNA Delivery

These sequenced-defined U-shape structures performed very well in pDNA and mRNA delivery and were subsequently also evaluated *in vitro* in siRNA polyplexes. The LAF oligomers form nanoparticles with control siRNA and eGFP-targeting siRNA (siGFP). Luo et al. have already reported the 1214 for siRNA formulations with high gene silencing efficiency.[296] Thus 1214 and SuccPEI were used as controls. Gene silencing experiments (**Figure 5.8**) were performed using the marker gene of N2A-eGFPLuc cells (enhanced green fluorescent protein/luciferase fusion protein). Specific silencing of the eGFPLuc fusion gene by siGFP was measured by a luminometric luciferase assay. Unspecific reduction of reporter activity was determined using the analogs siCtrl formulations. In general, the U-shape structures show higher functional siRNA transfer. These siRNA polyplexes at lower dose can reduce the toxicity but still possess high gene silencing effect, such as polyplexes formed of **1716**, **1717**, **1718** and **1719**. In sum, the screening for transfection-active polyplexes revealed the 1) LAF and 2) topologies) in the nucleic acid delivery as favorable elements.

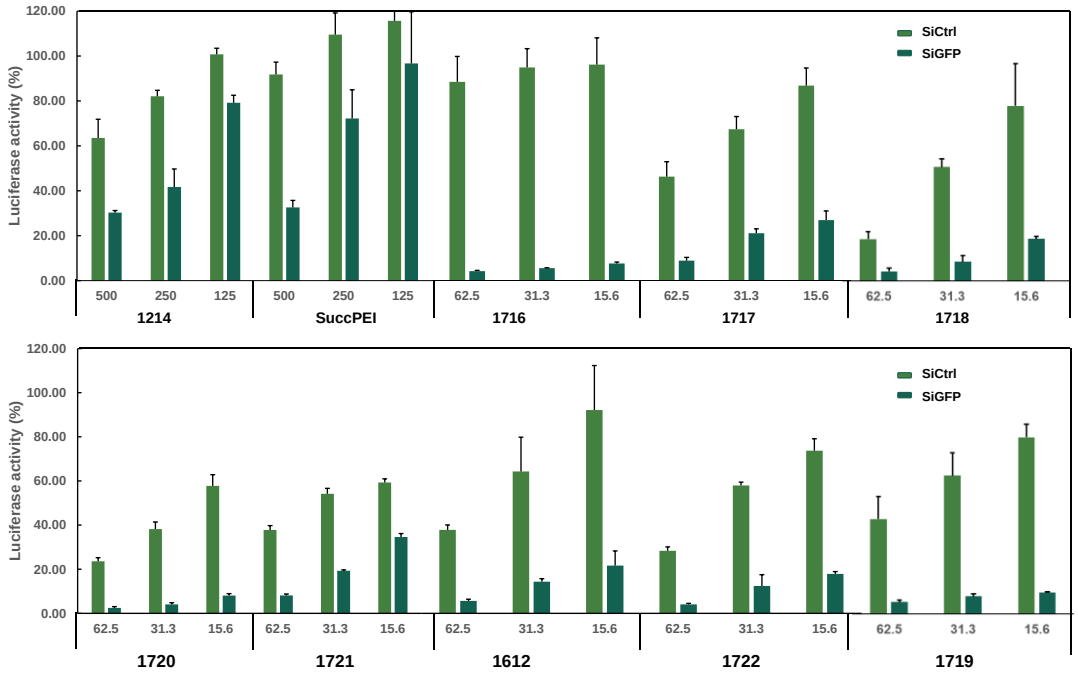

Figure 5.8. Gene silencing activity of siRNA formulations was tested by luciferase assays. Specific gene silencing (using siGFP) is compared with unspecific reporter silencing (by siCtrl formulations). Polyplexes were prepared at indicated N/P 18 in HBG and applied in indicated doses (15.6 ng to 62.5 ng /well) for transfection of N2A-eGFPLuc cell (5000 cells/well). Luciferase protein expression was determined at 48 hours after transfection. SuccPEI at w/w 4 was used as positive control. 1214 at N/P ratio 12 was used as control. The experiment was performed by Mina Yazdi, PhD student at LMU Pharmaceutical Biotechnology.

5.4 Conclusions

In summary, the use of novel, hydrophobic cationizable domains (LAFs), in combination with the previously established artificial amino acid succinoyl-tetraethylenpentamine (Stp) in solid-phase supported synthesis of sequence-defined oligomers provided novel efficient carriers for nucleic acid delivery. Our first examples already demonstrate that clear structure-activity relationship depends on the specific building blocks, sequences, topologies used on the carrier side and the type of nucleic acid. It turned out that the novel combination of building blocks/components is necessary for an astonishingly high effect. For example, some structures show very good efficiency for pDNA transfer, outstanding efficiency for packaging mRNA into lipopolyplexes, or good efficiency for siRNA transfer. We can also see that substituting the LAF building block with control building blocks (such as DodOc) led to a greatly reduced effect.

6 Summary of the thesis

Studies on tailor-made designs of carriers have already developed some novel nanoplatforms for combination chemotherapy and nucleic acid delivery, such as polymeric nanoparticles, solid lipid nanoparticles, micelles, dendrimers, liposomes, gold nanoparticles, they are changing the fate of various therapies in some cases. Conventional anticancer drug combinations suffer from major issues such as unequal bioavailability and unmatched pharmacokinetics/circulation half-lives among drug components. The optimized carriers for combinations of drugs with different intracellular targets are routinely used in tumor chemotherapy due to their increased efficiency and reduced risk for chemoresistance. Considering polymeric vesicles encapsulating both hydrophobic and hydrophilic drugs, it remains a considerable challenge to fabricate codelivery polymeric vesicles possessing structural stability during blood circulation, encapsulation stability toward both hydrophobic and hydrophilic drugs, and synchronized corelease features triggered by a specific pathological milieu. In addition, polymeric carriers have been explored for nucleic acid delivery for more than two decades, a series of novel therapeutic nucleic acids entered research and clinical valuation. For example, the cationic carriers, lipofection and LNPs have been used in clinical translation, however they still illustrate lower efficacy in comparison to viruses.

The study described in the first main chapter focuses on optimizing stable polyplexes with sequence-defined oligoaminoamides/oligomers and hydrophobic drugs. With this, the modification of drug analogs and oligomers, and the addition of helper lipid were applied to optimize combination chemotherapy. A combination effect of drug polyplexes was visible on L1210 cells compared to the effects of single pretubulysin (PT) and methotrexate (MTX). The cationizable lipo-oligomers 1198 and 1444 formed polyelectrolyte complexes with the anionic drug MTX (and analogs E2MTX and E5MTX) via electrostatic interactions and PT via hydrophobic and hydrophilic interactions. In addition, the modified drugs E2MTX and E5MTX show same efficiency of tumor treatment as MTX, but form more stable polyplexes. Adding cholesterol as a helper lipid and more hydrophobic domains in the cationic oligomers helps to stabilize the particles in the presence of FBS medium. Incorporating PT+MTX with several optimized modifications into the delivery systems increased the antitumoral efficiency of the drug combination in cell culture.

The second main chapter reviews recent tailor-made polymeric carrier designs that were optimized for nucleic acid cargos such as plasmid DNA, siRNA, and micro RNA, mRNA, or genome-modifying nucleic acids. The specific requirements for the various therapeutic cargos are discussed. It prospects the future directions including dynamic bioresponsive polymers as components of nanomachines, multifunctional sequence-defined carriers for evolution-based selective optimization, and organic−inorganic multicomponent nanoassemblies.

In the third main chapter, novel lipo-amino fatty acid (LAF) building blocks were synthesized for use in the solid-phase synthesis of novel nucleic acid delivery systems. The solid-phase methodology enabled the rapid parallel synthesis of LAF and succinoyl-tetraethylenpentamine (Stp) containing structures as carriers for nucleic acid delivery. The new synthetic platform was used to construct a small library of oligomers consisting of polar cationizable Stp domains and hydrophobic cationizable LAF domains in different ratios and topologies. Subsequent screening of the library for pDNA, mRNA and siRNA delivery identified a set of lead structures able to most favorably compete with gold standard polymeric carriers LPEI or SuccPEI.

7 Appendix

7.1 Abbreviations

Boc	*tert*-Butoxycarbonyl protecting group
DCM	Dichloromethane
DIPEA	*N,N*-Diisopropylethylamine
DLS	Dynamic light scattering
DMEM	Dulbecco's modified Eagle's medium
DMF	*N,N*-Dimethylformamide
DNA	Desoxyribonucleic acid
EDTA	Ethylendiaminetetraacetic acid
EGF/EGFR	Epidermal growth factor (receptor)
EtBr	Ethidium bromide
FBS	Fetal bovine serum
Fmoc	Fluorenylmethoxycarbonyl protecting group
FolA	Folic acid
FR	Folate receptor
HBG	Hepes-buffered glucose
HBTU	2-(1H-benzotriazole-1-yl)-1,1,3,3-tetramethyluronium hexafluorophosphate
HEPES	*N*-(2-hydroxethyl) piperazine-N'-(2-ethansulfonic acid)
HGF/HGFR	Hepatocyte growth factor (receptor)
HOBt	1-Hydroxybenzotriazole
kDa	Kilodalton
LMW	Low molecular weight
LPEI	Linear polyethylenimine
mM	Millimolar
mRNA	Messenger RNA
MTBE	Methyl *tert*-butyl ether
MTT	3-(4,5-dimethylthiazol-2-yl)-2,5-diphenyltetrazolium bromide
mV	Millivolt
MWCO	Molecular weight cut-off
N/P	Nitrogen to phosphates ratio
NEM	N-ethylmaleimide

NHS	*N*-Hydroxysuccinimide
nm	Nanometer
NMP	*N*-Methyl-2-pyrrolidone
NMR	Nuclear magnetic resonance
OleA	Oleic acid
PDI	Polydispersity index
pDNA	Plasmid DNA
PEG	Polyethylene glycol
pKa	$-\log_{10} K_a$ (acid dissociation constant)
PyBOP	Benzotriazol-1-yloxy-tripyrrolidinophosphonium hexafluorophosphate
RLU	Relative light units
RNA	Ribonucleic acid
succPEI	branched polyethylenimine with a succinylation degree of 10%
RP-HPLC	Reversed-phase high-performance liquid chromatography
RT	Room temperature
SEC	Size-exclusion chromatography
siRNA	Small interfering RNA
SPS	Solid-phase synthesis
Stp	Succinyl-tetraethylene pentamine
STOTDA	*N*-Fmoc-*N*″-succinyl-4,7,10-trioxa-1,13-tridecanediamine
TEPA	Tetraethylene pentamine
TFA	Trifluoroacetic acid
THF	Tetrahydrofuran
TIS	Triisopropylsilane

7.2 Summary of SPS derived oligomers

Table 7.1. Summary of SPS derived oligomers.

Oligomer ID	Topology	Sequence (N→C)	Proton. amines	Chapter
1198	T-Shape	(N3)K-C-Y_3-Stp_2-K-[K(OleA)$_{\alpha,\varepsilon}$]$_\varepsilon$-Stp_2-Y_3-C-OH	13	3
1444	T-shape	(N3)K-C-Y_6-Stp_2-K-[K(OleA)$_{\alpha,\varepsilon}$]$_\varepsilon$-Stp_2-Y_6-C-OH	13	3
1563	U-shape	H_2N-Stp_2-K(12Oc)-Stp_2-OH	14	5
1611	U-shape	H_2N-K(12Oc)-Stp-K(12Oc)-OH	6	5
1612	U-shape	K(12Oc)$_2$-Stp-K(12Oc)-K(12Oc)-OH	7	5
1613	Bundle	K[K(12Oc)$_2$]$_2$-Stp-OH	7	5
1614	Bundle	K(12Oc)$_2$-Stp-OH	5	5
1615	Comb	H_2N-[K(12Oc)]$_2$-Stp-OH	6	5
1616	Comb	H_2N-[K(12Oc)]4-Stp-OH	8	5
1617	Comb	H_2N-[K(12Oc)]$_6$-Stp-OH	10	5
1620	U-shape	K(8Oc)$_2$-Stp-K(8Oc)-K(8Oc)-OH	7	5
1621	Comb	H_2N-K[K(8Oc)$_2$]$_2$-Stp-OH	7	5
1680	U-shape	H2N-K(8Oc)-Stp_2 -K(8Oc)-OH	9	5
1681	U-shape	H_2N-K(12Oc)-Stp_2-K(12Oc)-OH	9	5
1682	U-shape	K(10Oc)$_2$-Stp-K(10Oc)-K(10Oc)-OH	7	5
1700	Comb	H_2N-Stp_{10}-OH	31	5
1701	Comb	H2N-K-K-Stp_{10}-OH	33	5
1704	Comb	H_2N-[K(12Oc)]$_2$-Stp_{10}-OH	33	5
1705	Comb	H_2N-[K(12Oc)]$_4$-Stp_{10}-OH	35	5
1706	Comb	H_2N-[K(12Oc)]$_6$-Stp_{10}-OH	37	5
1707	Comb	H_2N-[K(12Oc)]$_4$-Stp_2-OH	11	5
1708	Comb	H_2N-[K(12Oc)]$_2$-Stp_2-OH	9	5
1709	Comb	H_2N-[K(12Oc)]$_4$-Stp_4-OH	17	5
1710	Bundle	K(12Oc)$_2$-Stp_2-OH	8	5
1711	Bundle	K(12Oc)$_2$-$^\varepsilon$K-$^\varepsilon$K-6Aha -OH	4	5
1712	Bundle	K(DodOc)$_2$-Stp-OH	3	5
1713	Bundle	K[K(12Oc)$_2$]$_2$-Stp_2-OH	10	5
1714	T-shape	H_2N-Stp-[K(12Oc)]$_2$-Stp-OH	9	5
1715	T-shape	H_2N-Stp-K[K(12Oc)2]-Stp-OH	9	5
1716	U-shape	K(12Oc)$_2$-Stp-K[K(12Oc)$_2$]-OH	7	5
1717	U-shape	K(12Oc)2-Stp_2-K[K(12Oc)$_2$]-OH	10	5
1718	U-shape	H2N-[K(12Oc)]$_2$-Stp-[K(12Oc)]$_2$-OH	8	5
1719	U-shape	H2N-[K(12Oc)]$_2$-Stp_2-[K(12Oc)]$_2$-OH	11	5
1720	U-shape	H2N-K[K(12Oc)$_2$]-Stp-K[K(12Oc)$_2$]-OH	8	5
1721	U-shape	K[K(12Oc)2]-Stp_2-K[K(12Oc)$_2$]-OH	11	5
1722	U-shape	K(12Oc)$_2$-Stp_2-K(12Oc)-K12(Oc)-OH	10	5
1723	U-shape	K(12Oc)$_2$-($^\varepsilon$K-$^\varepsilon$K-6Aha)-K(12Oc)-K(12Oc)-OH	6	5
1724	U-shape	K(DodOc)$_2$-Stp-K(DodOc)-K(DodOc -OH	3	5
1725	U-shape	K(DodOc)$_2$-Stp_2-K(DodOc)-K(DodOc)-OH	6	5
1729	Bundle	K(8Oc)$_2$-Stp-OH	5	5

1730	Bundle	K[K[8Oc)$_2$]$_2$-Stp$_2$-OH	10	5
1731	U-shape	K(8Oc)$_2$-Stp$_2$-K(8Oc)-K(12Oc)-OH	10	5
1732	U-shape	K(8Oc)$_2$-Stp$_2$-K[K(8Oc)$_2$]-OH	10	5
1745	U-shape	H_2N-[K(8Oc)]$_2$-Stp$_2$-[K(8Oc)]$_2$-OH	11	5
1746	U-shape	H_2N-K(8Oc)-Stp-K(8Oc)-OH	6	5
1747	U-shape	H_2N-K(12Oc)-$^{\varepsilon}$K-$^{\varepsilon}$K-6Aha-K(12Oc)-OH	5	5
1748	U-shape	H_2N-K(DodOc)-Stp-K(DodOc)-OH	4	5
1749	U-shape	K(DodOc)$_2$-Stp-K[K(DodOc)$_2$]-OH	3	5
1750	U-shape	K(12Oc)$_2$-$^{\varepsilon}$K-$^{\varepsilon}$K-6Aha-K[K(12Oc)$_2$]-OH	6	5
1751	U-shape	[K(DodOc)]$_2$-Stp$_2$-[K(DodOc)]$_2$-OH	7	5

7.3 Summary of SPS derived shielding reagents

Table 7.2. Summary of SPS derived shielding reagents.

ID	Name	Sequence (C→N)	Chapter
	PEG	bisDBCO-PEG$_{24}$	3
	FolA	bisDBCO-PEG$_{24}$-FolA	3
	E4FolA	bisDBCO-PEG$_{24}$-E$_4$FolA	3

8 Analytical data

8.1 MALDI-TOF mass spectrometry of artificial peptides

1 µL matrix solution containing 10 mg/mL Super-DHB (90/10 m/m mixture of 2,5-dihydroxybenzoic acid and 2-hydroxy-5-methoxybenzoic acid) in 69.93/30/0.07 (v/v/v) H_2O/acetonitrile/trifluoroacetic acid was spotted on an MTP AnchorChip (Bruker Daltonics, Germany). After the matrix crystallized, 1 µL of sample solution (10 mg/mL in water) was added to the matrix spot. Samples were analyzed using an Autoflex II mass spectrometer (Bruker Daltonics, Germany). All spectra were recorded in positive ion mode.

Table 8.1. Summary of peptide data.

ID	Description	Molecular formula	$[M+H]^+$ calc.	$[M+H]^+$ found
	E2-MTX	$C_{30}H_{36}N_{10}O_{11}$	712.7	710.6
	E5-MTX	$C_{45}H_{57}N_{13}O_{20}$	1100.0	1097.8
1198	T-Shape	$C_{162}H_{264}N_{36}O_{28}S_2$	3228.2	3221.4
1444	T-Shape	$C_{216}H_{318}N_{42}O_{40}S_2$	4207.2	4195.4
	$DBCO_2$ –PEG_{24}-FolA	$C_{124}H_{178}N_{14}O_{37}$	2456.8	2453.3
	$DBCO_2$ –PEG_{24}-4FolA	$C_{124}H_{178}N_{14}O_{37}$	2973.3	2965.6
1563	U-shape	$C_{86}H_{177}N_{23}O_{11}$	1709.47	1703.6
1611	U-shape	$C_{88}H_{177}N_{11}O_7$	1501.42	1499.2
1612	U-shape	$C_{158}H_{315}N_{15}O_{10}$	2585.28	2580.6
1613	Bundle	$C_{158}H_{315}N_{15}O_{10}$	2585.29	2580.2
1614	Bundle	$C_{82}H_{165}N_9O_6$	1373.24	1370.0
1615	Comb	$C_{88}H_{177}N_{11}O_7$	1501.42	1499.2
1616	Comb	$C_{164}H_{327}N_{17}O_{11}$	2713.46	2700.8
1617	Comb	$C_{240}H_{477}N_{23}O_{15}$	3925.5	3912.6
1620	U-shape	$C_{126}H_{251}N_{15}O_{10}$	2136.44	2131.9
1621	Comb	$C_{126}H_{251}N_{15}O_{10}$	2136.44	2133.5
1681	U-shape	$C_{100}H_{202}N_{16}O_9$	1772.82	1769.1
1700	Comb	$C_{120}H_{252}N_{50}O_{21}$	2731.67	2726.4
1701	Comb	$C_{132}H_{276}N_{54}O_{23}$	2988.02	2983.5
1704	Comb	$C_{196}H_{402}N_{56}O_{25}$	3943.74	3934.3
1705	Comb	$C_{272}H_{552}N_{62}O_{29}$	5155.81	N.D.
1706	Comb	$C_{348}H_{702}N_{68}O_{33}$	6367.89	N.D.
1707	Comb	$C_{176}H_{352}N_{22}O_{13}$	2984.89	2981.5
1708	Comb	$C_{100}H_{202}N_{16}O_9$	1772.82	1765.0
1709	Comb	$C_{200}H_{402}N_{32}O_{17}$	3527.62	3516.5
1710	Bundle	$C_{94}H_{190}N_{14}O_8$	1644.64	1641.5
1711	Bundle	$C_{88}H_{175}N_9O_7$	1471.42	1467.8
1712	Bundle	$C_{58}H_{113}N_9O_8$	1064.6	1062.3
1713	Bundle	$C_{170}H_{340}N_{20}O_{12}$	2856.72	2849.98
1714	T-shape	$C_{100}H_{202}N_{16}O_9$	1772.82	1765.0
1715	T-shape	$C_{100}H_{202}N_{16}O_9$	1772.82	1769.1
1716	U-shape	$C_{158}H_{315}N_{15}O_{10}$	2585.35	2579.9
1717	U-shape	$C_{170}H_{340}N_{20}O_{12}$	2856.72	2849.9
1718	U-shape	$C_{164}H_{327}N_{17}O_{11}$	2713.53	2707.03
1719	U-shape	$C_{176}H_{352}N_{22}O_{13}$	2984.89	2977.1
1720	U-shape	$C_{164}H_{327}N_{17}O_{11}$	2713.53	2707.4

1721	U-shape	$C_{176}H_{352}N_{22}O_{13}$	2984.89	2977.9
1722	U-shape	$C_{170}H_{340}N_{20}O_{12}$	2856.72	2849.99
1723	U-shape	$C_{164}H_{325}N_{15}O_{11}$	2683.5	2676.8
1724	U-shape	$C_{110}H_{211}N_{15}O_{14}$	1967.99	1963.3
1725	U-shape	$C_{122}H_{236}N_{20}O_{16}$	2239.35	2234.5
1729	Bundle	$C_{66}H_{133}N_9O_6$	1148.85	1146.1
1730	Bundle	$C_{138}H_{276}N_{20}O_{12}$	2407.85	2402.3
1731	U-shape	$C_{138}H_{276}N_{20}O_{12}$	2407.85	2403.2
1732	U-shape	$C_{138}H_{276}N_{20}O_{12}$	2407.85	2402.9
1745	U-shape	$C_{144}H_{288}N_{22}O_{13}$	2536.03	2530.1
1746	U-shape	$C_{72}H_{145}N_{11}O_7$	1277.02	1274.2
1747	U-shape	$C_{94}H_{187}N_{11}O_8$	1599.6	1595.9
1748	U-shape	$C_{64}H_{125}N_{11}O_9$	1192.77	1189.97
1749	U-shape	$C_{110}H_{211}N_{15}O_{14}$	1967.99	1963.5
1750	U-shape	$C_{164}H_{325}N_{15}O_{11}$	2683.5	2677.01
1751	U-shape	$C_{128}H_{248}N_{22}O_{17}$	2367.53	2361.96

MALDI-TOF MS of E2-MTX

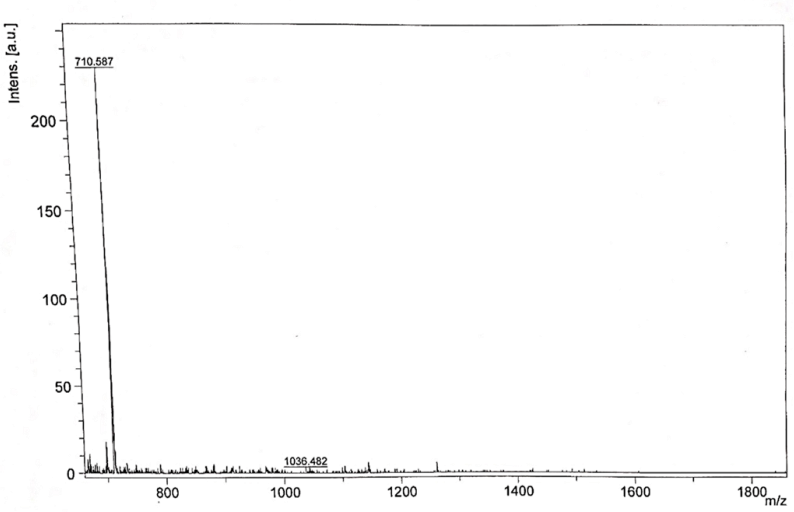

MALDI-TOF MS of E5-MTX

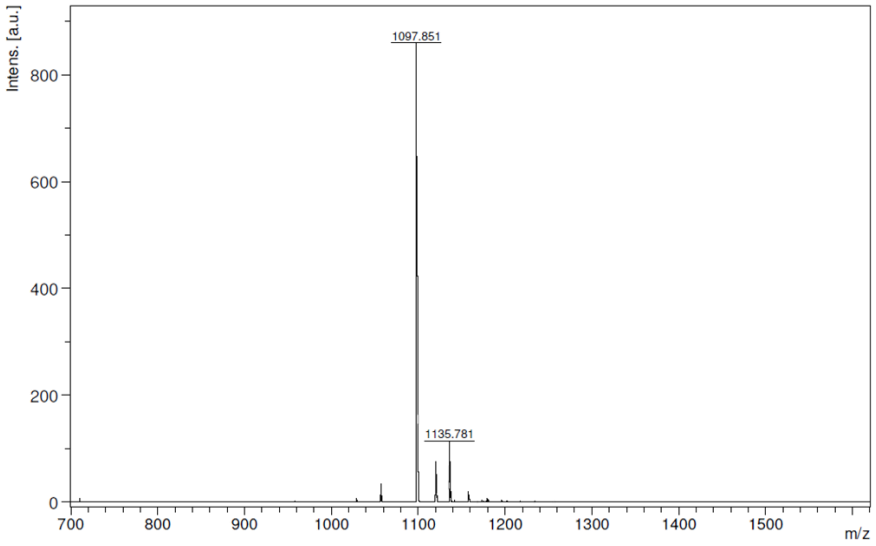

MALDI-TOF MS of 1198

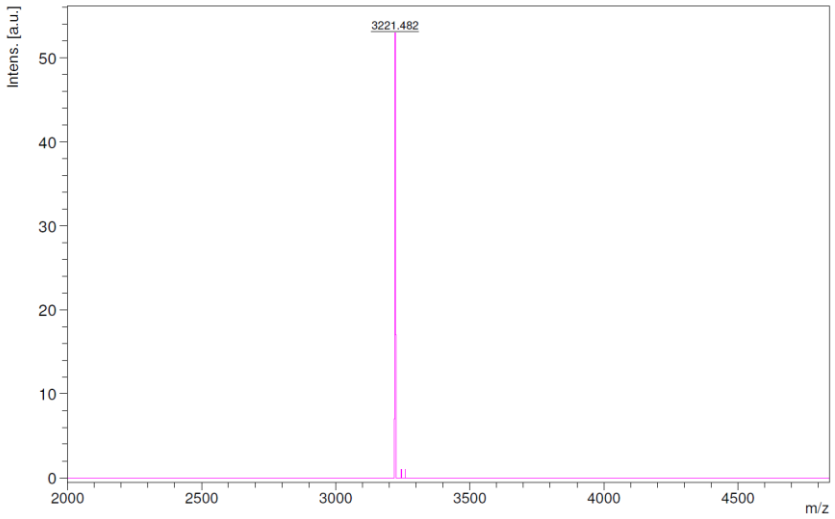

MALDI-TOF MS of 1444

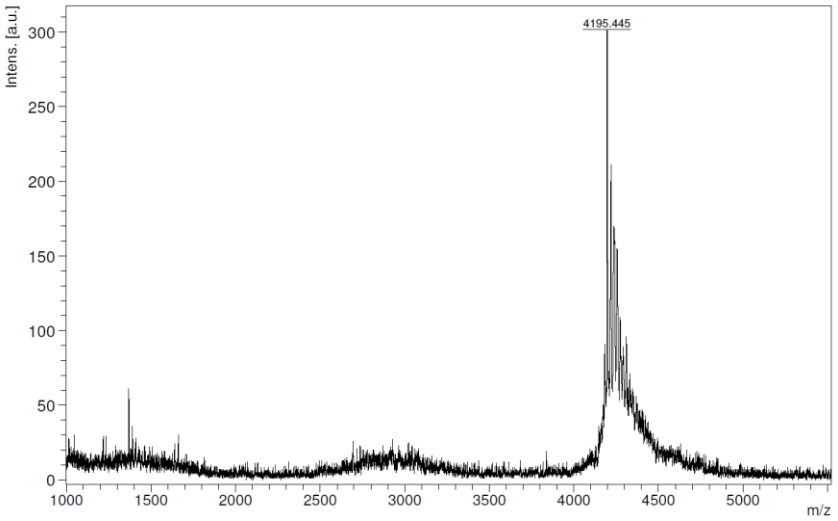

MALDI-TOF MS of $DBCO_2$- PEG_{24}- FolA

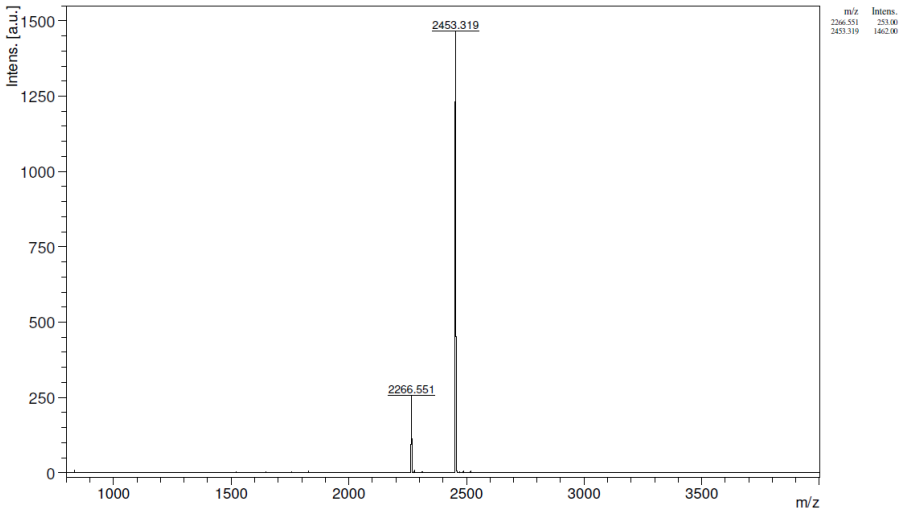

MALDI-TOF MS of $DBCO_2$- PEG_{24}- E4FolA

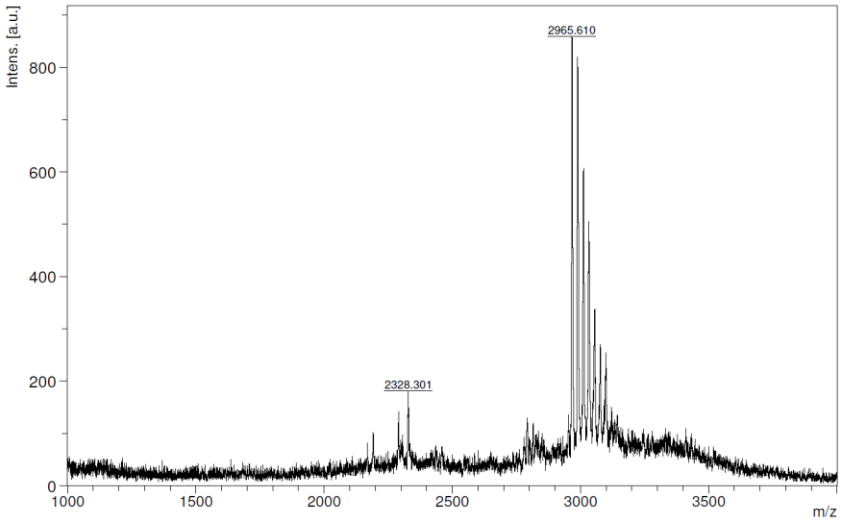

MALDI-TOF MS of cy5-labeled 1198

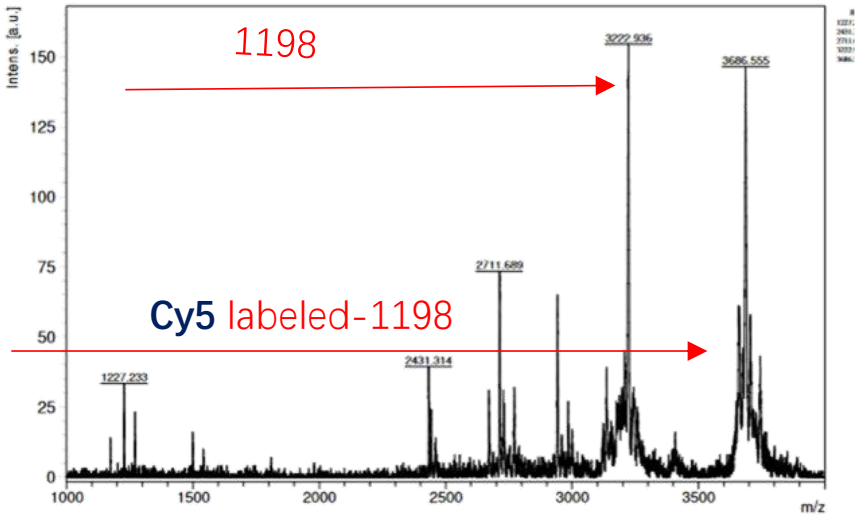

MALDI-TOF MS of 1700

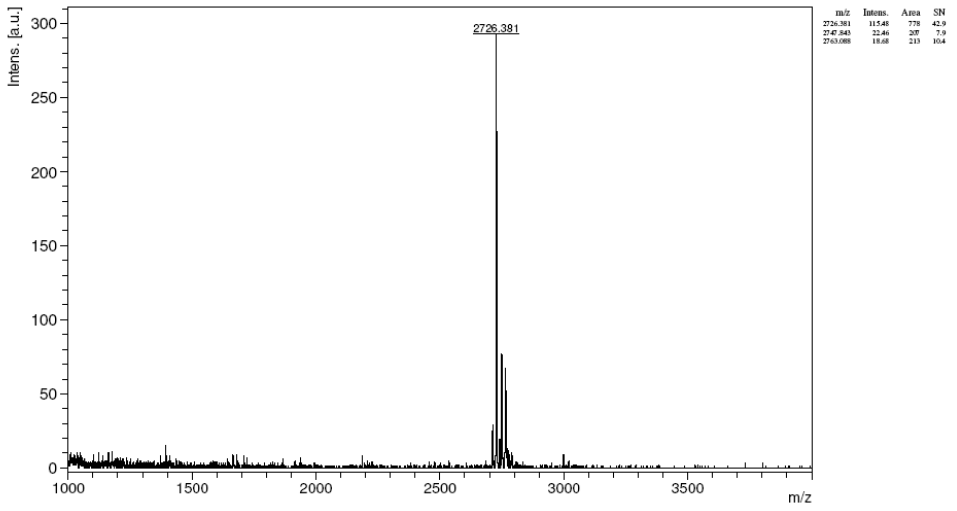

MALDI-TOF MS of 1701

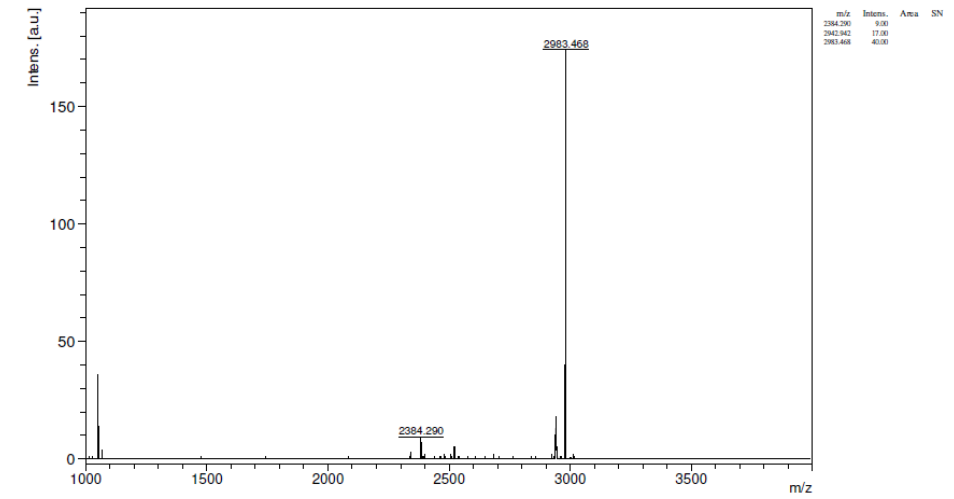

MALDI-TOF MS of 1615

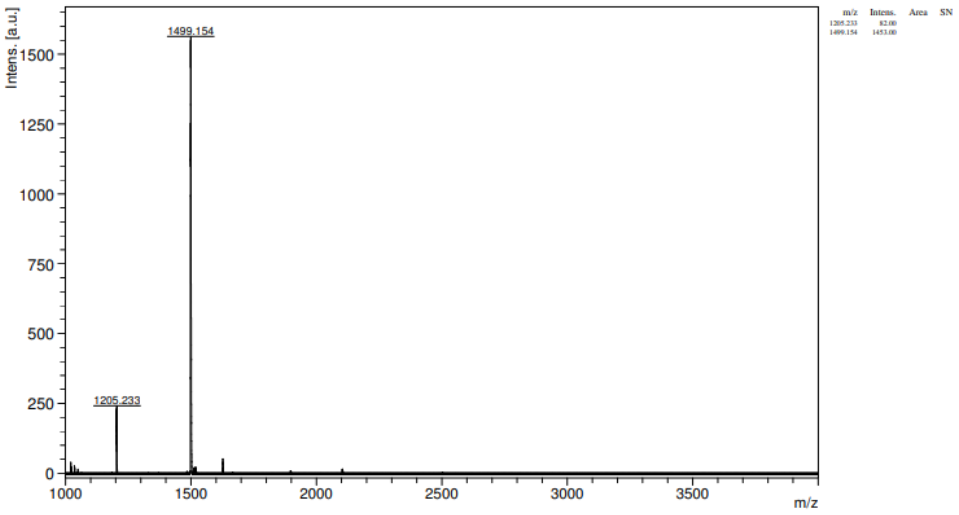

MALDI-TOF MS of 1616

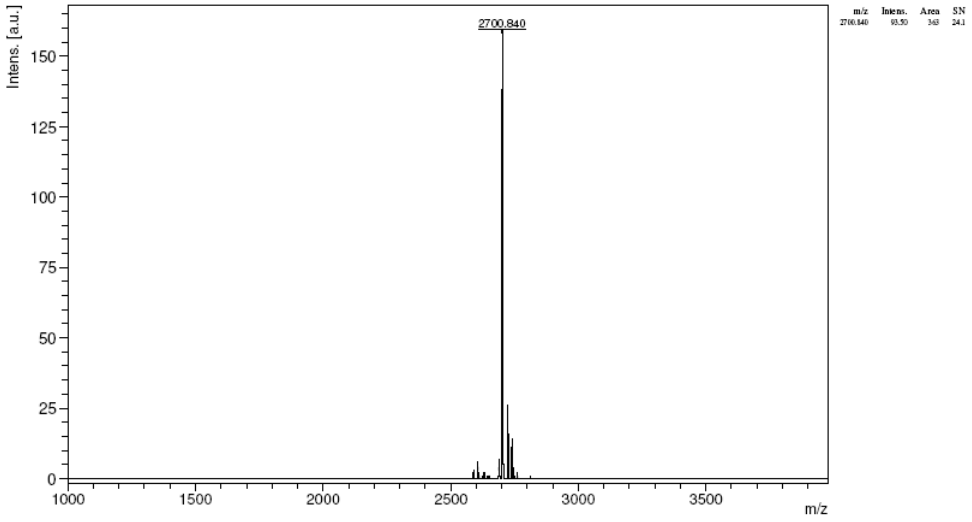

MALDI-TOF MS of 1617

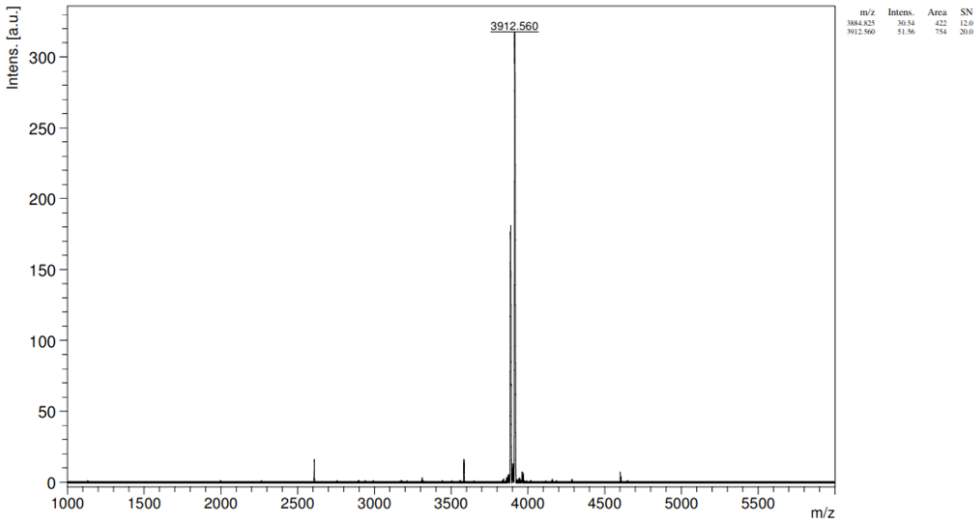

MALDI-TOF MS of 1704

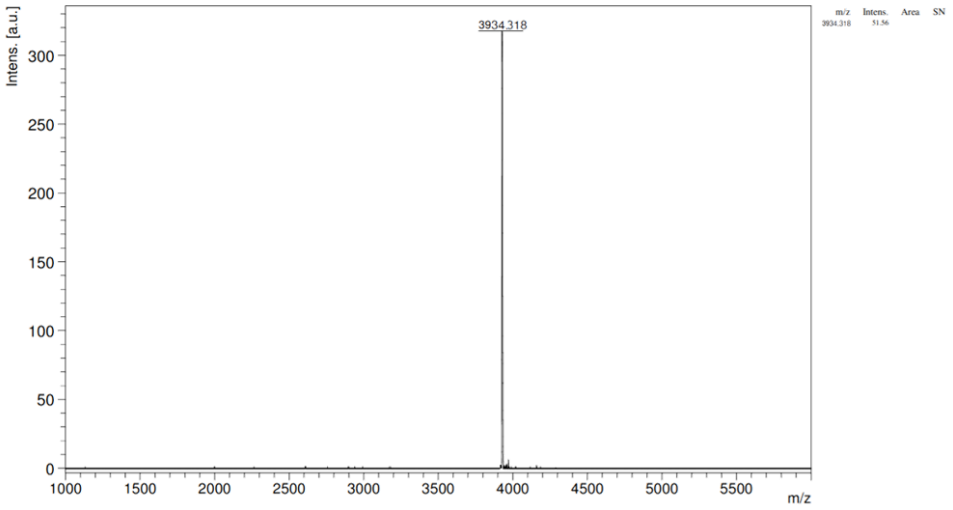

MALDI-TOF MS of 1707

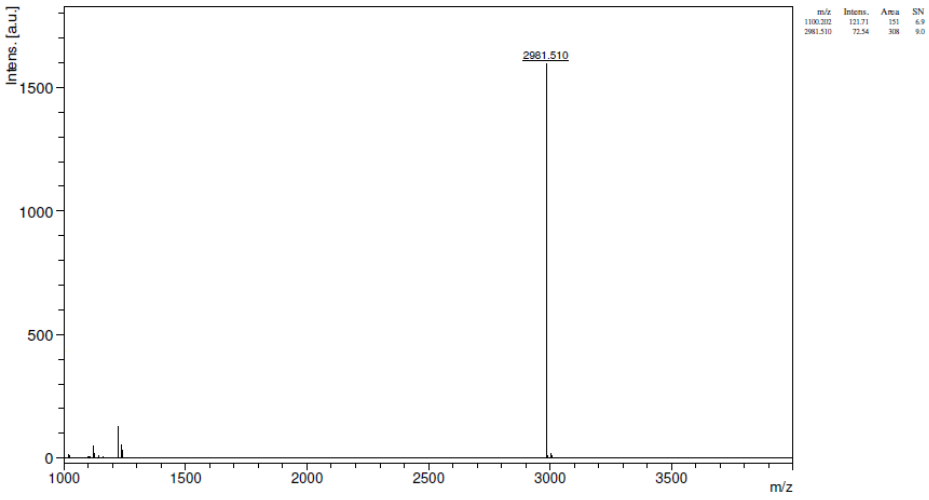

MALDI-TOF MS of 1708

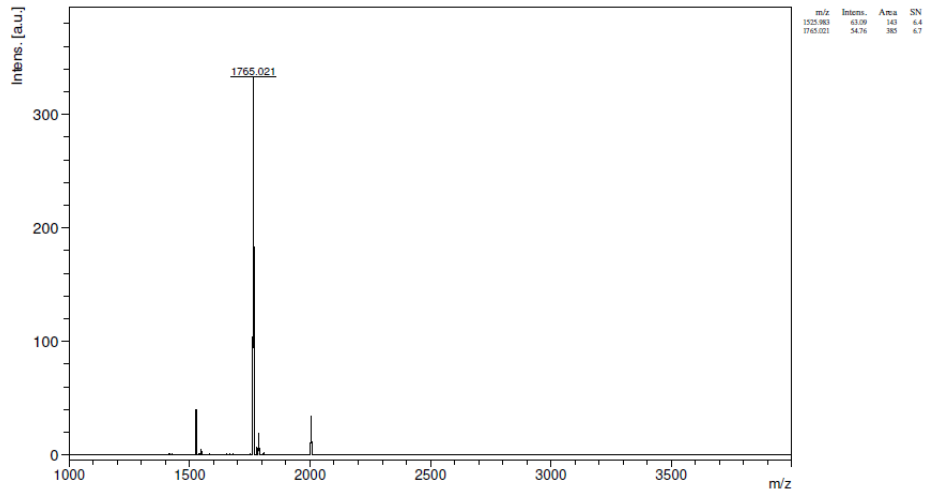

MALDI-TOF MS of 1709

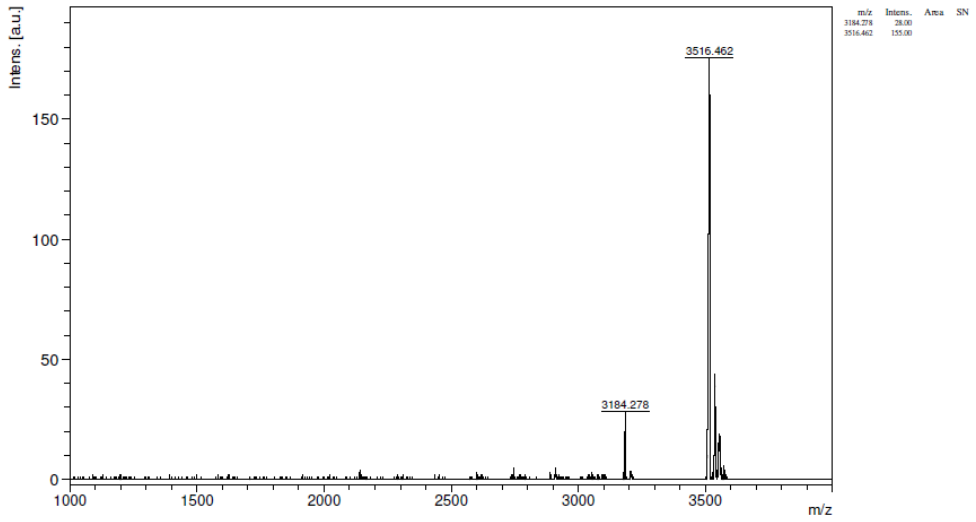

MALDI-TOF MS of 1563

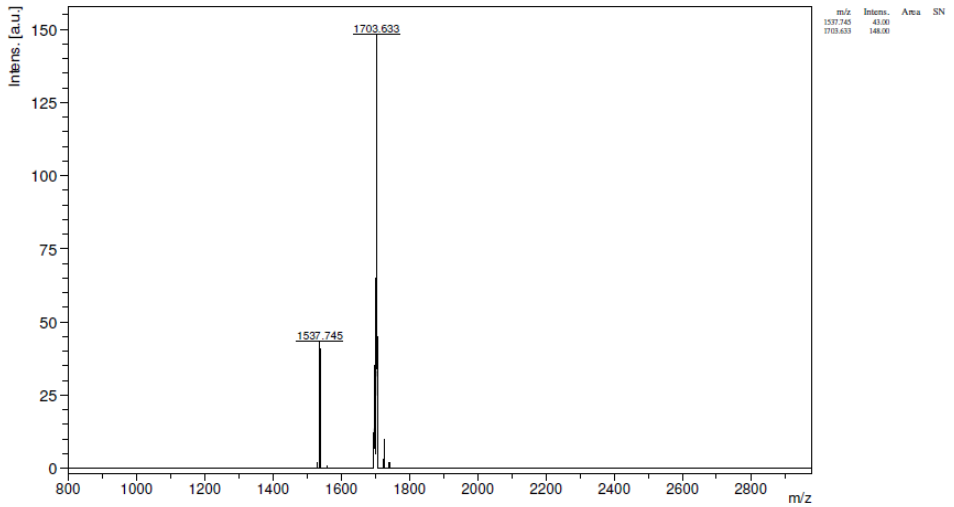

MALDI-TOF MS of 1714

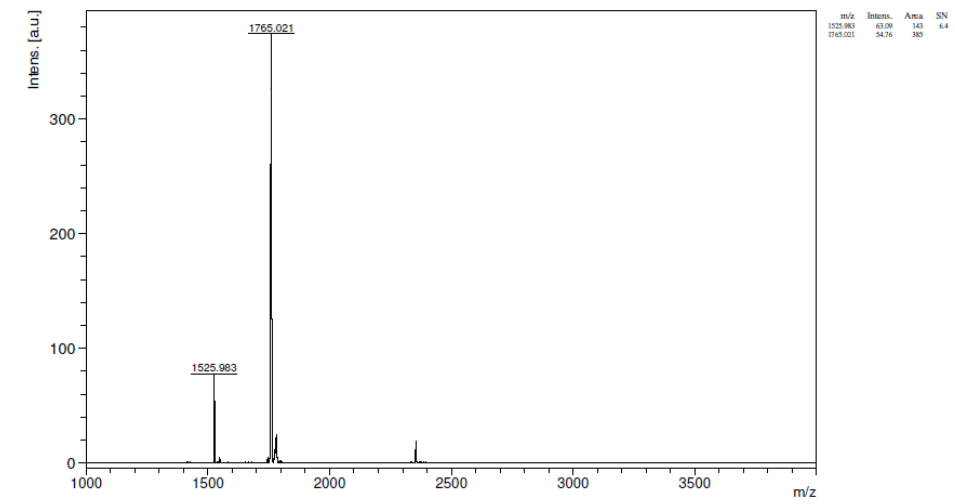

MALDI-TOF MS of 1715

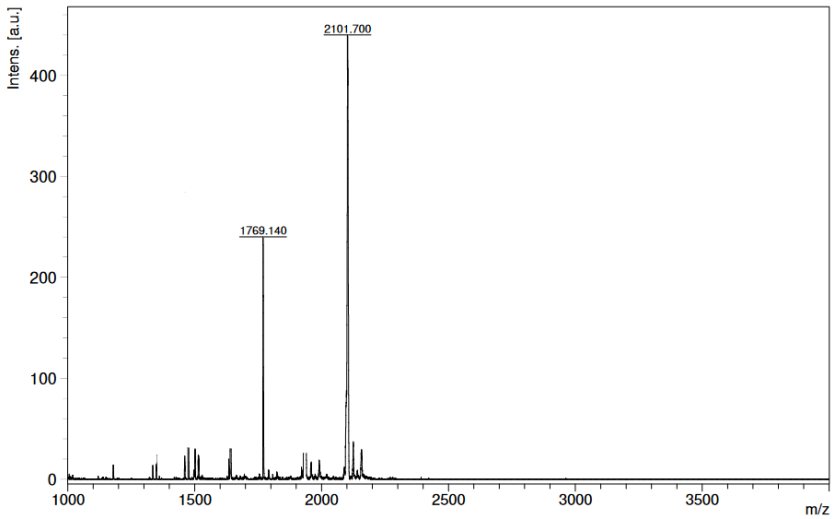

MALDI-TOF MS of 1614

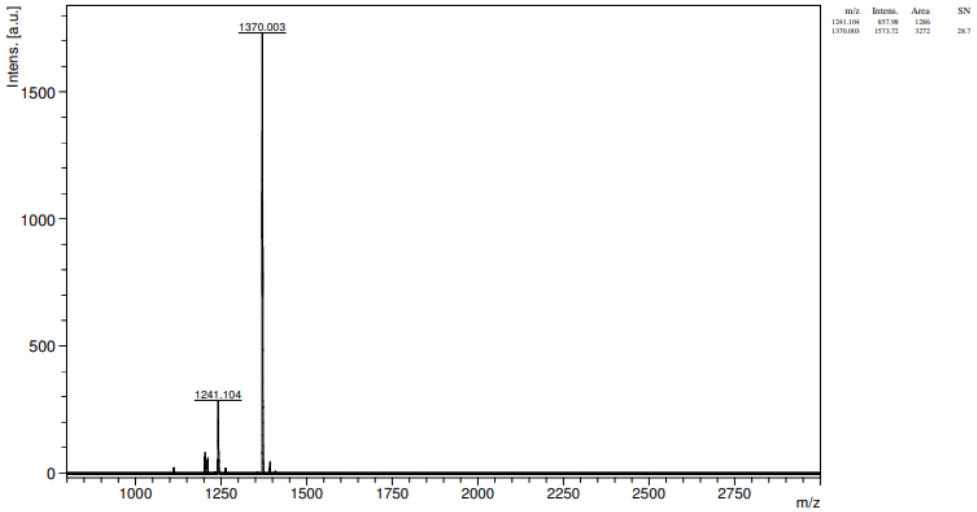

MALDI-TOF MS of 1710

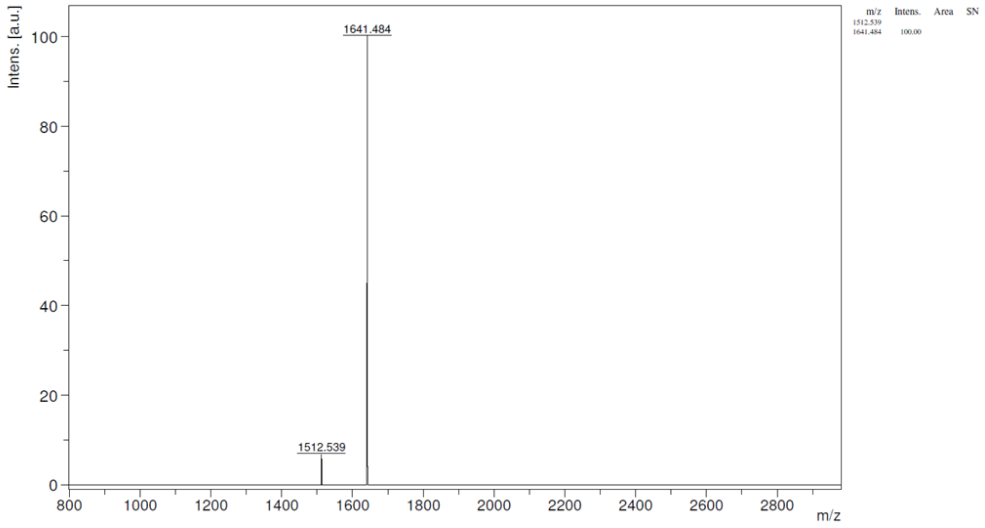

MALDI-TOF MS of 1711

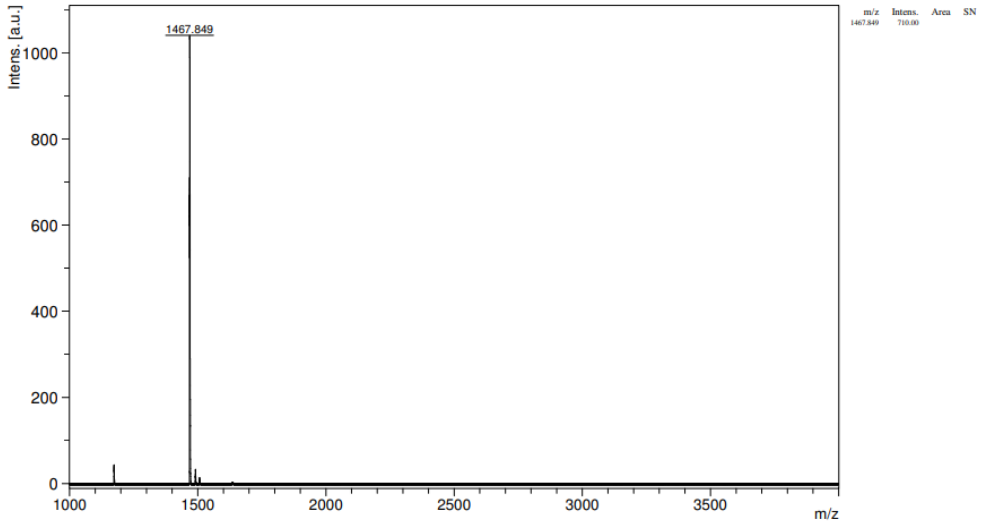

MALDI-TOF MS of 1712

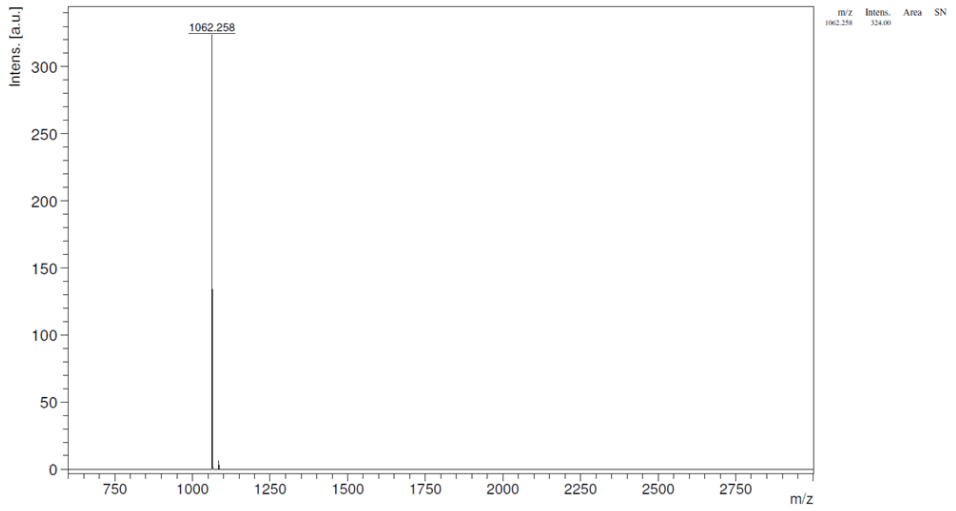

MALDI-TOF MS of 1613

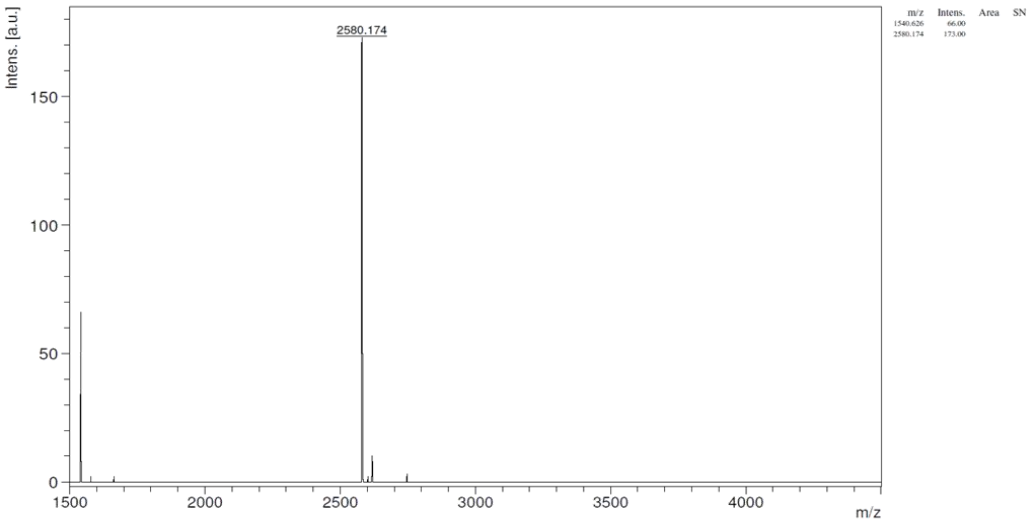

MALDI-TOF MS of 1713

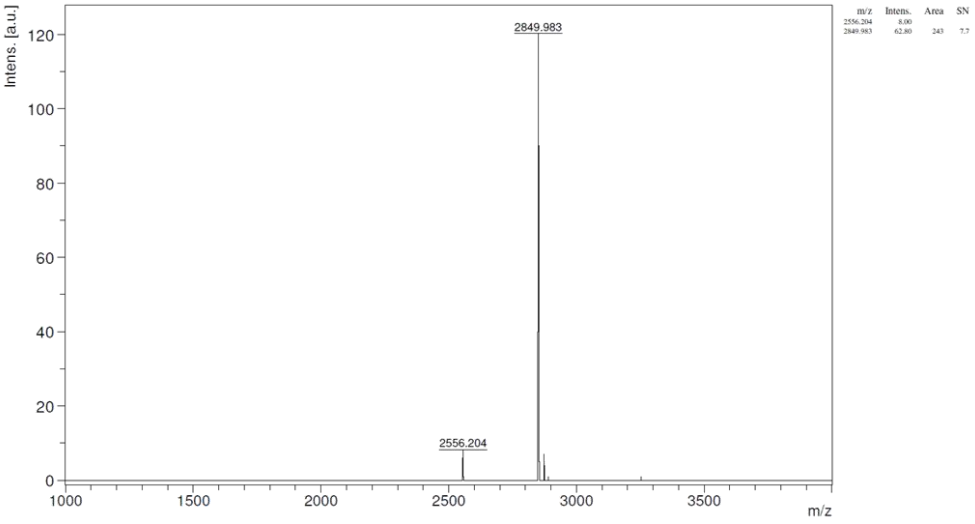

MALDI-TOF MS of 1621

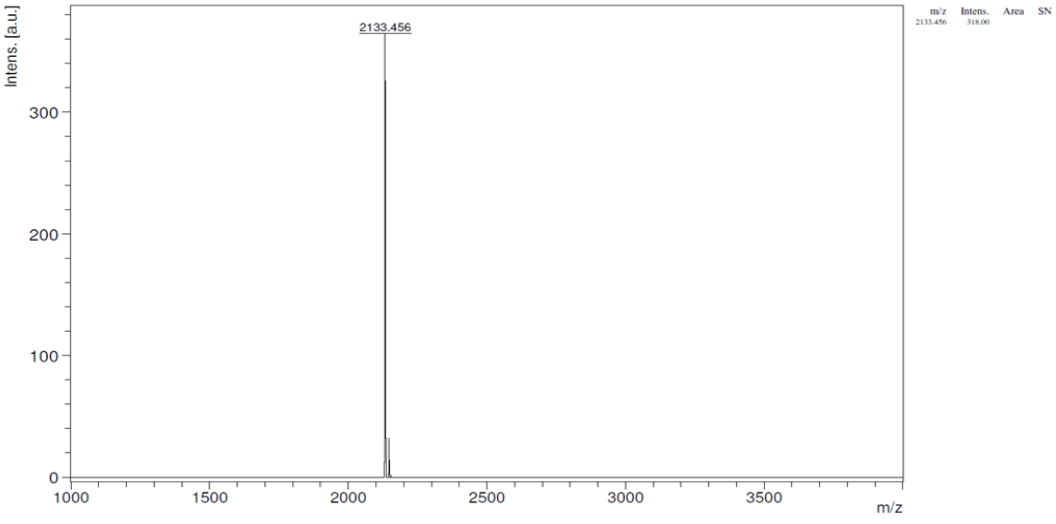

MALDI-TOF MS of 1681

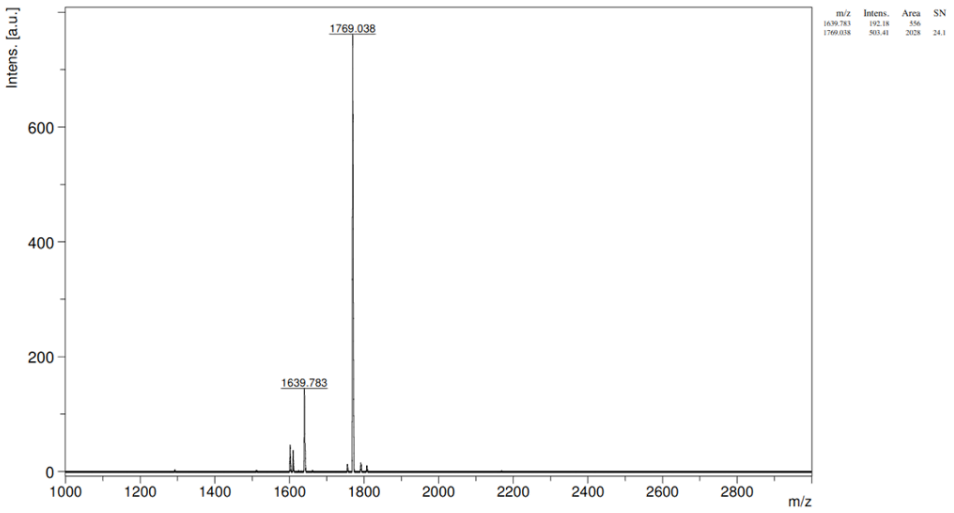

MALDI-TOF MS of 1716

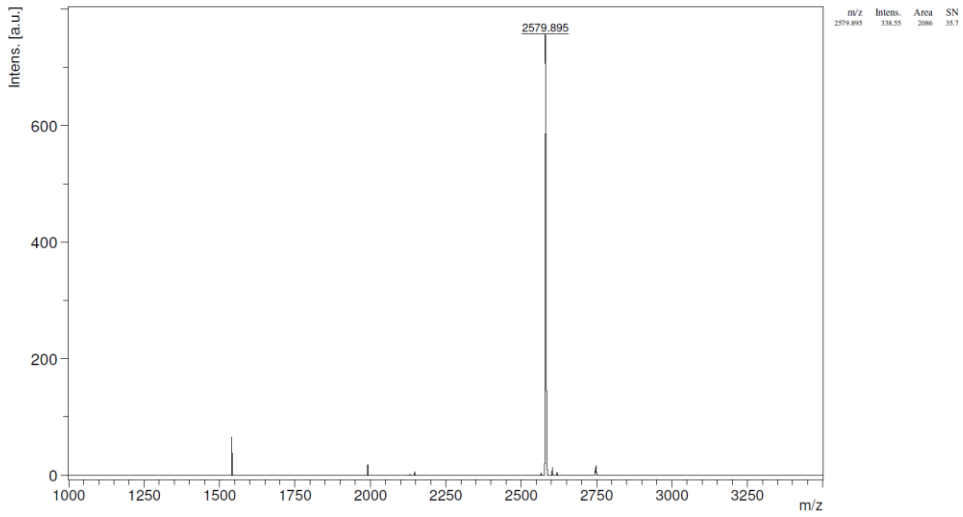

MALDI-TOF MS of 1717

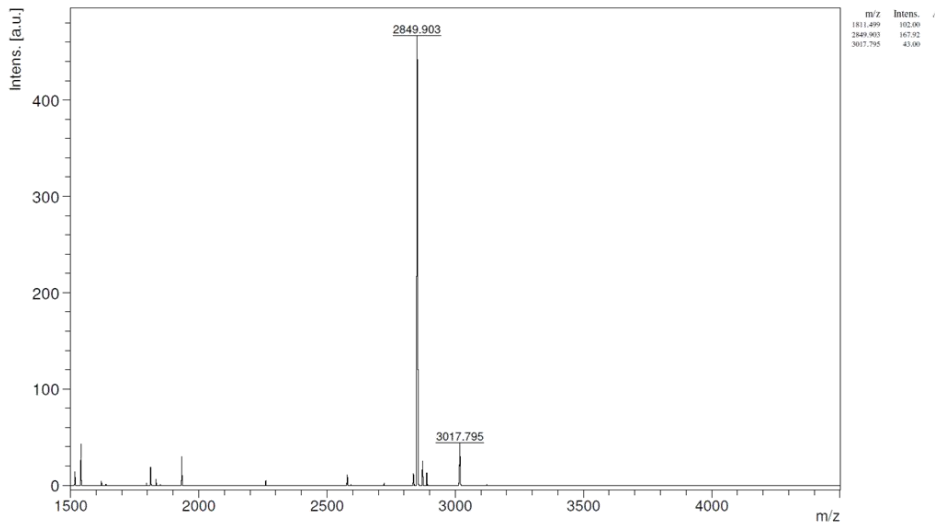

MALDI-TOF MS of 1718

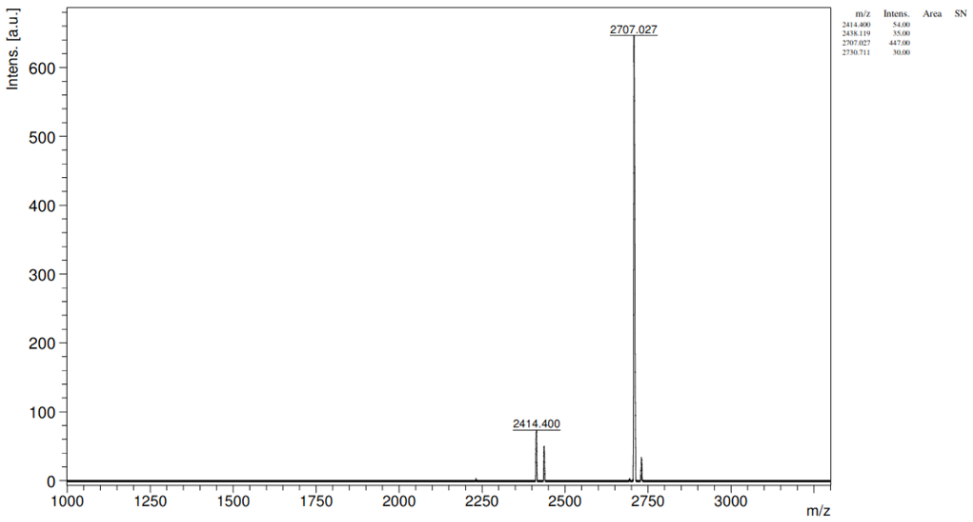

MALDI-TOF MS of 1719

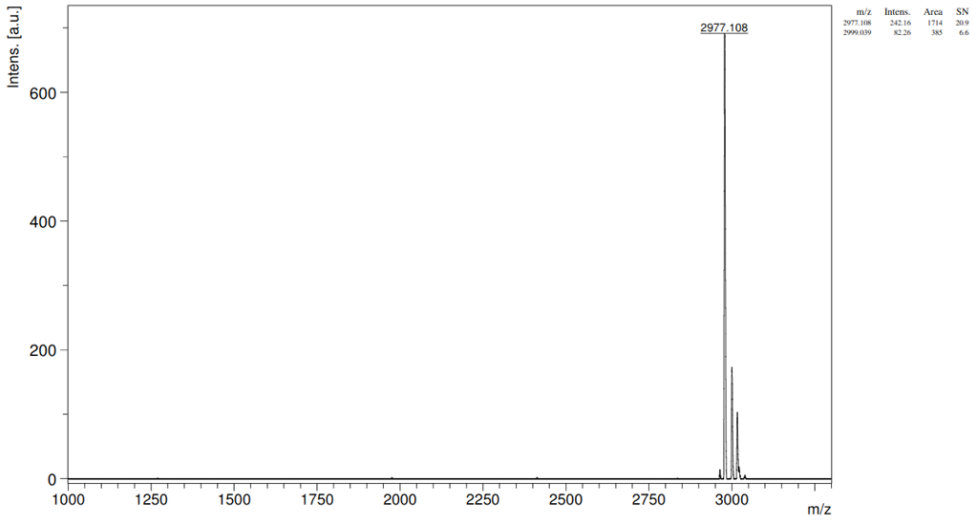

MALDI-TOF MS of 1720

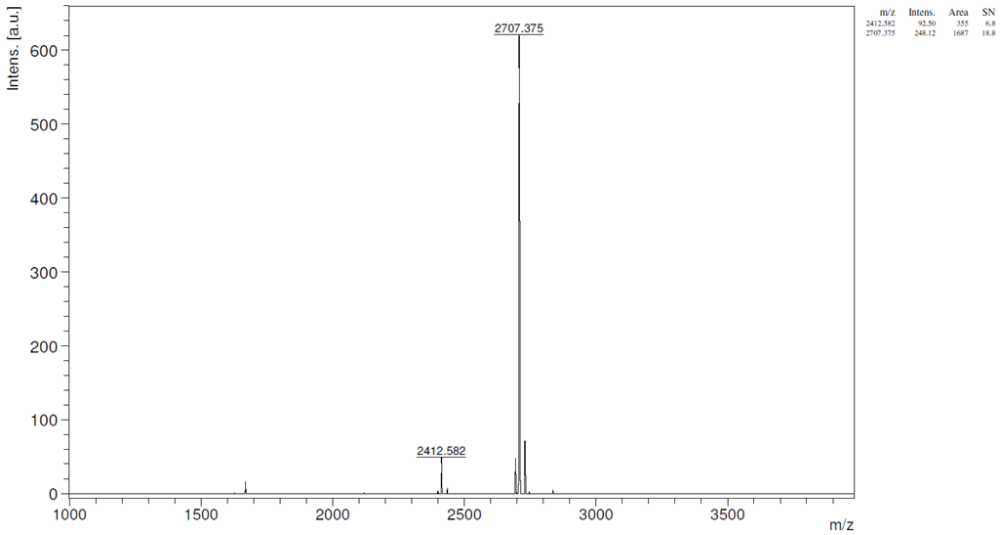

MALDI-TOF MS of 1721

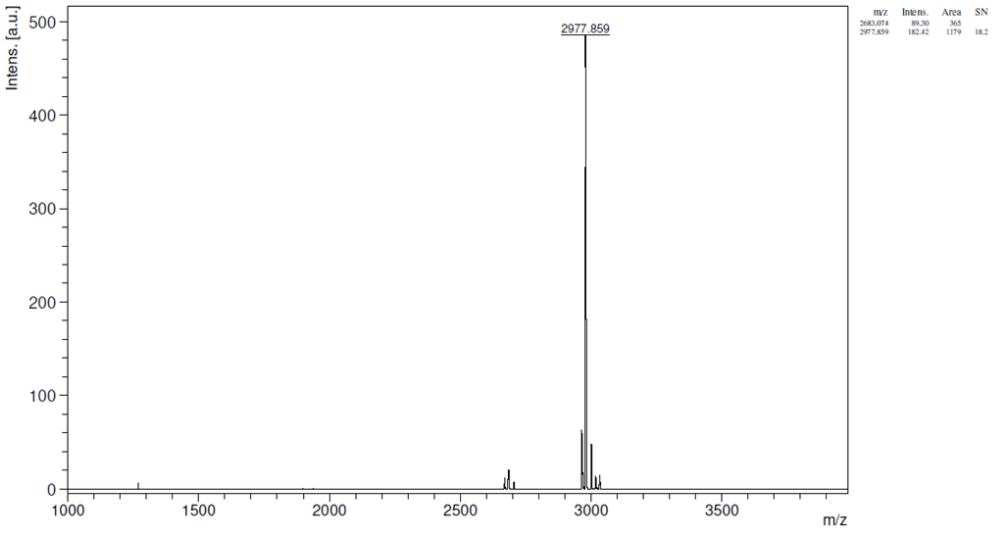

MALDI-TOF MS of 1722

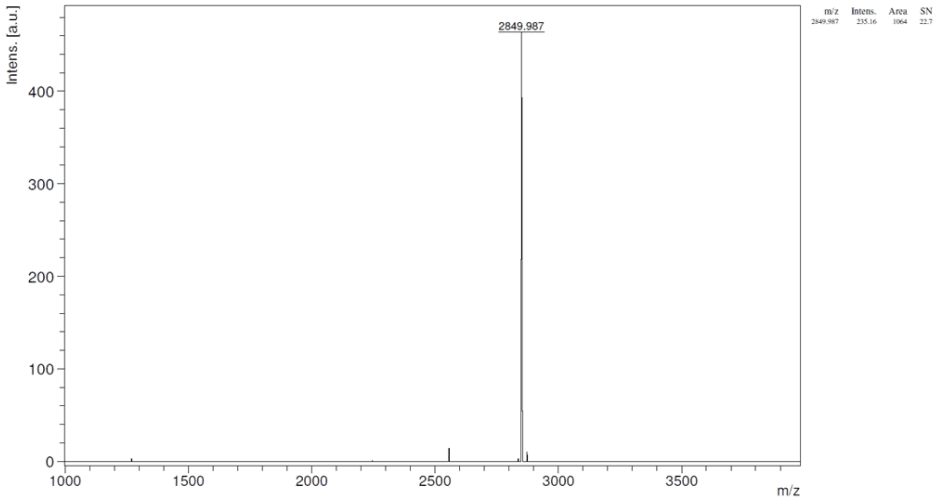

MALDI-TOF MS of 1723

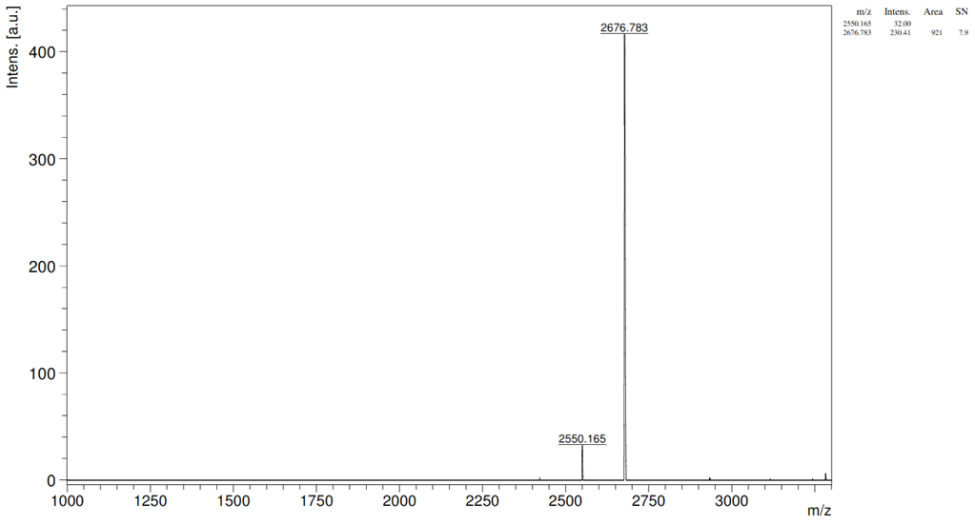

MALDI-TOF MS of 1725

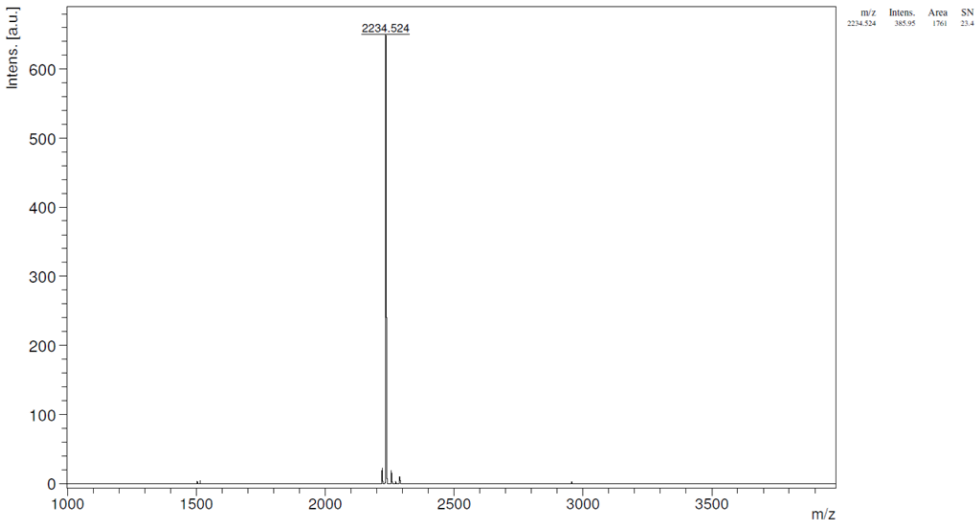

MALDI-TOF MS of 1611

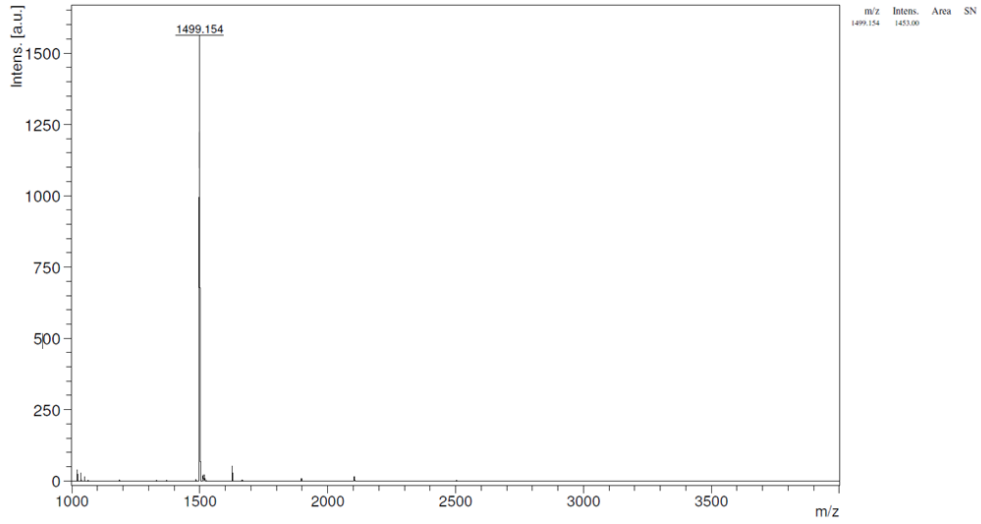

MALDI-TOF MS of 1612

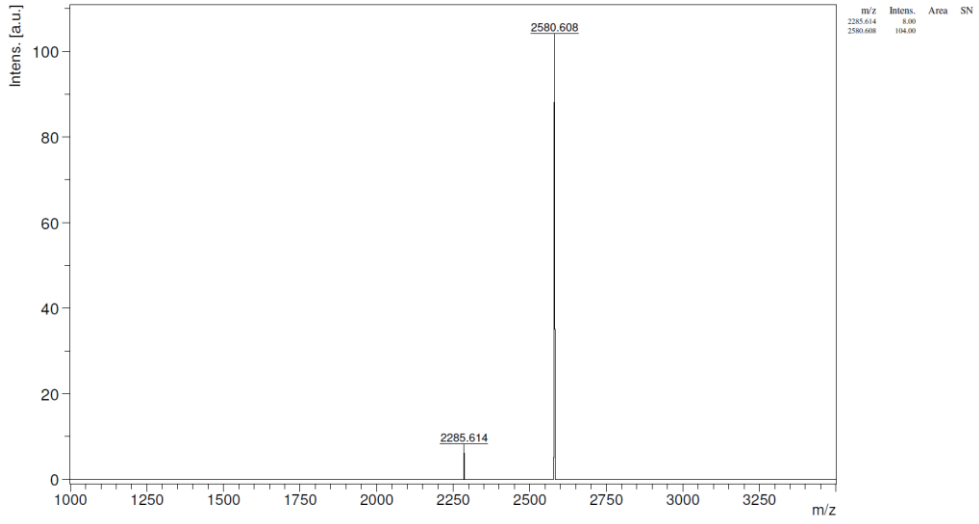

MALDI-TOF MS of 1620

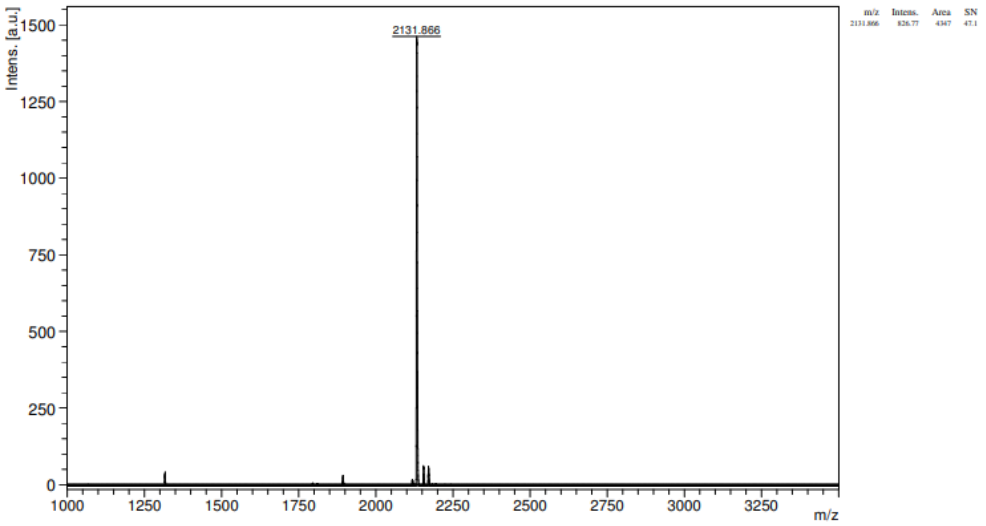

MALDI-TOF MS of 1724

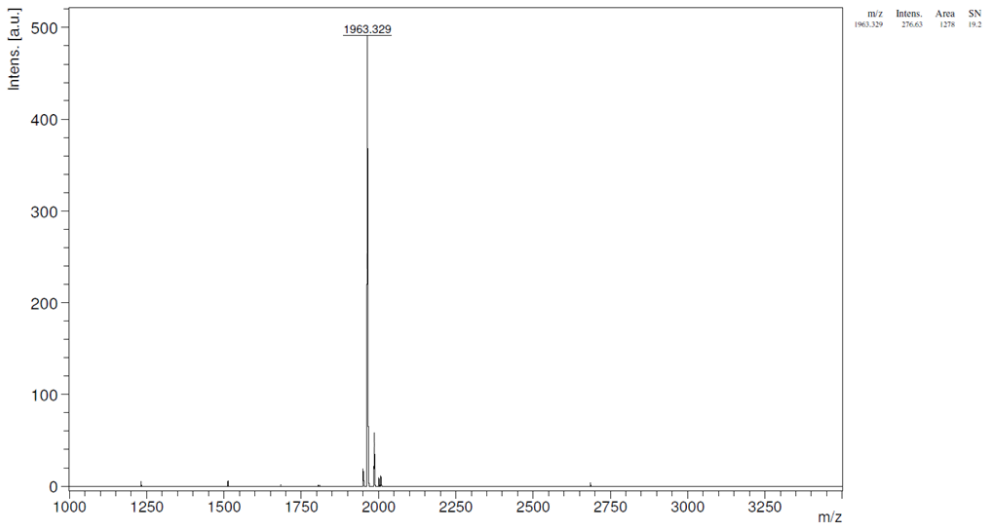

MALDI-TOF MS of 1729

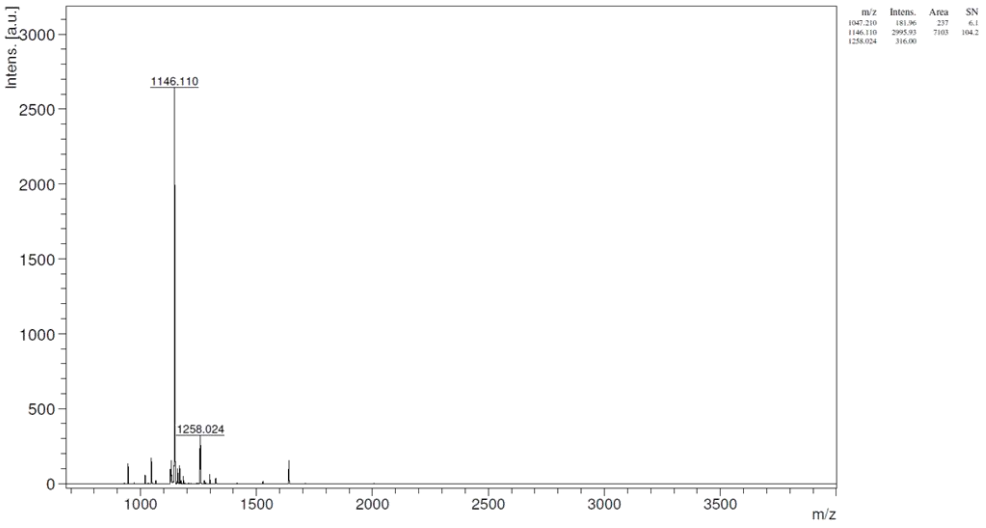

MALDI-TOF MS of 1730

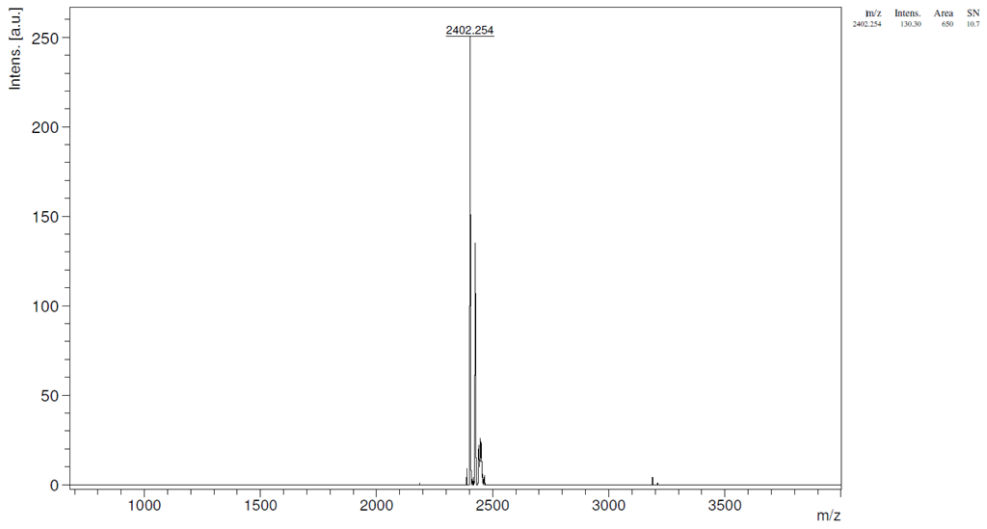

MALDI-TOF MS of 1731

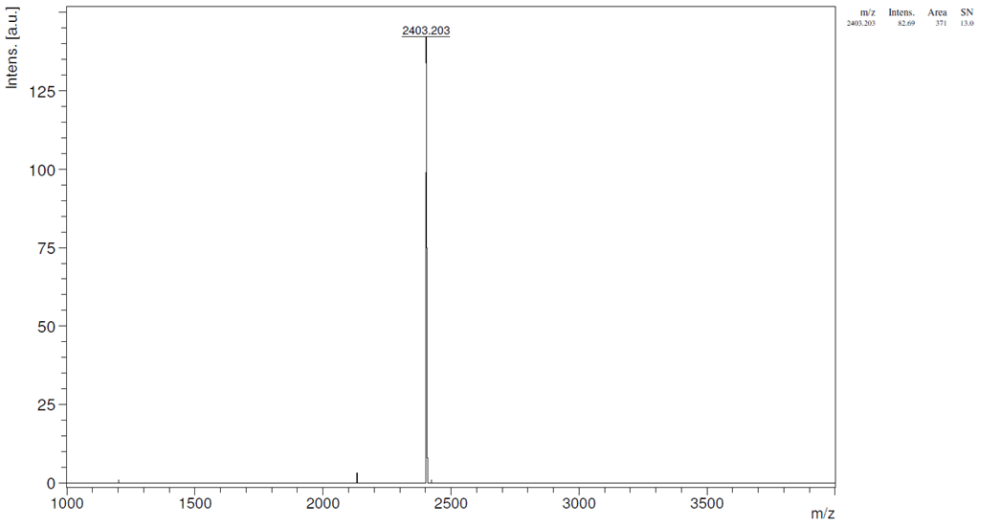

MALDI-TOF MS of 1732

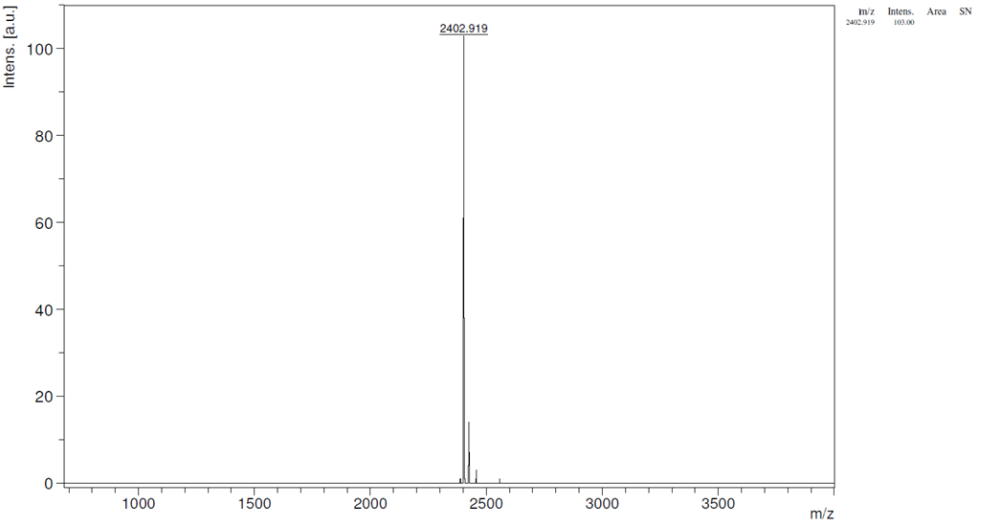

MALDI-TOF MS of 1745

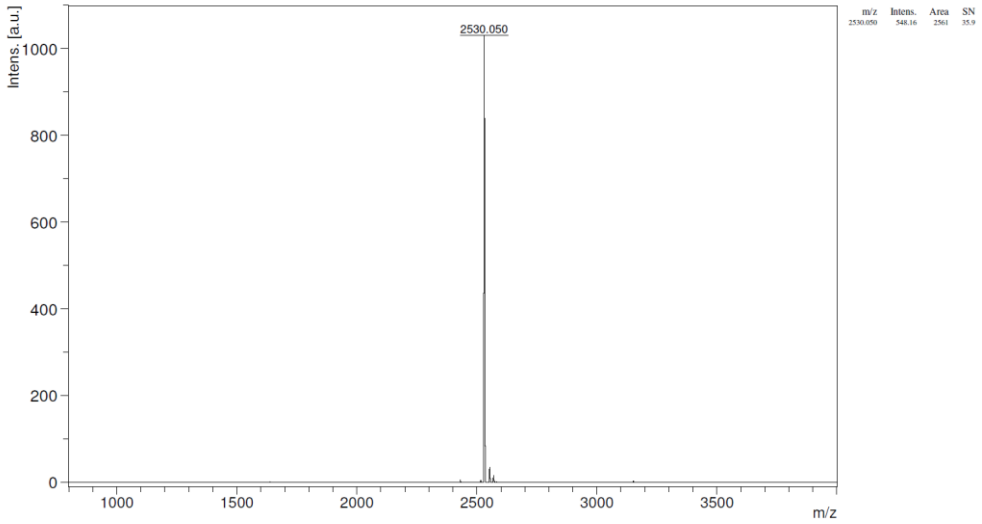

MALDI-TOF MS of 1746

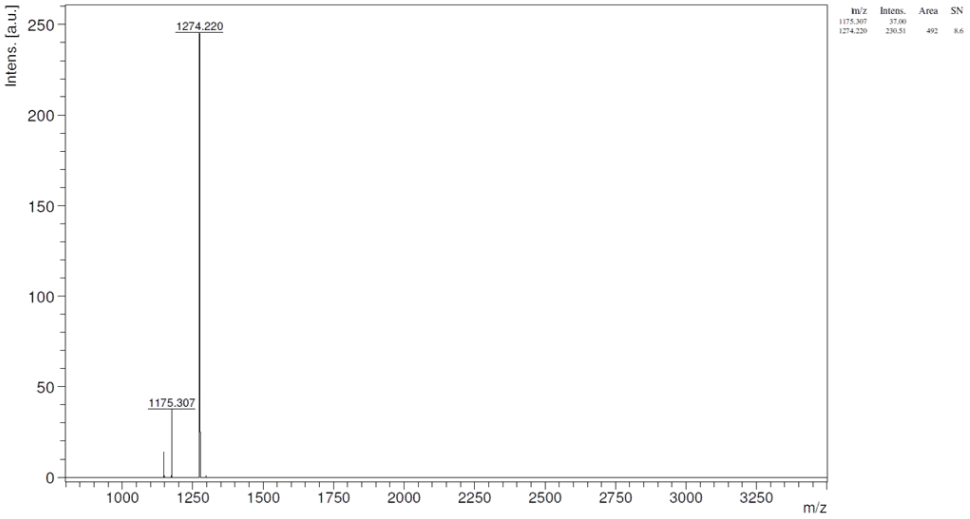

MALDI-TOF MS of 1747

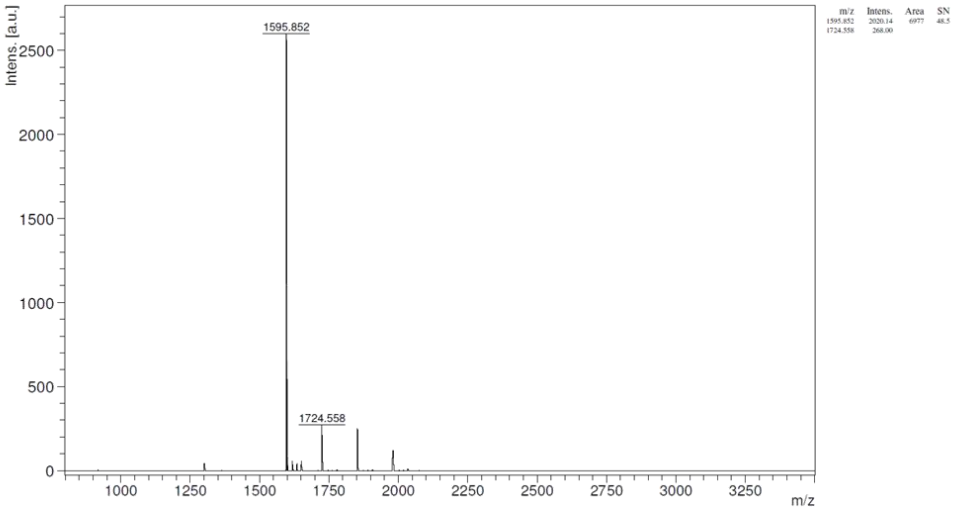

MALDI-TOF MS of 1748

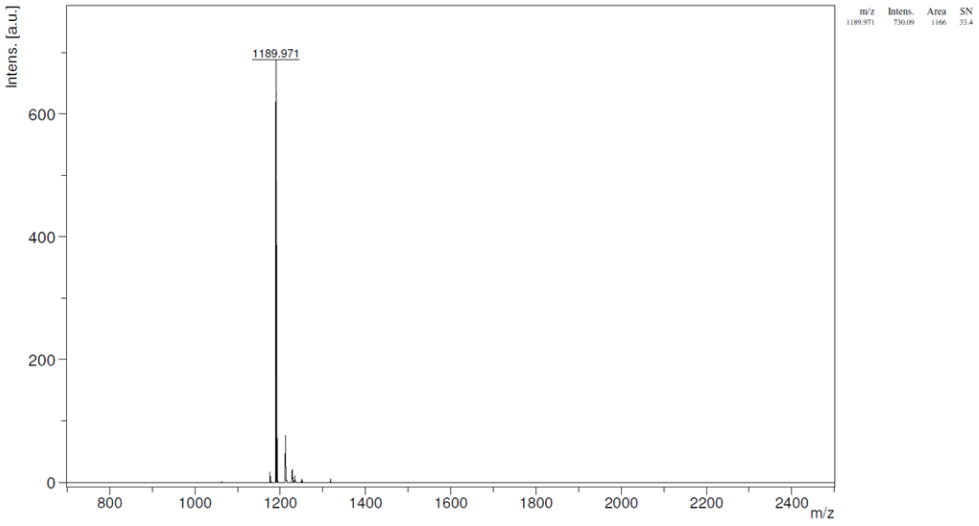

MALDI-TOF MS of 1749

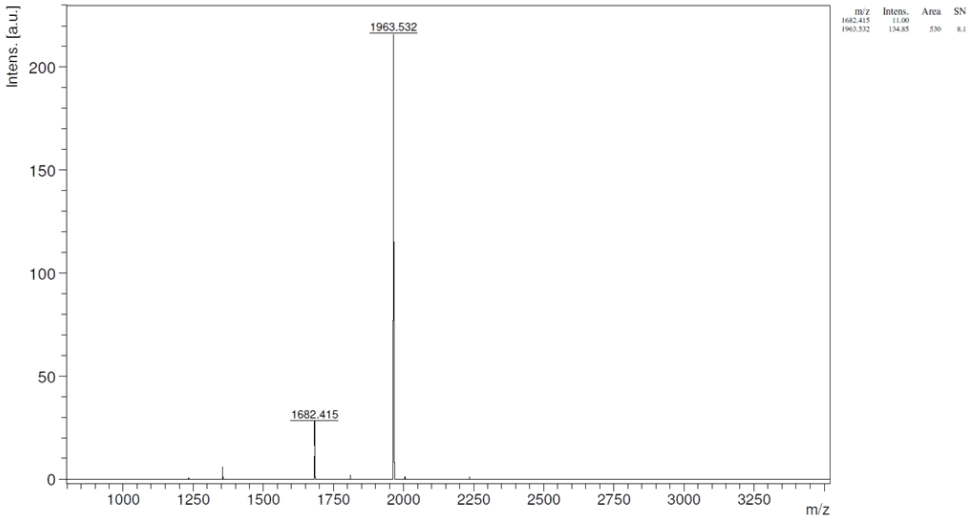

MALDI-TOF MS of 1750

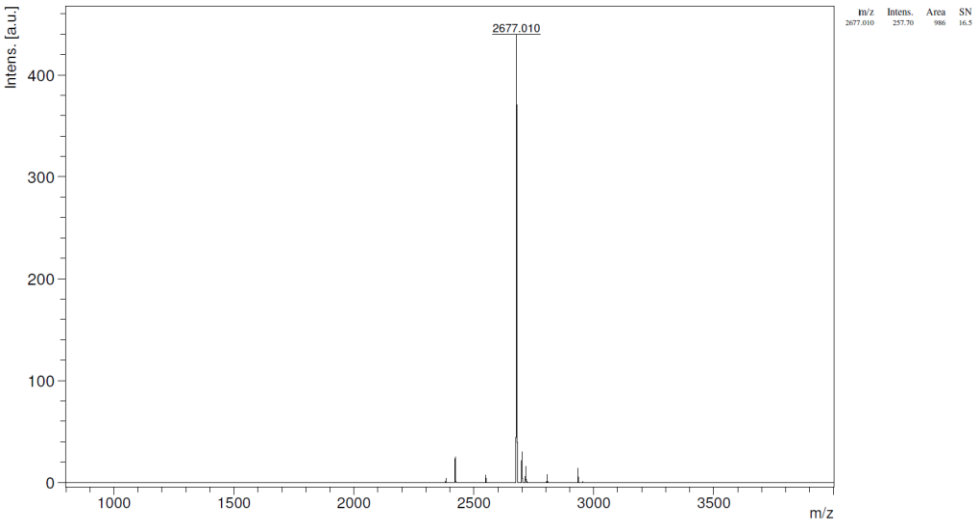

MALDI-TOF MS of 1751

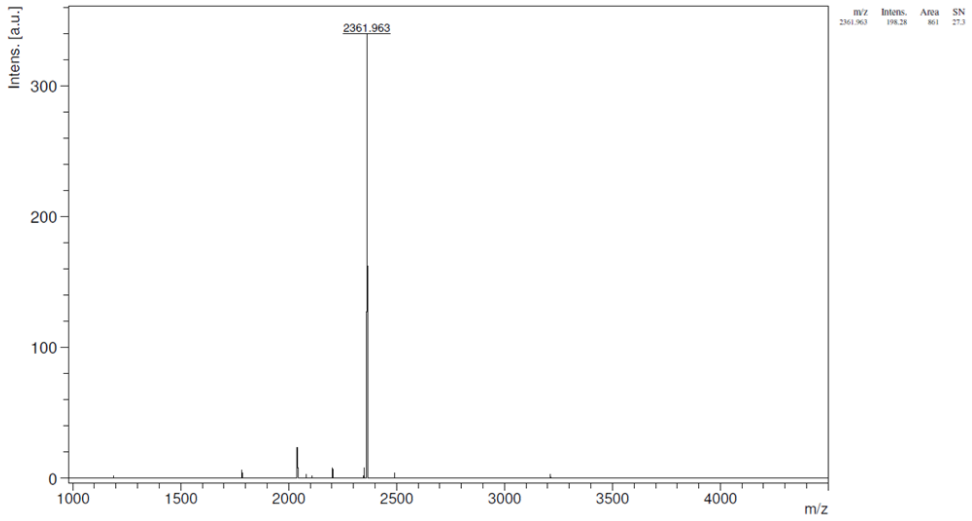

8.2 ESI-MS of LAFs (8Oc, 10Oc and 12Oc)

ESI- MS of 8Oc (in positive mode)

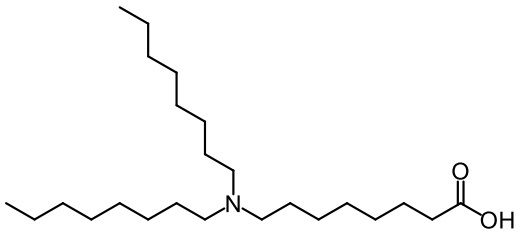

Chemical Formula: $C_{24}H_{49}NO_2$
Molecular Weight: 383.66

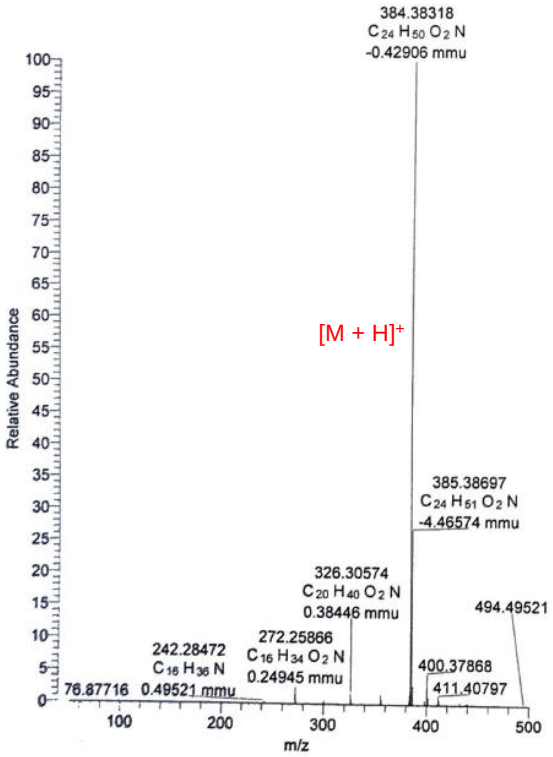

ESI- MS of 10Oc (in positive mode)

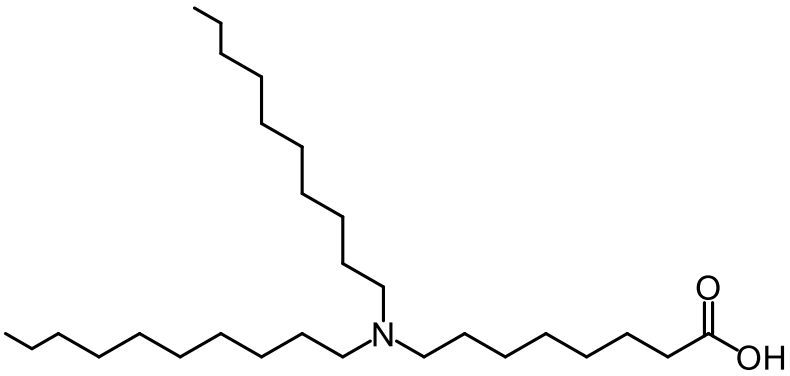

Chemical Formula: $C_{28}H_{57}NO_2$
Molecular Weight: 439.77

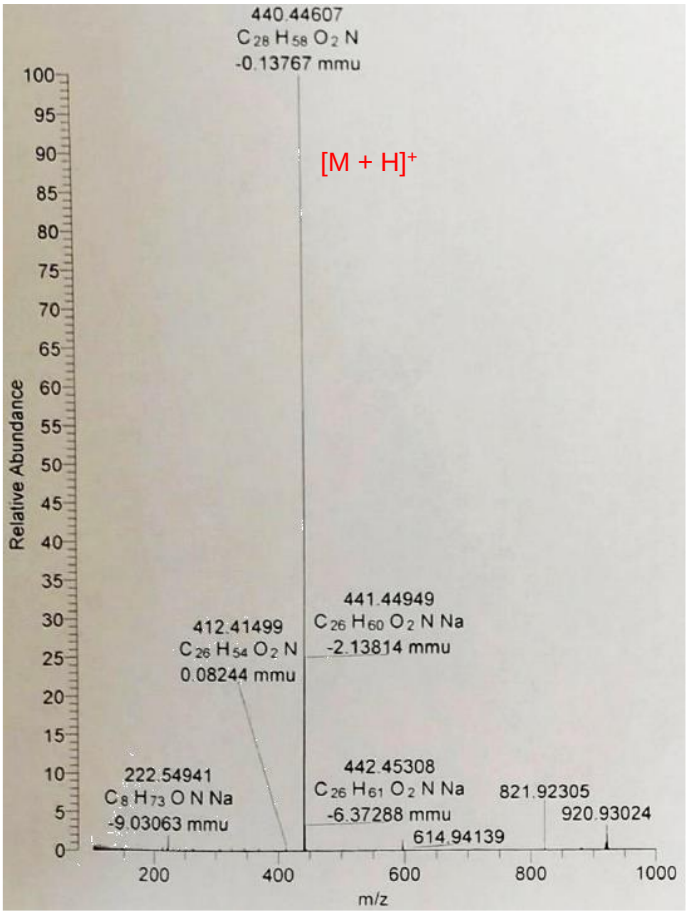

ESI- MS of 12Oc (in positive mode)

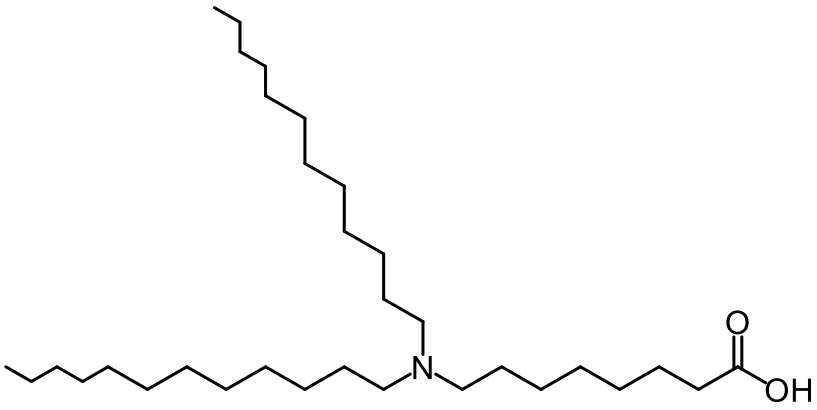

Chemical Formula: $C_{32}H_{65}NO_2$
Molecular Weight: 495.88

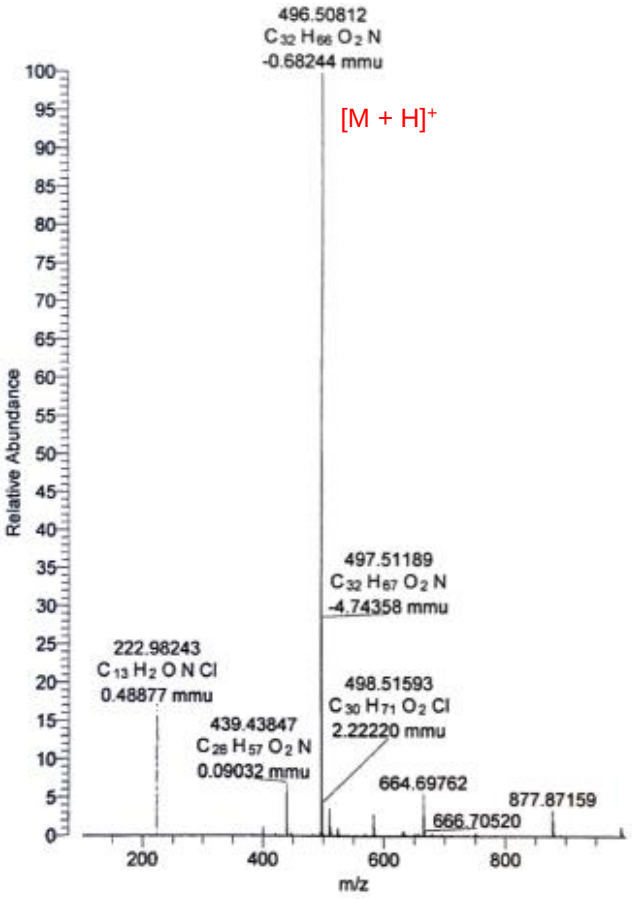

8.3 ^{1}H NMR spectra of building blocks and oligomers

1198: Sequence (N->C): K(N_3)-C-Y_3-Stp_2-K(K($OleA)_2$-Stp_2-Y_3-C

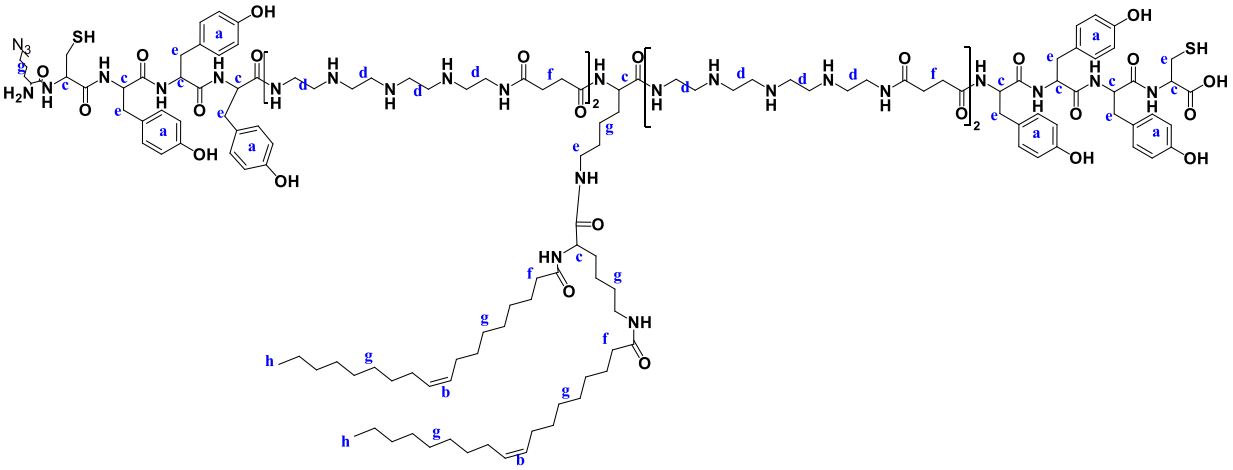

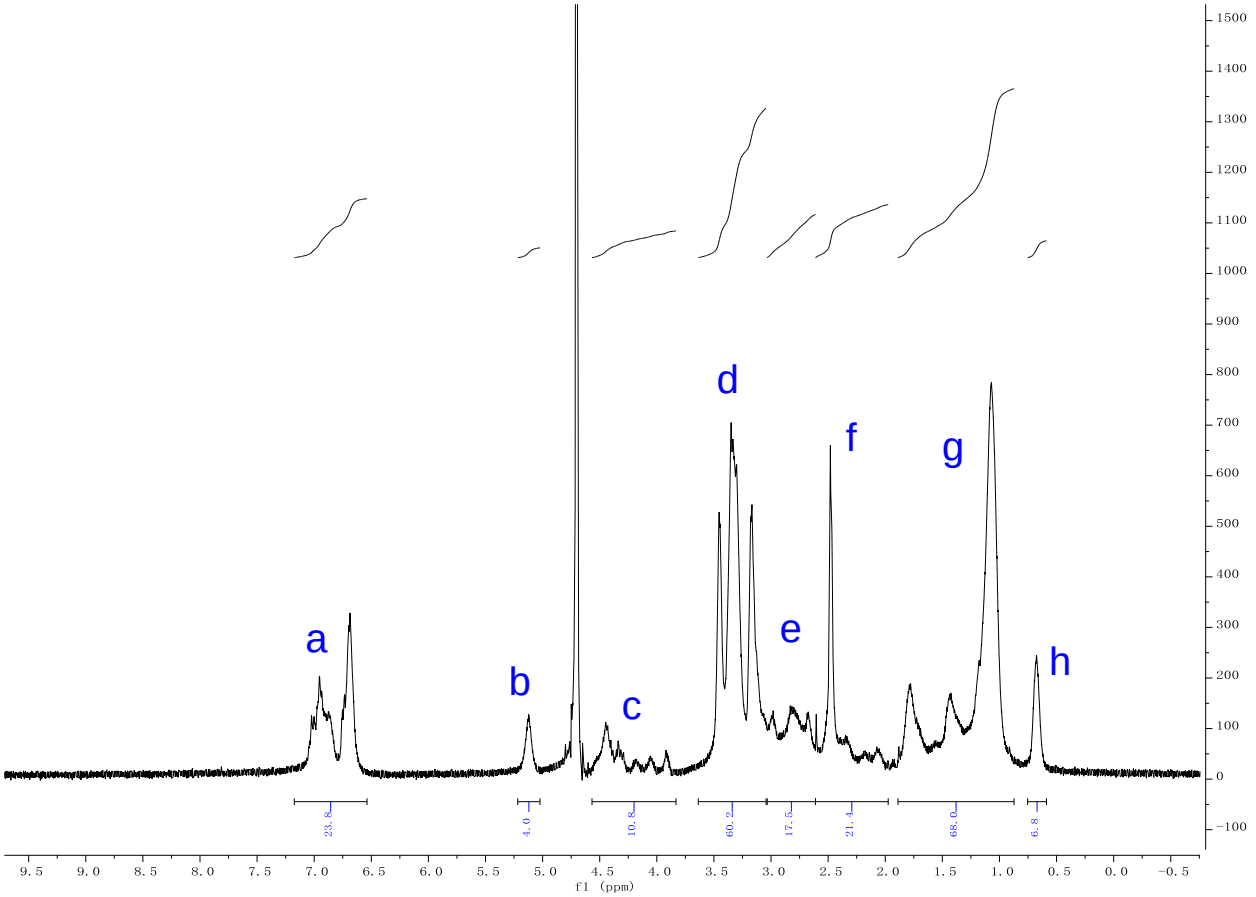

^{1}H NMR (400 MHz, Deuterium oxide) δ (ppm) = 0.65-0.85 (s, 6 H, -CH3 oleic acid), 0.85-1.95 (m, 64 H, βγδH lysine, -CH2- oleic acid), 2.0 -2.65 (m, 20 H, -CO-CH2-CH2- CO- Stp, -CO-CH2- oleic acid), 2.65-3.1 (m, 20 H, εH lysine, tyrosine, cysteine), 3.1-3.6 (m, 64 H, -CH2- Tp), 3.85-4.55 (m, 10 H, αH amino acids), 5.05-5.20 (s, 4 H, -CH=CH oleic acid), 6.55-7.10 (m, 24 H, -CH- tyrosine).

8Oc:

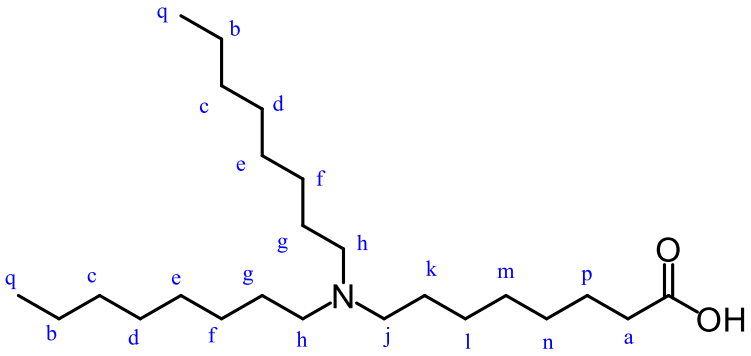

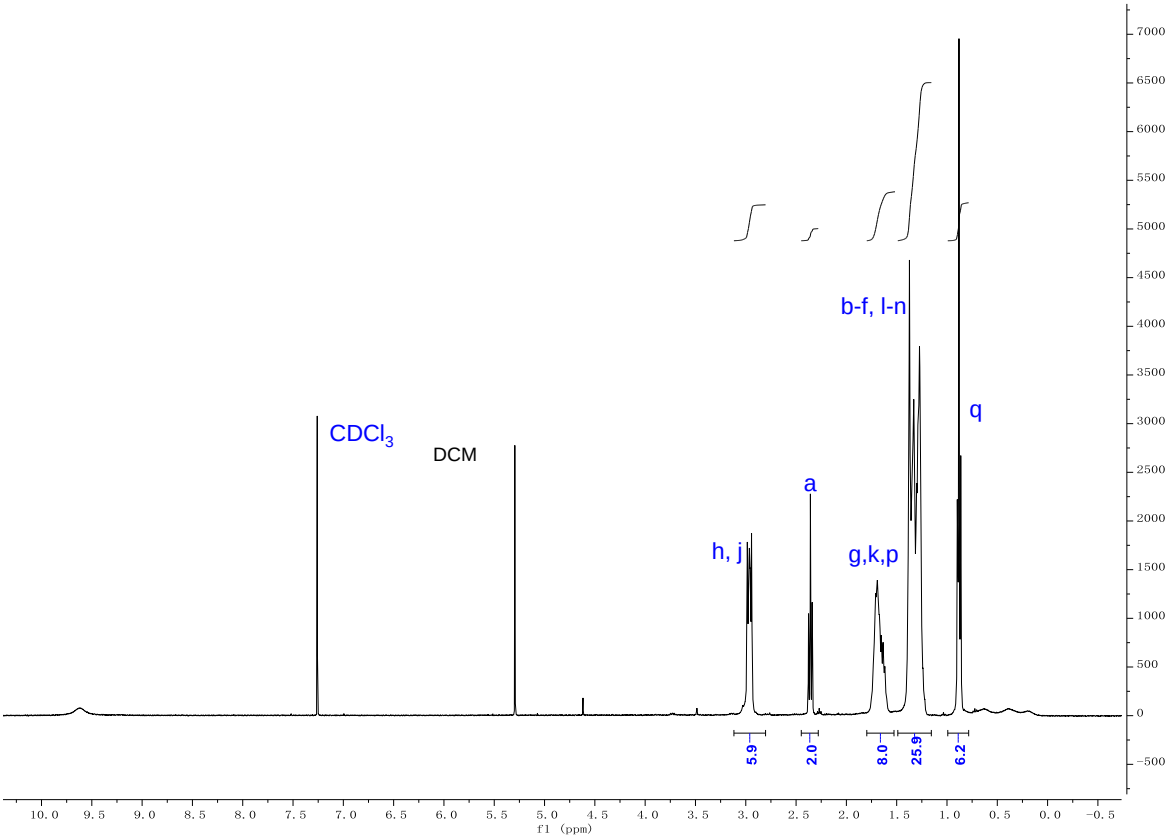

^{1}H NMR (400 MHz, Chloroform-d) δ (ppm) = 0.65–0.95 (m, 6H, -CH3, octanal), 1.15-1.53 (m, 26H, -CH2-CH2-), 1.55-1.88 (m, 8H, -CH2-), 2.24 – 2.44 (m, 2H, -CH2-CO-), 2.28-3.12 (m, 6H, -CH2-N-).

10Oc:

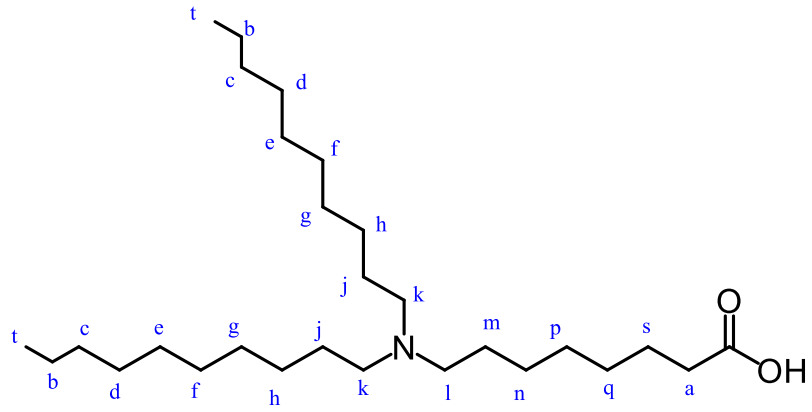

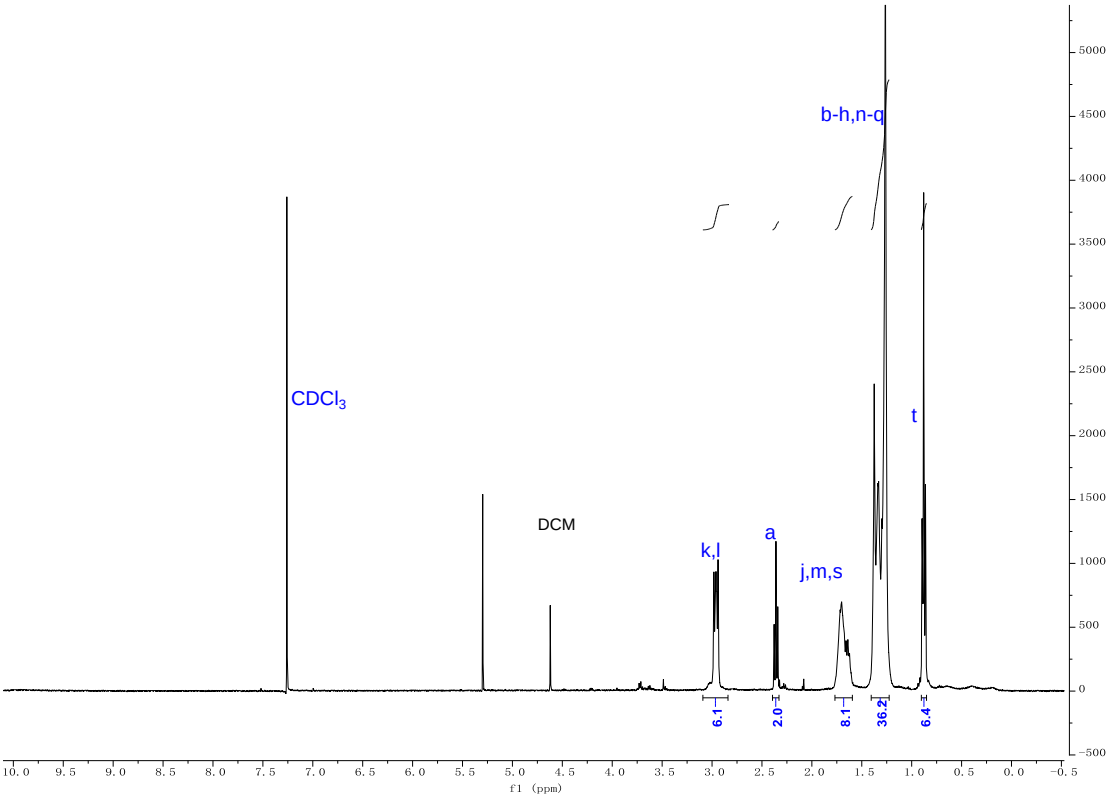

^{1}H NMR (400 MHz, Chloroform-d) δ (ppm) = 0.65–0.95 (m, 6H, -CH3, decatanal), 1.15-1.53 (m, 34H, -CH2-CH2-), 1.55-1.88 (m, 8H, -CH2-), 2.24 – 2.44 (m, 2H, -CH2-CO-), 2.28-3.12 (m, 6H, -CH2-N-).

12Oc:

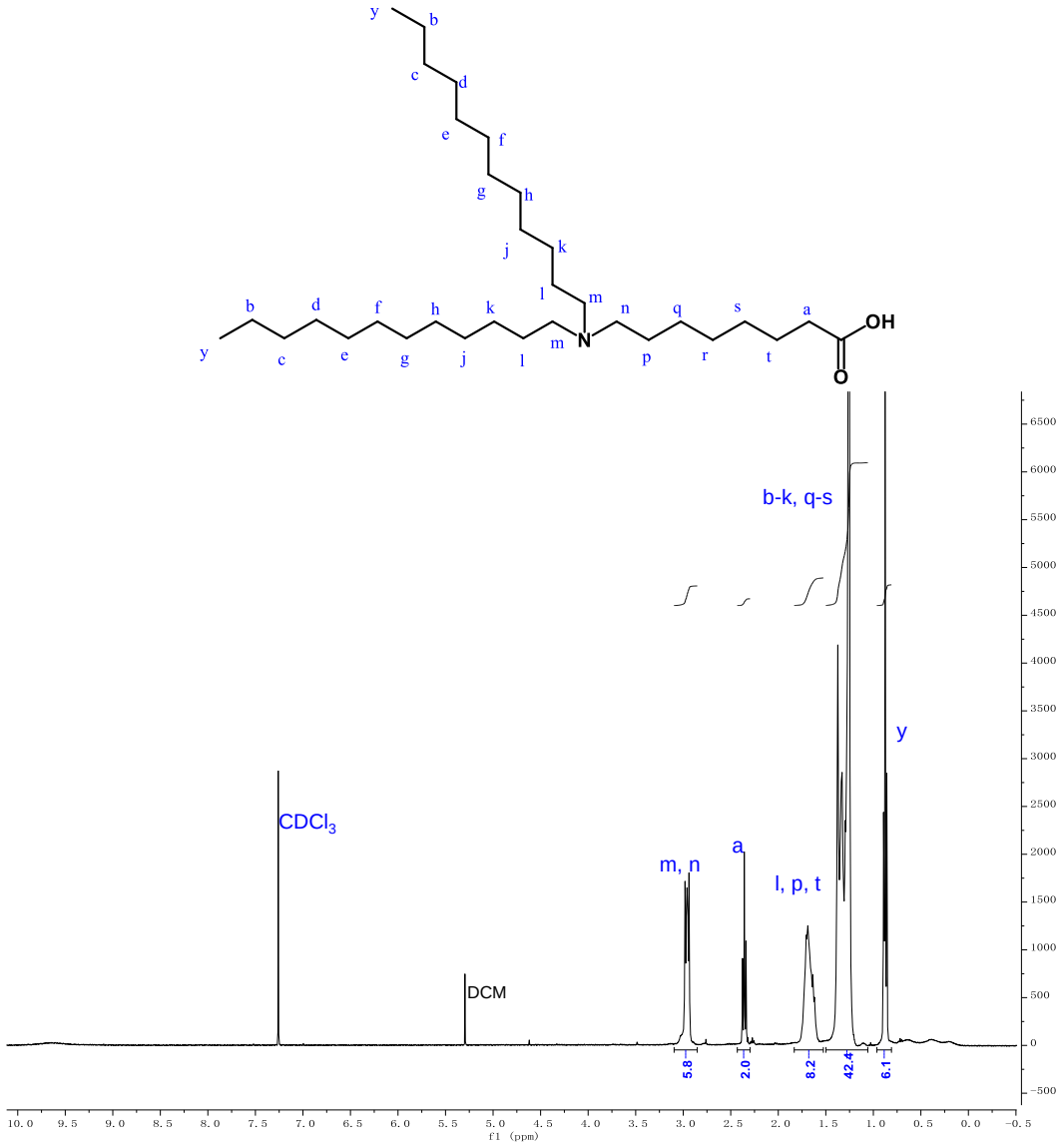

^{1}H NMR (400 MHz, Chloroform-d) δ (ppm) = 0.65–0.95 (m, 6H, -CH3, dodecatanal), 1.15-1.53 (m, 42H, -CH2-CH2-), 1.55-1.88 (m, 8H, -CH2-), 2.24 – 2.44 (m, 2H, -CH2-CO), 2.28-3.12 (m, 6H, -CH2-N-).

1612: Sequence (N->C): $K(12Oc)_2$-Stp-K(12Oc)-K(12Oc)-OH

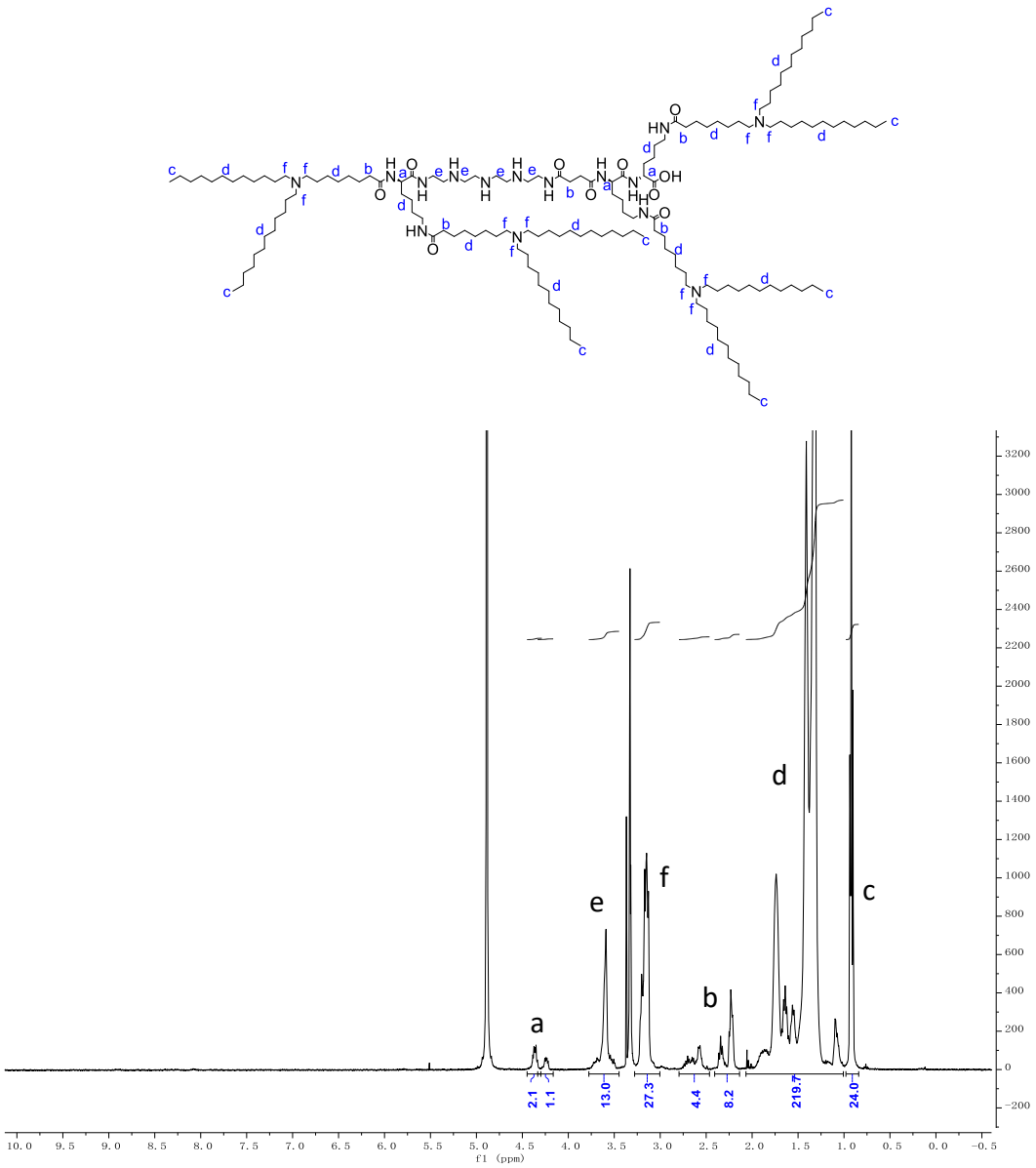

^{1}H NMR (400 MHz, Methanol-d4) δ (ppm) = 0.82 – 0.96 (m, 24H, -CH3), 0.99 – 2.05 (m, 220H, -CH2-CH2-), 2.11 – 2.71 (m, 12H, -CH2-CONH-), 2.98 – 3.26 (m, 24H, -CH2-N), 3.31 – 3.58 (m, 14H, -NH-CH2-CH2-NH-), 4.22-4.34 (3H, αH amino acids).

1620: Sequence (N->C): $K(8Oc)_2$-Stp-K(8Oc)-K(8Oc)-OH

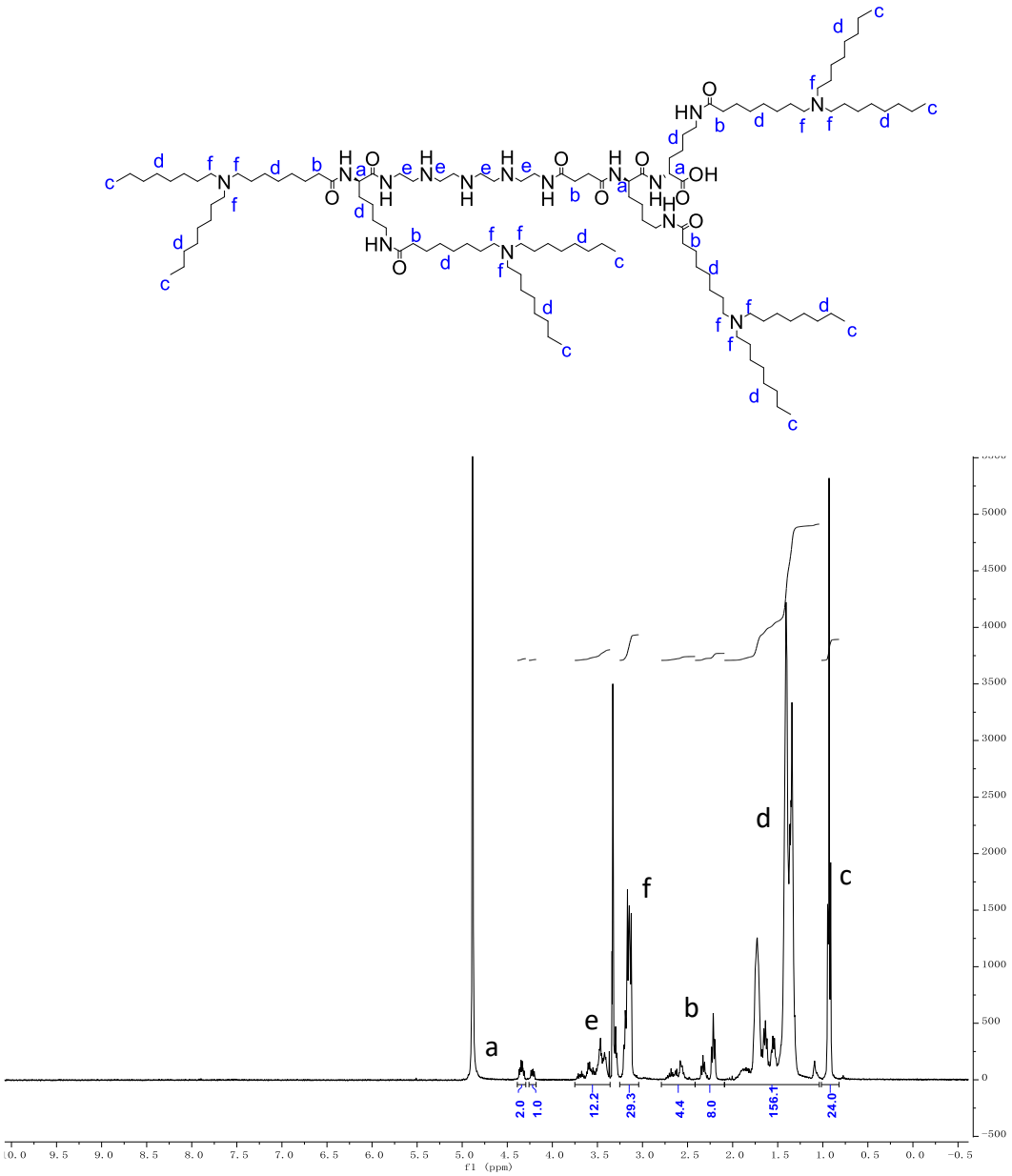

^{1}H NMR (400 MHz, Methanol-d4) δ (ppm) = 0.82 – 0.96 (m, 24H, -CH3), 0.99 – 2.05 (m, 156H, -CH2-CH2-), 2.11 – 2.71 (m, 12H, -CH2-CONH-), 2.98 – 3.26 (m, 24H, -CH2-N), 3.31 – 3.58 (m, 14H, -NH-CH2-CH2-NH-), 4.22-4.34 (3H, αH amino acids).

1621: Sequence (N->C): $K[K(8Oc)_2]_2$-Stp-OH

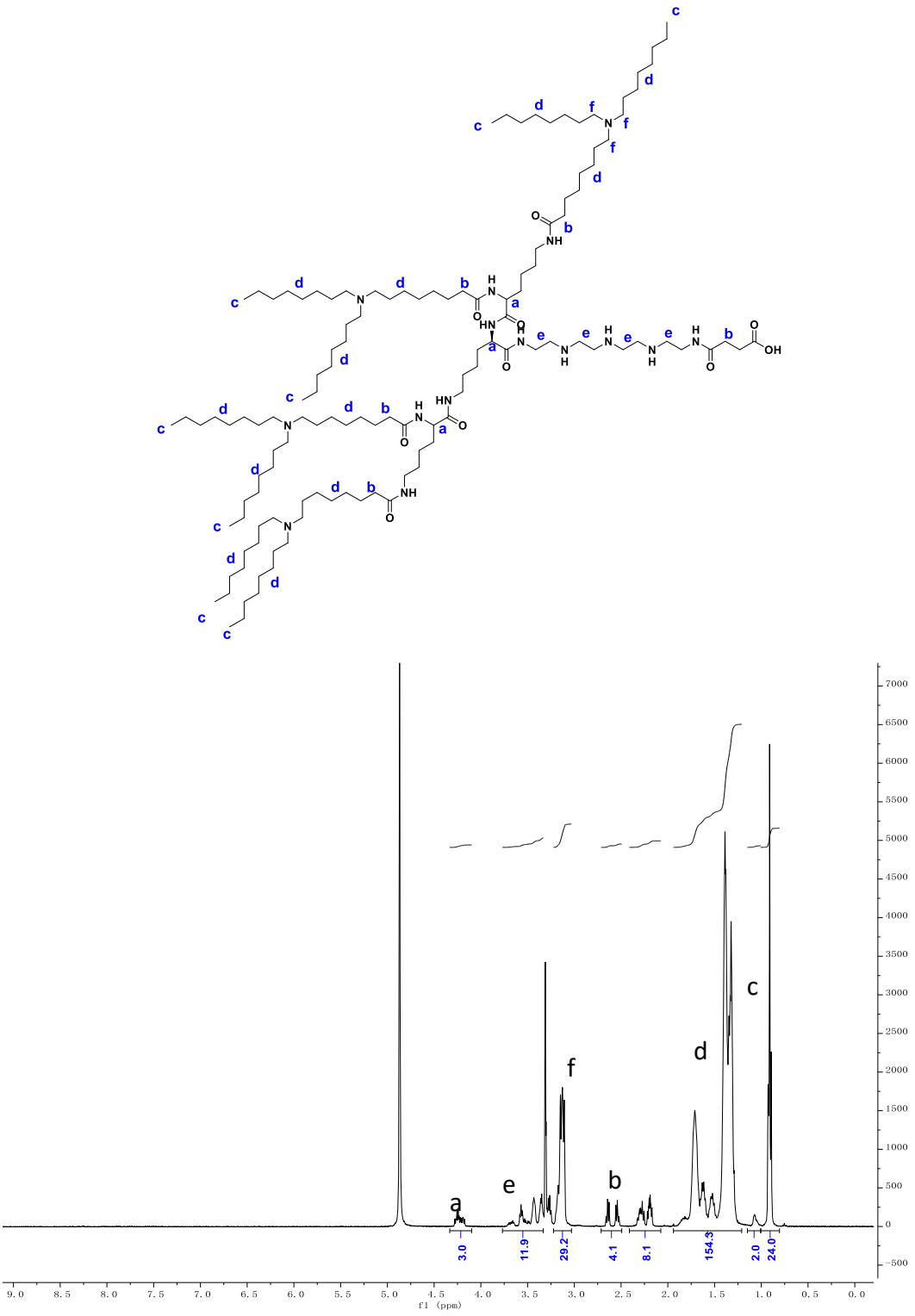

^{1}H NMR (400 MHz, Methanol-d4) δ (ppm) = 0.82 – 0.96 (m, 24H, -CH3), 0.99 – 2.05 (m, 156H, -CH2-CH2-), 2.11 – 2.71 (m, 12H, -CH2-CONH-), 2.98 – 3.26 (m, 24H, -CH2-N), 3.31 – 3.58 (m, 14H, -NH-CH2-CH2-NH-), 4.22-4.34 (3H, αH amino acids).

1722: Sequence (N->C): K(12Oc)$_2$-Stp$_2$-K(12Oc)-K12(Oc)-OH

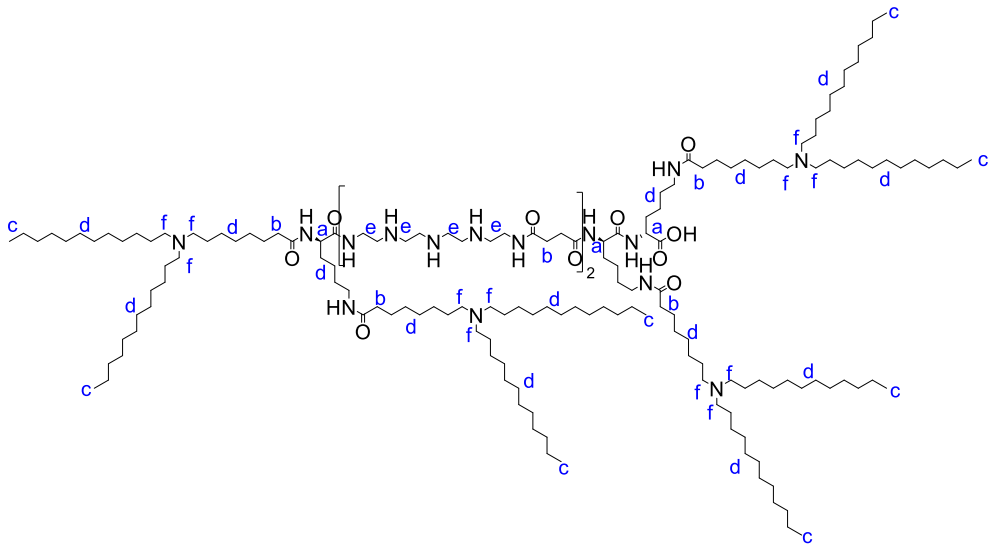

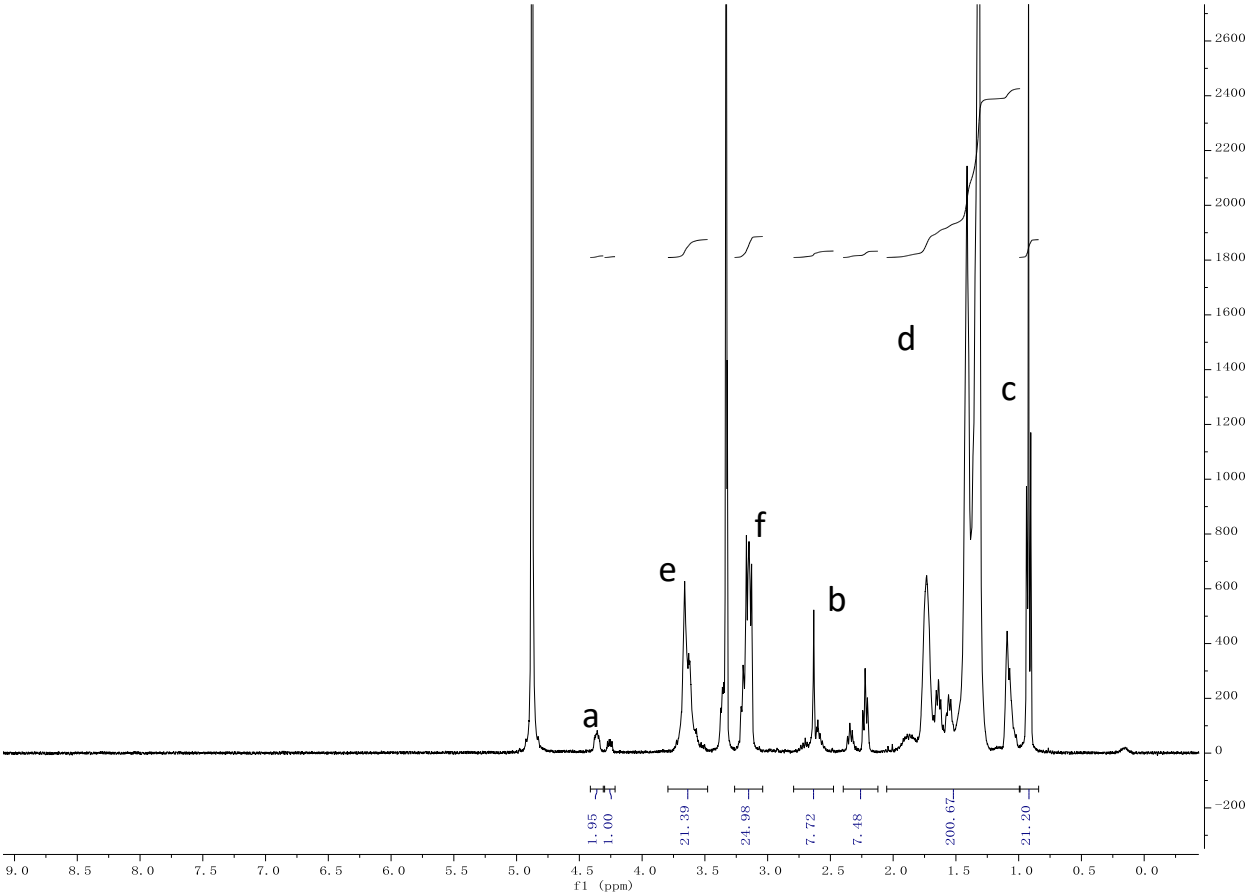

^{1}H NMR (400 MHz, Methanol-d4) δ (ppm) = 0.82 – 0.96 (m, 24H, -CH3), 0.99 – 2.05 (m, 220H, -CH2-CH2-), 2.11 – 2.71 (m, 12H, -CH2-CONH-), 2.98 – 3.26 (m, 24H, -CH2-N), 3.31 – 3.58 (m, 28H, -NH-CH2-CH2-NH-), 4.22-4.34 (3H, αH amino acids).

1713: Sequence (N->C): $K[K(12Oc)_2]_2$-Stp_2-OH

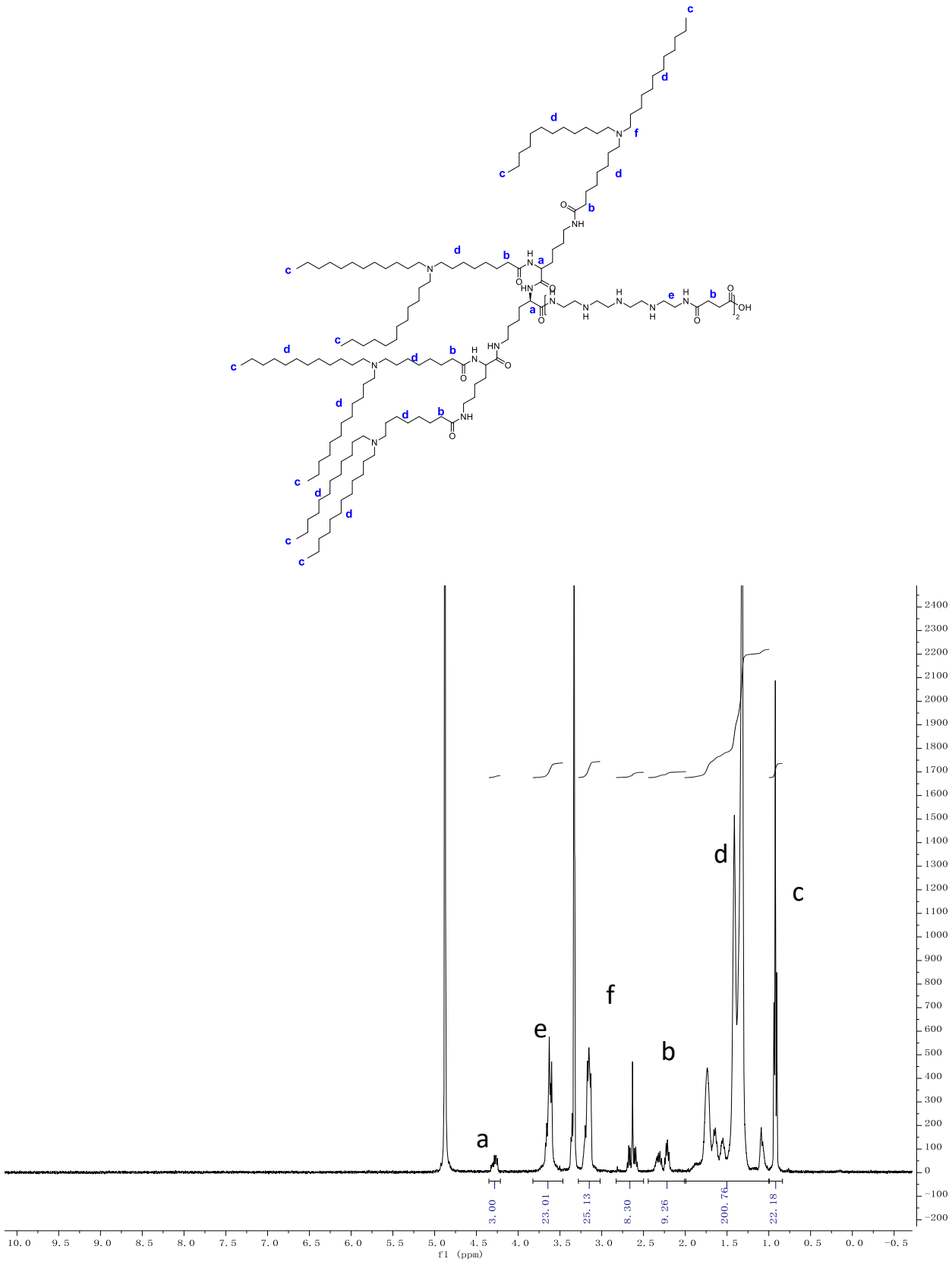

^{1}H NMR (400 MHz, Methanol-d4) δ (ppm) = 0.82 – 0.96 (m, 24H, -CH3), 0.99 – 2.05 (m, 220H, -CH2-CH2-), 2.11 – 2.71 (m, 12H, -CH2-CONH-), 2.98 – 3.26 (m, 24H, -CH2-N), 3.31 – 3.58 (m, 28H, -NH-CH2-CH2-NH-), 4.22-4.34 (3H, αH amino acids).

1613: Sequence (N->C): K[K(12Oc)$_2$]$_2$-Stp-OH

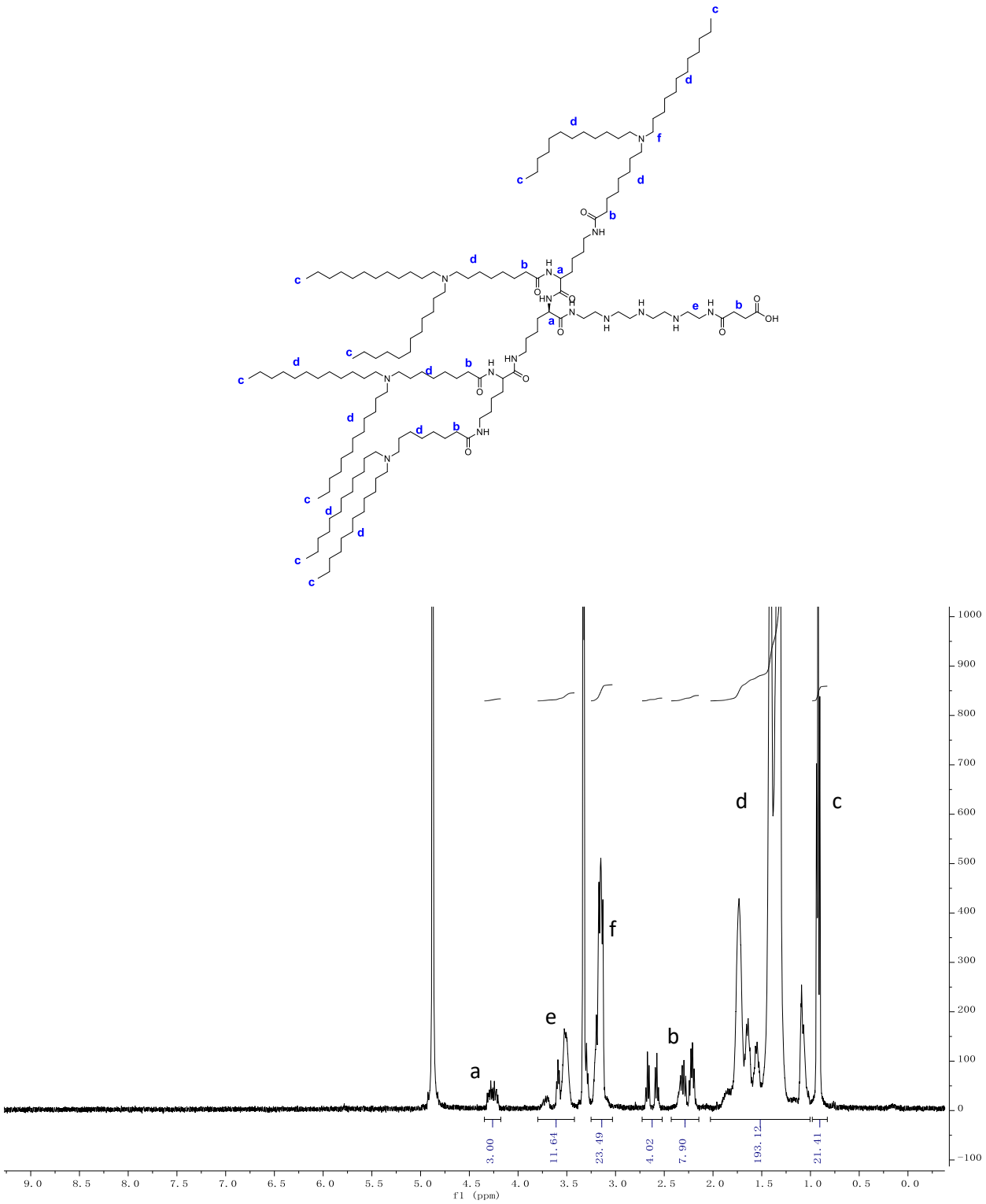

^{1}H NMR (400 MHz, Methanol-d4) δ (ppm) = 0.82 – 0.96 (m, 24H, -CH3), 0.99 – 2.05 (m, 220H, -CH2-CH2-), 2.11 – 2.71 (m, 12H, -CH2-CONH-), 2.98 – 3.26 (m, 24H, -CH2-N), 3.31 – 3.58 (m, 14H, -NH-CH2-CH2-NH-), 4.22-4.34 (3H, αH amino acids).

1615: Sequence (N->C): H2N-[K(12Oc)]$_2$-Stp-OH

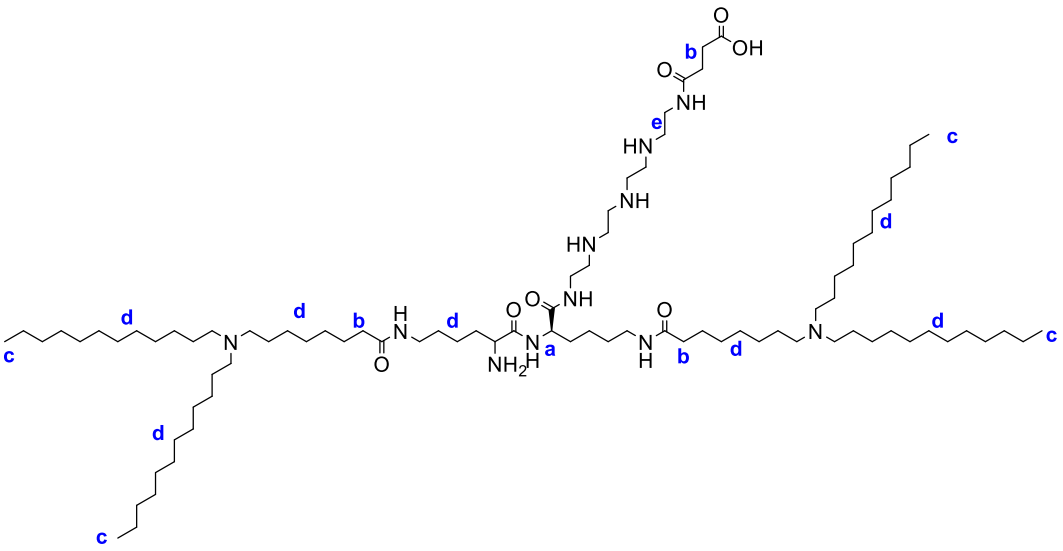

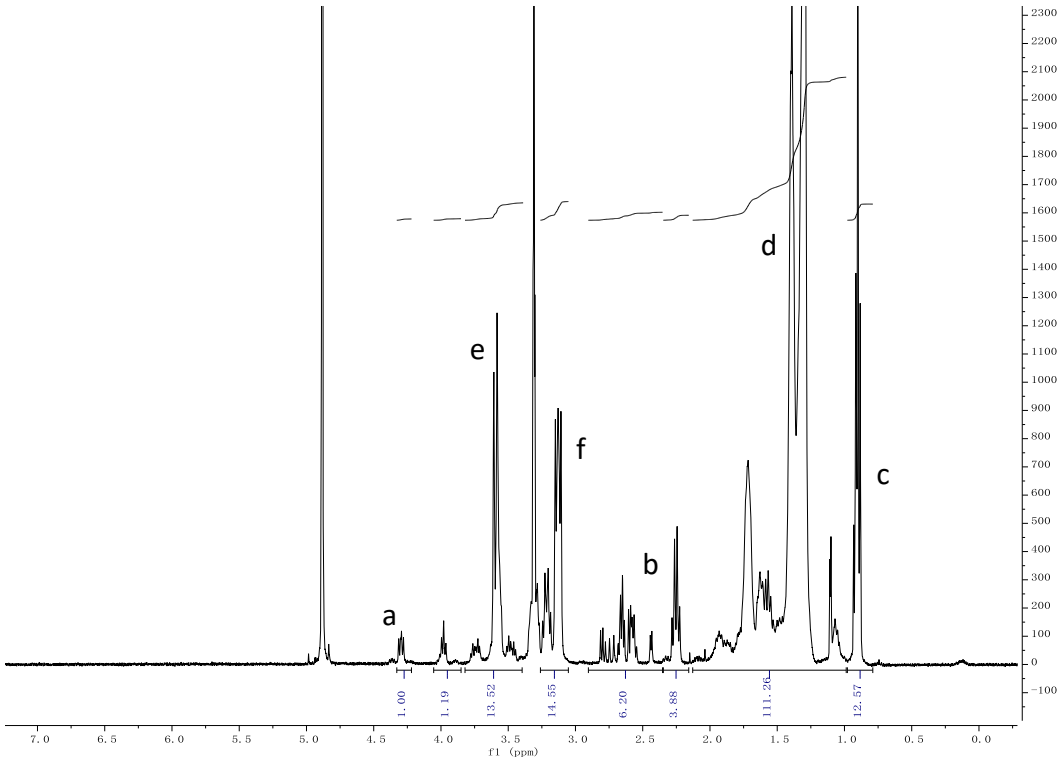

^{1}H NMR (400 MHz, Methanol-d4) δ (ppm) = 0.82 – 0.96 (m, 12H, -CH3), 0.99 – 2.05 (m, 110H, -CH2-CH2-), 2.11 – 2.71 (m, 8H, -CH2-CONH-), 2.98 – 3.26 (m, 12H, -CH2-N), 3.31 – 3.58 (m, 12H, -NH-CH2-CH2-NH-), 4.35-4.41 (1H, αH amino acids).

1716: Sequence (N->C): $K(12Oc)_2$-Stp_1-$K[K(12Oc)_2]$-OH

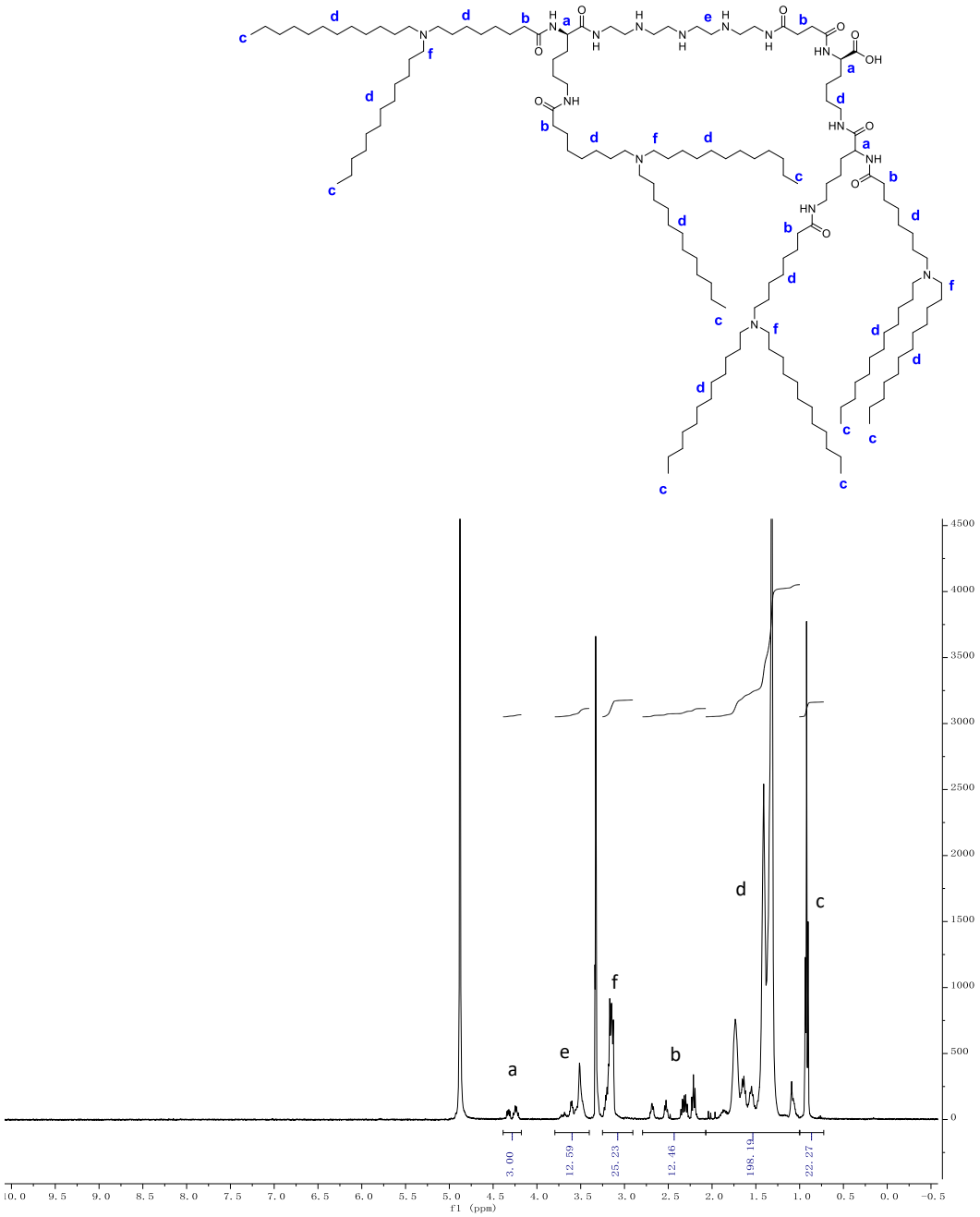

^{1}H NMR (400 MHz, Methanol-d4) δ (ppm) = 0.82 – 0.96 (m, 24H, -CH3), 0.99 – 2.05 (m, 220H, -CH2-CH2-), 2.11 – 2.71 (m, 12H, -CH2-CONH-), 2.98 – 3.26 (m, 24H, -CH2-N), 3.31 – 3.58 (m, 14H, -NH-CH2-CH2-NH-), 4.22-4.34 (3H, αH amino acids).

1717: Sequence (N->C): $K(12Oc)_2$-Stp_2-$K[K(12Oc)_2]$-OH

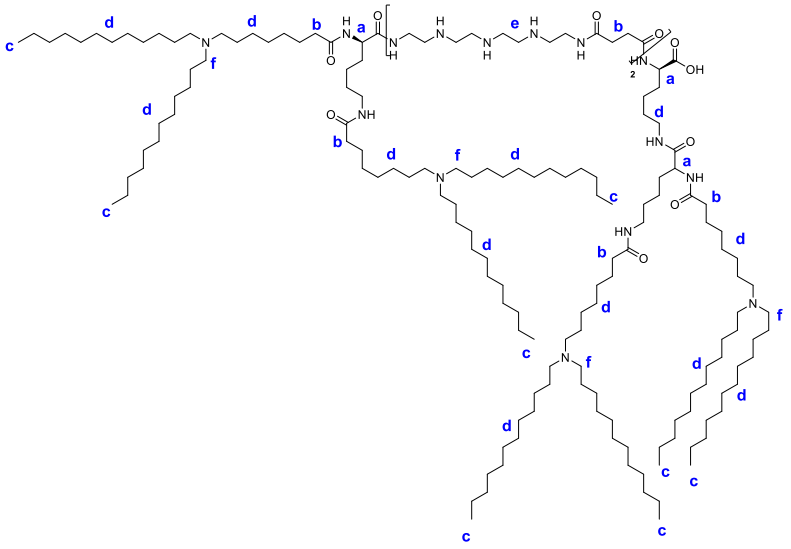

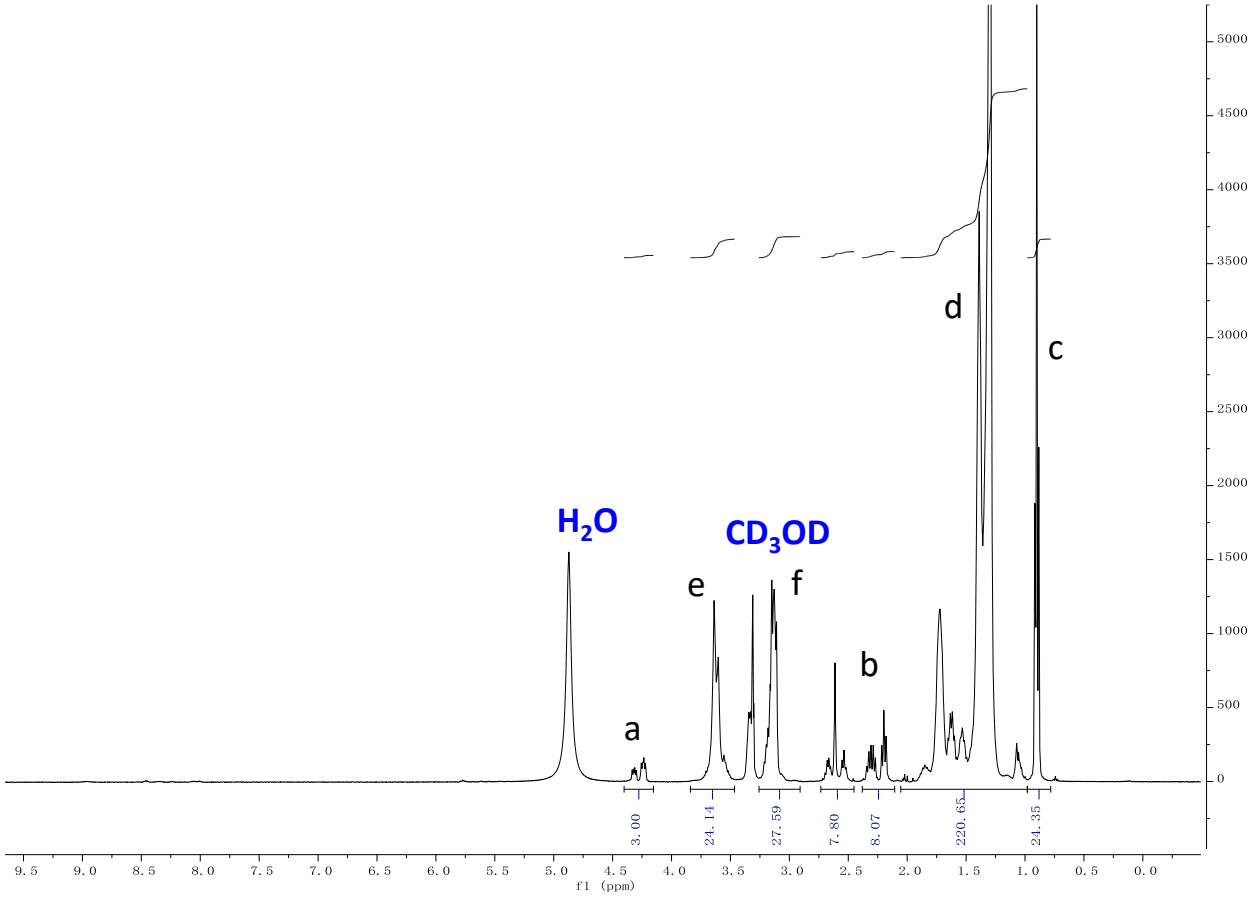

^{1}H NMR (400 MHz, Methanol-d4) δ (ppm) = 0.82 – 0.96 (m, 24H, -CH3), 0.99 – 2.05 (m, 220H, -CH2-CH2-), 2.11 – 2.71 (m, 12H, -CH2-CONH-), 2.98 – 3.26 (m, 24H, -CH2-N), 3.31 – 3.58 (m, 28H, -NH-CH2-CH2-NH-), 4.22-4.34 (3H, αH amino acids).

8.4 RP-HPLC of building blocks and oligomers

8Oc:

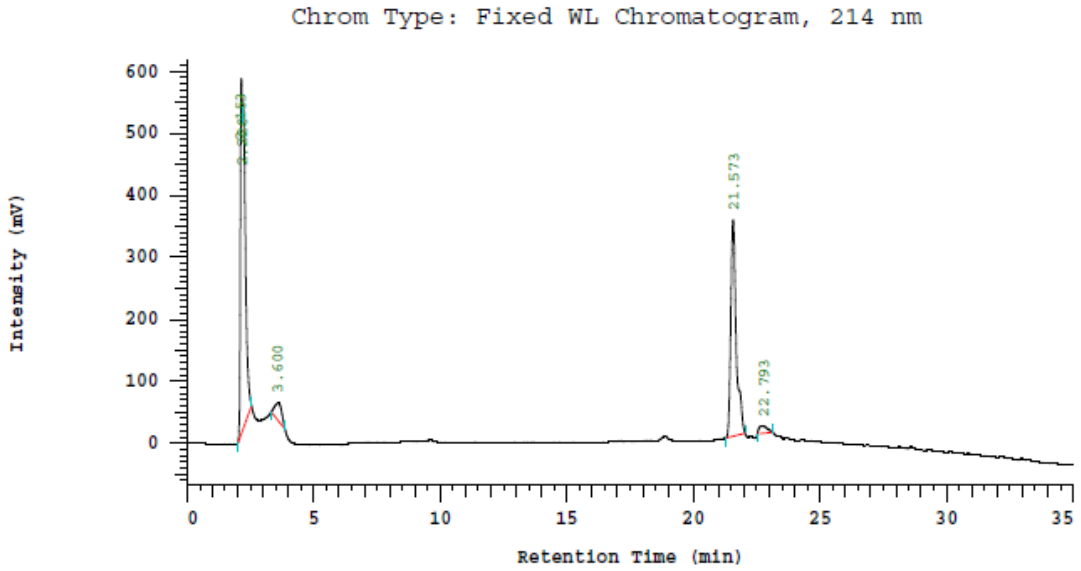

12Oc

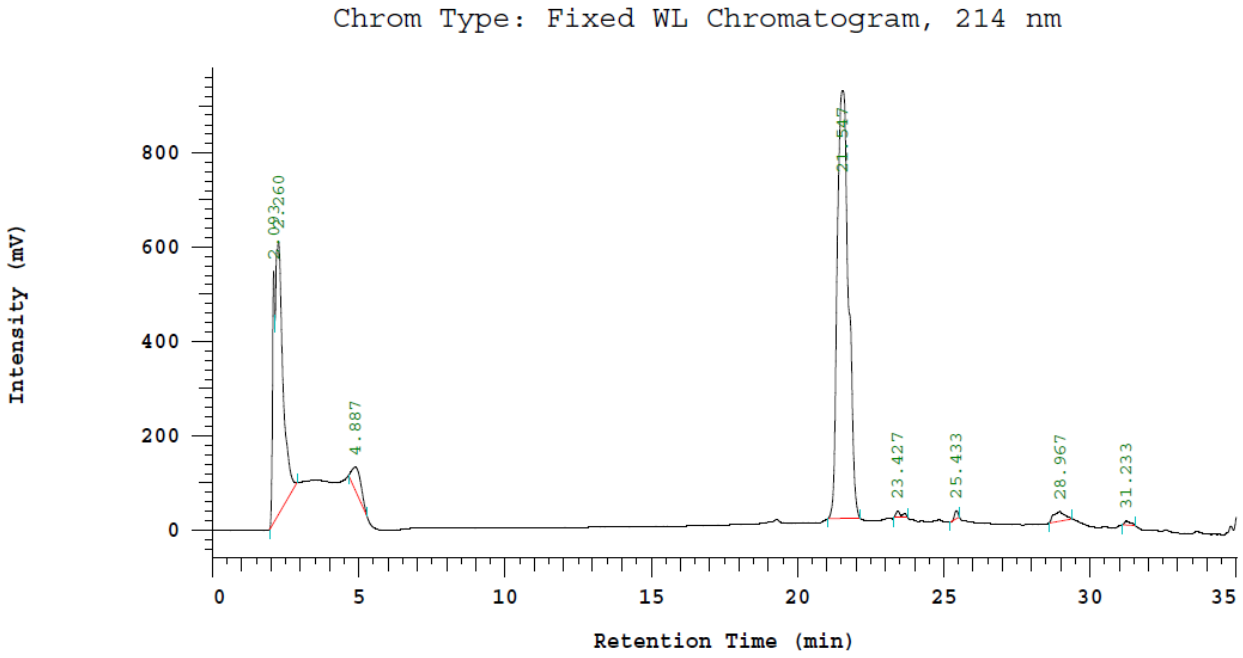

1620:

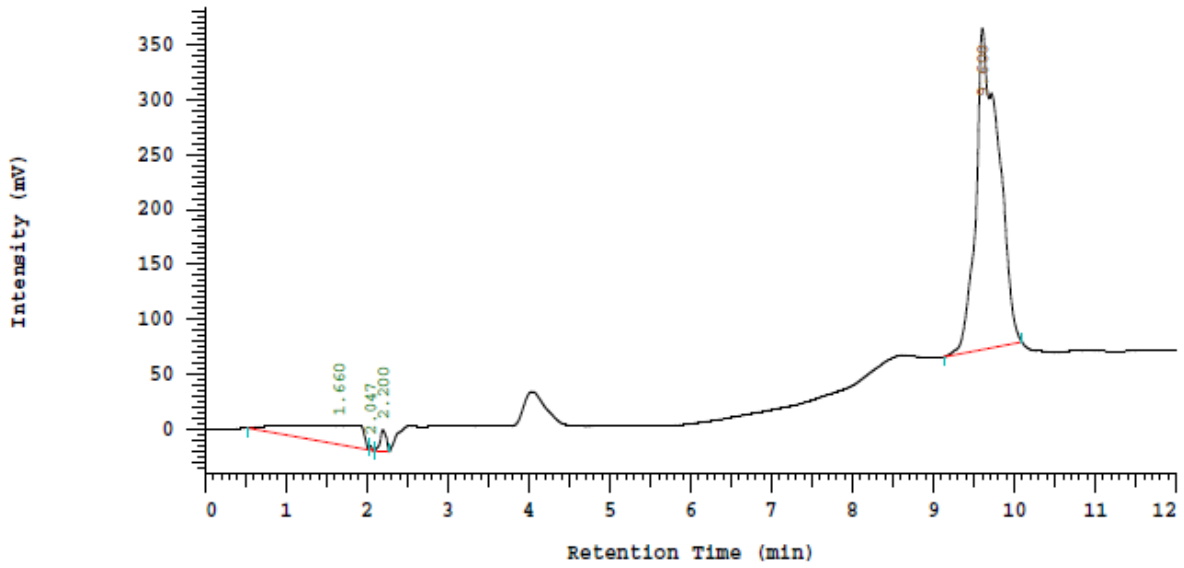
Intensity (mV)
350
300
250
200
150
100
50
0
1.660
2.047
2.200
0
1
2
3
4
5
6
7
8
9
10
11
12
Retention Time (min)

1613:

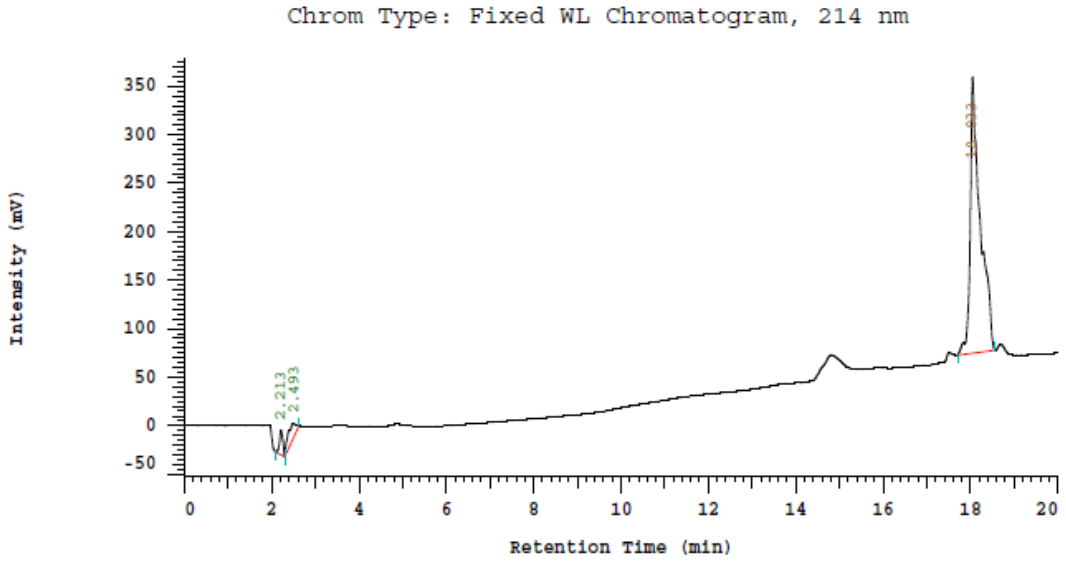
Chrom Type: Fixed WL Chromatogram, 214 nm
Intensity (mV)
350
300
250
200
150
100
50
0
-50
2.213
2.493
0
2
4
6
8
10
12
14
16
18
20
Retention Time (min)

1621:

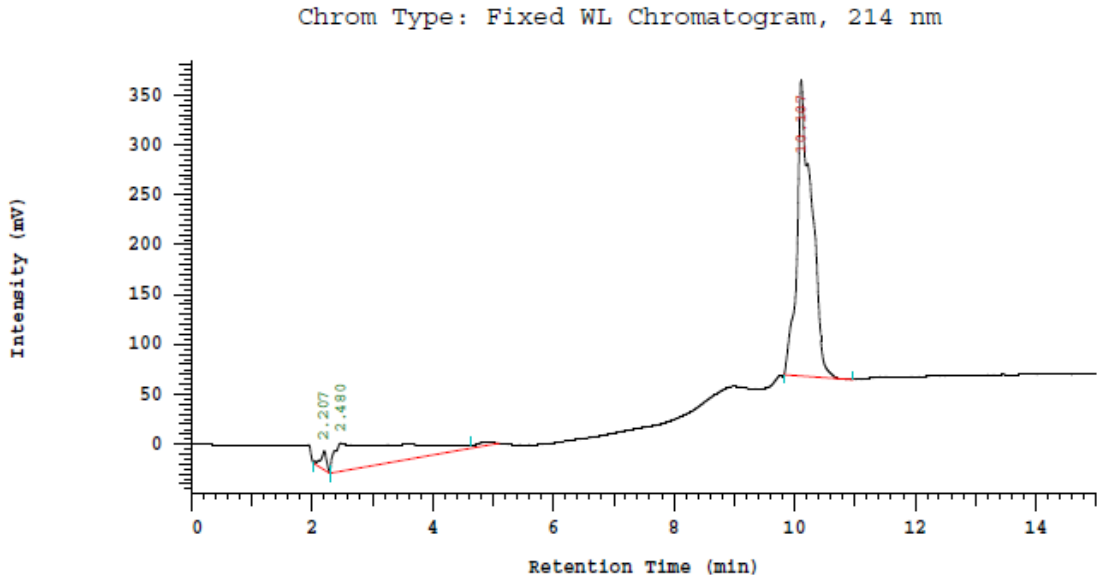
Chrom Type: Fixed WL Chromatogram, 214 nm
Intensity (mV)
Retention Time (min)
2.207
2.480
10.189

1722:

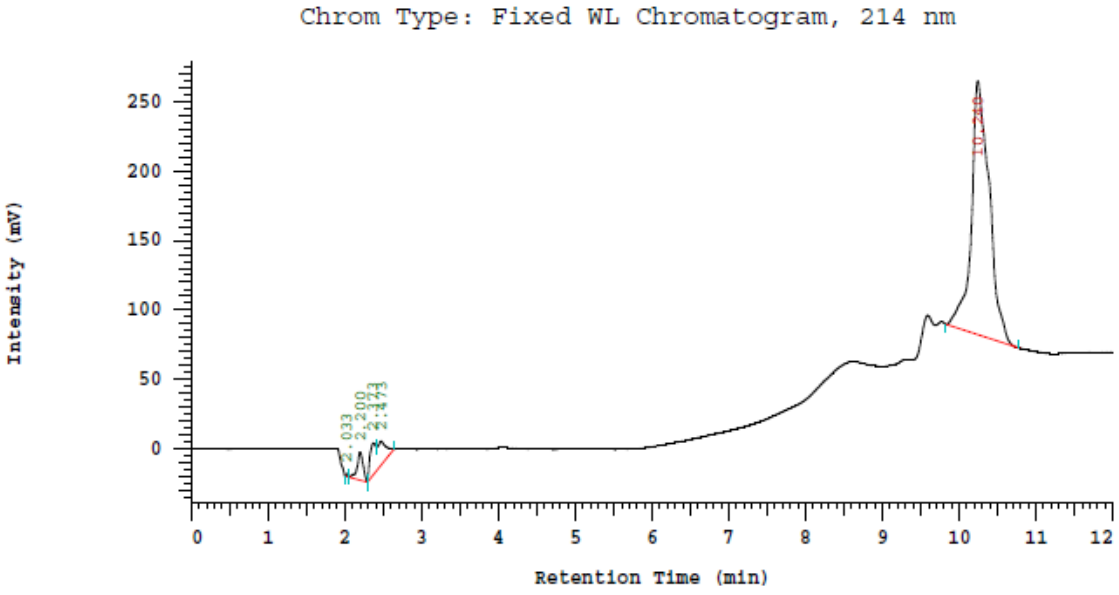
Chrom Type: Fixed WL Chromatogram, 214 nm
Intensity (mV)
Retention Time (min)
2.033
2.200
2.373
10.210

9 References

(1) Jemal, A.; Bray, F.; Center, M. M.; Ferlay, J.; Ward, E.; Forman, D. Global cancer statistics. *CA Cancer J Clin* **2011**, *61* (2), 69-90.
(2) Arnold, M.; Sierra, M. S.; Laversanne, M.; Soerjomataram, I.; Jemal, A.; Bray, F. Global patterns and trends in colorectal cancer incidence and mortality. *Gut* **2017**, *66* (4), 683-691.
(3) Siegel, R. L.; Miller, K. D.; Jemal, A. Cancer statistics, 2016. *CA Cancer J. Clin.* **2016**, *66* (1), 7-30.
(4) Mignani, S.; Bryszewska, M.; Klajnert-Maculewicz, B.; Zablocka, M.; Majoral, J. P. Advances in combination therapies based on nanoparticles for efficacious cancer treatment: an analytical report. *Biomacromolecules* **2015**, *16* (1), 1-27.
(5) Gilman, A. The initial clinical trial of nitrogen mustard. *Am J Surg* **1963**, *105*, 574-578.
(6) Zubrod, C. G.; Schepartz, S. A.; Carter, S. K. Historical background of the National Cancer Institute's drug development thrust. *Natl. Cancer Inst. Monogr.* **1977**, *45*, 7-11.
(7) FREI III, E.; Karon, M.; Levin, R. H.; FREIREICH, E. J.; Taylor, R. J.; Hananian, J.; Selawry, O.; Holland, J. F.; Hoogstraten, B.; Wolman, I. J. The effectiveness of combinations of antileukemic agents in inducing and maintaining remission in children with acute leukemia. *Blood* **1965**, *26* (5), 642-656.
(8) Lin, J.; Wang, S.; Huang, P.; Wang, Z.; Chen, S.; Niu, G.; Li, W.; He, J.; Cui, D.; Lu, G.; et al. Photosensitizer-Loaded Gold Vesicles with Strong Plasmonic Coupling Effect for Imaging-Guided Photothermal/Photodynamic Therapy. *ACS Nano* **2013**, *7* (6), 5320-5329.
(9) Bernstein, I. D.; Tam, M. R.; Nowinski, R. C. Mouse leukemia: therapy with monoclonal antibodies against a thymus differentiation antigen. *Science* **1980**, *207* (4426), 68-71.
(10) Kapse-Mistry, S.; Govender, T.; Srivastava, R.; Yergeri, M. Nanodrug delivery in reversing multidrug resistance in cancer cells. *Front. Pharmacol.* **2014**, *5*, 159, 1-22.
(11) Espinosa, E.; Zamora, P.; Feliu, J.; González Barón, M. Classification of anticancer drugs—a new system based on therapeutic targets. *Cancer Treat. Rev.* **2003**, *29* (6), 515-523.
(12) Wang, H.; Zhao, Y.; Wu, Y.; Hu, Y. L.; Nan, K.; Nie, G.; Chen, H. Enhanced anti-tumor efficacy by co-delivery of doxorubicin and paclitaxel with amphiphilic methoxy PEG-PLGA copolymer nanoparticles. *Biomaterials* **2011**, *32* (32), 8281-8290.
(13) Duong, H. H. P.; Yung, L.-Y. L. Synergistic co-delivery of doxorubicin and paclitaxel using multi-functional micelles for cancer treatment. *Int. J. Pharm.* **2013**, *454* (1), 486-495.
(14) Chen, Y.; Zhang, W.; Huang, Y.; Gao, F.; Sha, X.; Fang, X. Pluronic-based functional polymeric mixed micelles for co-delivery of doxorubicin and paclitaxel to multidrug resistant tumor. *Int. J. Pharm.* **2015**, *488* (1), 44-58.
(15) Qi, S. S.; Sun, J. H.; Yu, H. H.; Yu, S. Q. Co-delivery nanoparticles of anti-cancer drugs for improving chemotherapy efficacy. *Drug Deliv* **2017**, *24* (1), 1909-1926.
(16) Lv, S.; Tang, Z.; Li, M.; Lin, J.; Song, W.; Liu, H.; Huang, Y.; Zhang, Y.; Chen, X. Co-delivery of doxorubicin and paclitaxel by PEG-polypeptide nanovehicle for the treatment of non-small cell lung cancer. *Biomaterials* **2014**, *35* (23), 6118-6129.
(17) Zhang, R. X.; Cai, P.; Zhang, T.; Chen, K.; Li, J.; Cheng, J.; Pang, K. S.; Adissu, H. A.; Rauth, A. M.; Wu, X. Y. Polymer-lipid hybrid nanoparticles synchronize pharmacokinetics of co-encapsulated doxorubicin-mitomycin C and enable their spatiotemporal co-delivery and local bioavailability in breast tumor. *Nanomedicine* **2016**, *12* (5), 1279-1290.
(18) Eloy, J. O.; Claro de Souza, M.; Petrilli, R.; Barcellos, J. P.; Lee, R. J.; Marchetti, J. M. Liposomes as carriers of hydrophilic small molecule drugs: strategies to enhance encapsulation and delivery. *Colloids Surf B Biointerfaces* **2014**, *123*, 345-363.
(19) KOBAYASHI, T.; TSUKAGOSHI, S.; SAKURAI, Y. Enhancement of the cancer chemotherapeutic effect of cytosine arabinoside entrapped in liposomes on mouse

leukemia L-1210. *GANN Japanese Journal of Cancer Research* **1975**, *66* (6), 719-720.
(20) Patel, N. R.; Rathi, A.; Mongayt, D.; Torchilin, V. P. Reversal of multidrug resistance by co-delivery of tariquidar (XR9576) and paclitaxel using long-circulating liposomes. *Int. J. Pharm.* **2011**, *416* (1), 296-299.
(21) Truebenbach, I.; Kern, S.; Loy, D. M.; Hoehn, M.; Gorges, J.; Kazmaier, U.; Wagner, E. Combination chemotherapy of L1210 tumors in mice with pretubulysin and methotrexate lipo-oligomer nanoparticles. *Mol. Pharm.* **2019**, 16(6), 2405-2417.
(22) Amable, L.; Reed, E.; Chabner, B. A. Platinum analogues. *Cancer Chemotherapy, Immunotherapy and Biotherapy* **2019**, 234-248.
(23) Chan, E. S.; Cronstein, B. N. Methotrexate--how does it really work? *Nat. Rev. Rheumatol.* **2010**, *6* (3), 175-178.
(24) Sasse, F.; SIEINMETZ, H.; Heil, J.; Hoefle, G.; Reichenbach, H. Tubulysins, new cytostatic peptides from myxobacteria acting on microtubuli production, isolation, physico-chemical and biological properties. *J. Antibiot.* **2000**, *53* (9), 879-885.
(25) Newman, D. J. Natural Product Based Antibody Drug Conjugates: Clinical Status as of November 9, 2020. *J. Nat. Prod.* **2021**, *84* (3), 917-931.
(26) Ullrich, A.; Chai, Y.; Pistorius, D.; Elnakady, Y. A.; Herrmann, J. E.; Weissman, K. J.; Kazmaier, U.; Müller, R. Pretubulysin, a potent and chemically accessible tubulysin precursor from Angiococcus disciformis. *Angew. Chem. Int. Ed.* **2009**, *48* (24), 4422-4425.
(27) Braig, S.; Wiedmann, R. M.; Liebl, J.; Singer, M.; Kubisch, R.; Schreiner, L.; Abhari, B. A.; Wagner, E.; Kazmaier, U.; Fulda, S.; et al. Pretubulysin: a new option for the treatment of metastatic cancer. *Cell Death Dis.* **2014**, *5*, e1001.
(28) Kern, S.; Truebenbach, I.; Hohn, M.; Gorges, J.; Kazmaier, U.; Zahler, S.; Vollmar, A. M.; Wagner, E. Combined antitumoral effects of pretubulysin and methotrexate. *Pharmacol. Res. Perspect* **2019**, *7* (1), e00460.
(29) Kanapathipillai, M.; Brock, A.; Ingber, D. E. Nanoparticle targeting of anti-cancer drugs that alter intracellular signaling or influence the tumor microenvironment. *Adv. Drug Deliv. Rev.* **2014**, *79-80*, 107-118.
(30) Kesharwani, P.; Jain, K.; Jain, N. K. Dendrimer as nanocarrier for drug delivery. *Prog. Polym. Sci.* **2014**, *39* (2), 268-307.
(31) Li, X.; Zhao, Q.; Qiu, L. Smart ligand: aptamer-mediated targeted delivery of chemotherapeutic drugs and siRNA for cancer therapy. *J. Control. Release* **2013**, *171* (2), 152-162.
(32) Safdar, M. H.; Hussain, Z.; Abourehab, M. A. S.; Hasan, H.; Afzal, S.; Thu, H. E. New developments and clinical transition of hyaluronic acid-based nanotherapeutics for treatment of cancer: reversing multidrug resistance, tumour-specific targetability and improved anticancer efficacy. *Artif Cells Nanomed. Biotechnol.* **2018**, *46* (8), 1967-1980.
(33) Xu, L.; Bai, Q.; Zhang, X.; Yang, H. Folate-mediated chemotherapy and diagnostics: An updated review and outlook. *J. Control. Release* **2017**, *252*, 73-82.
(34) Fiehn, C. Methotrexate transport mechanisms: the basis for targeted drug delivery and β-folate-receptor-specific treatment. *Clin Exp Rheumatol* **2010**, *28* (5 Suppl 61), S40-45.
(35) Klein, P. M.; Kern, S.; Lee, D. J.; Schmaus, J.; Hohn, M.; Gorges, J.; Kazmaier, U.; Wagner, E. Folate receptor-directed orthogonal click-functionalization of siRNA lipopolyplexes for tumor cell killing *in vivo*. *Biomaterials* **2018**, *178*, 630-642.
(36) Yarden, Y. The EGFR family and its ligands in human cancer: signalling mechanisms and therapeutic opportunities. *Eur. J. Cancer* **2001**, *37*, 3-8.
(37) Drebin, J. A.; Link, V. C.; Stern, D. F.; Weinberg, R. A.; Greene, M. I. Down-modulation of an oncogene protein product and reversion of the transformed phenotype by monoclonal antibodies. *Cell* **1985**, *41* (3), 695-706.
(38) Morys, S.; Urnauer, S.; Spitzweg, C.; Wagner, E. EGFR targeting and shielding of pDNA lipopolyplexes via bivalent attachment of a sequence ‐ defined PEG agent. *Macromol. Biosci.* **2018**, *18* (1), 1700203.
(39) Li, Z.; Zhao, R.; Wu, X.; Sun, Y.; Yao, M.; Li, J.; Xu, Y.; Gu, J. Identification and

characterization of a novel peptide ligand of epidermal growth factor receptor for targeted delivery of therapeutics. *FASEB J* **2005**, *19* (14), 1978-1985.
(40) Zou, Y.; Xia, Y.; Meng, F.; Zhang, J.; Zhong, Z. GE11-Directed Functional Polymersomal Doxorubicin as an Advanced Alternative to Clinical Liposomal Formulation for Ovarian Cancer Treatment. *Mol. Pharm.* **2018**, *15* (9), 3664-3671.
(41) Muller, K.; Klein, P. M.; Heissig, P.; Roidl, A.; Wagner, E. EGF receptor targeted lipo-oligocation polyplexes for antitumoral siRNA and miRNA delivery. *Nanotechnology* **2016**, *27* (46), 464001.
(42) Truebenbach, I.; Zhang, W.; Wang, Y.; Kern, S.; Höhn, M.; Reinhard, S.; Gorges, J.; Kazmaier, U.; Wagner, E. Co-delivery of pretubulysin and siEG5 to EGFR overexpressing carcinoma cells. *Int. J. Pharm.* **2019**, *569*, 118570.
(43) Goswami, R.; Subramanian, G.; Silayeva, L.; Newkirk, I.; Doctor, D.; Chawla, K.; Chattopadhyay, S.; Chandra, D.; Chilukuri, N.; Betapudi, V. Gene Therapy Leaves a Vicious Cycle. *Front. Oncol.* **2019**, *9*, 297.
(44) MacLaren, R. E.; Groppe, M.; Barnard, A. R.; Cottriall, C. L.; Tolmachova, T.; Seymour, L.; Clark, K. R.; During, M. J.; Cremers, F. P. M.; Black, G. C. M.; et al. Retinal gene therapy in patients with choroideremia: initial findings from a phase 1/2 clinical trial. *The Lancet* **2014**, *383* (9923), 1129-1137.
(45) van Deutekom, J. C.; van Ommen, G. J. Advances in Duchenne muscular dystrophy gene therapy. *Nat. Rev. Genet.* **2003**, *4* (10), 774-783.
(46) Morrissey, D. V.; Lockridge, J. A.; Shaw, L.; Blanchard, K.; Jensen, K.; Breen, W.; Hartsough, K.; Machemer, L.; Radka, S.; Jadhav, V.; et al. Potent and persistent *in vivo* anti-HBV activity of chemically modified siRNAs. *Nat. Biotechnol.* **2005**, *23* (8), 1002-1007.
(47) Okumura, A.; Pitha Paula, M.; Harty Ronald, N. ISG15 inhibits Ebola VP40 VLP budding in an L-domain-dependent manner by blocking Nedd4 ligase activity. *Proc. Natl. Acad. Sci. U.S.A.* **2008**, *105* (10), 3974-3979.
(48) Shen, H.; Sun, T.; Ferrari, M. Nanovector delivery of siRNA for cancer therapy. *Cancer Gene Ther.* **2012**, *19* (6), 367-373.
(49) Davis, M. E.; Zuckerman, J. E.; Choi, C. H.; Seligson, D.; Tolcher, A.; Alabi, C. A.; Yen, Y.; Heidel, J. D.; Ribas, A. Evidence of RNAi in humans from systemically administered siRNA via targeted nanoparticles. *Nature* **2010**, *464* (7291), 1067-1070.
(50) Whitehead, K. A.; Langer, R.; Anderson, D. G. Knocking down barriers: advances in siRNA delivery. *Nat. Rev. Drug Discov.* **2009**, *8* (2), 129-138.
(51) Singha, K.; Namgung, R.; Kim, W. J. Polymers in small-interfering RNA delivery. *Nucleic Acid Ther.* **2011**, *21* (3), 133-147.
(52) Semple, S. C.; Akinc, A.; Chen, J.; Sandhu, A. P.; Mui, B. L.; Cho, C. K.; Sah, D. W.; Stebbing, D.; Crosley, E. J.; Yaworski, E.; et al. Rational design of cationic lipids for siRNA delivery. *Nat. Biotechnol.* **2010**, *28* (2), 172-176.
(53) Akinc, A.; Zumbuehl, A.; Goldberg, M.; Leshchiner, E. S.; Busini, V.; Hossain, N.; Bacallado, S. A.; Nguyen, D. N.; Fuller, J.; Alvarez, R.; et al. A combinatorial library of lipid-like materials for delivery of RNAi therapeutics. *Nat. Biotechnol.* **2008**, *26* (5), 561-569.
(54) Mo, R. H.; Zaro, J. L.; Shen, W. C. Comparison of cationic and amphipathic cell penetrating peptides for siRNA delivery and efficacy. *Mol. Pharm.* **2012**, *9* (2), 299-309.
(55) Yao, Y.-d.; Sun, T.-m.; Huang, S.-y.; Dou, S.; Lin, L.; Chen, J.-n.; Ruan, J.-b.; Mao, C.-q.; Yu, F.-y.; Zeng, M.-s.; et al. Targeted Delivery of PLK1-siRNA by ScFv Suppresses Her2+ Breast Cancer Growth and Metastasis. *Sci. Transl. Med.* **2012**, *4* (130), 130ra148-130ra148.
(56) Dassie, J. P.; Liu, X. Y.; Thomas, G. S.; Whitaker, R. M.; Thiel, K. W.; Stockdale, K. R.; Meyerholz, D. K.; McCaffrey, A. P.; McNamara, J. O., 2nd; Giangrande, P. H. Systemic administration of optimized aptamer-siRNA chimeras promotes regression of PSMA-expressing tumors. *Nat. Biotechnol.* **2009**, *27* (9), 839-849.
(57) Soutschek, J.; Akinc, A.; Bramlage, B.; Charisse, K.; Constien, R.; Donoghue, M.; Elbashir, S.; Geick, A.; Hadwiger, P.; Harborth, J.; et al. Therapeutic silencing of an

endogenous gene by systemic administration of modified siRNAs. *Nature* **2004**, *432* (7014), 173-178.
(58) Thomas, M.; Kularatne, S. A.; Qi, L.; Kleindl, P.; Leamon, C. P.; Hansen, M. J.; Low, P. S. Ligand-Targeted Delivery of Small Interfering RNAs to Malignant Cells and Tissues. *Annals of the New York Academy of Sciences* **2009**, *1175* (1), 32-39.
(59) Mallapaty, S.; Callaway, E.; Kozlov, M.; Ledford, H.; Pickrell, J.; Van Noorden, R. How COVID vaccines shaped 2021 in eight powerful charts. *Nature* **2021**, *600* (7890), 580-583.
(60) Mallapaty, S. India's DNA COVID vaccine is a world first–more are coming. *Nature* **2021**, *597* (7875), 161-162.
(61) Hardee, C. L.; Arevalo-Soliz, L. M.; Hornstein, B. D.; Zechiedrich, L. Advances in Non-Viral DNA Vectors for Gene Therapy. *Genes (Basel)* **2017**, *8* (2), 65.
(62) Tang, X.; Zhang, S.; Fu, R.; Zhang, L.; Huang, K.; Peng, H.; Dai, L.; Chen, Q. Therapeutic Prospects of mRNA-Based Gene Therapy for Glioblastoma. *Front. Oncol.* **2019**, *9*, 1208.
(63) Kumar, R.; Santa Chalarca, C. F.; Bockman, M. R.; Bruggen, C. V.; Grimme, C. J.; Dalal, R. J.; Hanson, M. G.; Hexum, J. K.; Reineke, T. M. Polymeric Delivery of Therapeutic Nucleic Acids. *Chem. Rev.* **2021**, *121* (18), 11527-11652.
(64) Meng, Z.; O'Keeffe-Ahern, J.; Lyu, J.; Pierucci, L.; Zhou, D.; Wang, W. A new developing class of gene delivery: messenger RNA-based therapeutics. *Biomater. Sci.* **2017**, *5* (12), 2381-2392.
(65) Fu, Y.; Chen, J.; Huang, Z. Recent progress in microRNA-based delivery systems for the treatment of human disease. *ExRNA* **2019**, *1* (1), 1-14.
(66) Yeh, C. D.; Richardson, C. D.; Corn, J. E. Advances in genome editing through control of DNA repair pathways. *Na.t Cell Biol.* **2019**, *21* (12), 1468-1478.
(67) Anzalone, A. V.; Koblan, L. W.; Liu, D. R. Genome editing with CRISPR-Cas nucleases, base editors, transposases and prime editors. *Nat. Biotechno.l* **2020**, *38* (7), 824-844.
(68) Liu, J.; Chang, J.; Jiang, Y.; Meng, X.; Sun, T.; Mao, L.; Xu, Q.; Wang, M. Fast and Efficient CRISPR/Cas9 Genome Editing *In Vivo* Enabled by Bioreducible Lipid and Messenger RNA Nanoparticles. *Adv. Mater.* **2019**, *31* (33), e1902575.
(69) Wang, P.; Zhang, L.; Zheng, W.; Cong, L.; Guo, Z.; Xie, Y.; Wang, L.; Tang, R.; Feng, Q.; Hamada, Y.; et al. Thermo-triggered Release of CRISPR-Cas9 System by Lipid-Encapsulated Gold Nanoparticles for Tumor Therapy. *Angew. Chem. Int. Ed.* **2018**, *57* (6), 1491-1496.
(70) Zhu, M.; Nie, G.; Meng, H.; Xia, T.; Nel, A.; Zhao, Y. Physicochemical Properties Determine Nanomaterial Cellular Uptake, Transport, and Fate. *Acc. Chem. Res.* **2013**, *46* (3), 622-631.
(71) Johannes, L.; Mayor, S. Induced domain formation in endocytic invagination, lipid sorting, and scission. *Cell* **2010**, *142* (4), 507-510.
(72) de Planque, M. R. R.; Aghdaei, S.; Roose, T.; Morgan, H. Electrophysiological Characterization of Membrane Disruption by Nanoparticles. *ACS Nano* **2011**, *5* (5), 3599-3606.
(73) Dasgupta, S.; Auth, T.; Gompper, G. Shape and orientation matter for the cellular uptake of nonspherical particles. *Nano Lett.* **2014**, *14* (2), 687-693.
(74) Herd, H.; Daum, N.; Jones, A. T.; Huwer, H.; Ghandehari, H.; Lehr, C.-M. Nanoparticle Geometry and Surface Orientation Influence Mode of Cellular Uptake. *ACS Nano* **2013**, *7* (3), 1961-1973.
(75) Li, Y.; Gu, N. Thermodynamics of Charged Nanoparticle Adsorption on Charge-Neutral Membranes: A Simulation Study. *J. Phys. Chem. B* **2010**, *114* (8), 2749-2754.
(76) Hühn, D.; Kantner, K.; Geidel, C.; Brandholt, S.; De Cock, I.; Soenen, S. J. H.; Rivera_Gil, P.; Montenegro, J.-M.; Braeckmans, K.; Müllen, K.; et al. Polymer-Coated Nanoparticles Interacting with Proteins and Cells: Focusing on the Sign of the Net Charge. *ACS Nano* **2013**, *7* (4), 3253-3263.
(77) Rozenberg, B. A.; Tenne, R. Polymer-assisted fabrication of nanoparticles and

nanocomposites. *Prog. Polym. Sci.* **2008**, *33* (1), 40-112.
(78) Li, Y.; Chen, X.; Gu, N. Computational Investigation of Interaction between Nanoparticles and Membranes: Hydrophobic/Hydrophilic Effect. *J. Phys. Chem. B* **2008**, *112* (51), 16647-16653.
(79) Karakoti, A. S.; Shukla, R.; Shanker, R.; Singh, S. Surface functionalization of quantum dots for biological applications. *Adv. Colloid Interface Sci.* **2015**, *215*, 28-45.
(80) Chompoosor, A.; Saha, K.; Ghosh, P. S.; Macarthy, D. J.; Miranda, O. R.; Zhu, Z. J.; Arcaro, K. F.; Rotello, V. M. The role of surface functionality on acute cytotoxicity, ROS generation and DNA damage by cationic gold nanoparticles. *Small* **2010**, *6* (20), 2246-2249.
(81) Yeh, Y. C.; Saha, K.; Yan, B.; Miranda, O. R.; Yu, X.; Rotello, V. M. The role of ligand coordination on the cytotoxicity of cationic quantum dots in HeLa cells. *Nanoscale* **2013**, *5* (24), 12140-12143.
(82) Steinborn, B.; Truebenbach, I.; Morys, S.; Lachelt, U.; Wagner, E.; Zhang, W. Epidermal growth factor receptor targeted methotrexate and small interfering RNA co-delivery. *J. Gene Med.* **2018**, *20* (7-8), e3041.
(83) Allen, T. M.; Cullis, P. R. Liposomal drug delivery systems: From concept to clinical applications. *Adv. Drug Deliv. Rev.* **2013**, *65* (1), 36-48.
(84) Jiang, D.; Lee, H.; Pardridge, W. M. Plasmid DNA gene therapy of the Niemann-Pick C1 mouse with transferrin receptor-targeted Trojan horse liposomes. *Sci Rep* **2020**, *10* (1), 13334.
(85) Miura, Y.; Takenaka, T.; Toh, K.; Wu, S.; Nishihara, H.; Kano, M. R.; Ino, Y.; Nomoto, T.; Matsumoto, Y.; Koyama, H.; et al. Cyclic RGD-Linked Polymeric Micelles for Targeted Delivery of Platinum Anticancer Drugs to Glioblastoma through the Blood–Brain Tumor Barrier. *ACS Nano* **2013**, *7* (10), 8583-8592.
(86) Osada, K.; Cabral, H.; Mochida, Y.; Lee, S.; Nagata, K.; Matsuura, T.; Yamamoto, M.; Anraku, Y.; Kishimura, A.; Nishiyama, N.; et al. Bioactive polymeric metallosomes self-assembled through block copolymer-metal complexation. *J. Am. Chem. Soc.* **2012**, *134* (32), 13172-13175.
(87) Fleige, E.; Quadir, M. A.; Haag, R. Stimuli-responsive polymeric nanocarriers for the controlled transport of active compounds: Concepts and applications. *Adv. Drug Deliv. Rev.* **2012**, *64* (9), 866-884.
(88) Quader, S.; Kataoka, K. Nanomaterial-Enabled Cancer Therapy. *Mol. Ther.* **2017**, *25* (7), 1501-1513.
(89) Chiang, N.-J.; Chang, J.-Y.; Shan, Y.-S.; Chen, L.-T. Development of nanoliposomal irinotecan (nal-IRI, MM-398, PEP02) in the management of metastatic pancreatic cancer. *Expert Opin. Pharmacother.* **2016**, *17* (10), 1413-1420.
(90) Lancet, J. E.; Uy, G. L.; Cortes, J. E.; Newell, L. F.; Lin, T. L.; Ritchie, E. K.; Stuart, R. K.; Strickland, S. A.; Hogge, D.; Solomon, S. R.; et al. CPX-351 (cytarabine and daunorubicin) Liposome for Injection Versus Conventional Cytarabine Plus Daunorubicin in Older Patients With Newly Diagnosed Secondary Acute Myeloid Leukemia. *J. Clin. Oncol.* **2018**, *36* (26), 2684-2692.
(91) Xu, L.; Liang, H. W.; Yang, Y.; Yu, S. H. Stability and Reactivity: Positive and Negative Aspects for Nanoparticle Processing. *Chem. Rev.* **2018**, *118* (7), 3209-3250.
(92) Gu, X.; Qiu, M.; Sun, H.; Zhang, J.; Cheng, L.; Deng, C.; Zhong, Z. Polytyrosine nanoparticles enable ultra-high loading of doxorubicin and rapid enzyme-responsive drug release. *Biomater. Sci.* **2018**, *6* (6), 1526-1534.
(93) Kim, C. S.; Tonga, G. Y.; Solfiell, D.; Rotello, V. M. Inorganic nanosystems for therapeutic delivery: Status and prospects. *Adv. Drug Deliv. Rev.* **2013**, *65* (1), 93-99.
(94) Garcia-Guerra, A.; Dunwell, T. L.; Trigueros, S. Nano-scale gene delivery systems: current technology, obstacles, and future directions. *Curr. Med. Chem.* **2018**, *25* (21), 2448-2464.
(95) Trigueros, S. Nano-gene-delivery: Overcoming one of the major challenges in gene therapy. *Research in Medical and Engineering Sciences* **2018**, *6* (2).

(96) Riley, R. S.; Day, E. S. Gold nanoparticle-mediated photothermal therapy: applications and opportunities for multimodal cancer treatment. *Nanomed. Nanobiotechnol.* **2017**, *9* (4), e1449.
(97) Mitchell, M. J.; Billingsley, M. M.; Haley, R. M.; Wechsler, M. E.; Peppas, N. A.; Langer, R. Engineering precision nanoparticles for drug delivery. *Nat. Rev. Drug Discov.* **2021**, *20* (2), 101-124.
(98) Trigueros, S.; Domenech, E. B.; Toulis, V.; Marfany, G. *In vitro* Gene Delivery in Retinal Pigment Epithelium Cells by Plasmid DNA-Wrapped Gold Nanoparticles. *Genes (Basel)* **2019**, *10* (4), 289.
(99) Adewale, O. B.; Davids, H.; Cairncross, L.; Roux, S. Toxicological Behavior of Gold Nanoparticles on Various Models: Influence of Physicochemical Properties and Other Factors. *In.t J. Toxicol.* **2019**, *38* (5), 357-384.
(100) Zrazhevskiy, P.; Gao, X. Multifunctional Quantum Dots for Personalized Medicine. *Nano Today* **2009**, *4* (5), 414-428.
(101) Buck, J.; Mueller, D.; Mettal, U.; Ackermann, M.; Grisch-Chan, H. M.; Thony, B.; Zumbuehl, A.; Huwyler, J.; Witzigmann, D. Improvement of DNA Vector Delivery of DOTAP Lipoplexes by Short-Chain Aminolipids. *ACS Omega* **2020**, *5* (38), 24724-24732.
(102) Eygeris, Y.; Patel, S.; Jozic, A.; Sahay, G. Deconvoluting Lipid Nanoparticle Structure for Messenger RNA Delivery. *Nano Lett.* **2020**, *20* (6), 4543-4549.
(103) Schoenmaker, L.; Witzigmann, D.; Kulkarni, J. A.; Verbeke, R.; Kersten, G.; Jiskoot, W.; Crommelin, D. J. A. mRNA-lipid nanoparticle COVID-19 vaccines: Structure and stability. *Int. J. Pharm.* **2021**, *601*, 120586.
(104) Eygeris, Y.; Gupta, M.; Kim, J.; Sahay, G. Chemistry of Lipid Nanoparticles for RNA Delivery. *Acc. Chem. Res.* **2022**, *55* (1), 2-12.
(105) Kalra, H.; Adda, C. G.; Liem, M.; Ang, C. S.; Mechler, A.; Simpson, R. J.; Hulett, M. D.; Mathivanan, S. Comparative proteomics evaluation of plasma exosome isolation techniques and assessment of the stability of exosomes in normal human blood plasma. *Proteomics* **2013**, *13* (22), 3354-3364.
(106) Meneksedag-Erol, D.; Tang, T.; Uludag, H. Probing the Effect of miRNA on siRNA-PEI Polyplexes. *J. Phys. Chem. B* **2015**, *119* (17), 5475-5486.
(107) Ho, L. W. C.; Liu, Y.; Han, R.; Bai, Q.; Choi, C. H. J. Nano-Cell Interactions of Non-Cationic Bionanomaterials. *Acc. Chem. Res.* **2019**, *52* (6), 1519-1530.
(108) Lächelt, U.; Wagner, E. Nucleic acid therapeutics using polyplexes: a journey of 50 years (and beyond). *Chem. Rev.* **2015**, *115* (19), 11043-11078.
(109) Estrella, V.; Chen, T.; Lloyd, M.; Wojtkowiak, J.; Cornnell, H. H.; Ibrahim-Hashim, A.; Bailey, K.; Balagurunathan, Y.; Rothberg, J. M.; Sloane, B. F.; et al. Acidity generated by the tumor microenvironment drives local invasion. *Cancer Res.* **2013**, *73* (5), 1524-1535.
(110) Swietach, P.; Vaughan-Jones, R. D.; Harris, A. L.; Hulikova, A. The chemistry, physiology and pathology of pH in cancer. *Philos Trans R Soc. Lond B Bio.l Sci.* **2014**, *369* (1638), 20130099.
(111) Ling, D.; Park, W.; Park, S. J.; Lu, Y.; Kim, K. S.; Hackett, M. J.; Kim, B. H.; Yim, H.; Jeon, Y. S.; Na, K.; et al. Multifunctional tumor pH-sensitive self-assembled nanoparticles for bimodal imaging and treatment of resistant heterogeneous tumors. *J. Am. Chem. Soc.* **2014**, *136* (15), 5647-5655.
(112) Casey, J. R.; Grinstein, S.; Orlowski, J. Sensors and regulators of intracellular pH. *Nat. Rev. Mol. Cell Biol.* **2010**, *11* (1), 50-61.
(113) Sonaje, K.; Lin, K.-J.; Wang, J.-J.; Mi, F.-L.; Chen, C.-T.; Juang, J.-H.; Sung, H.-W. Self-Assembled pH-Sensitive Nanoparticles: A Platform for Oral Delivery of Protein Drugs. *Adv. Funct. Mater.* **2010**, *20* (21), 3695-3700.
(114) Convertine, A. J.; Benoit, D. S. W.; Duvall, C. L.; Hoffman, A. S.; Stayton, P. S. Development of a novel endosomolytic diblock copolymer for siRNA delivery. *J. Control. Release* **2009**, *133* (3), 221-229.
(115) Adolph, E. J.; Nelson, C. E.; Werfel, T. A.; Guo, R.; Davidson, J. M.; Guelcher, S. A.;

Duvall, C. L. Enhanced Performance of Plasmid DNA Polyplexes Stabilized by a Combination of Core Hydrophobicity and Surface PEGylation. *J. Mater. Chem. B* **2014**, *2* (46), 8154-8164.
(116) Wang, X.; Wilhelm, J.; Li, W.; Li, S.; Wang, Z.; Huang, G.; Wang, J.; Tang, H.; Khorsandi, S.; Sun, Z.; et al. Polycarbonate-based ultra-pH sensitive nanoparticles improve therapeutic window. *Nat. Commun.* **2020**, *11* (1), 5828.
(117) Wang, Y.; Wang, C.; Li, Y.; Huang, G.; Zhao, T.; Ma, X.; Wang, Z.; Sumer, B. D.; White, M. A.; Gao, J. Digitization of Endocytic pH by Hybrid Ultra-pH-Sensitive Nanoprobes at Single-Organelle Resolution. *Adv. Mater.* **2017**, *29* (1), 1603794.
(118) Ma, X.; Wang, Y.; Zhao, T.; Li, Y.; Su, L. C.; Wang, Z.; Huang, G.; Sumer, B. D.; Gao, J. Ultra-pH-sensitive nanoprobe library with broad pH tunability and fluorescence emissions. *J. Am. Chem. Soc.* **2014**, *136* (31), 11085-11092.
(119) Peeler, D. J.; Sellers, D. L.; Pun, S. H. pH-Sensitive Polymers as Dynamic Mediators of Barriers to Nucleic Acid Delivery. *Bioconjug. Chem.* **2019**, *30* (2), 350-365.
(120) Peeler, D. J.; Thai, S. N.; Cheng, Y.; Horner, P. J.; Sellers, D. L.; Pun, S. H. pH-sensitive polymer micelles provide selective and potentiated lytic capacity to venom peptides for effective intracellular delivery. *Biomaterials* **2019**, *192*, 235-244.
(121) Zhang, P.; He, D.; Klein, P. M.; Liu, X.; Röder, R.; Döblinger, M.; Wagner, E. Enhanced Intracellular Protein Transduction by Sequence Defined Tetra-Oleoyl Oligoaminoamides Targeted for Cancer Therapy. *Adv. Funct. Mater.* **2015**, *25* (42), 6627-6636.
(122) Luo, J.; Wagner, E.; Wang, Y. Artificial peptides for antitumoral siRNA delivery. *J. Mater. Chem. B* **2020**, *8* (10), 2020-2031.
(123) Krhač Levačić, A.; Berger, S.; Müller, J.; Wegner, A.; Lächelt, U.; Dohmen, C.; Rudolph, C.; Wagner, E. Dynamic mRNA polyplexes benefit from bioreducible cleavage sites for *in vitro* and *in vivo* transfer. *J. Control. Release* **2021**, *339*, 27-40.
(124) Hill, S. A.; Gerke, C.; Hartmann, L. Recent Developments in Solid-Phase Strategies towards Synthetic, Sequence-Defined Macromolecules. *Chem. Asian J.* **2018**, *13* (23), 3611-3622.
(125) Cheng, Y.; Yumul, R. C.; Pun, S. H. Virus‐inspired polymer for efficient *in vitro* and *in vivo* gene delivery. *Angew. Chem. Int. Ed.* **2016**, *55* (39), 12013-12017.
(126) Jayaraman, M.; Ansell, S. M.; Mui, B. L.; Tam, Y. K.; Chen, J.; Du, X.; Butler, D.; Eltepu, L.; Matsuda, S.; Narayanannair, J. K.; et al. Maximizing the Potency of siRNA Lipid Nanoparticles for Hepatic Gene Silencing *In Vivo*. *Angew. Chem. Int. Ed.* **2012**, *51* (34), 8529-8533.
(127) Celasun, S.; Remmler, D.; Schwaar, T.; Weller, M. G.; Du Prez, F.; Borner, H. G. Digging into the Sequential Space of Thiolactone Precision Polymers: A Combinatorial Strategy to Identify Functional Domains. *Angew. Chem. Int. Ed.* **2019**, *58* (7), 1960-1964.
(128) Solleder, S. C.; Schneider, R. V.; Wetzel, K. S.; Boukis, A. C.; Meier, M. A. R. Recent Progress in the Design of Monodisperse, Sequence-Defined Macromolecules. *Macromol. Rapid. Commun.* **2017**, *38* (9), 1600711.
(129) Schaffert, D.; Troiber, C.; Salcher, E. E.; Frohlich, T.; Martin, I.; Badgujar, N.; Dohmen, C.; Edinger, D.; Klager, R.; Maiwald, G.; et al. Solid-phase synthesis of sequence-defined T-, i-, and U-shape polymers for pDNA and siRNA delivery. *Angew. Chem. Int. Ed.* **2011**, *50* (38), 8986-8989.
(130) Frohlich, T.; Edinger, D.; Klager, R.; Troiber, C.; Salcher, E.; Badgujar, N.; Martin, I.; Schaffert, D.; Cengizeroglu, A.; Hadwiger, P.; et al. Structure-activity relationships of siRNA carriers based on sequence-defined oligo (ethane amino) amides. *J. Control. Release* **2012**, *160* (3), 532-541.
(131) He, D.; Muller, K.; Krhac Levacic, A.; Kos, P.; Lachelt, U.; Wagner, E. Combinatorial Optimization of Sequence-Defined Oligo(ethanamino)amides for Folate Receptor-Targeted pDNA and siRNA Delivery. *Bioconjug. Chem.* **2016**, *27* (3), 647-659.
(132) Kuhn, J.; Lin, Y.; Krhac Levacic, A.; Al Danaf, N.; Peng, L.; Höhn, M.; Lamb, D. C.; Wagner, E.; Lächelt, U. Delivery of Cas9/sgRNA Ribonucleoprotein Complexes via

Hydroxystearyl Oligoamino Amides. *Bioconjug. Chem.* **2020**, *31* (3), 729-742.
(133) Kos, P.; Lächelt, U.; Herrmann, A.; Mickler, F. M.; Döblinger, M.; He, D.; Levačić, A. K.; Morys, S.; Bräuchle, C.; Wagner, E. Histidine-rich stabilized polyplexes for cMet-directed tumor-targeted gene transfer. *Nanoscale* **2015**, *7* (12), 5350-5362.
(134) Wang, S.; Reinhard, S.; Li, C.; Qian, M.; Jiang, H.; Du, Y.; Lächelt, U.; Lu, W.; Wagner, E.; Huang, R. Antitumoral cascade-targeting ligand for IL-6 receptor-mediated gene delivery to glioma. *Mol. Ther.* **2017**, *25* (7), 1556-1566.
(135) Schaffert, D.; Badgujar, N.; Wagner, E. Novel Fmoc-Polyamino Acids for Solid-Phase Synthesis of Defined Polyamidoamines. *Org. Lett.* **2011**, *13* (7), 1586-1589.
(136) Boussif, O.; Lezoualc'h, F.; Zanta, M. A.; Mergny, M. D.; Scherman, D.; Demeneix, B.; Behr, J.-P. A versatile vector for gene and oligonucleotide transfer into cells in culture and *in vivo*: polyethylenimine. *Proc. Natl. Acad. Sci. U.S.A.* **1995**, *92* (16), 7297-7301.
(137) Kaiser, E.; Colescott, R. L.; Bossinger, C. D.; Cook, P. I. Color test for detection of free terminal amino groups in the solid-phase synthesis of peptides. *Anal. Biochem.* **1970**, *34* (2), 595-598.
(138) Tsigelny, I. F. Artificial intelligence in drug combination therapy. *Brief Bioinform.* **2019**, *20* (4), 1434-1448.
(139) Jia, J.; Zhu, F.; Ma, X.; Cao, Z.; Cao, Z. W.; Li, Y.; Li, Y. X.; Chen, Y. Z. Mechanisms of drug combinations: interaction and network perspectives. *Nat. Rev. Drug Discov.* **2009**, *8* (2), 111-128.
(140) McGuire, J. J.; Mini, E.; Hsieh, P.; Bertino, J. R. Role of methotrexate polyglutamates in methotrexate- and sequential methotrexate-5-fluorouracil-mediated cell kill. *Cancer Res.* **1985**, *45* (12 Pt 1), 6395-6400.
(141) Truebenbach, I.; Gorges, J.; Kuhn, J.; Kern, S.; Baratti, E.; Kazmaier, U.; Wagner, E.; Lachelt, U. Sequence-Defined Oligoamide Drug Conjugates of Pretubulysin and Methotrexate for Folate Receptor Targeted Cancer Therapy. *Macromol. Biosci.* **2017**, *17* (10), 1600520.
(142) Wu, C.; Leroux, J. C.; Gauthier, M. A. Twin disulfides for orthogonal disulfide pairing and the directed folding of multicyclic peptides. *Nat. Chem.* **2012**, *4* (12), 1044-1049.
(143) Schaffert, D.; Troiber, C.; Salcher, E. E.; Fröhlich, T.; Martin, I.; Badgujar, N.; Dohmen, C.; Edinger, D.; Kläger, R.; Maiwald, G.; et al. Festphasen-basierte Synthese sequenzdefinierter T-, i- und U-Form-Polymere für den pDNA- und siRNA-Transfer. *Angew. Chem. Int. Ed.* **2011**, *123* (38), 9149-9152.
(144) Gu, X.; Wei, Y.; Fan, Q.; Sun, H.; Cheng, R.; Zhong, Z.; Deng, C. cRGD-decorated biodegradable polytyrosine nanoparticles for robust encapsulation and targeted delivery of doxorubicin to colorectal cancer *in vivo*. *J. Control. Release* **2019**, *301*, 110-118.
(145) Liu, D.; Huang, L.; Moore, M. A.; Anantharamaiah, G. M.; Segrest, J. P. Interactions of serum proteins with small unilamellar liposomes composed of dioleoylphosphatidylethanolamine and oleic acid: high-density lipoprotein, apolipoprotein A1, and amphipathic peptides stabilize liposomes 399. *Biochemistry* **1990**, *29*, 3637-3643.
(146) Goldstein, D. B. The effects of drugs on membrane fluidity 240. *Annu. Rev. Pharmacol. Toxicol.* **1984**, *24*, 43-64.
(147) Subbarao, N. K.; Fielding, C. J.; Hamilton, R. L.; Szoka, F. C., Jr. Lecithin:cholesterol acyltransferase activation by synthetic amphipathic peptides. *Proteins* **1988**, *3* (3), 187-198.
(148) Kulkarni, J. A.; Witzigmann, D.; Leung, J.; Tam, Y. Y. C.; Cullis, P. R. On the role of helper lipids in lipid nanoparticle formulations of siRNA. *Nanoscale* **2019**, *11* (45), 21733-21739.
(149) Lechanteur, A.; Sanna, V.; Duchemin, A.; Evrard, B.; Mottet, D.; Piel, G. Cationic Liposomes Carrying siRNA: Impact of Lipid Composition on Physicochemical Properties, Cytotoxicity and Endosomal Escape. *Nanomaterials (Basel)* **2018**, *8* (5), 270.
(150) Zhang, P.; Steinborn, B.; Lachelt, U.; Zahler, S.; Wagner, E. Lipo-Oligomer Nanoformulations for Targeted Intracellular Protein Delivery. *Biomacromolecules* **2017**, *18* (8), 2509-2520.

(151) Kang, H.; Rho, S.; Stiles, W. R.; Hu, S.; Baek, Y.; Hwang, D. W.; Kashiwagi, S.; Kim, M. S.; Choi, H. S. Size-Dependent EPR Effect of Polymeric Nanoparticles on Tumor Targeting. *Ad.v Healthc. Mater.* **2020**, *9* (1), e1901223.
(152) De Smedt, S. C.; Demeester, J.; Hennink, W. E. Cationic polymer based gene delivery systems. *Pharm. Res.* **2000**, *17* (2), 113-126.
(153) Duncan R, Dimitrijevic S, Evagorou E G. The role of polymer conjugates in the diagnosis and treatment of cancer[J]. *S.T.P. Pharma. Prat.* **1996**, *6*(4): 237-263.
(154) Duncan, R. The dawning era of polymer therapeutics. *Nat. Rev. Drug Discov.* **2003**, *2* (5), 347-360.
(155) Zhang, P.; Wagner, E. History of polymeric gene delivery systems. *Polymeric Gene Delivery Systems* **2017**, 1-39.
(156) Kwok, A.; Hart, S. L. Comparative structural and functional studies of nanoparticle formulations for DNA and siRNA delivery. *Nanomed.: Nanotechnol. Biol. Med.* **2011**, *7* (2), 210-219.
(157) Scholz, C.; Wagner, E. Therapeutic plasmid DNA versus siRNA delivery: common and different tasks for synthetic carriers. *J. Control. Release* **2012**, *161* (2), 554-565.
(158) Remaut, K.; Symens, N.; Lucas, B.; Demeester, J.; De Smedt, S. Cell division responsive peptides for optimized plasmid DNA delivery: the mitotic window of opportunity? *J. Control. Release* **2014**, *179*, 1-9.
(159) Goncalves, C.; Akhter, S.; Pichon, C.; Midoux, P. Intracellular availability of pDNA and mRNA after transfection: A comparative study among polyplexes, lipoplexes, and lipopolyplexes. *Mol. Pharm.* **2016**, *13* (9), 3153-3163.
(160) Hall, A.; Lächelt, U.; Bartek, J.; Wagner, E.; Moghimi, S. M. Polyplex evolution: understanding biology, optimizing performance. *Mol. Ther.* **2017**, *25* (7), 1476-1490.
(161) Kauffman, A. C.; Piotrowski-Daspit, A. S.; Nakazawa, K. H.; Jiang, Y.; Datye, A.; Saltzman, W. M. Tunability of biodegradable poly (amine-co-ester) polymers for customized nucleic acid delivery and other biomedical applications. *Biomacromolecules* **2018**, *19* (9), 3861-3873.
(162) Blakney, A. K.; Yilmaz, G.; McKay, P. F.; Becer, C. R.; Shattock, R. J. One size does not fit all: the effect of chain length and charge density of poly (ethylene imine) based copolymers on delivery of pDNA, mRNA, and RepRNA polyplexes. *Biomacromolecules* **2018**, *19* (7), 2870-2879.
(163) Andersen, H.; Parhamifar, L.; Hunter, A. C.; Shahin, V.; Moghimi, S. M. AFM visualization of sub-50 nm polyplex disposition to the nuclear pore complex without compromising the integrity of the nuclear envelope. *J. Control. Release* **2016**, *244*, 24-29.
(164) Levacic, A. K.; Morys, S.; Kempter, S.; Lächelt, U.; Wagner, E. Minicircle versus plasmid DNA delivery by receptor-targeted polyplexes. *Hum. Gene Ther.* **2017**, *28* (10), 862-874.
(165) Neu, M.; Germershaus, O.; Behe, M.; Kissel, T. Bioreversibly crosslinked polyplexes of PEI and high molecular weight PEG show extended circulation times *in vivo*. *J. Control. Release* **2007**, *124* (1-2), 69-80.
(166) Burke, R. S.; Pun, S. H. Extracellular barriers to *in vivo* PEI and PEGylated PEI polyplex-mediated gene delivery to the liver. *Bioconjugate chemistry* **2008**, *19* (3), 693-704.
(167) Hama, S.; Akita, H.; Ito, R.; Mizuguchi, H.; Hayakawa, T.; Harashima, H. Quantitative comparison of intracellular trafficking and nuclear transcription between adenoviral and lipoplex systems. *Mol. Ther.* **2006**, *13* (4), 786-794.
(168) Wightman, L.; Kircheis, R.; Rössler, V.; Carotta, S.; Ruzicka, R.; Kursa, M.; Wagner, E. Different behavior of branched and linear polyethylenimine for gene delivery *in vitro* and *in vivo*. *J. Gene Med.* **2001**, *3* (4), 362-372.
(169) Brunner, S.; Fürtbauer, E.; Sauer, T.; Kursa, M.; Wagner, E. Overcoming the nuclear barrier: cell cycle independent nonviral gene transfer with linear polyethylenimine or electroporation. *Mol. Ther.* **2002**, *5* (1), 80-86.
(170) Itaka, K.; Harada, A.; Yamasaki, Y.; Nakamura, K.; Kawaguchi, H.; Kataoka, K. In situ

single cell observation by fluorescence resonance energy transfer reveals fast intra‐cytoplasmic delivery and easy release of plasmid DNA complexed with linear polyethylenimine. *J. Gene Med.* **2004**, *6* (1), 76-84.
(171) Bishop, C. J.; Majewski, R. L.; Guiriba, T.-R. M.; Wilson, D. R.; Bhise, N. S.; Quiñones-Hinojosa, A.; Green, J. J. Quantification of cellular and nuclear uptake rates of polymeric gene delivery nanoparticles and DNA plasmids via flow cytometry. *Acta Biomater.* **2016**, *37*, 120-130.
(172) Christensen, M. D.; Nitiyanandan, R.; Meraji, S.; Daer, R.; Godeshala, S.; Goklany, S.; Haynes, K.; Rege, K. An inhibitor screen identifies histone-modifying enzymes as mediators of polymer-mediated transgene expression from plasmid DNA. *J. Control. Release* **2018**, *286*, 210-223.
(173) Takeda, K. M.; Osada, K.; Tockary, T. A.; Dirisala, A.; Chen, Q.; Kataoka, K. Poly (ethylene glycol) crowding as critical factor to determine pDNA packaging scheme into polyplex micelles for enhanced gene expression. *Biomacromolecules* **2017**, *18* (1), 36-43.
(174) Urnauer, S.; Morys, S.; Levacic, A. K.; Müller, A. M.; Schug, C.; Schmohl, K. A.; Schwenk, N.; Zach, C.; Carlsen, J.; Bartenstein, P. Sequence-defined cMET/HGFR-targeted polymers as gene delivery vehicles for the theranostic sodium iodide symporter (NIS) gene. *Mol. Ther.* **2016**, *24* (8), 1395-1404.
(175) Cheng, Y.; Sellers, D. L.; Tan, J.-K. Y.; Peeler, D. J.; Horner, P. J.; Pun, S. H. Development of switchable polymers to address the dilemma of stability and cargo release in polycationic nucleic acid carriers. *Biomaterials* **2017**, *127*, 89-96.
(176) Birnstiel, M. Coupling of adenovirus to transferrin-polylysine. *DNA* **1992**.
(177) Plank, C.; Oberhauser, B.; Mechtler, K.; Koch, C.; Wagner, E. The influence of endosome-disruptive peptides on gene transfer using synthetic virus-like gene transfer systems. *J. Biol. Chem.* **1994**, *269* (17), 12918-12924.
(178) Kichler, A.; Leborgne, C.; März, J.; Danos, O.; Bechinger, B. Histidine-rich amphipathic peptide antibiotics promote efficient delivery of DNA into mammalian cells. *Proc. Natl. Acad. Sci. U.S.A.* **2003**, *100* (4), 1564-1568.
(179) Boeckle, S.; Fahrmeir, J.; Roedl, W.; Ogris, M.; Wagner, E. Melittin analogs with high lytic activity at endosomal pH enhance transfection with purified targeted PEI polyplexes. *J. Control. Release* **2006**, *112* (2), 240-248.
(180) Douat, C.; Aisenbrey, C.; Antunes, S.; Decossas, M.; Lambert, O.; Bechinger, B.; Kichler, A.; Guichard, G. A Cell-Penetrating Foldamer with a Bioreducible Linkage for Intracellular Delivery of DNA. *Angew. Chem. Int. Ed.* **2015**, *54* (38), 11133-11137.
(181) Douat, C.; Bornerie, M.; Antunes, S.; Guichard, G.; Kichler, A. Hybrid cell-penetrating foldamer with superior intracellular delivery properties and serum stability. *Bioconjug. Chem.* **2019**, *30* (4), 1133-1139.
(182) Trützschler, A.-K.; Bus, T.; Reifarth, M.; Brendel, J. C.; Hoeppener, S.; Traeger, A.; Schubert, U. S. Beyond gene transfection with methacrylate-based polyplexes—the influence of the amino substitution pattern. *Bioconjug. Chem.* **2018**, *29* (7), 2181-2194.
(183) Heller, P.; Hobernik, D.; Lächelt, U.; Schinnerer, M.; Weber, B.; Schmidt, M.; Wagner, E.; Bros, M.; Barz, M. Combining reactive triblock copolymers with functional cross-linkers: A versatile pathway to disulfide stabilized-polyplex libraries and their application as pDNA vaccines. *J. Control. Release* **2017**, *258*, 146-160.
(184) Wilson, D. R.; Rui, Y.; Siddiq, K.; Routkevitch, D.; Green, J. J. Differentially branched ester amine quadpolymers with amphiphilic and pH-sensitive properties for efficient plasmid DNA delivery. *Mol. Pharm.* **2019**, *16* (2), 655-668.
(185) Sato, T.; Nakata, M.; Yang, Z.; Torizuka, Y.; Kishimoto, S.; Ishihara, M. *In vitro* and *in vivo* gene delivery using chitosan/hyaluronic acid nanoparticles: Influences of molecular mass of hyaluronic acid and lyophilization on transfection efficiency. *J. Gene Med.* **2017**, *19* (8), e2968.
(186) Caballero, I.; Riou, M.; Hacquin, O.; Chevaleyre, C.; Barc, C.; Pezant, J.; Pinard, A.; Fassy, J.; Rezzonico, R.; Mari, B. Tetrafunctional block copolymers promote lung gene

transfer in newborn piglets. *Molecular Therapy-Nucleic Acids* **2019**, *16*, 186-193.
(187) Kowalski, P. S.; Rudra, A.; Miao, L.; Anderson, D. G. Delivering the Messenger: Advances in Technologies for Therapeutic mRNA Delivery. *Mol Ther* **2019**, *27* (4), 710-728.
(188) Kranz, L. M.; Diken, M.; Haas, H.; Kreiter, S.; Loquai, C.; Reuter, K. C.; Meng, M.; Fritz, D.; Vascotto, F.; Hefesha, H.; et al. Systemic RNA delivery to dendritic cells exploits antiviral defence for cancer immunotherapy. *Nature* **2016**, *534* (7607), 396-401.
(189) Bhosle, S. M.; Loomis, K. H.; Kirschman, J. L.; Blanchard, E. L.; Vanover, D. A.; Zurla, C.; Habrant, D.; Edwards, D.; Baumhof, P.; Pitard, B.; et al. Unifying *in vitro* and *in vivo* IVT mRNA expression discrepancies in skeletal muscle via mechanotransduction. *Biomaterials* **2018**, *159*, 189-203.
(190) Kormann, M. S.; Hasenpusch, G.; Aneja, M. K.; Nica, G.; Flemmer, A. W.; Herber-Jonat, S.; Huppmann, M.; Mays, L. E.; Illenyi, M.; Schams, A.; et al. Expression of therapeutic proteins after delivery of chemically modified mRNA in mice. *Nat. Biotechnol.* **2011**, *29* (2), 154-157.
(191) Jarzebinska, A.; Pasewald, T.; Lambrecht, J.; Mykhaylyk, O.; Kummerling, L.; Beck, P.; Hasenpusch, G.; Rudolph, C.; Plank, C.; Dohmen, C. A Single Methylene Group in Oligoalkylamine-Based Cationic Polymers and Lipids Promotes Enhanced mRNA Delivery. *Angew. Chem. Int. Ed.* **2016**, *55* (33), 9591-9595.
(192) Nuhn, L.; Kaps, L.; Diken, M.; Schuppan, D.; Zentel, R. Reductive Decationizable Block Copolymers for Stimuli-Responsive mRNA Delivery. *Macromol. Rapid Commun.* **2016**, *37* (11), 924-933.
(193) Kaczmarek, J. C.; Patel, A. K.; Kauffman, K. J.; Fenton, O. S.; Webber, M. J.; Heartlein, M. W.; DeRosa, F.; Anderson, D. G. Polymer-Lipid Nanoparticles for Systemic Delivery of mRNA to the Lungs. *Angew. Chem. Int. Ed.* **2016**, *55* (44), 13808-13812.
(194) Kaczmarek, J. C.; Kauffman, K. J.; Fenton, O. S.; Sadtler, K.; Patel, A. K.; Heartlein, M. W.; DeRosa, F.; Anderson, D. G. Optimization of a Degradable Polymer-Lipid Nanoparticle for Potent Systemic Delivery of mRNA to the Lung Endothelium and Immune Cells. *Nano Lett.* **2018**, *18* (10), 6449-6454.
(195) Yan, Y.; Xiong, H.; Zhang, X.; Cheng, Q.; Siegwart, D. J. Systemic mRNA Delivery to the Lungs by Functional Polyester-based Carriers. *Biomacromolecules* **2017**, *18* (12), 4307-4315.
(196) Kowalski, P. S.; Capasso Palmiero, U.; Huang, Y.; Rudra, A.; Langer, R.; Anderson, D. G. Ionizable Amino-Polyesters Synthesized via Ring Opening Polymerization of Tertiary Amino-Alcohols for Tissue Selective mRNA Delivery. *Adv. Mater.* **2018**, e1801151.
(197) Chen, Q.; Qi, R.; Chen, X.; Yang, X.; Wu, S.; Xiao, H.; Dong, W. A Targeted and Stable Polymeric Nanoformulation Enhances Systemic Delivery of mRNA to Tumors. *Mol. Ther.* **2017**, *25* (1), 92-101.
(198) McKinlay, C. J.; Vargas, J. R.; Blake, T. R.; Hardy, J. W.; Kanada, M.; Contag, C. H.; Wender, P. A.; Waymouth, R. M. Charge-altering releasable transporters (CARTs) for the delivery and release of mRNA in living animals. *Proc. Natl. Acad. Sci. U.S.A.* **2017**, *114* (4), E448-E456.
(199) McKinlay, C. J.; Benner, N. L.; Haabeth, O. A.; Waymouth, R. M.; Wender, P. A. Enhanced mRNA delivery into lymphocytes enabled by lipid-varied libraries of charge-altering releasable transporters. *Proc. Natl. Acad. Sci. U.S.A.* **2018**, *115* (26), E5859-E5866.
(200) Haabeth, O. A. W.; Blake, T. R.; McKinlay, C. J.; Tveita, A. A.; Sallets, A.; Waymouth, R. M.; Wender, P. A.; Levy, R. Local Delivery of Ox40l, Cd80, and Cd86 mRNA Kindles Global Anticancer Immunity. *Cancer Res.* **2019**, *79* (7), 1624-1634.
(201) Benner, N. L.; Near, K. E.; Bachmann, M. H.; Contag, C. H.; Waymouth, R. M.; Wender, P. A. Functional DNA Delivery Enabled by Lipid-Modified Charge-Altering Releasable Transporters (CARTs). *Biomacromolecules* **2018**, *19* (7), 2812-2824.
(202) Adams, D.; Gonzalez-Duarte, A.; O'Riordan, W. D.; Yang, C.-C.; Ueda, M.; Kristen, A. V.; Tournev, I.; Schmidt, H. H.; Coelho, T.; Berk, J. L.; et al. Patisiran, an RNAi Therapeutic, for Hereditary Transthyretin Amyloidosis. *N. Engl. J. Med.* **2018**, *379* (1), 11-

21.
(203) Rozema, D. B.; Lewis, D. L.; Wakefield, D. H.; Wong, S. C.; Klein, J. J.; Roesch, P. L.; Bertin, S. L.; Reppen, T. W.; Chu, Q.; Blokhin, A. V.; et al. Dynamic PolyConjugates for targeted *in vivo* delivery of siRNA to hepatocytes. *Proc. Natl. Acad. Sci. U.S.A.* **2007**, *104* (32), 12982-12987.
(204) Gao, K.; Huang, L. Nonviral methods for siRNA delivery. *Mol. Pharm.* **2009**, *6* (3), 651-658.
(205) Nair, J. K.; Attarwala, H.; Sehgal, A.; Wang, Q.; Aluri, K.; Zhang, X.; Gao, M.; Liu, J.; Indrakanti, R.; Schofield, S.; et al. Impact of enhanced metabolic stability on pharmacokinetics and pharmacodynamics of GalNAc-siRNA conjugates. *Nucleic Acids Res.* **2017**, *45* (19), 10969-10977.
(206) Foster, D. J.; Brown, C. R.; Shaikh, S.; Trapp, C.; Schlegel, M. K.; Qian, K.; Sehgal, A.; Rajeev, K. G.; Jadhav, V.; Manoharan, M.; et al. Advanced siRNA Designs Further Improve *In Vivo* Performance of GalNAc-siRNA Conjugates. *Mol. Ther.* **2018**, *26* (3), 708-717.
(207) Chen, C.; Posocco, P.; Liu, X.; Cheng, Q.; Laurini, E.; Zhou, J.; Liu, C.; Wang, Y.; Tang, J.; Col, V. D.; et al. Mastering Dendrimer Self-Assembly for Efficient siRNA Delivery: From Conceptual Design to *In Vivo* Efficient Gene Silencing. *Small* **2016**, *12* (27), 3667-3676.
(208) Feldmann, D. P.; Cheng, Y.; Kandil, R.; Xie, Y.; Mohammadi, M.; Harz, H.; Sharma, A.; Peeler, D. J.; Moszczynska, A.; Leonhardt, H.; et al. *In vitro* and *in vivo* delivery of siRNA via VIPER polymer system to lung cells. *J. Control. Release* **2018**, *276*, 50-58.
(209) Chiper, M.; Tounsi, N.; Kole, R.; Kichler, A.; Zuber, G. Self-aggregating 1.8kDa polyethylenimines with dissolution switch at endosomal acidic pH are delivery carriers for plasmid DNA, mRNA, siRNA and exon-skipping oligonucleotides. *J. Control. Release* **2017**, *246*, 60-70.
(210) Creusat G, R. A., Weiss E, Elbaghdadi R, Remy JS, Mulherkar R, Zuber G. Proton Sponge Trick for pH-Sensitive Disassembly of Polyethylenimine-Based siRNA Delivery Systems. *Bioconjug. Chem.* **2010**, *21* (5), 994–1002.
(211) Creusat, G.; Thomann, J. S.; Maglott, A.; Pons, B.; Dontenwill, M.; Guerin, E.; Frisch, B.; Zuber, G. Pyridylthiourea-grafted polyethylenimine offers an effective assistance to siRNA-mediated gene silencing *in vitro* and *in vivo*. *J. Control. Release* **2012**, *157* (3), 418-426.
(212) Ewe, A.; Przybylski, S.; Burkhardt, J.; Janke, A.; Appelhans, D.; Aigner, A. A novel tyrosine-modified low molecular weight polyethylenimine (P10Y) for efficient siRNA delivery *in vitro* and *in vivo*. *J. Control. Release* **2016**, *230*, 13-25.
(213) Troiber, C.; Edinger, D.; Kos, P.; Schreiner, L.; Klager, R.; Herrmann, A.; Wagner, E. Stabilizing effect of tyrosine trimers on pDNA and siRNA polyplexes. *Biomaterials* **2013**, *34* (5), 1624-1633.
(214) Lee, D. J.; Kessel, E.; Lehto, T.; Liu, X.; Yoshinaga, N.; Padari, K.; Chen, Y. C.; Kempter, S.; Uchida, S.; Radler, J. O.; et al. Systemic Delivery of Folate-PEG siRNA Lipopolyplexes with Enhanced Intracellular Stability for *In Vivo* Gene Silencing in Leukemia. *Bioconjug. Chem.* **2017**, *28* (9), 2393-2409.
(215) Wu, C.; Li, J.; Wang, W.; Hammond, P. T. Rationally Designed Polycationic Carriers for Potent Polymeric siRNA-Mediated Gene Silencing. *ACS Nano* **2018**, *12* (7), 6504-6514.
(216) Ding, F.; Mou, Q.; Ma, Y.; Pan, G.; Guo, Y.; Tong, G.; Choi, C. H. J.; Zhu, X.; Zhang, C. A Crosslinked Nucleic Acid Nanogel for Effective siRNA Delivery and Antitumor Therapy. *Angew. Chem. Int. Ed.* **2018**, *57* (12), 3064-3068.
(217) An, S.; He, D.; Wagner, E.; Jiang, C. Peptide-like Polymers Exerting Effective Glioma-Targeted siRNA Delivery and Release for Therapeutic Application. *Small* **2015**, *11* (38), 5142-5150.
(218) Shi, Y.; Jiang, Y.; Cao, J.; Yang, W.; Zhang, J.; Meng, F.; Zhong, Z. Boosting RNAi therapy for orthotopic glioblastoma with nontoxic brain-targeting chimaeric polymersomes.

J. Control. Release **2018**, *292*, 163-171.
(219) Luo, J.; Höhn, M.; Reinhard, S.; Loy, D. M.; Klein, P. M.; Wagner, E. IL4-Receptor-Targeted Dual Antitumoral Apoptotic Peptide—siRNA Conjugate Lipoplexes. *Adv. Funct. Mater.* **2019**, *29* (25), 1900697.
(220) Krutzfeldt, J.; Rajewsky, N.; Braich, R.; Rajeev, K. G.; Tuschl, T.; Manoharan, M.; Stoffel, M. Silencing of microRNAs *in vivo* with 'antagomirs'. *Nature* **2005**, *438* (7068), 685-689.
(221) Wagner, E. Tumor-targeted Delivery of Anti-microRNA for Cancer Therapy: pHLIP is Key. *Angew. Chem. Int. Ed.* **2015**, *54* (20), 5824-5826.
(222) Ibrahim, A. F.; Weirauch, U.; Thomas, M.; Grunweller, A.; Hartmann, R. K.; Aigner, A. MicroRNA replacement therapy for miR-145 and miR-33a is efficacious in a model of colon carcinoma. *Cancer Res.* **2011**, *71* (15), 5214-5224.
(223) Lopez-Bertoni, H.; Kozielski, K. L.; Rui, Y.; Lal, B.; Vaughan, H.; Wilson, D. R.; Mihelson, N.; Eberhart, C. G.; Laterra, J.; Green, J. J. Bioreducible Polymeric Nanoparticles Containing Multiplexed Cancer Stem Cell Regulating miRNAs Inhibit Glioblastoma Growth and Prolong Survival. *Nano Letters* **2018**, *18* (7), 4086-4094.
(224) Paidikondala, M.; Rangasami, V. K.; Nawale, G. N.; Casalini, T.; Perale, G.; Kadekar, S.; Mohanty, G.; Salminen, T.; Oommen, O. P.; Varghese, O. P. An Unexpected Role of Hyaluronic Acid in Trafficking siRNA Across the Cellular Barrier: The First Biomimetic, Anionic, Non-Viral Transfection Method. *Angew. Chem. Int. Ed.* **2019**, *58* (9), 2815-2819.
(225) Zhang, Z.; Wan, T.; Chen, Y.; Chen, Y.; Sun, H.; Cao, T.; Songyang, Z.; Tang, G.; Wu, C.; Ping, Y.; et al. Cationic Polymer-Mediated CRISPR/Cas9 Plasmid Delivery for Genome Editing. *Macromol. Rapid Commun.* **2019**, *40* (5), e1800068.
(226) Zhang, H. X.; Zhang, Y.; Yin, H. Genome Editing with mRNA Encoding ZFN, TALEN, and Cas9. *Mol. Ther.* **2019**, *27* (4), 735-746.
(227) Sun, W.; Ji, W.; Hall, J. M.; Hu, Q.; Wang, C.; Beisel, C. L.; Gu, Z. Self-assembled DNA nanoclews for the efficient delivery of CRISPR-Cas9 for genome editing. *Angew. Chem. Int. Ed.* **2015**, *54* (41), 12029-12033.
(228) Kang, Y. K.; Kwon, K.; Ryu, J. S.; Lee, H. N.; Park, C.; Chung, H. J. Nonviral Genome Editing Based on a Polymer-Derivatized CRISPR Nanocomplex for Targeting Bacterial Pathogens and Antibiotic Resistance. *Bioconjug. Chem.* **2017**, *28* (4), 957-967.
(229) Rui, Y.; Wilson, D. R.; Sanders, K.; Green, J. J. Reducible Branched Ester-Amine Quadpolymers (rBEAQs) Codelivering Plasmid DNA and RNA Oligonucleotides Enable CRISPR/Cas9 Genome Editing. *ACS Appl. Mater. Interfaces* **2019**, *11* (11), 10472-10480.
(230) Miller, J. B.; Zhang, S.; Kos, P.; Xiong, H.; Zhou, K.; Perelman, S. S.; Zhu, H.; Siegwart, D. J. Non-Viral CRISPR/Cas Gene Editing *In vitro* and *In Vivo* Enabled by Synthetic Nanoparticle Co-Delivery of Cas9 mRNA and sgRNA. *Angew. Chem. Int. Ed.* **2017**, *56* (4), 1059-1063.
(231) Liu, C.; Wan, T.; Wang, H.; Zhang, S.; Ping, Y.; Cheng, Y. A boronic acid–rich dendrimer with robust and unprecedented efficiency for cytosolic protein delivery and CRISPR-Cas9 gene editing. *Sci. Adv.* **2019**, *5* (6), eaaw8922.
(232) Ginn, S. L.; Amaya, A. K.; Alexander, I. E.; Edelstein, M.; Abedi, M. R. Gene therapy clinical trials worldwide to 2017: An update. *J. Gene. Med.* **2018**, *20* (5), e3015.
(233) Wittrup, A.; Lieberman, J. Knocking down disease: a progress report on siRNA therapeutics. *Nat. Rev. Genet.* **2015**, *16* (9), 543-552.
(234) Oupický, D.; Diwadkar, V. Stimuli-responsive gene delivery vectors. *Curr. Opin. Mol. Ther.* **2003**, *5* (4), 345-350.
(235) Wagner, E. Programmed drug delivery: nanosystems for tumor targeting. *Expert Opin. Biol. Ther.* **2007**, *7* (5), 587-593.
(236) Sun, M.; Wang, K.; Oupicky, D. Advances in Stimulus-Responsive Polymeric Materials for Systemic Delivery of Nucleic Acids. *Adv. Healthc. Mater.* **2018**, *7* (4), 1701070.
(237) Hager, S.; Wagner, E. Bioresponsive polyplexes – chemically programmed for nucleic acid delivery. *Expert Opin. Drug Deliv.* **2018**, *15* (11), 1067-1083.

(238) Yu, C.; Qian, L.; Uttamchandani, M.; Li, L.; Yao, S. Q. Single-Vehicular Delivery of Antagomir and Small Molecules to Inhibit miR-122 Function in Hepatocellular Carcinoma Cells by using "Smart" Mesoporous Silica Nanoparticles. *Angew. Chem. Int. Ed.* **2015**, *54* (36), 10574-10578.
(239) Klein, P. M.; Reinhard, S.; Lee, D. J.; Muller, K.; Ponader, D.; Hartmann, L.; Wagner, E. Precise redox-sensitive cleavage sites for improved bioactivity of siRNA lipopolyplexes. *Nanoscale* **2016**, *8* (42), 18098-18104.
(240) Reinhard, S.; Wang, Y.; Dengler, S.; Wagner, E. Precise Enzymatic Cleavage Sites for Improved Bioactivity of siRNA Lipo-Polyplexes. *Bioconjug. Chem.* **2018**, *29* (11), 3649-3657.
(241) Das, D. K.; Govindan, R.; Nikic-Spiegel, I.; Krammer, F.; Lemke, E. A.; Munro, J. B. Direct Visualization of the Conformational Dynamics of Single Influenza Hemagglutinin Trimers. *Cell* **2018**, *174* (4), 926-937 e912.
(242) Carr, C. M.; Kim, P. S. A spring-loaded mechanism for the conformational change of influenza hemagglutinin. *Cell* **1993**, *73* (4), 823-832.
(243) Luo, T.; Liang, H.; Jin, R.; Nie, Y. Virus-inspired and mimetic designs in non-viral gene delivery. *J. Gene Med.* **2019**, *21* (7), e3090.
(244) Wagner, E. Strategies to Improve DNA Polyplexes for *in Vivo* Gene Transfer: Will “Artificial Viruses” Be the Answer? *Pharm. Res.* **2004**, *21* (1), 8-14.
(245) Berg, K.; Folini, M.; Prasmickaite, L.; Selbo, K. P.; Bonsted, A.; Engesaeter, O. B.; Zaffaroni, N.; Weyergang, A.; Dietzea, A.; Maelandsmo, M. G.; et al. Photochemical Internalization: A New Tool for Drug Delivery. *Curr. Pharm. Biotechnol.* **2007**, *8* (6), 362-372.
(246) Plank, C.; Zelphati, O.; Mykhaylyk, O. Magnetically enhanced nucleic acid delivery. Ten years of magnetofection-progress and prospects. *Adv. Drug. Deliv. Rev.* **2011**, *63* (14-15), 1300-1331.
(247) De Cock, I.; Zagato, E.; Braeckmans, K.; Luan, Y.; de Jong, N.; De Smedt, S. C.; Lentacker, I. Ultrasound and microbubble mediated drug delivery: Acoustic pressure as determinant for uptake via membrane pores or endocytosis. *J. Control. Release* **2015**, *197*, 20-28.
(248) Maier, C. M.; Huergo, M. A.; Milosevic, S.; Pernpeintner, C.; Li, M.; Singh, D. P.; Walker, D.; Fischer, P.; Feldmann, J.; Lohmuller, T. Optical and Thermophoretic Control of Janus Nanopen Injection into Living Cells. *Nano Lett.* **2018**, *18* (12), 7935-7941.
(249) Chen, W.; Glackin, C. A.; Horwitz, M. A.; Zink, J. I. Nanomachines and Other Caps on Mesoporous Silica Nanoparticles for Drug Delivery. *Acc. Chem. Res.* **2019**, *52* (6), 1531-1542.
(250) Liu, D.; Garcia-Lopez, V.; Gunasekera, R. S.; Greer Nilewski, L.; Alemany, L. B.; Aliyan, A.; Jin, T.; Wang, G.; Tour, J. M.; Pal, R. Near-Infrared Light Activates Molecular Nanomachines to Drill into and Kill Cells. *ACS Nano* **2019**, *13* (6), 6813-6823.
(251) Lu, X.; Shen, H.; Zhao, K.; Wang, Z.; Peng, H.; Liu, W. Micro-/Nanomachines Driven by Ultrasonic Power Sources. *Chem. Asian J.* **2019**, *14* (14), 2406-2416.
(252) Scholz, C.; Kos, P.; Leclercq, L.; Jin, X.; Cottet, H.; Wagner, E. Correlation of length of linear oligo(ethanamino) amides with gene transfer and cytotoxicity. *ChemMedChem* **2014**, *9* (9), 2104-2110.
(253) Paunovska, K.; Sago, C. D.; Monaco, C. M.; Hudson, W. H.; Castro, M. G.; Rudoltz, T. G.; Kalathoor, S.; Vanover, D. A.; Santangelo, P. J.; Ahmed, R.; et al. A Direct Comparison of *in vitro* and *in Vivo* Nucleic Acid Delivery Mediated by Hundreds of Nanoparticles Reveals a Weak Correlation. *Nano Lett.* **2018**, *18* (3), 2148-2157.
(254) Paunovska, K.; Da Silva Sanchez, A. J.; Sago, C. D.; Gan, Z.; Lokugamage, M. P.; Islam, F. Z.; Kalathoor, S.; Krupczak, B. R.; Dahlman, J. E. Nanoparticles Containing Oxidized Cholesterol Deliver mRNA to the Liver Microenvironment at Clinically Relevant Doses. *Adv. Mater.* **2019**, *31* (14), e1807748.
(255) Moller, K.; Muller, K.; Engelke, H.; Brauchle, C.; Wagner, E.; Bein, T. Highly efficient

siRNA delivery from core-shell mesoporous silica nanoparticles with multifunctional polymer caps. *Nanoscale* **2016**, *8* (7), 4007-4019.
(256) Timin, A. S.; Muslimov, A. R.; Lepik, K. V.; Epifanovskaya, O. S.; Shakirova, A. I.; Mock, U.; Riecken, K.; Okilova, M. V.; Sergeev, V. S.; Afanasyev, B. V.; et al. Efficient gene editing via non-viral delivery of CRISPR-Cas9 system using polymeric and hybrid microcarriers. *Nanomedicine* **2018**, *14* (1), 97-108.
(257) Kim, H. S.; Son, Y. J.; Mao, W.; Leong, K. W.; Yoo, H. S. Atom Transfer Radical Polymerization of Multishelled Cationic Corona for the Systemic Delivery of siRNA. *Nano Lett.* **2018**, *18* (1), 314-325.
(258) Yi, Y.; Kim, H. J.; Zheng, M.; Mi, P.; Naito, M.; Kim, B. S.; Min, H. S.; Hayashi, K.; Perche, F.; Toh, K.; et al. Glucose-linked sub-50-nm unimer polyion complex-assembled gold nanoparticles for targeted siRNA delivery to glucose transporter 1-overexpressing breast cancer stem-like cells. *J. Control. Release* **2019**, *295*, 268-277.
(259) Friedmann, T.; Roblin, R. Gene Therapy for Human Genetic Disease? Proposals for genetic manipulation in humans raise difficult scientific and ethical problems. *Science* **1972**, *175* (4025), 949-955.
(260) Cavazzana, M.; Six, E.; Lagresle-Peyrou, C.; André-Schmutz, I.; Hacein-Bey-Abina, S. Gene therapy for X-linked severe combined immunodeficiency: where do we stand? *Hum. Gene Ther.* **2016**, *27* (2), 108-116.
(261) Sahin, U.; Kariko, K.; Tureci, O. mRNA-based therapeutics--developing a new class of drugs. *Nat. Rev. Drug Discov.* **2014**, *13* (10), 759-780.
(262) Hajj, K. A.; Whitehead, K. A. Tools for translation: non-viral materials for therapeutic mRNA delivery. *Nat. Rev. Mater.* **2017**, *2* (10), 1-17.
(263) Wadhwa, A.; Aljabbari, A.; Lokras, A.; Foged, C.; Thakur, A. Opportunities and Challenges in the Delivery of mRNA-based Vaccines. *Pharmaceutics* **2020**, *12* (2).
(264) Zeng, C.; Zhang, C.; Walker, P. G.; Dong, Y. Formulation and Delivery Technologies for mRNA Vaccines. *Curr. Top Microbiol. Immunol.* **2020**.
(265) Alameh, M.-G.; Weissman, D.; Pardi, N. Messenger RNA-Based Vaccines Against Infectious Diseases. Springer Berlin Heidelberg, pp 1-35.
(266) Tombacz, I.; Weissman, D.; Pardi, N. Vaccination with messenger RNA: a promising alternative to DNA vaccination. *DNA Vaccines* **2021**, 13-31.
(267) Guevara, M. L.; Persano, F.; Persano, S. Advances in Lipid Nanoparticles for mRNA-Based Cancer Immunotherapy. *Front. Chem.* **2020**, *8*, 589959.
(268) Cheng, Q.; Wei, T.; Farbiak, L.; Johnson, L. T.; Dilliard, S. A.; Siegwart, D. J. Selective organ targeting (SORT) nanoparticles for tissue-specific mRNA delivery and CRISPR-Cas gene editing. *Nat. Nanotechnol.* **2020**, *15* (4), 313-320.
(269) Xiong, Q.; Lee, G. Y.; Ding, J.; Li, W.; Shi, J. Biomedical applications of mRNA nanomedicine. *Nano Res.* **2018**, *11* (10), 5281-5309.
(270) Gebre, M. S.; Brito, L. A.; Tostanoski, L. H.; Edwards, D. K.; Carfi, A.; Barouch, D. H. Novel approaches for vaccine development. *Cell* **2021**, *184* (6), 1589-1603.
(271) Meng, C.; Chen, Z.; Li, G.; Welte, T.; Shen, H. Nanoplatforms for mRNA Therapeutics. *Adv. Ther.* **2020**, *4* (1).
(272) Baden, L. R.; El Sahly, H. M.; Essink, B.; Kotloff, K.; Frey, S.; Novak, R.; Diemert, D.; Spector, S. A.; Rouphael, N.; Creech, C. B.; et al. Efficacy and Safety of the mRNA-1273 SARS-CoV-2 Vaccine. *N. Engl. J. Med.* **2021**, *384* (5), 403-416.
(273) Polack, F. P.; Thomas, S. J.; Kitchin, N.; Absalon, J.; Gurtman, A.; Lockhart, S.; Perez, J. L.; Perez Marc, G.; Moreira, E. D.; Zerbini, C.; et al. Safety and Efficacy of the BNT162b2 mRNA Covid-19 Vaccine. *N. Engl. J. Med.* **2020**, *383* (27), 2603-2615.
(274) Gallops, C.; Ziebarth, J.; Wang, Y. A Polymer Physics Perspective on Why PEI Is an Effective Nonviral Gene Delivery Vector. In *Polymers in Therapeutic Delivery*, ACS Symposium Series, Vol. 1350; American Chemical Society, 2020; pp 1-12.
(275) Bettinger, T.; Carlisle, R. C.; Read, M. L.; Ogris, M.; Seymour, L. W. Peptide-mediated RNA delivery: a novel approach for enhanced transfection of primary and post-mitotic cells.

Nucleic Acids Res. **2001**, *29* (18), 3882-3891.
(276) Hall, A.; Lachelt, U.; Bartek, J.; Wagner, E.; Moghimi, S. M. Polyplex Evolution: Understanding Biology, Optimizing Performance. *Mol. Ther.* **2017**, *25* (7), 1476-1490.
(277) Krhac Levacic, A.; Berger, S.; Muller, J.; Wegner, A.; Lachelt, U.; Dohmen, C.; Rudolph, C.; Wagner, E. Dynamic mRNA polyplexes benefit from bioreducible cleavage sites for *in vitro* and *in vivo* transfer. *J. Control. Release* **2021**, *339*, 27-40.
(278) Yoshinaga, N.; Uchida, S.; Dirisala, A.; Naito, M.; Osada, K.; Cabral, H.; Kataoka, K. mRNA loading into ATP-responsive polyplex micelles with optimal density of phenylboronate ester crosslinking to balance robustness in the biological milieu and intracellular translational efficiency. *J. Control. Release* **2021**, *330*, 317-328.
(279) Cheng, Y.; Yumul, R. C.; Pun, S. H. Virus-Inspired Polymer for Efficient *In vitro* and *In Vivo* Gene Delivery. *Angew. Chem. Int. Ed.* **2016**, *55* (39), 12013-12017.
(280) Baldassi, D.; Ambike, S.; Feuerherd, M.; Cheng, C. C.; Peeler, D. J.; Feldmann, D. P.; Porras-Gonzalez, D. L.; Wei, X.; Keller, L. A.; Kneidinger, N.; et al. Inhibition of SARS-CoV-2 replication in the lung with siRNA/VIPER polyplexes. *J. Control. Release* **2022**, *345*, 661-674.
(281) Reinhard, S.; Zhang, W.; Wagner, E. Optimized Solid-Phase-Assisted Synthesis of Oleic Acid Containing siRNA Nanocarriers. *ChemMedChem* **2017**, *12* (17), 1464-1470.
(282) Berger, S.; Krhac Levacic, A.; Horterer, E.; Wilk, U.; Benli-Hoppe, T.; Wang, Y.; Ozturk, O.; Luo, J.; Wagner, E. Optimizing pDNA Lipo-polyplexes: A Balancing Act between Stability and Cargo Release. *Biomacromolecules* **2021**, *22* (3), 1282-1296.
(283) Alexis, F.; Pridgen, E.; Molnar, L. K.; Farokhzad, O. C. Factors affecting the clearance and biodistribution of polymeric nanoparticles. *Mol. Pharm.* **2008**, *5* (4), 505-515.
(284) Lv, H.; Zhang, S.; Wang, B.; Cui, S.; Yan, J. Toxicity of cationic lipids and cationic polymers in gene delivery. *J. Control. Release* **2006**, *114* (1), 100-109.
(285) Zhang, Z.; Qiu, N.; Wu, S.; Liu, X.; Zhou, Z.; Tang, J.; Liu, Y.; Zhou, R.; Shen, Y. Dose-Independent Transfection of Hydrophobized Polyplexes. *Adv. Mater.* **2021**, *33* (25), e2102219.
(286) Nelson, C. E.; Kintzing, J. R.; Hanna, A.; Shannon, J. M.; Gupta, M. K.; Duvall, C. L. Balancing cationic and hydrophobic content of PEGylated siRNA polyplexes enhances endosome escape, stability, blood circulation time, and bioactivity *in vivo*. *ACS Nano* **2013**, *7* (10), 8870-8880.
(287) Liu, Z.; Zhang, Z.; Zhou, C.; Jiao, Y. Hydrophobic modifications of cationic polymers for gene delivery. *Prog. Polym. Sci.* **2010**, *35* (9), 1144-1162.
(288) Nayerossadat, N.; Maedeh, T.; Ali, P. A. Viral and nonviral delivery systems for gene delivery. *Adv. Biomed. Res.* **2012**, *1*, 27.
(289) Yin, H.; Kanasty, R. L.; Eltoukhy, A. A.; Vegas, A. J.; Dorkin, J. R.; Anderson, D. G. Non-viral vectors for gene-based therapy. *Nat. Rev. Genet.* **2014**, *15* (8), 541-555.
(290) Sato, Y.; Hatakeyama, H.; Sakurai, Y.; Hyodo, M.; Akita, H.; Harashima, H. A pH-sensitive cationic lipid facilitates the delivery of liposomal siRNA and gene silencing activity *in vitro* and *in vivo*. *J. Control. Release* **2012**, *163* (3), 267-276.
(291) Sun, M.; Dang, U. J.; Yuan, Y.; Psaras, A. M.; Osipitan, O.; Brooks, T. A.; Lu, F.; Di Pasqua, A. J. Optimization of DOTAP/chol Cationic Lipid Nanoparticles for mRNA, pDNA, and Oligonucleotide Delivery. *AAPS PharmSciTech* **2022**, *23* (5).
(292) Pinnaduwage, P.; Schmitt, L.; Huang, L. Use of a quaternary ammonium detergent in liposome mediated DNA transfection of mouse L-cells. *Biochimica et Biophysica Acta (BBA)-Biomembranes* **1989**, *985* (1), 33-37.
(293) Wang, Y.; Luo, J.; Truebenbach, I.; Reinhard, S.; Klein, P. M.; Hohn, M.; Kern, S.; Morys, S.; Loy, D. M.; Wagner, E.; et al. Double Click-Functionalized siRNA Polyplexes for Gene Silencing in Epidermal Growth Factor Receptor-Positive Tumor Cells. *ACS Biomater. Sci. Eng.* **2020**, *6* (2), 1074-1089.
(294) Neu, M.; Germershaus, O.; Behe, M.; Kissel, T. Bioreversibly crosslinked polyplexes of PEI and high molecular weight PEG show extended circulation times *in vivo*. *J. Control.*

Release **2007**, *124* (1), 69-80.
(295) Boussif, O.; Lezoualc'h, F.; Zanta, M. A.; Mergny, M. D.; Scherman, D.; Demeneix, B.; Behr, J. P. A versatile vector for gene and oligonucleotide transfer into cells in culture and *in vivo*: polyethylenimine. *Proc. Natl. Acad. Sci. U.S.A.* **1995**, *92* (16), 7297-7301.
(296) Luo, J.; Schmaus, J.; Cui, M.; Horterer, E.; Wilk, U.; Hohn, M.; Dather, M.; Berger, S.; Benli-Hoppe, T.; Peng, L.; et al. Hyaluronate siRNA nanoparticles with positive charge display rapid attachment to tumor endothelium and penetration into tumors. *J. Control. Release* **2021**, *329*, 919-933.

10 Publications

Original articles

Luo, J., Schmaus, J., Cui, M., Hörterer, E., Wilk, U., Höhn, M., Däther, M., Berger, S., Benli-Hoppe, T., **Peng, L.**, Wagner, E. Hyaluronate siRNA nanoparticles with positive charge display rapid attachment to tumor endothelium and penetration into tumors. J Control Release ***2021***, 329: 919-933.

Kuhn, J., Lin, Y., Krhac Levacic, A., Al Danaf N., **Peng L.,** Höhn, M., Lamb, DC., Wagner, E., Lächelt, U. Delivery of Cas9/sgRNA Ribonucleoprotein Complexes via Hydroxystearyl Oligoamino Amides. *Bioconjug Chem.* ***2020***, 31, 3, 729–742.

Review

Peng, L., Wagner, E., Polymeric Carriers for Nucleic Acid Delivery: Current Designs and Future Directions*. Biomacromolecules* ***2019****, 20, 10, 3613–3626.*

Patent

Wagner, E., **Peng**, **L.**, Berger, S., Schlögl, S., Folda, P., Haase, F., Grau M., Germer, J. New sequence-defined carriers for DNA or messenger RNA delivery. (Patent filing in progress)

11 Acknowledgements

After an intensive period of almost four years, my Ph.D. study ends. It has been a period of intense learning for me, both in the scientific and personal areas. Writing this dissertation has had a significant impact on me. I want to reflect on the people who have supported and helped me so much throughout the years.

First, I thank my supervisor, Professor Dr. Ernst Wagner, for allowing me to work on my dissertation within his research group. I am very grateful for his wise supervision and personal as well as scientific support during the whole time. Also, I want to thank him for his encouragement to develop my own projects and experiments.

I also especially want to thank Mina, Sophie, and Paul for spending so much time on cell culture work to test my synthesized oligomers, and we have very great collaboration. All synthetic work would be irrelevant without your contribution! It was great teamwork that added up perfectly within different projects. I thank Melina and Shuyuan for helping me with the synthesis of the projects.

I thank Teoman and Tobias for the MALDI-TOF-MS measurements. They really support my work on this very important characterization.

Many thanks to Ulrich and Jana for carrying out in vivo animal experiments and Markus for caring for the animals.

I would like to thank Dr. Ines Trübenbach, Dr. Philipp Klein, Dr. Jie Luo, and Simone for teaching me solid-phase synthesis during my first weeks in the lab and for providing scientific advice whenever needed.

Many thanks to Wolfgang for supporting our technical equipment, repairing almost any broken instruments or computers, ensuring technical maintenance, quick test kits for Covid-19, and a good atmosphere within room D3.002. I'm also grateful for Olga's support whenever needed.

Many thanks to Prof. Dr. Ulrich Lächelt for preparing the traditional Weißwurst, St. Nicholas chocolate, and lovely Glühwein. And thank him for the scientific advice in the research.

I want to thank current members of AK Wagner research group for the great atmosphere during my time in the lab. I especially want to thank our lunch groups, Dr.

Jie Luo, Yi Lin, Meng Lyu, Faqian Shen, Fengrong Zhang, and Xianjin Luo. We have great meals and talk happily during every lunch. Special thanks to China Scholarship Council for supporting my study and life in Munich. Many thanks to all my friends for helping and caring for me all the time.

Finally, I would also like to thank my parents for their constant support and trust throughout my life. I want to thank my girlfriend, Hui Zhang, who has been waiting for me in my motherland for four years, and she always makes me optimistic.